Spring 2020

Efficient Design Optimization Methodology for Manufacturable Variable Stiffness Laminated Composite Structures

Mazen Albazzan

EFFICIENT DESIGN OPTIMIZATION METHODOLOGY FOR MANUFACTURABLE VARIABLE STIFFNESS LAMINATED COMPOSITE STRUCTURES

by

Mazen Albazzan

Bachelor of Engineering
Lebanese American University, 2016

Master of Science
University of South Carolina, 2018

Submitted in Partial Fulfillment of the Requirements

For the Degree of Doctor of Philosophy in

Mechanical Engineering

College of Engineering and Computing

University of South Carolina

2020

Accepted by:

Zafer Gürdal, Major Professor

Ramy Harik, Major Professor

Brian Tatting, Committee Member

Adriana W. Blom-Schieber, Committee Member

Cheryl L. Addy, Vice Provost and Dean of the Graduate School

ACKNOWLEDGEMENTS

I would like to thank the Boeing Company for their support of the presented work. This research was mostly performed under contract SSOW-BRT-W0915-0002 through the University of South Carolina and the Ronald E. McNAIR Center for Aerospace Innovation and Research.

It is difficult to find the accurate words that express my sincere gratitude to my advisors Dr. Ramy Harik and Dr. Zafer Gürdal. I would like to thank Ramy for granting me the wonderful opportunity of being part of the McNAIR Center, for the energetic and welcoming atmosphere that he has created, and for the unconditional brotherly support and guidance throughout these years. I would also like to thank Zafer for introducing me to the challenging and interesting topic of structural optimization as well as the research enthusiasm that he has passed over throughout these years. I have enjoyed the journey and the challenges throughout each step of this project, and I am thankful for having the opportunity to work on your research topic for the past years. I am also grateful to my committee member Dr. Brian Tatting for his major contributions to this work and for the invaluable knowledge and expertise shared. A wonderful thing about Brian is that a new idea pops out every time we have a fruitful discussion; I highly appreciate all the valuable time that you have spent with me going through technical details while always improving my work. I would also like to appreciatively thank Dr. Adriana W. Blom for being part of my committee and for the rewarding discussions that we had over several ideas in this work. Thank you so much Agnes for the critical questions that you always asked; your

valuable contributions and comments have made me reconsider my explanations along the way, and this improved the quality of the work significantly. It has been a great pleasure and privilege to work with all of you.

I would like to my friends at McNAIR for their support and valuable time spent together throughout these years, including Roudy Wehbe, Aniz Baz Radwan, Christopher Sacco, and Andrew Anderson. The steering experiment we did in the AFP room was a memorable experience that we all enjoyed, so thank you Ramy for this opportunity. I would also like to thank my colleagues at McNAIR for the time spent together and the discussions we had.

Finally, I would like to express my deep appreciation for everyone who stood by my side through every step of the way. To my beloved father and brother, thank you for shaping my life to strive with motivation, pride, and love. To my lovely mother, thank you for providing me with everlasting love and for enduring my physical absence from home, and making me feel as if I am still at home. To my sister and brothers who I miss every day, thank you for your constant love and support. To my girlfriend, I am blessed and grateful for all the love and support. Thank you all for making this a successful achievement.

ABSTRACT

Because of their superior mechanical and environmental properties compared to traditional metals, fiber-reinforced composite materials have earned a widespread acceptance for different structural applications. The tailoring potential of composites to achieve high specific stiffness and strength has promoted them as promising candidates for constructing lightweight structures. From that aspect, designers have tackled the problem of designing composite laminates, which is inherently challenging due to the presence of non-linear, non-convex, and multi-dimensional optimization problems with discrete and continuous design variables. However, despite their increased usage, the possible improvements that can be achieved by composite laminates have not been fully exploited. With the introduction of new manufacturing technologies such as advanced fiber placement, engineers now have the capability to harness the full potential of nonconventional variable stiffness composite laminates using in-plane fiber steering. This can be a blessing as well as a curse for the designer, where the additional improvements can be attained at the expense of an increased complexity of the design problem. To circumvent this difficulty, this research aims to develop appropriate design tools to help unlock the advancements achieved by nonconventional variable stiffness laminates. The purpose is to adopt an efficient design optimization methodology to abandon the traditional usage of straight fiber composite laminates in the favor of exploring the structural improvements that can be achieved by steered laminated composite structures, subject to

manufacturing constraints and industry design guidelines. This represents a remarkable step in the development of energy-efficient light-weight structures and in their certification.

The complexity of the optimization problem imposes the need for an efficient multi-level optimization approach to achieve a global optimum design. In this work, the importance of including a design-manufacturing mesh is demonstrated in each optimization step of the multi-level optimization framework. In the first step (Stiffness Optimization), a theoretical optimum stiffness distribution parameterized in terms of lamination parameters is achieved that accounts for optimum structural performance while maintaining smoothness and robustness. The design-manufacturing mesh allows the spatial stiffness distribution to be expressed as a B-spline or NURBS surface defined by the control points of the design-manufacturing mesh. The fiber angle distribution is then obtained in the second optimization step (Stacking Sequence Retrieval) to match the optimum stiffness properties from the first optimization step while accounting for the maximum steering constraint and laminate design guidelines to attain manufacturability and feasibility. A bilinear *sine* angle variation is presented to obtain smooth fiber angle distributions, and the maximum steering constraint is derived to guarantee a certain degree of manufacturability at the second optimization step. Using the design-manufacturing mesh, a constant curvature arc solution is developed in the third optimization step (Fiber Path Construction) to generate manufacturable fiber paths with piecewise constant curvature arcs that match the optimal fiber orientation angles from the second optimization step while locally satisfying the maximum curvature constraint. To minimize gaps and overlaps obtained due to fiber steering, a design-for-manufacturing tool is developed to

generate tow-by-tow descriptions of the steered plies in the form of manufacturing boundaries for the AFP machine with optimized cut and restart positions.

The design of cylindrical shells under bending with a specified cutout is chosen as an aerospace application to demonstrate the effectiveness of using nonconventional variable stiffness laminates compared to traditional conventional laminates. The presence of the cutout in the cylindrical shell imposes severe stress concentrations yielding a need to use variable stiffness laminates that have continuously varying fiber orientation angles to redistribute the stresses and obtain a structurally optimal design. A design-manufacturing mesh was introduced to perform the buckling load optimization, where both circumferential and longitudinal stiffness variations were considered to physically understand the importance of the stiffness tailoring mechanism in efficient load redistribution and local reinforcements around the regions of the cutouts. The multi-level optimization framework is utilized to obtain a manufacturable fiber-steered laminate that improves the buckling load significantly. The design-for-manufacturing tool developed then generates the tow-level information in the form of exported AFP boundaries. The designed cylindrical shell is imported into CATIA V5® for composite design programming to demonstrate the applicability of the design-for-manufacturing tool developed.

TABLE OF CONTENTS

LIST OF TABLES

LIST OF FIGURES

LIST OF SYMBOLS

σ	In-plane normal stress
τ	In-plane shear stress
ε	In-plane normal strain
γ	In-plane shear strain
Q_{ij}	Components of reduced lamina stiffness matrix
E_1	Material's longitudinal modulus
E_2	Material's transverse modulus
G_{12}	Material's shear modulus
ν_{12}	Material's Poisson ratio
$\boldsymbol{\varepsilon}^0$	Mid-plane strains
$\boldsymbol{\kappa}$	Curvatures related to out-of-plane bending
θ_k	Fiber orientation angle of k^{th} layer of laminate
U_i	Material invariant properties
N	Stress resultants
M	Moment resultants
A_{ij}	Components of in-plane stiffness matrix
B_{ij}	Components of extension-bending coupling stiffness matrix
D_{ij}	Components of out-of-plane stiffness matrix
$T_{0,1}$	Initial (0) and final (1) orientation angles defining linear fiber angle path variation

ϕ Angle defining rotation of axis of variation x' with respect to x axis in linear fiber angle path variation

$L_{i,j}$ Lobatto polynomials

T_{ij} Coefficients associated with Lobatto polynomials

κ In-plane fiber path curvature

V_{iA} In-plane lamination parameters

V_{iB} Coupling lamination parameters

V_{iD} Out-of-plane lamination parameters also denoted as W_i

Γ_i Material invariant matrices

$I_{1,2}$ Volumetric strain invariants I_1 and maximum shear strain I_2

$X_{t,c}$ Longitudinal tensile and compressive failure stresses

$Y_{t,c}$ Transverse tensile and compressive failure stresses

S Shear failure stress

F_{ij} Tsai-Wu criterion failure coefficients

G_{ij} Tsai-Wu criterion failure coefficients in terms of strain

$\boldsymbol{x_i}$ i^{th} region design variable vector

h_i i^{th} region laminate thickness

α_i i^{th} region term containing derivatives for terms that depend explicitly on laminate thickness

$\breve{\Psi}_{i,j}^{m}$ Damped sensitivity matrix containing derivatives of j^{th} response with respect to laminate in-plane stiffness matrix of i^{th} region

$\breve{\Psi}_{i,j}^{b}$ Damped sensitivity matrix containing derivatives of j^{th} response with respect to laminate out-of-plane stiffness matrix of i^{th} region

$\breve{\Phi}_{i,j}^{m}$ Damped sensitivity matrix containing derivatives of j^{th} response with respect to inverse of laminate in-plane stiffness matrix of i^{th} region

$\breve{\Phi}_{i,j}^{b}$ Damped sensitivity matrix containing derivatives of j^{th} response with respect to inverse of laminate out-of-plane stiffness matrix of i^{th} region

P_{rs} Control points in B-spline lamination parameter distribution

$\Gamma_{rs}^{(\tau)}$ Coefficients representing lamination parameters for each control point P_{rs}

μ, ν Denote outer and inner iterations in GCMMA

$\alpha_j^{(\mu)}$ Upper moving asymptotes in GCMMA

$\beta_j^{(\mu)}$ Lower moving asymptotes in GCMMA

$p_{ij}^{(\mu,\nu)}$ Associated with positive sensitivities and upper moving asymptote in GCMMA

$q_{ij}^{(\mu,\nu)}$ Associated with negative sensitivities and lower moving asymptote in GCMMA

$r_i^{(\mu,\nu)}$ Denotes difference between objective function and response approximation

$\Psi_{(x,y)}$ Stream function

$t_{(x,y)}$ Smeared thickness distribution

$\theta_{(x,y)}$ Fiber angle distribution

$\boldsymbol{P}_{i,j}$ Bidirectional net of control points of design-manufacturing mesh

$N_{i,p}$ P^{th} degree B-spline basis functions along ξ

$N_{j,q}$ Q^{th} degree B-spline basis functions along η

Ξ Knot vector of $N_{i,p}$ along ξ

H Knot vector of $N_{j,q}$ along η

R Radius of cylindrical shell

L Length of cylindrical shell

θ Spherical coordinate corresponding to azimuthal angle

ρ Spherical coordinate corresponding to radial distance

φ_{uv} Fiber angle distribution in $\{u, v\}$ domain

$w_{i,j}$ Weights of control points in a NURBS surface representation

$\tilde{f}_0$ Objective function in approximate subproblem

$\tilde{f}_j$ Constraints in approximate subproblem

$\mathcal{L}$ Lagrangian of the primal convex subproblem

$\mathcal{L}_C$ Complementary Lagrangian

μ_j Dual variables or Lagrange multipliers

$\tilde{f}_j$ Conservative convex separable approximation of structural response

$\sin\varphi_{uv}$ Bilinear sine angle variation for $\{u, v\}$ domain

$\vec{e}_{u,v}$ Surface unit vectors

κ_g Geodesic curvature (in-plane)

κ_n Normal curvature (out-of-plane)

f_{GA} Fitness function for genetic algorithm

Ψ_{GA} Augmented fitness function for genetic algorithm

φ_P Initial starting angle for constant curvature arc solution

φ_E Fiber orientation angle at edge from constant curvature arc solution

κ Curvature of constant curvature arc

$\Delta\varphi$ Angle subtended by the constant curvature arc

C Chord length for constant curvature arc solution

φ_C Chord angle for constant curvature arc solution

κ_{max} Maximum curvature constraint for constant curvature arc solution

$\theta_{1,2}$ Constant curvature arc bounds

$\Delta\varphi_{Path}$ Fiber angle deviation along constant curvature arc

f_C Conservative convex approximations for error and gap

r Radius of cutouts

β Circumferential location of cutouts

t_{ply} Thickness of ply

r_b Inverse of buckling load factor λ

μ_b Lagrange multipliers associated with r_b

LIST OF ABBREVIATIONS

AFP ..... Automated Fiber Placement

ATL ..... Automated Tape Laying

CFRP ..... Carbon Fiber Reinforced Polymer

CLT ..... Classical Lamination Theory

FEM ..... Finite Element Method

FPFF ..... First Ply Fiber Failure

FRP ..... Fiber Reinforced Polymer

GA ..... Genetic Algorithm

GCMMA ..... Globally Convergent Method of Moving Asymptotes

GFRP ..... Glass Fiber Reinforced Polymer

KKT ..... Karush-Kuhn-Tucker

MCL ..... Minimum Cut Length

MCT ..... Multi-Continuum Theory

MDO ..... Multidisciplinary Design Optimization

NURBS ..... Non-Uniform Rational B-Spline

PFA ..... Progressive Failure Analysis

SLP ..... Sequential Linear Programming

RTM ..... Resin Transfer Molding

VARTM ..... Vacuum Assisted Resin Transfer Molding

XDSM ..... Extended Design Structure Matrix

CHAPTER 1

INTRODUCTION

1.1 OVERVIEW OF COMPOSITE MATERIALS

With the emergence of several cutting-edge research in the composite material field, it is often difficult to accurately define a composite material. In fact, instead of trying to describe a composite as it is now, we can help broaden its definition via continuous innovation ranging from a nanoscale to a macroscopic scale. On a macroscopic level, a composite can be characterized as a material system that can be obtained through a combination of two or more materials that possess distinctly different chemical and physical properties. The constituents are essentially insoluble in each other, and their combination would generally yield desirable properties that cannot be achieved by any of the constituents alone.

Composite materials have been used since the earliest ages. For example, the Pharaohs of the ancient Egyptian civilization used to combine chopped straws with mud to create reinforced bricks for their structures. Wood is also, without doubt, the most multipurpose composite material that has accompanied human evolution through all times. It has been used for building structures, transportation systems, weapons, bridges, and even airplanes [1]. However, their use gradually decreased after human civilizations started discovering stronger material systems. During the Stone Age, early civilizations started utilizing stone to build stronger and more complex structures. With the emergence of the

Bronze and Iron Ages, civilizations then revealed the importance of melting metals and their benefits in construction. The discovery of conventional metals was accompanied with the opportunity to produce stronger but heavier structures. The industrial revolution and the use of combustion engines then had a major effect on the usage of materials. Energy consumption increased immensely and heavy metals such as steel became dominant as an engineering metal. Traditional metals have been improved immensely throughout the years, and efficient alloy systems emerged and are still used nowadays heavily for structural applications. However, with the increase of the world population and the depletion of fossil fuel resources over decades, energy consumption became costly. As a result, the use of conventional metals has peaked around 1960, when consistent pressuring to produce lighter transportation systems became evident to decrease energy consumption and minimize cost [2,3] .

The material system chosen for a structure plays a significant role in terms of energy consumption. In the aerospace industry, the search for innovative light-weight structural solutions is persistent to improve structural reliability and energy efficiency. The structure of the aircraft has several purposes from carrying all the loads on the aircraft to protecting the passengers and providing a comfortable environment for them. During the First World War, wooden frames on airplanes were replaced by steel frames, and then came the first all metal airplane in 1920's which was made of steel iron. Several problems appeared with these metal airplanes such as buckling, corrosion, and fatigue. After the Second World War, improved types of aluminum appeared, which were more resistant to corrosion, accompanied with the birth of a stressed-skin semi-monocoque design that made the skin an essential element of the aircraft fuselage [4]. The continuous change in material

and design concepts were driven by the need to reduce structural weight, while increasing safety, reliability, durability, and structural performance of the aircraft. The reduction in structural weight directly reduces the lift required to sustain a steady-state flight. This decreases the amount of drag that is experienced by the aircraft and less thrust force is required to propel an aircraft. As a result, saving weight directly affects the amount of fuel being consumed, which allows the range of the aircraft flight to be extended or the payload to be increased, thus minimizing transportation costs. Consequently, the need for efficient light-weight structures promotes advanced composite materials to be ideal candidates for aerospace applications because of their high specific stiffness and high specific strength. In addition, maintenance costs are considered lower for advanced composite materials, because they are less sensitive to fatigue and corrosion than traditional metals [5].

In the last four decades, composite materials have witnessed an evolutionary era, where they constitute one of the major material systems that the aerospace industry is exploring to satisfy the ever-increasing structural efficiency requirements. Metals with high strength-to-weight ratios such as aluminum (20%), titanium (15%), and steel (10%) have found temporary prosperity in modern aircraft such as the Boeing 787, whereas advanced composite materials currently make up around 50% of structural weight of the Boeing 787 as shown in Figure 1.1 [6].

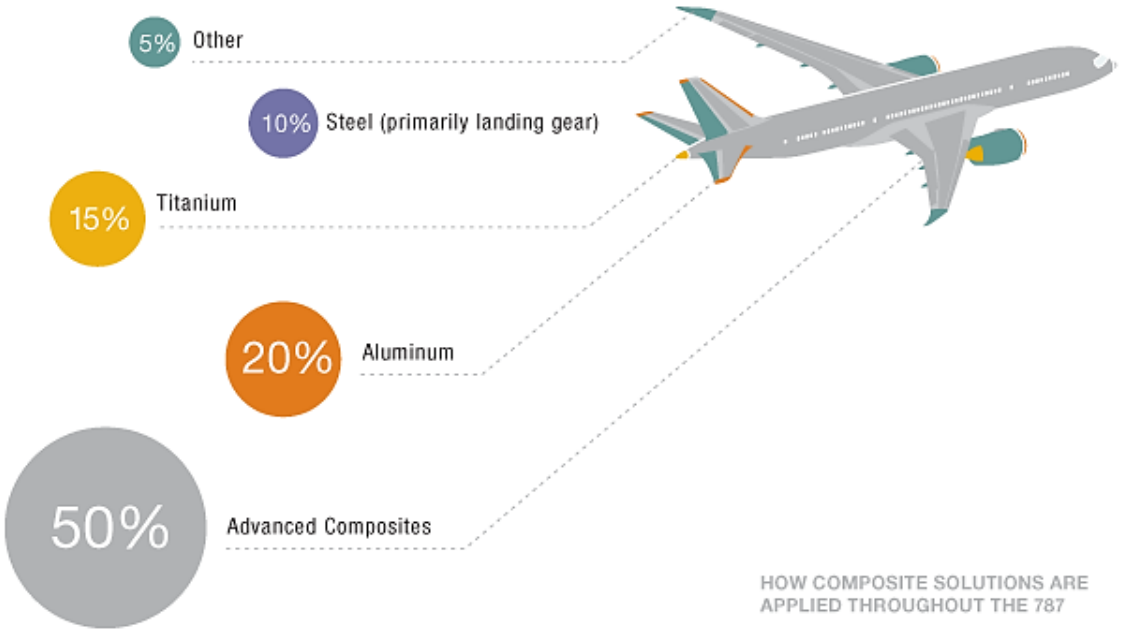

Figure 1.1 Boeing 787 Dreamliner Material Composition [6]

Because of their superior mechanical and environmental properties compared to traditional metals, fiber-reinforced composite materials have earned a prevalent acceptance for different structural applications not only in the aerospace industry, but also in the automotive, naval, and wind-energy industries. To produce light-weight structures, advanced composites such as carbon fiber-reinforced polymer (CFRP) and glass fiber-reinforced polymer (GFRP) have been utilized. Because of their composition, fiber-reinforced polymers (FRP) possess ideal specific strength and stiffness, which promote them as ideal candidates for constructing light-weight structures. In FRP, fibers that are characterized by their high stiffness and strength are embedded in a relatively low-stiffness and strength polymer matrix. The fibers constitute the major load carrying elements and the matrix acts as a binding material that holds the fiber in their position and transfers the stresses between the fibers. Because of the different chemical compositions of the separate

material systems, an interphase may exist between the fibers and the matrix to enhance the properties of the composite [7].

Fibrous materials are found in several different forms, ranging from discontinuous short fibers to woven fabrics to unidirectional continuous tapes or tows. Unidirectional continuous fibers are predominantly used in aerospace applications to produce laminated composites. Laminated composites are obtained by stacking multiple thin layers. These layers, which are commonly referred to as a lamina or ply, are held together by the polymer matrix after curing to constitute a laminate as shown in Figure 1.2.

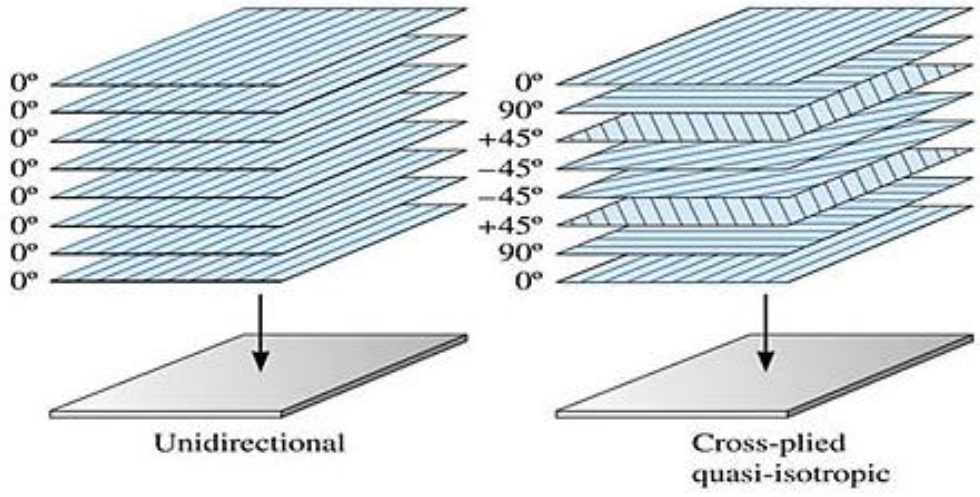

Figure 1.2 Example of composite laminates produced from multiple laminae [8]

Each layer usually has fibers that are placed straight and parallel at a certain orientation angle measured from the principal material axis. Specific desirable stiffness properties can be obtained by choosing the fiber orientation angles constituting a laminate, the thickness and number of the plies, and their order in the laminate. This laminate configuration is referred to as the stacking sequence of the composite laminate. Altering the stacking sequence of a laminate can significantly affect the in-plane and bending

stiffness properties of the laminate, without modifying the thickness, because of the directional properties of the layers. Composite laminates thus exhibit an important feature that distinguishes them from conventional metals, by providing highly directional or orthotropic properties depending on the direction of the fibers in each layer. This allows the designer to design the material by modifying the mechanical properties to satisfy the load requirements of the structure. This is considered a primary advantage of fiber-reinforced laminated composites, where the designer has the ability not only to change the size and shape of the structure, but also to 'optimize the material properties', which is often referred to as tailoring of composite laminates.

1.2 COMPOSITE LAMINATE MANUFACTURING

The stacked fibers must be embedded in a matrix material to produce a composite laminate. Two different matrix material systems exist, namely thermosets and thermoplastics. Thermosets usually consist of a resin and a hardener that cure upon their combination in the appropriate mixture ratio specified by the manufacturer. The curing process for thermosets is irreversible because it involves a cross-linking mechanism, whereas thermoplastics solidify when cured and can be transformed back to liquid state if reheated to their processing temperature [9].

Traditionally, composite laminates were manufactured by using a manual hand layup process. During hand layup, the layers of fibers are cut from the fabric roll and then stacked on an open mold successively according to the predefined stacking sequence. For dry fiber hand layup, the fiber layers are stacked on the surface of the mold, and then matrix material is infused to impregnate the laminate using resin transfer molding (RTM) or vacuum assisted resin transfer molding (VARTM). The impregnated fibers can then be

cured using an elevated temperature in the oven to achieve desirable properties [10]. Dry fiber impregnation usually suffers from relatively higher void regions in the laminate resulting in lower fiber volume fraction, which affects the performance of the laminate. As a result, wet layup with pre-impregnated fibers or prepregs, are usually used to manufacture laminates with desirable industrial performance while reducing the time taken for the impregnation process. The prepreg layup is then placed in an autoclave with adequate pressure and temperature at a certain cure cycle to minimize the void content and accomplish the anticipated properties [11]. In addition to the fiber and matrix system used, the manufacturing process requires a mold that shapes the composite part to be produced.

This demonstrates that the resulting manufactured part is strongly affected by the manufacturing process. In fact, some of the manufactured laminates can exhibit different mechanical properties because hand layup is prone to errors in fiber alignment and stacking. As a result, the traditional manufacturing processes depended on skilled labor to precisely manufacture laminated composites. Improving the manufacturing process plays a significant role in the production of advanced composite structures.

To increase the efficiency of composite laminate production, the aerospace industry has invested heavily in developing innovative manufacturing technologies to reduce costs and improve efficiency. Axisymmetric parts such as pressure vessels and tubes were initially automated using filament winding. In the 1970's, Automated Tape Laying (ATL) was established to manufacture large parts with non-convex shapes. ATL consists of placing a wide tape of prepreg to reduce the time required for high volume production, generally on low-contour non-convex surfaces. However, the commercial interest in composite material development continued to increase, and innovative manufacturing

processes were still being developed to satisfy the production of high-quality parts with complex shapes. Therefore, Automated Fiber Placement (AFP) was commercially available in the 1980's for accurate and relatively fast layup on complex surfaces. AFP is considered a unique manufacturing technology that combines the benefits of individual tow control in filament winding machines as well as the compaction and cut-restart capabilities of ATL. Most AFP machines currently process thermoset pre-impregnated materials, while thermoplastic and dry fiber placement are showing potential promise for future applications [12]. In AFP, the wide tapes are replaced by several narrow prepreg strips called tows. AFP machines were an inevitable solution to the increase of flexibility of the manufacturing process as well as the reduction of material waste and rejected parts. With this innovative manufacturing technology, manual labor was reduced, and production volume was increased, while also improving product quality and reproducibility. The process parameters of automated layup such as the processing temperature, layup speed and compaction pressure must be tuned based on the material being used to achieve an appropriate layup quality [12,13].

AFP machines are usually composed of a numerically control arm, a robotic arm or a gantry system, a material storage center and a fiber placement head. The fiber placement head is mounted on the robotic arm or gantry system, which is controlled via the control unit to deliver material with required position and orientation. An example of the fiber placement head is shown in Figure 1.3. It has enough degrees of freedom to access every point of the tool surface. An extra degree of freedom is available via the mandrel rotation for complex parts. Stools are used in the material storage chamber to store the pre-impregnated tows where the climate is controlled. A controlled tension mechanism is used

to guide the prepreg tows to the tool surface through the rollers. Before tow placement on the tool surface, the prepregs are subjected to controlled heating to increase their tackiness in order to enhance the adhesion properties with the mold surface. The preheated tows are then placed on the surface with a compaction roller that helps in removing the entrapped air between the tow and the surface to securely adhere the tows to the surface and avoid void content. Friction between the tow, compaction roller, and the tool surface acts as the driving force which pulls the tows from the spools to the surface.

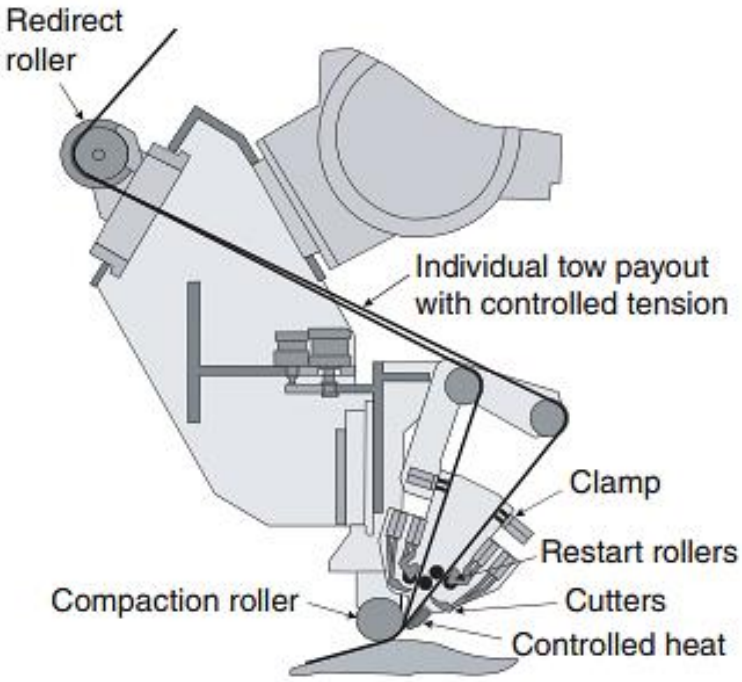

Figure 1.3 Schematic of fiber placement head in AFP [14]

AFP normally supplies multiple tows in a single sequence to form a course within each pass, while a sequence of courses constitutes a ply or layer. In order to maximize production rates, industry tends to use wider tows to fill a ply with the minimum time required. However, different tow widths can be used depending on the complexity of the manufactured part to avoid defects and achieve the desired product. Tows can also be cut

and restarted individually via a cutting mechanism and restart rollers to reduce material waste. The smallest feature that can be manufactured is limited by the minimal course length of the cutting and restart mechanism which corresponds to the distance between the nip point and the cutting mechanism [14]. An advanced fiber placement head laying material on a cylindrical mandrel is shown in Figure 1.4.

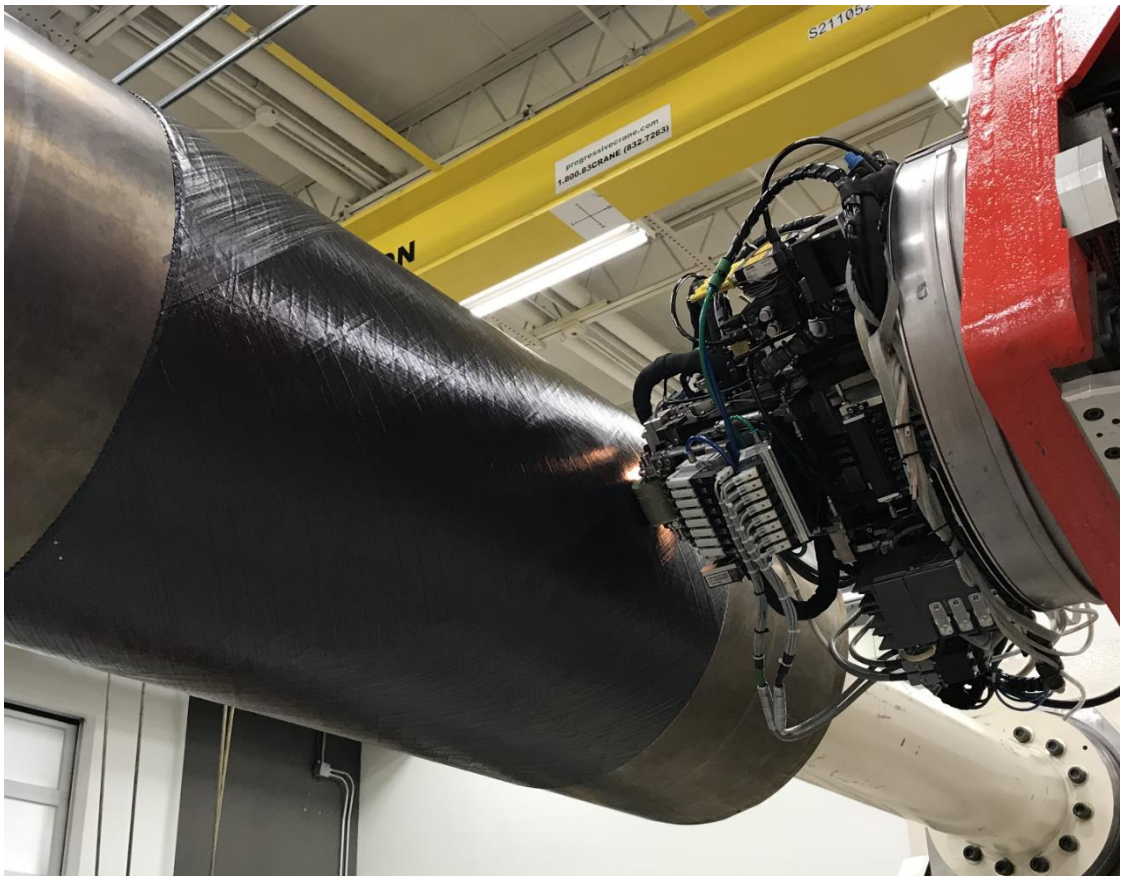

Figure 1.4 Working AFP head on a cylindrical mandrel at McNAIR Center for Aerospace Innovation and Research

1.3 CONVENTIONAL AND NONCONVENTIONAL COMPOSITE LAMINATES

Laminate tailoring is traditionally done by designing the laminate stacking sequence for each structural application to improve its performance. Each layer within the laminate is assigned a constant fiber orientation angle leading to a constant stiffness laminate. Fiber-reinforced composite laminates utilized are still predominantly restricted

to fiber orientation angles composed of 0°, ±45°, and 90°. The choice of these layups was initially motivated by the manufacturing capability when manual hand layup was still used because it was generally difficult to accurately align fibers at arbitrary fiber orientation angles. Composite laminates that are composed using fiber orientation angles restricted to 0°, ±45°, and 90° are defined as conventional laminates in this work.

The use of conventional laminates has been an essential stage in the development of advanced composite laminates. Although they were only limited to a restricted set of 0°, ±45°, and 90° fiber orientation angles, conventional laminates demonstrated the significant advantages that are achieved by composite structures compared to traditional metals. In fact, these fiber orientation angles are not completely arbitrary, as they refer to the maximum degree of axial (0°), transverse (90°), and shear stiffness (±45°), and a composite laminate designed using these set of angles yields desirable properties for several structural applications. Consequently, conventional laminates were experimentally tested for various applications, which led to the certification of conventional laminates and the availability of several test data. This enhanced the industry's experience and confidence in using them. This accumulated experience over decades also helped in developing laminate design guidelines, which help the designer exploit the composite laminate's strength while alleviating its weaknesses.

In practical design applications of realistic structures, a uniform stress state is rarely the case. On the contrary, the stress state in a structure usually varies spatially, which means that a composite structure composed of a conventional stacking sequence throughout may be subjected to different local loading conditions at different locations. As a result, the full potential of the composite laminate is not fully exploited at different regions of the

structure. By enlarging the design space and allowing arbitrary fiber orientation angles for a stacking sequence, the performance of a laminate can be improved, but the effective use of the composite material is still limited to local regions within the structure. However, by modifying the local design of the laminate spatially to counteract the loading conditions of a specific application, the mechanical behavior of the laminate can be significantly improved, and the weight of the structure can also be reduced. Hence, local laminate tailoring is essential for the effective utilization of the anisotropic properties of composite materials in order to improve the performance of a structure. With the introduction of AFP into the aerospace industry, designers have explored novel means to exploit the benefits of this innovative manufacturing technology. Because fiber tows can be placed accurately in any direction as well as the capability of in-plane fiber steering and tow-dropping, nonconventional laminates emerged in laminate design optimization. Nonconventional laminates attempt to harness the full potential of composite laminates by enlarging the design space creating significantly more efficient structural designs. Nonconventional laminates can be separated into two categories:

1. **Constant stiffness nonconventional laminates**: Each layer has a constant fiber orientation angle that is not restricted to any set of angles, and the stiffness properties are constant independent of the spatial location.
2. **Variable stiffness nonconventional laminates:** The fiber orientation angles vary spatially in a layer yielding different stiffness properties at each point in the laminate. The stiffness variation can be achieved by modifying the stacking sequences at each location, either by using blending laminates (patch design), or by steering the fibers in

each ply to produce continuous curvilinear fiber paths, which are also referred to as variable angle tow laminates.

a. **Blended Laminates:** They are obtained from discrete regions with different stacking sequences and number of layers. Some layers are dropped between neighboring regions and some constitute the stacking guide which is common between different design zones. Continuity of the structure is ensured by blending the neighboring laminates through the common layers. As a result, manufacturing and feasibility constraints are applied in the design of blended laminates. The discrete stiffness variation results in improvements in structural performance and weight reduction compared to constant stiffness laminates because a larger design space is utilized.

b. **Steered Fiber Laminates:** Using the built-in capabilities of AFP, the fibers can be steered in curvilinear paths in each layer in the laminate. Because of the continuous fiber angle variation, each point in the laminate possesses different stiffness properties, aiming to attain the maximum performance of the structure. This is the most general case of variable stiffness laminates, where the full potential of composite laminates can be harnessed if the thickness at each point is also allowed to vary spatially. However, it is accompanied with an additional complexity in structural optimization problems to guarantee manufacturability and feasibility.

An example of constant and variable stiffness (blended and steered) laminates is shown in Figure 1.5.

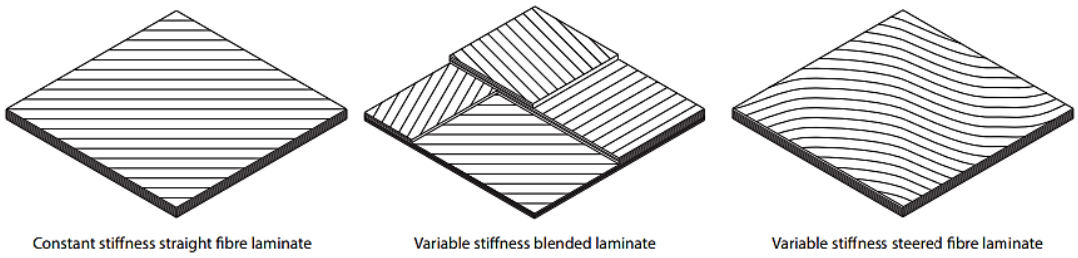

Figure 1.5 Constant and variable stiffness laminate configurations [15]

Given the achievable capacity of AFP machines, nonconventional laminate designs have emerged to improve the structural efficiency of composite laminates. The versatility of AFP unlocks the door for several design possibilities that were not attainable using the traditional composite manufacturing techniques used in aerospace. Complex fiber architectures can now be manufactured using fiber steering, and variable thickness composites can also be obtained by using ply dropping. As a result, the optimal performance of composite laminates can be attained by using these additional capabilities in composite laminate tailoring.

1.4 THESIS OBJECTIVES AND LAYOUT

Fiber-reinforced composite materials have earned a prevalent acceptance for different structural applications. The tailoring potential of composites to achieve high specific stiffness and strength has promoted them as promising candidates for constructing lightweight structures. From that aspect, designers have tackled the problem of designing composite laminates, which is inherently challenging because of the presence of non-linear, non-convex, and multi-dimensional problems with discrete and continuous design variables. Witnessing the introduction of AFP manufacturing, engineers now have the capability of exploiting the full potential of composites by using nonconventional variable stiffness laminates that introduce complex design problems.

It has been shown that constant stiffness nonconventional laminates increase the elastic tailoring capabilities resulting in a more efficient structure because of an enlarged design space [16–19]. However, the design of nonconventional constant stiffness laminates with arbitrary fiber orientation angles was not tackled extensively in the past years. On the contrary, the design of nonconventional variable stiffness laminates has indeed gained much more interest, perhaps because of its challenge and promising performance both theoretically and experimentally [20–26]. By providing the largest possible design space, variable stiffness laminates allow the full potential of composite materials to be harnessed. This could be a blessing and a curse for the designer, where the maximum achievable performance can be attained at the expense of an increased complexity of the design problem. Composite structures inherently present a challenge to obtain the global optimum design because of the complexity of modeling, analysis, and optimization [27–33].

The primary goal of this research was to develop appropriate design tools to help unlock the advancements that can be achieved by nonconventional laminates while considering the manufacturability and the feasibility of the designed composite structure. By adopting an efficient design optimization methodology, the traditional usage of conventional composite laminates can be abandoned in specific design applications in favor of exploring the structural improvements that can be achieved by nonconventional variable stiffness laminated composite structures. A major contribution of this research is the development of a design-for-manufacturing tool that accounts for AFP manufacturing constraints and detailed course-level and tow-level information of the designed structure as well as the feasibility in terms of industry design guidelines. This represents a

remarkable step in the development of nonconventional light-weight structures and in their certification. The thesis is organized as follows:

Chapter 2 Reviews the current state of the art extensively. Composite laminate parameterization is described briefly, followed by popular modeling techniques used for the design of nonconventional laminates. Lamination parameters are introduced, and the multi-level optimization methodologies used by researchers are then demonstrated to explain the efficient steps in obtaining an optimum laminate design while satisfying manufacturing constraints and laminate design rules. Because of the complexity of variable stiffness laminate design optimization, a multi-level optimization approach is demanded to efficiently achieve a global optimum design. In the first optimization step (Stiffness Optimization), a theoretical optimum stiffness distribution parameterized in terms of lamination parameters is obtained that accounts for optimum structural performance design drivers such as stiffness, strength, and buckling. Parameterizing the problem in terms of lamination parameters retains the convex nature of the problem aiming to attain a global optimum design. After the optimum stiffness requirements are obtained, the next level (Stacking Sequence Retrieval) aims to convert the optimum stiffness properties to optimal fiber orientation angle distributions while satisfying industry design guidelines to attain robustness and feasibility. The third level (Fiber Path Construction) constructs the continuous fiber paths from the retrieved fiber angle distributions while controlling gaps and overlaps for AFP manufacturing.

Chapter 3 Introduces the proposed multi-level optimization methodology that includes a design-manufacturing mesh in the framework to obtain optimal nonconventional steered fiber laminates while accounting for manufacturing constraints and industry design guidelines. A design-manufacturing mesh is introduced in the multi-level optimization to solve the variable stiffness optimization problem using two decoupled but dependent meshes. The analysis mesh, which is a finer mesh, is used to evaluate the finite element solutions, whereas the design-manufacturing mesh is used to define the spatial stiffness distribution of the laminated structure by mapping the values of the design variables to the analysis mesh. A design-manufacturing mesh is utilized in each optimization step to improve the efficiency, manufacturability, and feasibility of the variable stiffness design. A B-spline or NURBS surface in the first optimization step allows the spatial stiffness distribution to be defined mathematically with the nodes of the design-manufacturing mesh serving as the control points. In the second optimization step, a bilinear variation of the *sine* of the angles of the control points of each element of the design-manufacturing is proposed. The fiber angle distribution in the second optimization step can be used to constrain the lamination parameter distribution in the first optimization step to guarantee the final obtained design can match closely the designed stiffness variation. In the third optimization step, a constant curvature arc solution is developed for the considered fiber angle distribution, and a local maximum steering constraint is defined along each fiber path to guarantee manufacturability. A design-for-manufacturing tool was developed using

Mathematica® to match the optimal fiber orientation angle distribution from the second optimization step while minimizing gaps and overlaps obtained due to fiber steering. The developed tool generates tow-by-tow descriptions of the steered plies in the form of manufacturing boundaries for the AFP machine with optimized cut and restart positions.

Chapter 4 Implements the multi-level optimization methodology using a design-manufacturing mesh for an aerospace design application. A cylindrical shell with a cutout is designed under bending loads using a nonconventional variable stiffness steered laminate to demonstrate the potential buckling load improvements that can be obtained by using variable stiffness nonconventional laminates. The presence of the cutout in the cylindrical shell imposes severe stress concentrations yielding a need to use variable stiffness laminates that have continuously varying fiber orientation angles to redistribute the stresses and reinforce the regions around the cutout. The mechanisms behind the improved buckling load of the variable stiffness cylindrical shell are explained in the first optimization step, where global circumferential and longitudinal stiffness variations are considered as well as global-local variations to obtain an optimal variable stiffness laminate. The fiber angle distributions are then retrieved in the second optimization step to match the optimal stiffness properties while imposing industry design guidelines. Finally, the fiber paths are constructed using the developed design-for-manufacturing tool to match the optimal fiber angles while guaranteeing manufacturability and generating

detailed tow-level information of the steered layup with optimized cut and restart positions.

Chapter 5 Presents the manufacturing stage of the design application in **Chapter 4**. This demonstrates the applicability of the design-for-manufacturing tool developed to generate manufacturable optimal variable stiffness steered fiber laminates. An experimental study was conducted as a team collaboration to study the effect of AFP process parameters (feed-rate, temperature, and compaction pressure) on the layup quality of steered constant curvature paths on a cylinder. The optimal set of process parameters was chosen after doing an image analysis and identification of defects such as wrinkles, gaps, and overlaps. The designed steered laminate from the design application in **Chapter 4** is then transformed to the surface of the cylinder, imported into CATIA V5®, and programmed using iCPS® (Ingersoll Composite Programming System) for final AFP manufacturing.

Chapter 6 Concludes the presented research work with important findings related to design, manufacturing, and analysis of nonconventional steered fiber laminates as well as their certification and future work that can be continued.

CHAPTER 2

STATE OF THE ART

This chapter aims to provide the current state of the art regarding the use of lamination parameters for the multi-level optimization of robust and manufacturable nonconventional laminates by integrating the optimization process with manufacturing constraints and industry design guidelines. The parameterization of composite laminates is first discussed in Section 2.1 to characterize the mechanical behavior of composite laminates. Section 2.2 reviews popular modeling techniques that have been used by designers for modeling nonconventional variable stiffness laminates. Lamination parameters, which are intermediate variables for laminate stiffness parameterization, are introduced in Section 2.3. The different steps of the multi-level optimization methodology are then described in Section 2.4 along with methodologies that designers used at each level. In order to achieve a manufacturable and robust nonconventional laminate design, the integration of the design process with manufacturing constraints and industry design guidelines is discussed in each optimization level. Finally, a brief summary is presented in Section 2.5.

2.1 COMPOSITE LAMINATE PARAMETERIZATION

The basis of laminate stiffness is usually formulated using the Classical Lamination Theory (CLT) satisfying the classical Kirchhoff-Love assumptions for the laminate, with a through-the-thickness line perpendicular to the mid-plane that remains inextensible, straight, and perpendicular to the mid-plane after deformation. The strains in the out-of-

plane direction are neglected, and the stress component is also assumed to be negligible satisfying the plane stress assumption. The stresses can be related to the strains by the following constitutive relation for orthotropic materials [27]:

$$\begin{Bmatrix} \sigma_1 \\ \sigma_2 \\ \tau_{12} \end{Bmatrix} = \begin{bmatrix} Q_{11} & Q_{12} & 0 \\ Q_{12} & Q_{22} & 0 \\ 0 & 0 & Q_{66} \end{bmatrix} \begin{Bmatrix} \varepsilon_1 \\ \varepsilon_2 \\ \gamma_{12} \end{Bmatrix}, \tag{2.1}$$

where Q_{ij}'s are the reduced lamina stiffness components, obtained from the material's longitudinal modulus (E_1), transverse modulus (E_2), shear modulus (G_{12}), and the Poisson ratio (ν_{12}):

$$Q_{11} = \frac{E_1}{1-\nu_{12}\nu_{21}}, \quad Q_{12} = \frac{E_1\nu_{12}}{1-\nu_{12}\nu_{21}}, \quad Q_{22} = \frac{E_2}{1-\nu_{12}\nu_{21}}, \qquad Q_{66} = G_{12}\,. \tag{2.2}$$

The laminate is obtained upon stacking multiple layers, each with thickness, t_k, and fiber orientation angle, θ_k, with respect to the principal material axis. Using CLT assumptions, the stresses within each k^{th} layer are given by:

$$\begin{Bmatrix} \sigma_x \\ \sigma_y \\ \tau_{xy} \end{Bmatrix} = \begin{bmatrix} \bar{Q}_{11} & \bar{Q}_{12} & \bar{Q}_{16} \\ \bar{Q}_{12} & \bar{Q}_{22} & \bar{Q}_{26} \\ \bar{Q}_{16} & \bar{Q}_{26} & \bar{Q}_{66} \end{bmatrix} \begin{Bmatrix} \varepsilon_x^0 + z\,\kappa_x^0 \\ \varepsilon_y^0 + z\,\kappa_y^0 \\ \gamma_{xy}^0 + z\,\kappa_{xy}^0 \end{Bmatrix}, \tag{2.3}$$

where $z_{k-1} < z < z_k$, $\boldsymbol{\varepsilon}^0$ and $\boldsymbol{\kappa}^0$ are the mid-plane strains and curvatures. $\bar{Q}_{ij}$'s are the laminate stiffness components in the laminate coordinate system of each k^{th} layer, which are obtained by:

$$\begin{aligned} \bar{Q}_{11} &= U_1 + U_2\cos 2\theta_k + U_3\cos 4\theta_k\,, \\ \bar{Q}_{12} &= U_4 - U_3\cos 4\theta_k\,, \\ \bar{Q}_{22} &= U_1 - U_2\cos 2\theta_k + U_3\cos 4\theta_k\,, \\ \bar{Q}_{66} &= U_5 - U_3\cos 4\theta_k\,, \\ \bar{Q}_{16} &= (U_2\sin 2\theta_k + 2U_3\sin 4\theta_k)/2\,, \\ \bar{Q}_{26} &= (U_2\sin 2\theta_k - 2U_3\sin 4\theta_k)/2\,. \end{aligned} \tag{2.4}$$

U_i's are the invariant material properties and are defined by:

$$U_1 = \frac{(3Q_{11} + 3Q_{22} + 2Q_{12} + 4Q_{66})}{8},$$

$$U_2 = \frac{(Q_{11} - Q_{22})}{2},$$

$$U_3 = \frac{(Q_{11} + Q_{22} - 2Q_{12} - 4Q_{66})}{8}, \tag{2.5}$$

$$U_4 = \frac{(Q_{11} + Q_{22} + 6Q_{12} - 4Q_{66})}{8},$$

$$U_5 = \frac{(Q_{11} + Q_{22} - 2Q_{12} + 4Q_{66})}{8}.$$

The strains are assumed to have a linear variation through-the-thickness of the laminate. As a result, the stresses in each layer can be either constant or linear depending on the laminate curvatures κ_i and the fiber orientation angle of each layer θ_k. Because of the discontinuity in the stress variation, the stress resultants per unit length are obtained by integrating the layer stresses throughout the laminate thickness, h. These are referred to as force and moment resultants N and M, respectively, and can be expressed as:

$$N_x = \int_{-\frac{h}{2}}^{\frac{h}{2}} \sigma_x dz\,, \qquad N_y = \int_{-\frac{h}{2}}^{\frac{h}{2}} \sigma_y dz\,, \qquad N_{xy} = \int_{-\frac{h}{2}}^{\frac{h}{2}} \tau_{xy} dz\,,$$

$$M_x = \int_{-\frac{h}{2}}^{\frac{h}{2}} \sigma_x z dz\,, \qquad M_y = \int_{-\frac{h}{2}}^{\frac{h}{2}} \sigma_y z dz\,, \qquad M_{xy} = \int_{-\frac{h}{2}}^{\frac{h}{2}} \tau_{xy} z dz\,. \tag{2.6}$$

Substituting the stresses of each layer with equation (2.3), the constitutive relations for the composite laminate are obtained:

$$\begin{Bmatrix} N_x \\ N_y \\ N_{xy} \\ M_x \\ M_y \\ M_{xy} \end{Bmatrix} = \begin{bmatrix} A_{11} & A_{12} & A_{16} & B_{11} & B_{12} & B_{16} \\ A_{12} & A_{22} & A_{26} & B_{12} & B_{22} & B_{26} \\ A_{16} & A_{26} & A_{66} & B_{16} & B_{26} & B_{66} \\ B_{11} & B_{12} & B_{16} & D_{11} & D_{12} & D_{16} \\ B_{12} & B_{22} & B_{26} & D_{12} & D_{22} & D_{26} \\ B_{16} & B_{26} & B_{66} & D_{16} & D_{26} & D_{66} \end{bmatrix} \begin{Bmatrix} \varepsilon_x^0 \\ \varepsilon_y^0 \\ \gamma_{xy}^0 \\ \kappa_x \\ \kappa_y \\ \kappa_{xy} \end{Bmatrix}, \tag{2.7}$$

where A_{ij}, B_{ij}, and D_{ij} are expressed by:

$$A_{ij} = \sum_{k=1}^{N} \left(\bar{Q}_{ij}\right)_k (z_k - z_{k-1})$$

$$B_{ij} = \frac{1}{2} \sum_{k=1}^{N} \left(\bar{Q}_{ij}\right)_k (z_k^2 - z_{k-1}^2) \tag{2.8}$$

$$D_{ij} = \frac{1}{3} \sum_{k=1}^{N} \left(\bar{Q}_{ij}\right)_k (z_k^3 - z_{k-1}^3)$$

The laminate stiffness is represented by the extensional matrix **[A]**, the flexural (bending) matrix **[D],** and the bending-extension coupling matrix **[B]**. The **[A]** matrix relates the in-plane force resultants to the mid-plane strains, and the **[D]** matrix relates the moment resultants to the curvatures. The **[B]** matrix couples the in-plane force resultants to the curvatures and the moment resultants to the mid-plane strains. These matrices characterize the macro-mechanical behavior of composite laminates following the classical lamination theory and the stiffness terms found in each matrix appear directly in either objective functions or constraints in composite design applications. In some applications such as wind turbines, the **[B]** matrix might be useful to achieve extension-bending coupling, but generally for aerospace applications, this coupling is not desired and can be avoided by using mid-plane symmetric laminates. Bending-extension coupling can also be avoided by a different class of laminates such as fully isotropic ones [34,35].

2.2 NONCONVENTIONAL LAMINATE MODELING METHODOLOGIES

An extensive overview of optimization tools that can be used for optimizing laminated composites is provided by Ghiasi et al. [29,30]. The purpose here is to introduce the modeling techniques that can be used for nonconventional laminates. Each technique can affect the complexity and properties of the optimization problem directly with its own benefits and drawbacks. Because variable stiffness is a generalization of constant stiffness, the modeling of variable stiffness laminates is considered and it can be divided into three parts [36]:

2.2.1 Discrete Fiber Angle Representation:

The laminate is directly modeled with discrete fiber orientation angles at each point in the structure yielding different stacking sequences. The laminate is usually discretized based on the underlying discretization of the structure such as the finite element [37] or cellular automata discretization [38]. Several authors have used direct fiber orientation angle modeling to design variable stiffness laminates. Hyer and Charrete were among the first to investigate variable stiffness laminates by aligning the fibers along the principal directions of the stress field where strength was enhanced without accounting for buckling [39]. A follow-up study was conducted by Hyer and Lee to improve buckling loads by using fiber orientation angles as design variables with a gradient search method as shown in Figure 2.1 [40].

Katz et al. used sequential linear programming to minimize the maximum strain ratio based on the maximum strain energy showing potential improvements [41]. Setoodeh et al. conducted variable stiffness designs based on cellular automata [38,42] and finite elements [37] showing improvements of variable stiffness laminates. The optimal fiber

angle distribution obtained for a simple supported and clamped plate under biaxial loading is shown in Figure 2.2.

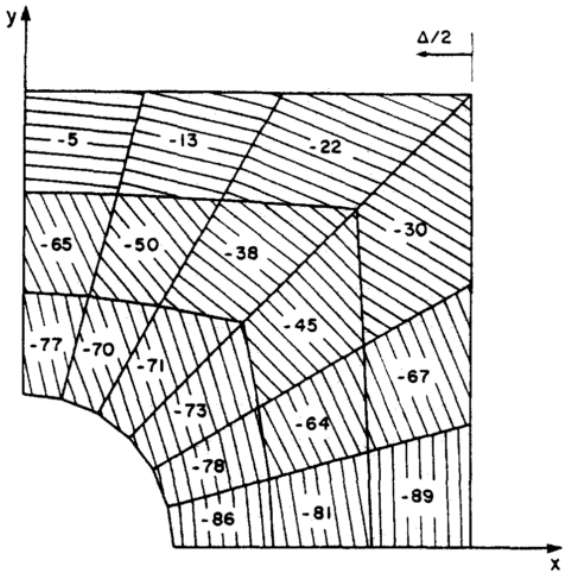

Figure 2.1 Optimal discrete fiber angle distribution to maximize buckling of simply supported square plate with a hole loaded in compression [40]

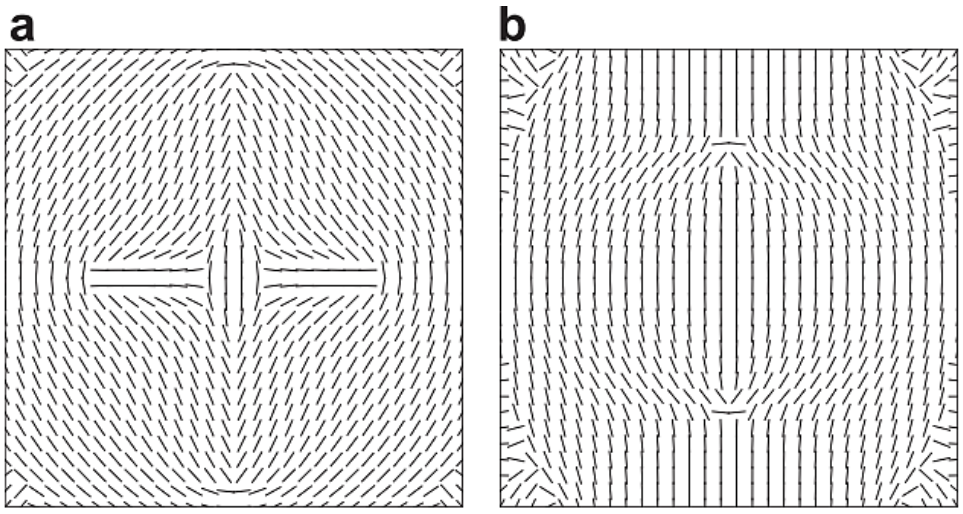

Figure 2.2 Optimal discrete fiber angle distribution for square plate under uniaxial transverse loading for (a) Simply supported (b) Clamped [37]

van Tooren et al. [43] and Barazanchy et al. [44] also used fiber orientation angles as design variables with a manufacturing finite element mesh framework, where promising improvements were achieved.

However, it is well known that these problems are highly non-linear, non-convex and usually suffer from ill-conditioned objective functions with many local optima even for constant stiffness laminate designs [16,45–48]. In addition, it is computationally expensive to achieve convergence and guarantee the continuity of a designed variable stiffness laminate with fiber angles as design variables. Tauchert and Adibhatla used a random jump technique with built-in learning to spray the design space and avoid local optima, but this is computationally expensive for a large design space with several design variables [45]. Because of the non-convexity and the presence of several local optima, gradient search algorithms were masked by direct stochastic search algorithms for such problems. Genetic algorithms (GAs) are by far the most popular stochastic methods dealing with discrete fiber angle representation [29]. The major benefit of using a GA is that it does not require gradient information, which is generally computationally expensive for complex structures. Several authors worked on developing genetic algorithms and improving the genetic operators as well as fine-tuning parameters [49–51]. However, genetic algorithms can be computationally expensive for more complex design problems and may suffer from local optima and convergence issues, especially when coupled with finite element analyses [52,53].

2.2.2 Fiber Path Parameterization:

This is achieved by using a curvilinear function to describe the fiber path. Gürdal and Olmedo were the first to introduce a fiber path parameterization where the fiber

orientation angle varies linearly [54]. The linear angle variation was later generalized by Tatting and Gürdal to vary along an arbitrarily defined axis, such that the fiber orientation angle is defined as [55]:

$$\theta(x') = \phi + (T_1 - T_0)\frac{|x'|}{d} + T_0 \tag{2.9}$$

where T_0 and T_1 are the fiber orientation angles at the beginning and end of the characteristic length d over which the variation occurs, as demonstrated in Figure 2.3. The angle ϕ defines the orientation of x' with respect to the global x axis.

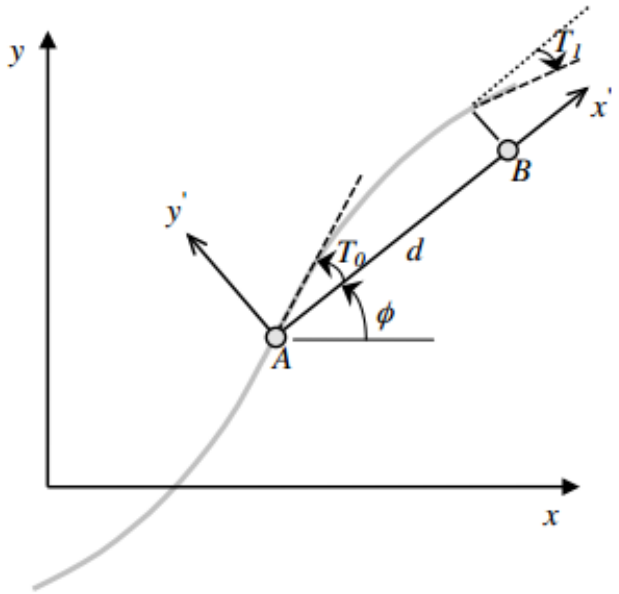

Figure 2.3 Fiber path definition using linear fiber orientation angle variation [55]

This fiber path parameterization was extensively used to design variable stiffness laminates for strength [23,56,57], thermomechanical response [58], and coupled strength-buckling optimization problems [55,59]. Nagendra et al. also used global fiber paths constructed by a linear combination of non-uniform rational B-splines (NURBS). They studied the design of optimal frequency and buckling load where the design variables were

multipliers of the different basis fiber paths [60]. Alhajahmad et al. used a non-linear fiber path expressed in terms of more complex functions such as Lobatto polynomials following the work conducted by Setoodeh et al. [61] to increase the number of design variables and achieve better laminate performance for pressure pillowing [62]. The non-linear fiber angle distribution with normalized coordinates (ζ, η) can be expresses as:

$$\theta(\zeta,\eta) = \sum_{i=0}^{m-1}\sum_{j=0}^{n-1} T_{ij} L_i(\zeta) L_j(\eta) \tag{2.10}$$

where L_i and L_j are the Lobatto polynomials, T_{ij} are the unknown coefficients used as design variables, and m and n are the number of basis functions used. By increasing the number of basis functions m and n the number of design variables increases, thus offering more design freedom. An example of fiber paths obtained using Lobatto polynomials is shown in Figure 2.4.

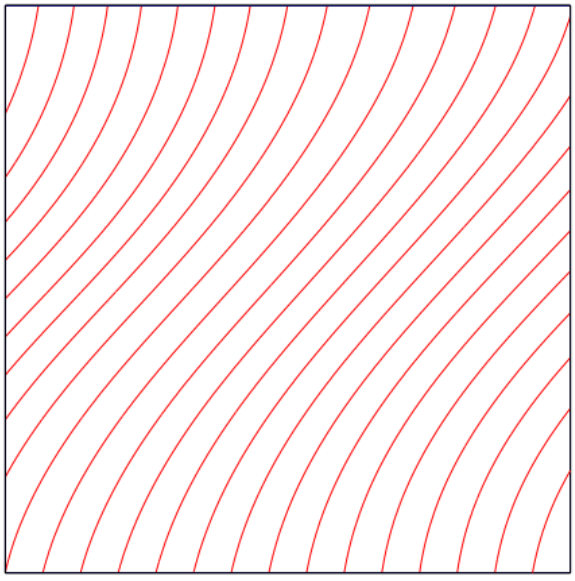

Figure 2.4 Optimal Fiber paths for pressure pillowing using Lobatto polynomials with m=4, n=9 [62]

Blom et al. also investigated several path definitions (geodesic, constant angle, linearly varying angle, and constant curvature) for conical shells [63]. These different path definitions are demonstrated graphically in Figure 2.5.

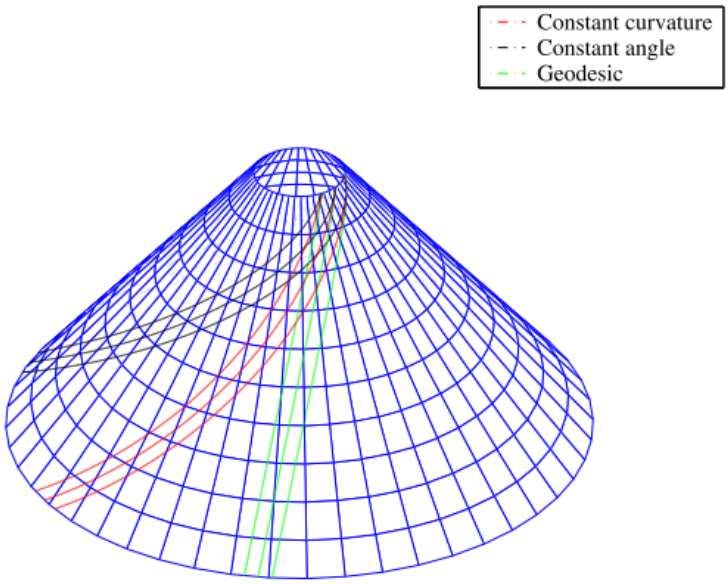

Figure 2.5 Different path definition on 3D cone [63]

The different path functions were used to maximize the fundamental frequency of conical shells including multiple-stage angle variations [64], as presented in Figure 2.6.

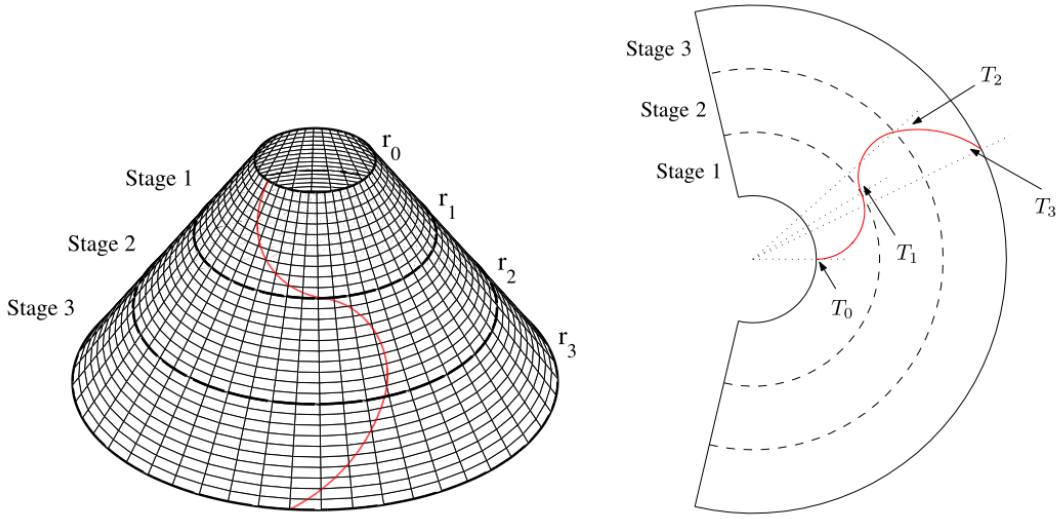

Figure 2.6 Fiber path optimization using multiple-stage angle variations [64]

Blom et al. then extended the formulation of linear angle variation to include multiple segments of variation at different predefined stages providing an additional design freedom for circumferential tailoring of cylinders [65], as presented in Figure 2.7.

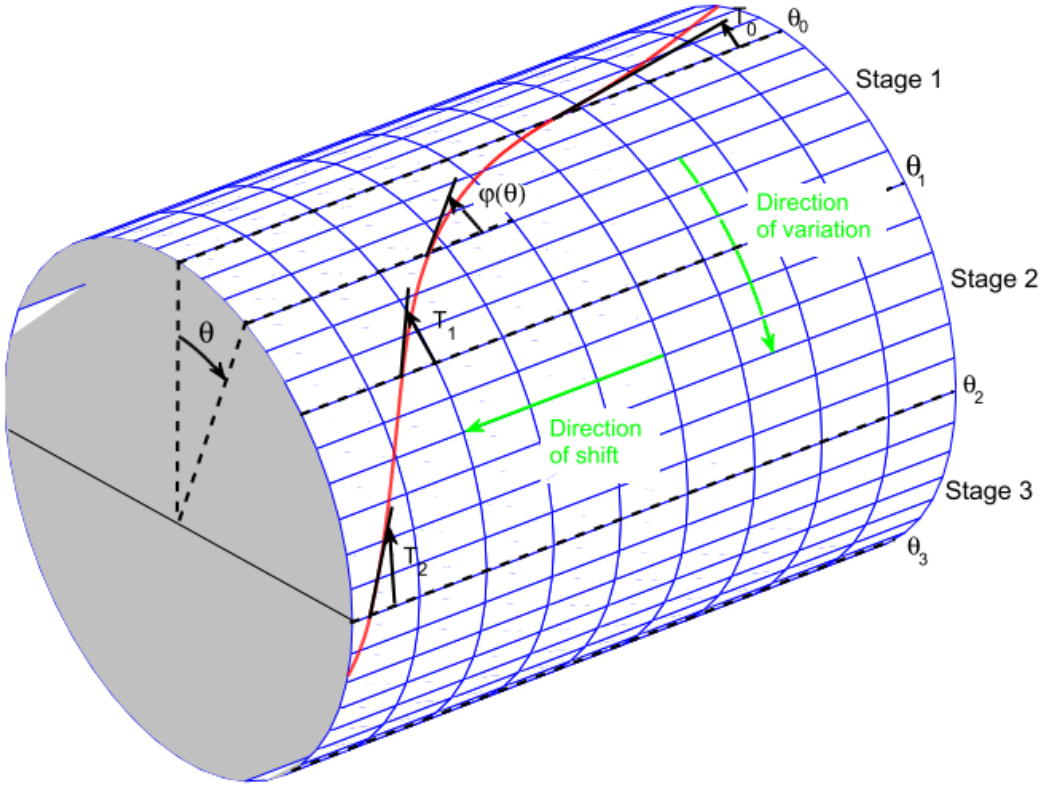

Figure 2.7 Circumferential multi-stage angle variation on cylinder [65]

The path definition was chosen to have a constant in-plane curvature, defined as:

$$\cos\varphi\,(\theta) = \cos T_i + (\cos T_{i+1} - \cos T_i)\frac{\theta - \theta_i}{\theta_{i+1} - \theta_i} \tag{2.11}$$

This helps in easily evaluating the curvature constraint within a segment to account for manufacturability of the fiber path. The values of T_i are the fiber orientation angles at the θ_i locations around the circumference. For a cylinder with radius R, the in-plane curvature κ within a segment, which can be used as a constraint in the optimization problem, is expressed as:

$$\kappa = \frac{\cos T_i - \cos T_{i+1}}{R(\theta_{i+1} - \theta_i)} \tag{2.12}$$

The optimal fiber paths of the variable stiffness layers obtained by using this fiber path definition to tailor the circumferential stiffness are shown in Figure 2.8.

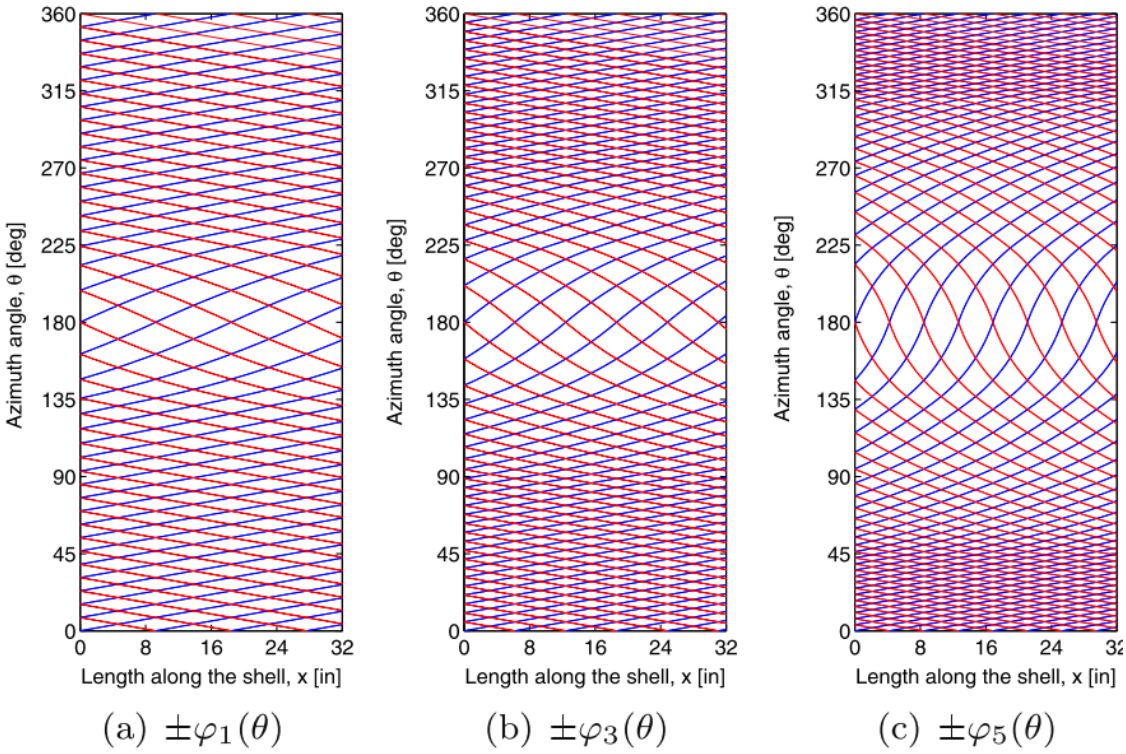

Figure 2.8 Optimal fiber paths in the variable stiffness layers for buckling load optimization of cylinder under bending [65]

As a result, modeling nonconventional laminates using fiber paths has the potential benefit of guaranteeing continuity and implementing curvature constraints efficiently, yet the design space is still non-convex, the modeling is always limited to the set of design variables used for the parameterization, and it requires path definitions for different surfaces.

2.2.3 Direct Stiffness Modeling:

The analysis of a composite laminate is usually done in terms of the stiffness matrices. Thus, instead of using local stacking sequences at each point in the laminate, the

terms of the **[A]**, **[B]**, and **[D]** matrices from the Classical Lamination Theory (CLT) are considered as design variables. One major difficulty is that the design variables are interrelated and cannot be chosen arbitrarily. As a result, lamination parameters can be used as intermediate variables to define a laminate's stiffness properties uniquely. In the most general case, the **[ABD]** matrix is a function of 12 lamination parameters and the laminate's thickness.

A significant advantage of using lamination parameters is decreasing the number of design variables, where they become independent of the number of layers in a laminate. In addition, it is well known that the optimization problem is always non-convex in the space of fiber orientation angles because it is non-bijective. The convexity of a given optimization problem depends on both the objective and the constraint functions. Using a multi-level optimization, the global optimum is attainable by parametrizing the first step of the optimization problem in the lamination parameter space. Lamination parameters have been found to be a finite set of continuous design variables defined by a convex feasible region, which makes them suitable to be used in efficient gradient search algorithms.

The responses to be optimized are usually non-convex as well, yet if convex structural approximations can be expressed as a function of lamination parameters, global optimality can be obtained in most cases. To determine the actual fiber angle from the lamination parameter distribution, a post-processing step is required. A hybrid multi-level approach is utilized which combines the benefits of gradient search using lamination parameters and evolutionary algorithms while alleviating their drawbacks. A conceptual optimum stiffness is achieved at the first stage using lamination parameters; then the

lamination parameter distribution is converted to optimal stacking sequences at the second stage, and the curvilinear fiber paths are then constructed at the final stage.

It is noteworthy to mention that the modeling technique presented by Vannucci and Verchery can also be used for direct stiffness modeling [66,67]. The polar method is a mathematical formulation that uses true tensor invariants for representing a general planar tensor. A fourth-order elasticity-like tensor requires only six polar parameters to be defined, two isotropic moduli, two anisotropic moduli, and two polar angles. Five polar parameters are invariants and they are related to all the possible elastic symmetries of the tensor (orthotropy, square symmetry, R0-orthotropy, and isotropy). Vannucci et al. utilized the polar method to find several classes of laminates, which are difficult to be identified otherwise, such as fully-isotropic laminates [68]. The concept of quasi-trivial solutions, initially introduced by Vannucci et al. [68], has been generalized for thick laminates by Garulli et al. [69]. In addition, Montemurro has extended the polar method to first-order shear deformation theory (FSDT) [67,70] and third-order shear deformation theory (TSDT) [71]. Catapano et al. have also carried out analysis of strength using the polar method at each scale [72], and analytical relations between laminate strength and stiffness polar parameters have been derived [73].

The polar method has also been successfully used for laminate design optimization. Over the last decade, a general multi-scale two-level (MS2L) optimization framework based on the polar method has also been developed by Montemurro et al. [74–79]. The optimization problem is split into two levels. The first level aims to optimize both the topology and the stiffness/strength properties of the laminate using the polar parameters with the use of high-order shear deformation theories [67,70]. At the first optimization

level, the structural requirements are considered such as mass, stiffness, buckling load, laminate strength, as well as manufacturing requirements. At the second optimization level, the goal is to find a suitable stacking sequence for each laminate compromising the structure to match the optimum combination of their geometrical and polar parameters obtained at the first optimization level. No restrictions were imposed on the laminate stack during the second optimization level to achieve the optimum stiffness properties.

The multi-scale two-level optimization framework has been applied to realistic engineering problems utilizing constant stiffness laminates. Montemurro et al. conducted design optimization of sandwich panels [76,80,81] as well as stiffened panels [74,75,77] with manufacturing constraints. Nonconventional stacking sequences with no restrictions have been retrieved at the second optimization step to match the optimum polar parameters in terms of buckling, stiffness, and strength requirements. The multi-scale two level optimization has also been further generalized for the design optimization of variable stiffness laminates [79,82,83]. The utilization of higher order theories (FSDT and TSDT) in the optimization framework has a great advantage of incorporating the effect of the transverse shear stiffness on the behavior of the variable stiffness laminate. This allows the adequate design of thin as well as moderately thick laminates. Discussing the optimization of composite laminates using the polar method in detail is outside the scope of this thesis. However, a very brief summary was presented here for the interested reader.

The complexity of the variable stiffness optimization problem necessitates the use of multi-level optimization with lamination parameters to utilize their benefits at the first stage to achieve efficient global optimization. This helps in eliminating the shortcomings

faced when using different modeling techniques. A schematic of the multi-level optimization process is shown in Figure 2.9.

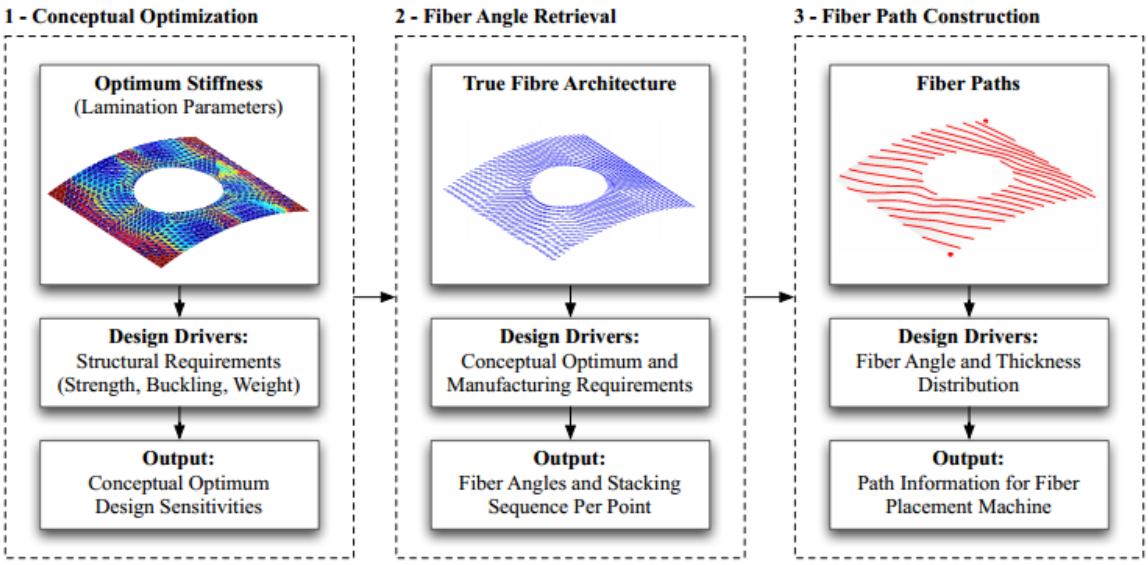

Figure 2.9 Schematic overview of the multi-level optimization process [36]

The benefits and drawbacks of each modeling technique in structural design of nonconventional laminates are summarized in Table 2.1. To demonstrate the efficiency of the multi-level optimization, lamination parameters are first reviewed extensively in Section 2.3, and then the optimization levels are discussed in Section 2.4 along with manufacturing constraints and industry design guidelines to discuss how designers implemented these constraints in nonconventional laminate design optimization to ensure manufacturability and robustness.

Table 2.1 Benefits and Drawbacks of Different Nonconventional Laminate Modeling Techniques

Modeling Technique	Benefits	Drawbacks
Discrete Fiber Angle Representation	• Entire design space encompassed	• Poorly conditioned design problem • Computationally expensive with convergence issues • Highly non-linear and non-convex • Requires post-processing for fiber path
Fiber Path Parametrization	• Few number of design variables • Continuous smooth path • Function definition eases curvature constraint application	• Limited design space by path function • Highly non-linear and non-convex • Requires function definitions for different surfaces
Direct Stiffness Modeling (Lamination Parameters)	• Entire design space encompassed • Set of continuous design variables defined by a convex region • Number of design variables independent of number of layers	• Multi-level optimization required for post-processing fiber angles and fiber path • Feasible region required for interrelating stiffness properties

2.3 LAMINATION PARAMETERS

Lamination parameters, first introduced by Tsai and Pagano [84] and Tsai and Hahn [85], allow the stiffness properties of a laminate to be described in a compact notation. Lamination parameters are non-dimensional through-the-thickness integrated trigonometric functions that express the laminate properties in 12 variables regardless of the number of layers as shown below.

$$(V_{1A}, V_{2A}, V_{3A}, V_{4A}) = \int_{-\frac{1}{2}}^{\frac{1}{2}} (cos\, 2\theta\, , sin\, 2\theta\, , cos\, 4\theta\, , sin\, 4\theta)\, d\bar{z}\, ,$$

$$(V_{1B}, V_{2B}, V_{3B}, V_{4B}) = 4 \int_{-\frac{1}{2}}^{\frac{1}{2}} \bar{z}(cos\, 2\theta\, , sin\, 2\theta\, , cos\, 4\theta\, , sin\, 4\theta)\, d\bar{z}\, , \qquad (2.13)$$

$$(V_{1D}, V_{2D}, V_{3D}, V_{4D}) = 12 \int_{-\frac{1}{2}}^{\frac{1}{2}} \bar{z}^2(cos\, 2\theta\, , sin\, 2\theta\, , cos\, 4\theta\, , sin\, 4\theta)\, d\bar{z}\, ,$$

where V_{iA}, V_{iB}, and V_{iD} are in-plane, coupling, and flexural lamination parameters, respectively; $\bar{z}$ is the normalized through the thickness dimension and θ is the layer fiber orientation angle.

The **[ABD]** matrix obtained from the Classical Lamination Theory characterizes the macro-mechanical behavior of composite laminates, and the stiffness terms found in each matrix appears directly in either objective functions or constraints in a composite structure design application. Because they are interrelated, lamination parameters are used as intermediate variables to represent the **[ABD]** matrix in a convenient form for

optimization problems. The **[A]**, **[B]**, and **[D]** matrices can be expressed as a linear function of material invariants and lamination parameters as follows:

$$\begin{aligned} A &= h\,(\Gamma_0 + \Gamma_1 V_{1A} + \Gamma_2 V_{2A} + \Gamma_3 V_{3A} + \Gamma_4 V_{4A})\,, \\ B &= {h^2}/{4}\;(\Gamma_1 V_{1B} + \Gamma_2 V_{2B} + \Gamma_3 V_{3B} + \Gamma_4 V_{4B})\,, \\ D &= {h^3}/{12}\;(\Gamma_0 + \Gamma_1 V_{1D} + \Gamma_2 V_{2D} + \Gamma_3 V_{3D} + \Gamma_4 V_{4D})\,, \end{aligned} \tag{2.14}$$

where Γ_i's are defined by the material invariants as:

$$\Gamma_0 = \begin{bmatrix} U_1 & U_4 & 0 \\ U_4 & U_1 & 0 \\ 0 & 0 & U_5 \end{bmatrix},\ \Gamma_1 = \begin{bmatrix} U_2 & 0 & 0 \\ 0 & -U_2 & 0 \\ 0 & 0 & 0 \end{bmatrix},\ \Gamma_2 = \begin{bmatrix} 0 & 0 & \frac{U_2}{2} \\ 0 & 0 & \frac{U_2}{2} \\ \frac{U_2}{2} & \frac{U_2}{2} & 0 \end{bmatrix},$$

$$\Gamma_3 = \begin{bmatrix} U_3 & -U_3 & 0 \\ -U_3 & U_3 & 0 \\ 0 & 0 & -U_3 \end{bmatrix},\ \Gamma_4 = \begin{bmatrix} 0 & 0 & U_3 \\ 0 & 0 & -U_3 \\ U_3 & -U_3 & 0 \end{bmatrix}. \tag{2.15}$$

The linear dependence of the **[ABD]** matrix on lamination parameters is beneficial for convex design optimization as demonstrated by Grenestedt et al., who proved that the feasible regions of lamination parameters are convex [86].

Assuming mid-plane symmetry reduces V_{iB} to zero and balancing the off-axis plies sets $V_{2A} = V_{4A} = 0$. In addition, several designers have assumed orthotropic laminates during the design of composite laminates, where bending-twisting coupling is assumed negligible having $V_{2D}, V_{4D} \approx 0$. Hence, the designer is left with four design variables V_{1A} (or V_1), V_{3A} (or V_3), V_{1D} (or W_1), and V_{3D} (or W_3). For variable stiffness laminates, several design variables are required to vary the properties at each spatial location. Thus, using fiber angles of several layers as design variables complicates the design problem by making it computationally expensive as well as non-convex. The complexity of the optimization

problem is directly influenced by the number of design variables as well as their nature. As a result, using lamination parameters as continuous design variables ensures robustness and efficiency.

One of the primary difficulties faced with lamination parameters is the development of explicit relations to define the feasible region of 12 lamination parameters. Researchers have tackled this problem where an analytical expression of the feasible region combining all 12 variables is still not available. However, this problem has been advanced progressively by several authors. Miki [87,88] and Miki et al. [89] were the first authors to pioneer the use of lamination parameters. They proposed a graphical design approach to design effective engineering constants of an orthotropic laminate. Miki defined the feasible region, known as the Miki diagram shown in Figure 2.10, describing two in-plane or two flexural lamination parameters characterizing the stiffness of an orthotropic laminate:

$$\begin{aligned} V_3 &\geq 2V_1^2 - 1 \,, \\ -1 \leq V_i &\leq 1 \; (i = 1,3) \,. \end{aligned} \tag{2.16}$$

Grenestedt et al. also studied the in-plane shear buckling optimization using four out-of-plane lamination parameters by using two-dimensional projections of the feasible region [90].

After that, Fukunaga and Sekine presented the feasible region of four in-plane or four flexural lamination parameters as follows:

$$\begin{aligned} 2V_1^2(1 - V_3) + 2V_2^2(1 + V_3) + V_3^2 + V_4^2 - 4V_1V_2V_4 &\leq 1 \,, \\ V_1^2 + V_2^2 &\leq 1 \,, \\ -1 \leq V_3 &\leq 1 \,. \end{aligned} \tag{2.17}$$

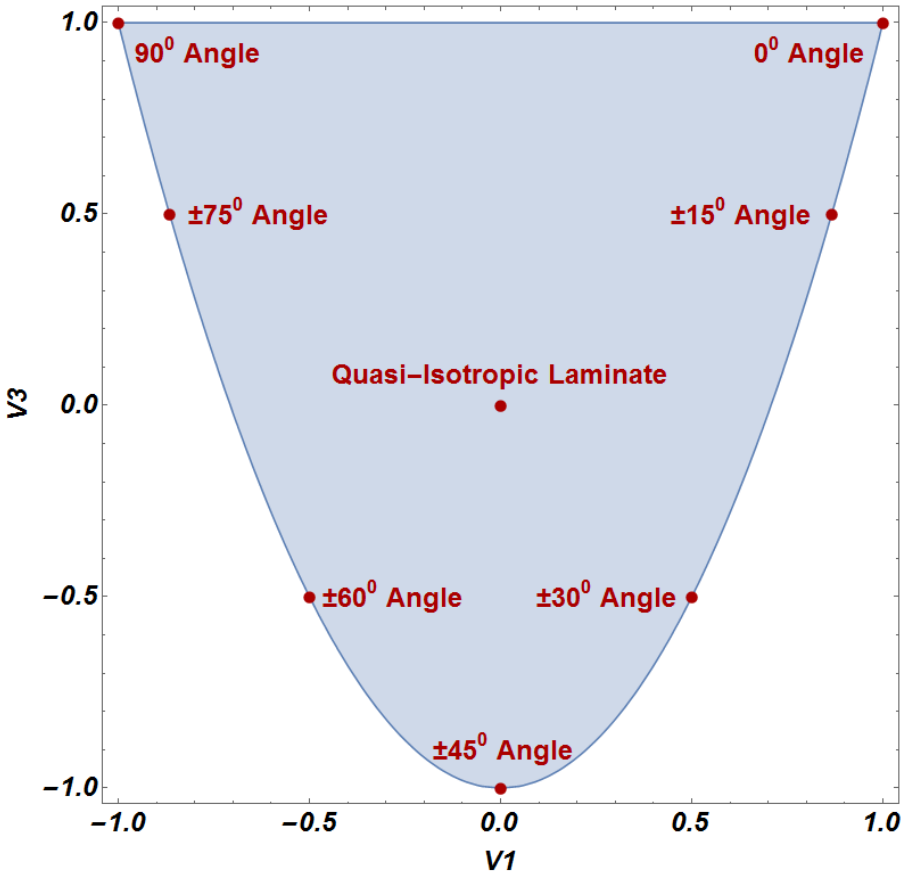

Figure 2.10 Miki diagram with some physical stacking sequence representation

They presented the importance of including bending-twisting coupling in aeroelastic tailoring of a composite wing and shear buckling optimization [91,92]. Hammer et al. used the four-dimensional feasible region for optimal compliance design of composite laminates [93]. To account for manufacturing practice, Setoodeh derived the feasible domain of two in-plane lamination parameters for an increasing number of equal thickness layers of balanced symmetric laminates. It was then used for optimal compliance design of variable stiffness laminates [94]. van Campen et al. also derived the feasible region for two out-of-plane lamination parameters of realistic laminates with equal layer thicknesses [95].

These derived feasible regions consider in-plane or flexural lamination parameters separately and can be applied to design applications that depend on either in-plane or out-

of-plane lamination parameters. However, practical structural design applications laminates require both in-plane and out-of-plane lamination parameters, because they depend on both extensional and flexural stiffness properties. As a result, a combined feasible region must be defined for both in-plane and out-of-plane lamination parameters. Fukunaga and Vanderplaats examined a geometrical method to determine the combined feasible region of orthotropic laminates for the buckling optimization of cylindrical shells [96]. It was later shown by Grenestedt et al. that it is smaller than the actual feasible region by using a variational approach [86]. Diaconu and Sekine utilized the variational approach to implicitly build the feasible region numerically in the general design space of 12 lamination parameters [97], and they proposed an optimization approach that was used to maximize the fundamental frequency of thick plates [98]. Liu et al. derived a hexagonal feasible region of flexural lamination parameters for the case where the amounts of 0, ±45, and 90-degree plies of a laminate are given [99]. Diaconu and Sekine later derived explicit equations relating in-plane, coupling and flexural lamination parameters for the conventional set of fiber angles (0°, ±45°, and 90°), which were used to optimize the buckling load of cylindrical shells [100]. Liu et al. utilized this explicit feasible region to conduct a bi-level optimization strategy with conventional laminates, where lamination parameters were optimized at the top level, and a GA was used to find the optimum integer number of plies that best matches the obtained lamination parameters [101]. Setoodeh et al. then established a method based on successive convex hull approximations to approximate the boundary of the general feasible region of lamination parameters with no restrictions on fiber angles. The final approximation was presented in the form of a huge number linear inequalities that could be included explicitly as constraints [102].

Bloomfield et al. also presented a method to derive the feasible region of lamination parameters for any predefined set of ply angles [103] and derived an expanded feasible region for the set of (0°, ±30°, ±45°, ±60°, and 90°) that was used for mass optimization of long anisotropic plates subject to buckling and strength constraints [18]. An explicit feasible region combining four coupled lamination parameters of orthotropic laminates was finally derived by Wu et al. By recognizing the importance of the Cauchy-Schwarz inequality and the algebraic identity relating in-plane, coupling, and flexural lamination parameters, the authors developed explicit expressions as follows [104,105]:

$$\begin{aligned} 5(V_{1A}-V_{1D})^2-2(1+V_{3A}-2V_{1A}^2)\le 0,\\ (V_{3A}-4tV_{1A}+1+2t^2)^3-4(1+2|t|+t^2)^2(V_{3D}-4tV_{1D}+1+2t^2)\le 0,\\ (4tV_{1A}-V_{3A}+1+4|t|)^3-4(1+2|t|+t^2)^2(4tV_{1D}-V_{3D}+1+4|t|)\le 0. \end{aligned} \quad (2.18)$$

where t = [-1, -0.75, -0.5, -0.25, 0, 0.25, 0.5, 0.75, 1] or the interval can be discretized more for better accuracy. These 19 non-linear constraints are adequate and can be considered the most efficient equations for expressing the boundary of the feasible region for orthotropic laminates to be included in optimization problems. Raju et al. further developed this work and derived explicit relations relating four in-plane and four flexural lamination parameters which was used to maximize the shear buckling performance of symmetric variable stiffness laminates [106].

One of the restrictions to using lamination parameters as design variables has been the difficulty of evaluating the strength on a ply-by-ply basis because the laminate configuration is not present. As a result, a conservative failure envelope is used for strength evaluation, which was developed by Ijsselmuiden et al. based on the Tsai-Wu failure criterion [107]. By mapping the Tsai-Wu failure criterion onto the strain space, the ply angles appear explicitly in the formulation. The conservative failure envelope is

constructed by finding a region in the strain space that is safe regardless of the ply angle. The obtained failure envelope is valid for any ply angle and depending on the laminate configuration used, the failure index obtained can be close to the one obtained using the Tsai-Wu criterion, or it may be more conservative. The Tsai-Wu failure criterion can be expressed in terms of the material strain tensor components as:

$$G_{11}\,{\epsilon_1}^2 + G_{22}\,{\epsilon_2}^2 + G_{66}\,{\epsilon_{12}}^2 + G_1\,\epsilon_1 + G_2\,\epsilon_2 + 2G_{12}\,\epsilon_1\epsilon_2 = 1, \tag{2.19}$$

where the strain coefficients, G_{ij} , are obtained using:

$$\begin{aligned} G_{11} &= {Q_{11}}^2 F_{11} + {Q_{12}}^2 F_{22} + 2F_{12}Q_{11}Q_{12}\,, \\ G_{22} &= {Q_{12}}^2 F_{11} + {Q_{22}}^2 F_{22} + 2F_{12}Q_{12}Q_{22}\,, \\ G_1 &= Q_{11}F_1 + Q_{12}F_2\,, \\ G_2 &= Q_{12}F_1 + Q_{22}F_2\,, \\ G_{12} &= Q_{11}Q_{12}F_{11} + Q_{12}Q_{22}F_{22} + F_{12}{Q_{12}}^2 + F_{12}Q_{11}Q_{22}\,, \\ G_{66} &= 4{Q_{66}}^2 F_{66}\,, \end{aligned} \tag{2.20}$$

and F_{ij} are defined from the Tsai-Wu failure criterion in Eq. (2.21), where X_t is the longitudinal tensile strength, Y_t is the transverse tensile strength, X_c is the longitudinal compressive strength, Y_c is the transverse compressive strength, and S is the shear strength of the composite material being used.

$$
\begin{aligned}
F_{11} &= \frac{1}{X_t X_c}, \\
F_{22} &= \frac{1}{Y_t Y_c}, \\
F_1 &= \frac{1}{X_t} - \frac{1}{X_c}, \\
F_2 &= \frac{1}{Y_t} - \frac{1}{Y_c}, \\
F_{12} &= \frac{-1}{2\sqrt{X_t X_c Y_t Y_c}}, \\
F_{66} &= \frac{1}{S^2},
\end{aligned}
\tag{2.21}
$$

Materials strains ($\epsilon_1, \epsilon_2, \epsilon_{12}$) can be related to laminate strains ($\epsilon_x, \epsilon_y, \epsilon_{xy}$) by using the transformation matrix:

$$
\begin{bmatrix}
\frac{1}{2}(1+c) & \frac{1}{2}(1-c) & s \\
\frac{1}{2}(1-c) & \frac{1}{2}(1+c) & -s \\
-\frac{1}{2}s & \frac{1}{2}s & c
\end{bmatrix},
\tag{2.22}
$$

where $s = \sin(2\theta)$ and $c = \cos(2\theta)$. Substituting the transformed strains in Eq. (2.19) yields a failure envelope equation in terms of laminate strains and ply angles:

$$
F(\epsilon_x, \epsilon_y, \epsilon_{xy}, s, c) = 0\,,
\tag{2.23}
$$

and the trigonometric functions satisfy the equation:

$$
s^2 + c^2 = 1\,,
\tag{2.24}
$$

The equation for the failure envelope is obtained by eliminating s and c from Eq. (2.23). The elimination is achieved by using Dixon's resultant for the elimination of

polynomial equations. This yields the two following equations, each one representing a surface traced out by the Tsai-Wu failure criterion in strain space for all ply orientations:

$$4{u_6}^2{I_2}^2 - 4u_6u_1{I_2}^2 + 4\left(1 - u_2I_1 - u_3{I_1}^2\right)(u_1 - u_6) + (u_4 + u_5I_1)^2 = 0\,,$$

$$u_1{}^2{I_2}^4 - {I_2}^2(u_4 + u_5I_1)^2 - 2u_1{I_2}^2\left(1 - u_2I_1 - u_3{I_1}^2\right) \qquad (2.25)$$

$$-\left(1 - u_2I_1 - u_3{I_1}^2\right)^2 = 0$$

where $I_1$is the volumetric strain invariant and I_2 is the maximum shear strain defined as:

$$I_1 = \epsilon_x + \epsilon_y\,,$$

$$I_2 = \sqrt{\frac{\left(\epsilon_x - \epsilon_y\right)^2}{2} + {\epsilon_{xy}}^2}\,, \qquad (2.26)$$

and the terms u_i are defined in terms of the strain coefficients G_{ij}:

$$u_1 = G_{11} + G_{22} - 2G_{12}\,,$$

$$u_2 = \frac{G_1 + G_2}{2},$$

$$u_3 = \frac{(G_{11} + G_{22} + 2G_{12})}{4}\,, \qquad (2.27)$$

$$u_4 = G_1 - G_2\,,$$

$$u_5 = G_{11} - G_{22}\,,$$

$$u_6 = G_{66}\,,$$

This formulation represents a conservative approximation of the Tsai-Wu failure criterion in terms of the strain invariants. The first equation in Eq. (2.25) is a second order equation with respect to strain and the second one is a fourth order equation. The safe region is the smallest common region between the two equations. The envelope equation describing the inner envelope is used to evaluate the laminate strength. Whether the second order or the fourth order envelope is critical depends on the material properties used. A

failure index was defined and used in optimization problems to design composite plates for maximum strength [107]. Khani et al. also investigated the conservative failure envelope further for the strength design of variable stiffness panels and presented a convexifying approach to guarantee its convexity in optimization problems [108].

Lamination parameters have been used extensively for distinctive design problems. Foldager et al. presented a general approach using fiber angle orientations as design variables while utilizing the convex nature of lamination parameters to control the sensitivities of the response [109]. Fukunaga et al. designed the thermo-elastic properties of symmetric laminates by minimizing the coefficient of thermal expansion using lamination parameters [110]. Miki et al. and Kogiso et al. applied lamination parameters for reliability-based optimization to design composite plates under probabilistic conditions [111,112]. Kameyama et al. used lamination parameters for damping and minimum weight optimization subjected to aeroelastic constraints [113,114]. Thuwis et al. exploited the benefits of passive aeroelastic tailoring to reduce the induced drag of the rear wing of a Formula One car at higher velocities. Lamination parameters were applied as design variables to optimize the variable material properties of the upper and lower skin of the torsion box of the rear wing main element [115]. Stanford et al. studied weight reduction of transport wings utilizing both structural and control surface tailoring schemes including flutter constraints. Composite laminate tailoring was achieved with lamination parameters as design variables, where a considerable reduction in wing mass was obtained [116,117]. Wu et al. derived an asymptotic closed-form solution, which was used for post-buckling optimization of composite plates using lamination parameters [118]. Dutra et al. utilized a formulation for hybrid laminates in terms of lamination parameters and optimized

composite plates for stiffness using a quadratic metamodel [119]. Liu et al. also used lamination parameters for the smeared stiffness-based approach to optimize a multi-panel subject to performance and blending constraints [120]. In addition, Maquart et al. derived blending constraints in the lamination parameter space to guarantee manufacturability and structural continuity from the optimal lamination parameter distribution [121]. These manufacturing constraints were then used for aeroelastic optimization of a composite wing structure [122]. Abdalla et al. presented a generalized reciprocal approximation using finite element analysis in the design of variable stiffness plates for maximum fundamental frequency while parametrizing the problem in terms of lamination parameters [123]. Ijsselmuiden et al. further developed the generalized reciprocal approximation and optimized variable stiffness panels for maximum buckling load [124] and presented a method for including thermal loads into the optimization framework [125]. Khani et al. utilized this optimization framework to optimize the buckling load of variable stiffness cylindrical shells [126] subjected to strength constraints [127] as well as longitudinally stiffened shells using a semi-analytical finite difference technique [128]. Dillinger et al. also used this optimization framework to investigate the aeroelastic stiffness optimization of forward swept composite wings considering structural and aeroelastic responses [129]. Wu et al. optimized the buckling load of variable stiffness panels by representing the lamination parameter distribution as a Lagrangian polynomial series [104]. The authors later advanced their optimization framework to benefit from the convex properties of B-splines to define the spatial variation of lamination parameters [105]. Raju et al. then utilized the developed 8^{th} dimensional feasible region to maximize the shear buckling performance of symmetric variable stiffness laminates [106].

2.4 MULTI-LEVEL OPTIMIZATION METHODOLOGY

Because of the complexity of nonconventional laminate design optimization, a multi-level optimization approach is demanded to achieve a global optimum design. Structural performance design drivers such as stiffness, strength, buckling, post-buckling, and frequency are considered at the first level (Stiffness Optimization), where the theoretical optimum stiffness is obtained using lamination parameters. After the optimum stiffness requirements are obtained, the next level (Stacking Sequence Retrieval) aims to convert the stiffness properties to optimal fiber orientation angles. This step usually suffers from theoretical performance loss when additional design guidelines and manufacturing constraints are applied at the conversion process. This is because of the discrepancies between the continuous and the discrete optimization steps. For fiber-steered variable stiffness designs, the third level (Fiber Path Construction) constructs the continuous fiber paths from the retrieved fiber angle distribution for manufacturing. The difficulty of this step lies in matching the optimal fiber orientation angles as well as satisfying the manufacturing constraints with the layup strategy used.

Nonconventional laminates are designed to exploit the benefits of fiber placement technologies. However, AFP manufacturing introduces limitations that must be integrated into the design process to ensure manufacturability. The fact that theoretically optimal designs and manufacturing processes are conflicting objectives necessitates the incorporation process to maintain structural integrity. Lozano et al. presented a thorough literature review of the design for manufacturing, where research needs were highlighted [14]. The purpose here is to recall how some critical manufacturing constraints were included by researchers in the design optimization process. Manufacturing constraints

include a jagged boundary, minimum cut length, fiber bridging, machine collision, minimum turning radius (maximum allowable curvature), continuity and smoothness, gaps and overlaps, fiber angle deviation, and deposition rate. Ijsselmuiden and Lozano et al. explained these in detail, where it is not a trivial task to incorporate all the manufacturing constraints in the design process [14,36].

In addition, laminate design guidelines have been introduced over time in traditional composite design, guaranteeing the robustness of the composite laminate. An unquantifiable amount of experience has played a vital role in the development of these design guidelines for composite materials to help the designer exploit the material's strength while alleviating its weaknesses. Highly desirable properties of designed composites include high specific stiffness and strength, corrosion resistance, negligible thermal expansion, enhanced fatigue life and improved fracture toughness [130]. However, some of the weaknesses encompass very low interlaminar tension strength making them vulnerable to out-of-plane loads, non-linear, and rate-dependent response of polymer resins. These weaknesses may induce creep and structural failure after sufficient loading cycles, micro-cracking of the polymer matrix, differences in the coefficient of thermal expansion, and reduction in strength due to impact-induced damage [131]. As a result, design guidelines have been developed to mitigate these weaknesses. These design guidelines include having mid-plane symmetric laminates, balanced laminates, a maximum number of consecutive plies, a minimum ply count percentage, a maximum ply angle jump, a minimum ply angle jump, and ±45 degree surface layers.

To ensure manufacturability and robustness of the laminate, each optimization level should account for manufacturing related criteria and design guidelines. However, it is

difficult to pose the constraints in the lamination parameter space because the laminate configuration is required but not present. If a constraint is possible to implement as a function of lamination parameters while maintaining convexity of the feasible region, it will generally result in a theoretically optimum design by reducing the discrepancies between the continuous lamination parameter solution and the discrete stacking sequence design. As a result, negligible performance loss would be observed at the conversion process if the theoretical design already satisfies these constraints. Each optimization level will be reviewed below along with manufacturing constraints and industry design guidelines that were used by designers to demonstrate their importance in achieving a manufacturable and robust laminate design.

2.4.1 Laminate Stiffness Optimization

Two efficient structural optimization frameworks have been presented for obtaining the optimal lamination parameter distribution. Both optimization frameworks incorporate gradient-based optimization methods and can be divided into:

1. **Finite Element Analysis Framework** [36,132]**:**

Ijsselmuiden et al. developed a convex conservative separable structural approximation framework following the work presented by Svanberg [133]. The structure is discretized using finite elements, and the lamination parameters are associated with nodes rather than elements with a reciprocal interpolation scheme to guarantee continuity and smoothness of the distribution. Svanberg has demonstrated that these approximations are globally convergent, which guarantees that an optimum design will be found. The framework expresses the structural response to be optimized as a Taylor series expansion in terms of stiffness matrices and their corresponding inverses. The approximation of the

response resembles the conservative structural approximation developed by Braibant and Fleury [28]. The optimization problem consists of a convergence control loop with inner global and local loops associated with the dual problem. To account for multiple buckling modes, Ijsselmuiden et al. utilized the bound formulation presented by Olhoff [134] which can be solved using the dual method developed by Fleury [135]. The approximate sub-problem is solved iteratively in the local loop, and the global loop solves for the Lagrange multipliers associated with the constraints. The primal-dual solution guarantees the convexity of the problem if the duality gap converges to zero while satisfying the KKT conditions [28]. The convergence control loop has a damping term that is chosen to maintain convexity and conservativeness and to control the convergence while improving the design with each optimization step. An adaptive damping scheme is implemented to update the damping after each iteration to reach an optimally converged design with the minimum number of finite element analysis required. The developed approximation scheme has been improved progressively by the authors to ensure homogeneity in stiffness space and convexity of lamination parameter space. The conservative convex separable approximation of a structural response, f_j, can be expressed as:

$$f_j = \sum_{i=1}^{N} (\breve{\Psi}_{i,j}^{m} : A_i + \breve{\Psi}_{i,j}^{b} : D_i + \breve{\Phi}_{i,j}^{m} : A_i^{-1} + \breve{\Phi}_{i,j}^{b} : D_i^{-1} + \breve{\alpha}_{i,j} h_i) + C_0 \qquad (2.28)$$

where $\breve{\Psi}_{i,j}^{m}$ and $\breve{\Psi}_{i,j}^{b}$ are the damped sensitivity matrices with elements representing the derivatives of the j^{th} response with respect to the elements of the in-plane and out-of-plane stiffness matrices, A_i and D_i, respectively, for the i^{th} design region including the convexifying terms obtained from damping. Similarly, $\breve{\Phi}_{i,j}^{m}$ and $\breve{\Phi}_{i,j}^{b}$ are the damped sensitivity matrices with elements representing the derivatives of the j^{th} response with

respect to the elements of the inverse of the in-plane and out-of-plane stiffness matrices, A_i^{-1} and D_i^{-1}, respectively, for the i^{th} design region. A variable thickness design can also be obtained by including $\breve{\alpha}_{i,j}$ in the response approximation, which represents the derivatives of the response which depend explicitly on the laminate thickness, h_i. C_0 represents all remaining constant terms. Because of the separability of the structural approximation, the optimization problem can be conducted as N independent local optimization problems as:

$$\min_{x_i} \left(\breve{\Psi}_i^m : A_i + \breve{\Psi}_i^b : D_i + \breve{\Phi}_i^m : A_i^{-1} + \breve{\Phi}_i^b : D_i^{-1} + \breve{\alpha}_i h_i \right) \tag{2.29}$$

where x_i is the vector of design variables containing the lamination parameters and thickness of each design region subject to the constraints imposed on the design variables. In addition, its separable nature facilitates parallel computing to reduce the computational time of the stiffness optimization step. In complex structures, the finite element analysis is typically the most computationally expensive for design sensitivity analysis. As such, the Adjoint method is widely used to obtain the gradient information to reduce computational cost. It is noteworthy to mention that a manufacturing finite element mesh framework can also be efficient and beneficial in decreasing the number of design variables as presented by van Tooren et al. [43] and Barazanchy et al. [44] to reduce the complexity of the problem.

2. Isogeometric Analysis Framework [105]**:**

Wu et al. developed an optimization framework for the buckling optimization of variable stiffness panels to describe the spatial variation of lamination parameters using B-splines. A set of control points and a prescribed knot vector determine a given degree B-spline curve or surface. Lamination parameters are associated with each control point over

the plate domain. The design flexibility can be accustomed by changing the location and number of control points, the degree of the B-spline, and the knot vector of spline functions. This optimization framework has the benefit of harnessing the smoothness and convex hull property of B-splines. It usually requires fewer design variables than the finite element approach and smoothness is guaranteed by the properties of the B-splines. In addition, it captures point-wise stiffness variation that is guaranteed to satisfy the laminate feasibility constraints. This reduces the computational expense of the optimization problem. The distribution of four lamination parameters $V_{1A}, V_{3A}, V_{1D}, V_{3D}$ representing an orthotropic variable stiffness laminate configuration can be represented in terms of the B-spline surface in Eq. (2.30), where $B_{rs}^{(x)}$ and $B_{rs}^{(y)}$ represent the location of the control points P_{rs} along the x and y axes, respectively, as shown in Figure 2.11. The coefficients $\Gamma_{rs}^{(\tau)}$ represent the values of the lamination parameters at each control point P_{rs}, which are used as design variables in the optimization problem.

$$
\begin{aligned}
x(\bar{u},\bar{v}) &= \sum_r \sum_s B_{rs}^{(x)}\, N_r^{(k)}(\bar{u})\, N_s^{(k)}(\bar{v})\,, \\
y(\bar{u},\bar{v}) &= \sum_r \sum_s B_{rs}^{(y)}\, N_r^{(k)}(\bar{u})\, N_s^{(k)}(\bar{v})\,, \\
V_{1,3}^{A,D}(\bar{u},\bar{v}) &= \sum_r \sum_s \Gamma_{rs}^{(\tau)}\, N_r^{(k)}(\bar{u})\, N_s^{(k)}(\bar{v})\,,
\end{aligned}
\tag{2.30}
$$

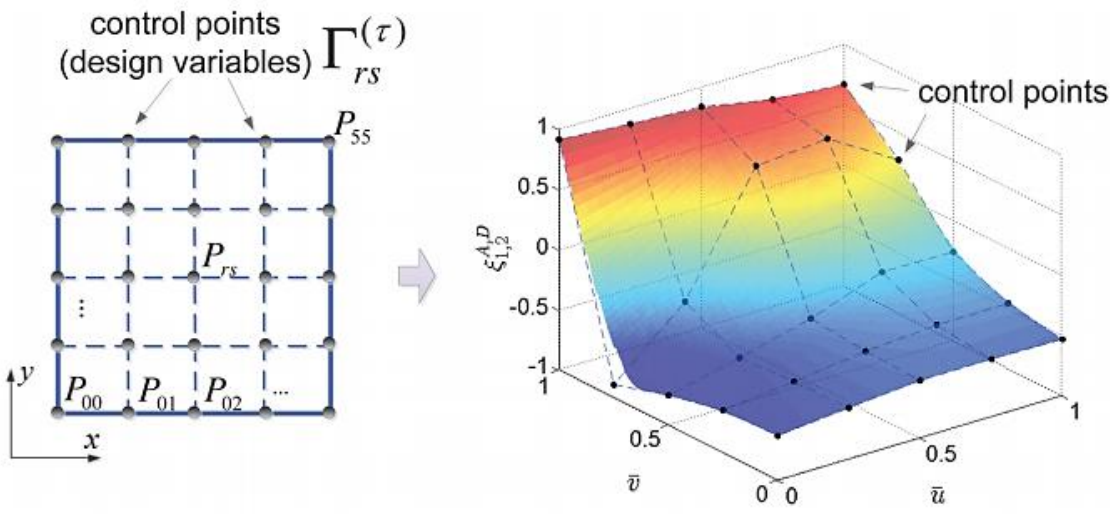

Figure 2.11 B-spline surface lamination parameter distribution five-by-five control points [105]

The authors employed a globally convergent method of moving asymptotes (GCMMA) with a damping factor to control convergence, as explained by Svanberg [133]. The objective function is approximated based on the gradient information computed and expressed in convex separable forms as:

$$f_i^{(\mu,\nu)}(\Gamma) = \sum_{j=1}^{n}\left(\frac{p_{ij}^{(\mu,\nu)}}{\alpha_j^{(\mu)} - \Gamma_j} + \frac{q_{ij}^{(\mu,\nu)}}{\Gamma_j - \beta_j^{(\mu)}}\right) + r_i^{(\mu,\nu)} \tag{2.31}$$

where μ and ν signify the outer and inner iterations, respectively. The terms $\alpha_j^{(\mu)}$ and $\beta_j^{(\mu)}$ are the upper and lower moving asymptotes, respectively. The values of $p_{ij}^{(\mu,\nu)}$ and $q_{ij}^{(\mu,\nu)}$ are associated with the positive and negative sensitivities for each design variable, as well as the upper and lower moving asymptotes, respectively. $r_i^{(\mu,\nu)}$ denotes the difference between the objective function and the approximation formula for the original design at the start of each outer iteration. Damping is introduced into the terms of the approximation to ensure convexity and conservativeness and the approximation can be solved using the dual method. In GCMMA routine, local optimization problems are solved iteratively by

updating the damping factor until complete conservativeness is achieved, and each outer iteration computes the buckling load and sensitivities, and it regenerates a new local optimization problem until convergence is achieved. The useful properties of B-Splines have attracted designers to use it as a modeling technique for variable stiffness laminates. Montemurro et al. have also utilized the B-Spline surfaces to express the spatial variation of the laminate polar parameters over the structure in their developed M2SL optimization strategy [79,82]. Similarly, the polar parameters are defined at each control point over the domain. The possibility of imposing the constraints only on the control points of the domain is a great advantage for reducing the complexity of the optimization problem. However, the use of B-splines is not adaptable for complex geometries, and the use of the NURBS-based approach in an isogeometric analysis framework may significantly raise the difficulty of evaluating the sensitivities of the responses and the computational cost of the optimization process.

Ensuring Manufacturability:

If the isogeometric framework is used for obtaining the optimum lamination parameters, the **continuity and smoothness** of the distribution is automatically guaranteed. Wu et al. maintain continuity of the lamination parameter distribution by using B-splines to model the spatial variation [105]. However, using the finite element framework, the fiber angle distribution and consequently the lamination parameter distribution must be continuously smooth to ensure a manufacturable fiber path. This constraint also affects the **minimum turning radius** constraint applied at the stacking sequence retrieval step, because it modifies the discrete nature obtained from the finite element discretization to maintain smoothness and continuity across the elements. Setoodeh et al. presented a

heuristic pattern-matching technique to maintain continuity of the fiber angle distribution [38], but this is computationally expensive for complex structural design problems. After that, Abdalla et al. proposed a reciprocal interpolation scheme to associate design variables with nodes rather than elements, where the continuity of the lamination parameter distribution was successfully achieved [123].

As for the **minimum turning radius** constraint, it has not been formulated yet in the lamination parameter space. However, Montemurro et al. have recently further developed the multi-scale two-level optimization strategy to integrate the minimum turning radius constraint in the polar parameter space [79]. The authors exploited the beneficial properties of the polar angles that are linked to the main orthotropy directions as well as the properties of the B-Spline derivatives. By utilizing the analogy with the problem of streamlines, the minimum steering radius constraint has been transformed to a very general constraint on the laminate polar angles without restrictions on the laminate stacking sequence. This major improvement in variable stiffness optimization ensures the stiffness properties obtained at the first optimization step satisfy the manufacturing requirements, which eases the problem of constructing an optimal fiber path.

However, it should be noted that the definition of the minimum steering radius must be confined to that of a course being placed during AFP manufacturing to minimize defects that may be obtained, and the exact critical steering radius value should not be applied during the optimization of the stiffness properties so that the designer does not overconstrain a highly non-linear stiffness variation that can be obtained in the first optimization step.

Ensuring Robustness:

Laminate design rules are usually applied at the second step during the fiber orientation angles retrieval because the laminate configuration is available. However, imposing the constraint at the lamination parameter optimization step ensures that the optimum stiffness distribution obtained also satisfies the laminate design rules. Because the convexity of the problem is still maintained, negligible performance loss is obtained when retrieving the stacking sequences matching the optimum stiffness properties.

Laminate design rules that can be easily incorporated in the stiffness optimization step include having **null extension-bending coupling** and **null extension-shear coupling**. By setting V_{iB} = 0, the designer obtains a null **[B]** matrix to uncouple the membrane and bending responses. Uncoupling the responses simplifies analysis, testing, and the manufacturing process because it prevents warping effects under thermal loading. In addition, laminates who have an uncoupled behavior remove excessive deflections that decrease the buckling strength. It is well known that mid-plane symmetric laminates uncouple the membrane and bending responses. However, it is noteworthy to mention that having mid-plane symmetric laminates is a sufficient but not necessary condition to uncouple the membrane and bending behaviors. It has been demonstrated by Verchery that this guideline can be limiting to the design of composite laminate, because uncoupling can be achieved with a different class of laminates without having mid-plane symmetry [34]. In addition, by setting V_{2A} = $V_{4A} = 0$, a null extension-shear coupling is obtained where $\boldsymbol{A_{16}} = \boldsymbol{A_{26}} = 0$. Extension shear uncoupling can be obtained by having balanced laminates, where a positive angle is present for every opposite negative one in the stacking sequence. Yet, having a balanced laminate to achieve a null extension-shear coupling is also a

sufficient but not necessary condition [68]. However, extension-shear coupling can be beneficial in certain applications such as aeroelastic tailoring. The laminate bending-twisting coupling may also be simplified if the problem in hand does not require a coupled response by assuming negligible $\boldsymbol{D_{16}}$, $\boldsymbol{D_{26}} \approx 0$. The bending-twisting coupling is never zero in mid-plane symmetric laminates, but by having angle plies dispersed together in the laminate in ± pairs, the bending-twisting terms are relatively insignificant compared to other terms in the **[D]** matrix for relatively thick laminates. This can be achieved by setting $V_{2D} = V_{4D} = 0$ in the stiffness optimization problem.

Designers have also tackled the problem of deriving constraints representing other important design guidelines in the lamination parameter or stiffness space. The **minimum ply count percentage**, also known as the 10% rule, has been developed based on experience to produce robust laminates that are less susceptible to the weaknesses associated with highly orthotropic laminates. The rule states that 10% of the laminate layer orientations should be in the direction of each of 0, ±45, and 90-degree angles. This introduces some degree of in-plane isotropy to ensure robustness against secondary loadings which are considered difficult to be modeled during the design process. In addition, it helps in avoiding micro-cracking, excessive coefficients of thermal expansion, and reducing free-edge stresses. Abdalla et al. derived a feasible region for the 10% rule as a constraint in the lamination parameter space using the concept of sub-laminates [136].

Laminate Blending:

In addition to manufacturing constraints of constant thickness variable stiffness laminates, additional continuity constraints must be used for variable thickness variable stiffness designs. In certain practical design applications of real structures, a uniform

distribution of load is rarely the case. The designer must present a structure that is not overdesigned, where specific locations that are subjected to low loads in the panel can have ply drops. To tailor the design of specific regions with ply drops, an optimization approach must be used while accounting for variable thickness and continuity constraints. Ensuring continuity between the separate locations in the composite panel is referred to as blending of composite laminates. Some examples of blending patterns are shown in Figure 2.12. Dropping plies from the surface of the laminate is termed outer blending, whereas dropping them from the mid-plane of the laminate is inner blending [137]. More complicated and general blending patterns can be used as well to enlarge the design space [138]. Blending is posed as a pure discrete optimization problem and can be efficiently tackled using evolutionary algorithms. However, blending constraints can be included in the stiffness optimization step following the work conducted by Macquart et al. [121]. The authors derived a set of blending constraints in the lamination parameter space to reduce the discrepancies between the continuous lamination parameter distribution and the discrete stacking sequence designs obtained. The authors validated the importance of the constraints based on the benchmark 18-panel horseshoe problem [121], and then they applied the blending constraints in aeroelastic optimization of a wing model [122]. The numerical results demonstrate that applying the blending constraints significantly increases the chance of retrieving optimal stacking sequences that closely match the lamination parameter distribution while reducing the number of iterations required to obtain the final blended designs.

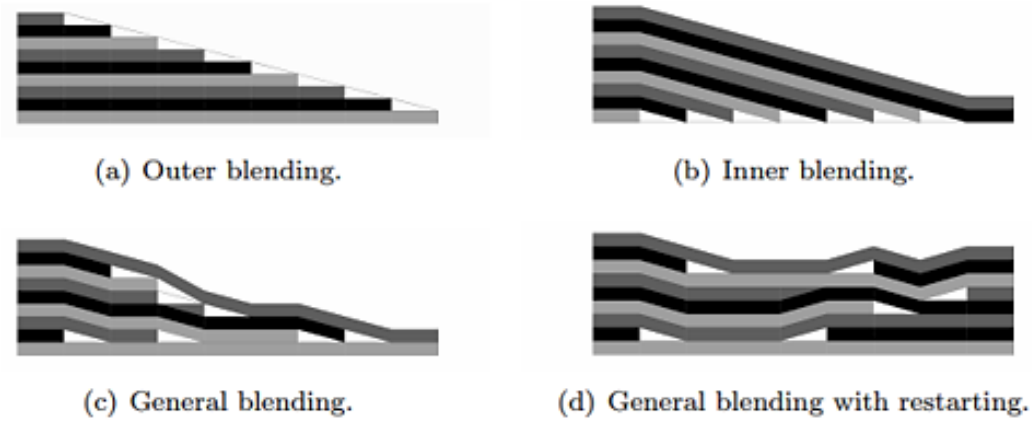

Figure 2.12 Examples of laminate blending patterns [137]

2.4.2 Stacking Sequence Retrieval

After obtaining the conceptual optimum stiffness, the next step is to convert the lamination parameter distribution into a practical laminate design in terms of fiber orientation angles. However, this inverse problem is no longer convex because it is posed in terms of fiber angles. As a result, designers have usually used evolutionary algorithms to avoid the non-convexity in retrieving the optimal fiber angles. This problem has been progressively developed by designers to minimize the performance loss in the conversion process. Earlier work aimed to present closed-form solutions for the inverse problem. Fukunaga et al. presented a method for determining constant stiffness layup configurations for the case of pure in-plane or flexural problems having four different fiber orientation angles [91] and then generalized it for any laminate [92]. However, these solutions do not account for equal thickness discrete layers, where a closed-form solution is not valid.

Evolutionary algorithms are the most widely used in the conversion step because of their discrete nature. Autio utilized a genetic algorithm to retrieve the optimal fiber orientation angles from the lamination parameters of constant stiffness laminates [139]. To reduce the computational expense accompanied with a genetic algorithm, global response

surface approximations have been also used in the first step to approximate the buckling loads for a constant stiffness laminate [140]. Todoroki et al. used a response surface to approximate the buckling load in terms of lamination parameters, and they retrieved the layup configuration using a genetic algorithm [141]. Todoroki et al. also presented a branch and bound method using the fractal nature of lamination parameters to design laminates restricted to 0°, ±45°, and 90°. The fractal branch and bound method is used in combination with a response surface approximation in terms of lamination parameters. The algorithm can easily apply design guidelines by pruning out violating branches. It was used efficiently for the design of composite laminates and stiffened structures [142–144]. Bloomfield et al. utilized a particle swarm optimization to retrieve the laminate configuration from the optimal set of lamination parameters [18]. Setoodeh et al. presented a curve fitting technique using Lobatto polynomials to retrieve fiber angle orientations of variable stiffness laminates in the least square sense [61]. van Campen et al. presented a point-wise retrieval method that can be efficiently used for a variable stiffness laminate having point-wise two different fiber angle orientations with equal thickness layers [95]. van Campen et al. later developed an efficient algorithm to convert the spatial lamination parameter distribution by using a genetic algorithm to supply initial points for a gradient-based optimizer in a CA paradigm. The authors studied the efficiency of implementing a least-square fitness function versus a sensitivity-based fitness function. It was realized that the sensitivity based achieves a minimum loss in performance because the approximation can be built based on the sensitivities computed at the stiffness optimization step [145]. However, the local nature of the response approximation indicates loss of accuracy away from the approximation point. This can either be remedied by updating the sensitivities

during the retrieval process [146] or by presenting a multipoint structural approximation as was developed by Irisarri et al. by using an improved Shephard method [147]. The conservative convex separable approximation that is updated at each iteration in the first optimization step is used to construct the multiple point approximation. These points are combined using a distance measure in the stiffness space to obtain a global approximation. This method has shown to be efficient in constant stiffness and patch designs and has still not been extended to variable stiffness laminates. Wu et al. also used a genetic algorithm to obtain the optimal fiber orientation angles at the control points in the B-spline lamination parameter distribution. The fiber angle distribution is then described using Lagrangian polynomials to interpolate the fiber angles at the control points to obtain a continuous and smooth distribution [105].

Ensuring Manufacturability:

A major manufacturing constraint for fiber-steered variable stiffness laminates is the **minimum turning radius.** Because the inner radius of a steered tow is smaller than the outer one, the inner edge is subjected to compressive forces while the outer edge is in tension. When the compressive forces exceed a certain limit, fiber buckling will take place. The laminate properties are directly affected by the subsequent out-of-plane undulations that are undesirable. Therefore, a minimum turning radius constraint can be defined to avoid fiber buckling. The use of curvilinear fiber paths to model variable stiffness laminates make the constraint trivial, yet by using direct stiffness or fiber angle distribution modeling, this is no longer the case.

Setoodeh et al. presented curve fitting techniques to retrieve the optimal fiber angle distribution from lamination parameters by using Lobatto polynomials and controlling

curvature constraints [61]. However, designers have found an easier way to interpret this constraint as a measure of the rate of change or norm of the gradient of fiber angle orientations between adjacent locations. Peeters et al. compared the use of global and local steering constraints to account for manufacturability of variable stiffness laminates. The problem was posed in terms of a continuous quadratic approximation in fiber angle space, where the local approach was found to provide more accurate control of the steering at the expense of increasing the number of constraints [148]. van Campen et al. presented a point-wise curvature constraint for a variable stiffness laminate with point-wise two different fiber orientation angles [145]. van Campen et al. later used the local fiber steering constraint with a CA paradigm to retrieve the stacking sequences of a variable stiffness laminate from the optimal lamination parameter distribution. A genetic algorithm was used to treat the steering constraint by using a penalty approach and provide starting points for a gradient-based optimizer, where minimum loss of performance was achieved in the retrieval process [145,149].

Brooks et al. [150] also presented a methodology to account for the minimum steering radius and for gaps and overlaps obtained from the fiber angle distribution. A mathematical formulation is developed by considering a tow-steered layer as a 2D unit vector field. A relationship is provided between the tow path curvature and vector field curl as well as gap/overlap propagation rate and the divergence of the vector field.

However, it should also be noted that the definition of the minimum steering radius must be defined locally along the fiber path of a course being placed during AFP manufacturing. By applying the steering constraint as a measure of rate of change of an angle, the designer might be overconstraining a highly non-linear fiber angle variation that

can be achieved in the third optimization step by fully utilizing the additional tow-dropping capability of the AFP machine. The exact critical steering radius value should not be applied during the optimization of each steered ply, but a small measure of a steering constraint (non-conservative) must be applied to reduce the number of tow-dropping that might take place in the third optimization step. Generally, there should be an acceptable trade-off between the amount of fiber steering that help achieve the desirable variable stiffness properties and the number of tow-drops to help maintain the reliability of the AFP manufacturing process and reduce fiber angle discontinuities.

Ensuring Robustness:

The laminate configuration is obtained at the stacking sequence retrieval step. As a result, it is possible to implement all the laminate design rules in this conversion step. These design guidelines are applied to accomplish the robust design of a composite laminate. When applied at the stacking sequence retrieval step using evolutionary algorithms, either a penalty approach or a repair strategy is usually used to ensure design feasibility [49–51]. In the case of variable stiffness laminates, they must be applied locally at each point in the structure to maintain structural integrity, or a laminate configuration satisfying these design rules can be used. A combination of having optimal nonconventional laminates with these design guidelines would result in a structurally feasible laminate design. This demonstrates the importance of these design guidelines in laminate design optimization [16,151].

The laminate should satisfy the conditions of having **null extension-bending coupling** and **extension-shear coupling**, and it should satisfy the **minimum ply count percentage** constraint as obtained from the stiffness optissmization step. As mentioned earlier, having a balanced and symmetric laminate constitutes a sufficient but not necessary

condition to satisfy null coupling of the responses. Hence, the designer should not impose these restrictions a priori on the stacking sequence to utilize the whole design space. In addition, the maximum number of consecutive plies at each point should be limited to 2-4 layers. This is known as the **ply contiguity rule**, which instructs the designer to avoid stacking too many plies to decrease the chance of having delamination, micro-cracking, and residual stresses. Autio utilized a genetic algorithm with a penalty approach to account for a maximum number of consecutive plies while retrieving fiber orientation angles from the lamination parameters of constant stiffness laminates [139].

Another design rule that should be implemented at the stacking sequence retrieval step is the angle jump between successive layers. A **maximum ply angle jump** is imposed by the designer to decrease the inter-laminar stresses that arise because of the mismatch in the stiffness, Poisson's ratio, and the coefficient of thermal expansion between plies with different fiber orientations. Constraining the fiber angle jump between adjacent plies reduces free-edge stresses that may cause delamination. In addition, a **minimum ply angle jump** can also be used to obtain dispersed laminates. Dispersion in laminates helps to withstand impacts and may improve post-impact behavior. By maintaining a minimal difference in fiber angles between consecutive plies, a better resistance is achieved which reduces the inter-laminar shear stress. Peeters et al. imposed the constraint by superimposing the sine function on the difference of the Poisson's ratio as a function of the angle difference to capture the periodicity. Fiber angles were used as design variables, and the constraint was formulated as a sinusoidal function of consecutive fiber angle difference between plies [16].

One additional design guideline is constraining the laminate with **±45 degree surface layers**. This improves the damage tolerance and the buckling load of thin laminates. The surface layers also protect the primary load carrying plies, so they are not easily damaged by minor impacts. For variable stiffness laminates, the surface layers can act as sandwiching layers to protect the fiber-steered layers. Having the ±45° angles in contact also minimizes inter-laminar shear. Another constraint that can also be used is having only one 45 degree surface layer to still respect the maximum ply angle jump constraint while still providing a better damage tolerance.

Laminate Blending:

As mentioned earlier, blending is formulated as a purely discrete optimization problem and can be efficiently tackled using evolutionary algorithms. However, single step stacking sequence optimization using evolutionary algorithms with blending constraints are prone to the curse of dimensionality [121]. On the contrary, using a multi-level optimization approach can result in an optimal blended design trying to match the continuous convex design solution that is obtained at the stiffness optimization step. Several designers have improved the blending problem definition to efficiently tackle the optimization of variable thickness laminates. Zabinsky et al. proposed a "greater-than-or-equal-to" blending rule, where a key region subjected to maximum loads is identified and fewer plies are obtained away from this region [32]. Liu and Haftka used material composition and stacking sequence continuity to implement blending [152]. Soremekun et al. utilized the concept of design variable zones and sub-laminates to gain full control over the blending procedure. The design variable zones contain information related to design constraints, and the sub-laminates define the laminate configuration [153]. A guiding stack

was later presented by Adams et al. where a set of outermost or innermost layers are deleted from the guide laminate [154]. Ijsselmuiden used the guiding stack approach and developed a multi-step optimization framework for blending design of composite panels subjected to buckling constraints [146]. van Campen et al. generalized the guiding stack approach and implemented two new definitions with a multi-chromosomal GA [138]. Seresta et al. illustrated an efficient way to implement blending of laminated composite structures in a GA framework [155]. Liu et al. implemented a smeared stiffness based-approach to achieve blending of a composite wing structure [120]. Irisarri et al. designed a blended laminate with design guidelines using stacking sequence tables and evolutionary algorithms [156]. Meddaikar et al. also presented a novel optimization strategy for blending using a multipoint structural approximation with a genetic algorithm and stacking sequence tables [157]. Peeters et al. formulated the ply drop boundary using topology optimization techniques and used a genetic algorithm to optimize the ply order. Significant improvements of blended variable thickness fiber-steered structures were obtained [158].

2.4.3 Fiber Path Construction

The last step of the multi-level optimization for variable stiffness steered-fiber laminates is to construct the fiber path that can be supplied to the fiber placement machine for manufacturing. The fiber path must match the optimal fiber orientation angle distribution in each ply as well as satisfy AFP manufacturing constraints. To construct a fiber-steered layup, multiple tows are required to be placed adjacently. Two well-known layup strategies for a fiber-steered layup are the parallel and shifted layup strategies, where the steered fiber tows are derived from one reference curve. However, using a parallel or shifted fiber layup strategy does not necessarily match the optimal fiber angle distribution

obtained from the second optimization step. Several researchers tackled the problem of generating manufacturable fiber-steered paths that match the optimal fiber orientation distribution.

Blom et al. presented a streamline methodology to generate continuous fiber paths from the optimal fiber angle distributions [159]. By using a fluid flow analogy, streamlines can be used to represent the centerline of a course. If streamlines are not parallel, successfully placed tows having a finite width will certainly result in gaps and overlaps. The distance between centerlines directly affects the amount of overlap. If this distance is decreased, more overlaps will be present. A smeared thickness approximation was used to account for thickness build-up resulting from matching the optimal fiber orientation angle distribution. The smeared thickness distribution is obtained from solving a partial differential equation with user-defined boundary conditions. After the smeared thickness is obtained, it can be used to obtain the stream functions, and the finite courses are extrapolated to generate the continuous fiber paths. A short summary of the streamline formulation is presented here. Mathematically, a streamline is represented by a stream function:

$$\Psi(x, y) = C\ , \tag{2.32}$$

which connects all the points with a constant value C. For a giver fiber angle distribution $\theta(x, y)$, the streamlines can be found by solving the following partial differential equation:

$$\frac{d\Psi}{ds} = \frac{d\Psi}{dx}\frac{dx}{ds} + \frac{d\Psi}{dy}\frac{dy}{ds} = \Psi_{,x}\cos\theta + \Psi_{,y}\sin\theta = 0\ , \tag{2.33}$$

A unique solution for the stream function and thus the location of the streamlines depends on the boundary conditions because it is a partial differential equation. By understanding

the physics behind the thickness buildup mechanism, Blom et al. found a direct relation between the thickness at a certain point and the partial derivative of the stream function with respect to the normal of the streamline n as:

$$t \propto \frac{1}{|\boldsymbol{dn}|} = \frac{1}{d\Psi/\Psi_{,n}} = \frac{\Psi_{,n}}{d\Psi} \propto \Psi_{,n}\,, \tag{2.34}$$

Although these overlaps are discrete, a first approximation to the amount of overlap could be made by smearing out this discrete overlap to form a continuous thickness distribution. If $d\Psi$ is assumed to be a unity, then $t = \Psi_{,n}$, which can be used to derive a direct correlation between the thickness distribution and the fiber angle variation:

$$-\vec{s}.\vec{\nabla}(\ln t) = \vec{n}.\vec{\nabla}\theta\,, \tag{2.35}$$

where the following definitions are used:

$$\vec{n} = \begin{pmatrix} -\sin\theta \\ \cos\theta \end{pmatrix}, \qquad \vec{s} = \begin{pmatrix} \cos\theta \\ \sin\theta \end{pmatrix},$$
$$\vec{\nabla}\theta = \begin{pmatrix} \theta_{,x} \\ \theta_{,y} \end{pmatrix}, \qquad \vec{\nabla}(\ln t) = \begin{pmatrix} t_{,x}/t \\ t_{,y}/t \end{pmatrix}, \tag{2.36}$$

Equation (2.35) states that the change in thickness along a streamline depends on the change of the fiber orientation perpendicular to that streamline. Since both vectors $\vec{s}$ and $\vec{n}$ depend on the given fiber angle distribution $\theta(x,y)$, the only unknown is the thickness. There exists an infinite number of possible boundary conditions for which the thickness distribution associated with the streamlines can be found, but the most difficult part is to find the ones that are physically sensible for the problem in hand. To obtain a general solution, a change of variables is used: $\tau = \ln t$, where Eq. (2.35) becomes:

$$-\vec{s}.\vec{\nabla}\tau = \vec{n}.\vec{\nabla}\theta \ . \tag{2.37}$$

Equation (2.37) is solved numerically by discretizing the derivatives, so that it is written as:

$$[M]\,\vec{\tau} = \vec{B}\ , \tag{2.38}$$

where $[M]$ is the matrix that represents the left-hand side of Eq. (2.37), $\vec{\tau}$ is a vector that represents τ at every grid point and $\vec{B}$ is the vector that represents the right-hand side of Eq. (2.37) in addition to the boundary conditions. If the thickness at the inflow boundaries is assumed to be equal to one everywhere ($\tau = \ln t = \ln 1 = 0$), a nominal solution can be found for $\vec{\tau}$, which will be referred to as $\vec{\tau}_0$. A general solution of Eq. (2.38) can be expresses as:

$$\vec{\tau} = \vec{\tau}_0 + [T]\vec{\tau}_{in}\ , \tag{2.39}$$

where each column j in matrix $[T]$ represents the influence of boundary grid point j on the thickness distribution in the complete domain, while satisfying Eq. (2.38). Because these columns are independent of each other and Eq. (2.38) is a linear equation, so any linear combination of these columns also represents a solution. The entries in $\vec{\tau}_{in}$ all render the thickness at a single point on the inflow boundary. By substituting Eq. (2.39) in Eq. (2.38), the thickness can be optimized for different criteria, such as minimizing maximum thickness or maximizing smoothness of the fiber path, by using $\vec{\tau}_{in}$ as design variables. Once the smeared thickness distribution is obtained through one of the optimization problems, the corresponding stream function can be obtained by integrating $\Psi_{,n}$ over dn:

$$\Psi(x,y) = \int \Psi_{,n} dn = \int \frac{d\Psi}{dx}\frac{dx}{dn} dn + \int \frac{d\Psi}{dy}\frac{dy}{dn} dn = \int \Psi_{,x} dx + \int \Psi_{,y} dy \ , \quad (2.40)$$

The derivatives of $\Psi(x,y)$ with respect to *x* and *y* can be expressed as functions of $\Psi_{,s}$ and $\Psi_{,n}$ as follows:

$$\begin{aligned} \Psi_{,x} &= \Psi_{,s}\, cos\, \theta - \Psi_{,n}\, sin\, \theta \ , \\ \Psi_{,y} &= \Psi_{,s}\, sin\, \theta + \Psi_{,n}\, cos\, \theta \ , \end{aligned} \quad (2.41)$$

Because $\Psi_{,s} = 0$ and $\Psi_{,n} = t$, replacing Eq. (2.41) in (2.40) gives:

$$\Psi(x,y) = -\int_0^x t(x^*, y^*)\, sin\, \theta(x^*, y^*)\, dx^* + \int_0^y t(x^*, y^*)\, cos\, \theta(x^*, y^*)\, dy^* \ . \quad (2.42)$$

Both $t(x,y)$ and $\theta(x,y)$ are known functions, so that $\Psi(x,y)$ can be solved. By plotting the contour lines of Ψ at fixed increments the streamlines are found and represent the centerlines of the actual fiber courses. Once the course centerlines are known, discrete courses can be constructed by calculating the course edges. If a point on the path centerline is defined by $\{x_c, y_c\}$ the course edges are found by:

$$\begin{aligned} x_e &= x_c \mp p \sin\theta_c \ , \\ y_e &= y_c \pm p \cos\theta_c \ , \end{aligned} \quad (2.43)$$

where p is half the total course width and θ_c is the fiber orientation angle at $\{x_c, y_c\}$, as shown in Figure 2.13. At the domain boundary, one edge will still be inside the domain, hence the centerline should be extrapolated until both edges are outside the boundary domain.

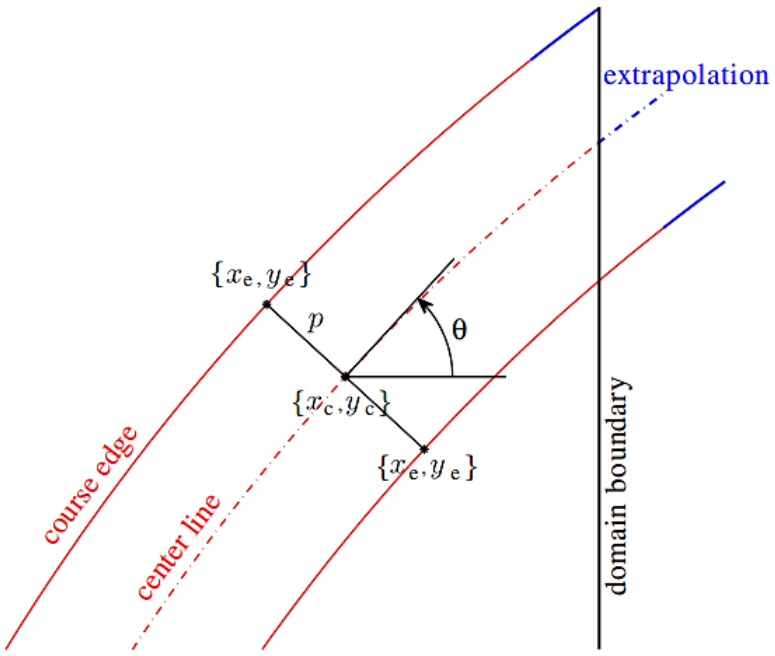

Figure 2.13 Finite width course with path extrapolation [159]

In a follow up study, extra streamlines were requested halfway between the center lines to serve as cut lines that define the boundary of each tow when it hits the lines [137]. In Figure 2.14, the streamlines in red are the center lines, and cut lines are obtained by shifting the streamline perpendicularly using Eq. (2.43) with different values of p as multiples of tow width to obtain the cut lines in black. A full gap strategy was used, so that the tow is cut when the outer edge touches the cut line. If a full overlap strategy were to be used, the tow would be cut when its inner edge touches the cut line. Figure 2.15 shows a tow-by-tow description, without any overlap appearing. However, gaps clearly appear at the edges, so extrapolation needs to be performed for complete coverage of the layer. In addition, some tows are too short to be laid down because they violate the minimum cut length constraint of the AFP machine, hence they should be extended or removed completely.

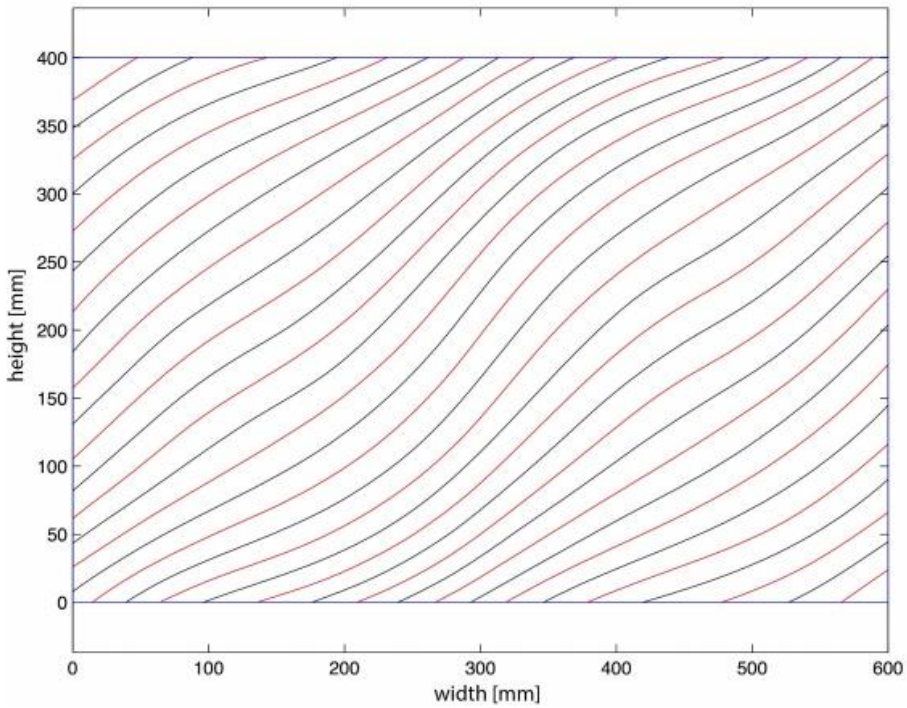

Figure 2.14 Streamlines in red and cut lines in black of a single layer [137]

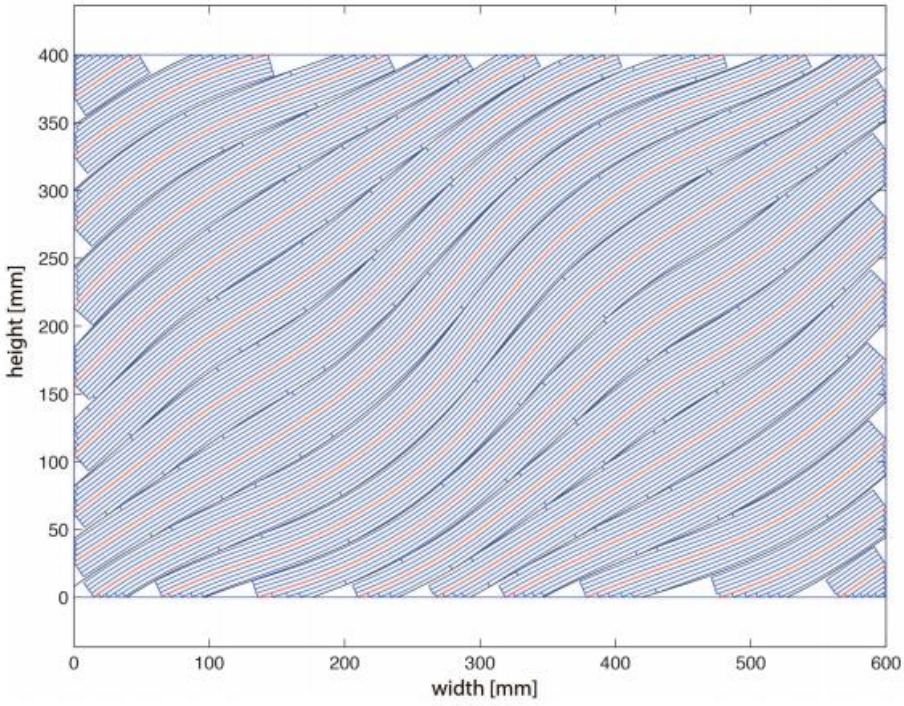

Figure 2.15 Example of fiber path construction for a variable stiffness layer [137]

van Tooren [43] et al. also presented a method for generating continuous fiber paths based on a manufacturing mesh finite element framework. The fiber angle distribution at the centroid of each element is obtained using Lagrange polynomials. To construct the fiber path, a polygon is positioned within the boundaries of the manufacturing mesh for the ply under consideration, where its edges are used for seeding the fiber path. The polygon defines the area that will be covered with tows. The seeds on each edge of the polygon are generated based on the fiber orientation angles resulting from the optimization process, and then they are used to define the tow path.

Wu et al. [105] defined the non-linear fiber orientation angle distribution by using Lagrange polynomials to interpolate the optimal fiber angle at the control points in the B-spline variation. Once a smooth fiber orientation angle distribution is obtained, the fiber paths are constructed using parabolic path functions varying either in one direction of the axes or both.

Lozano et al. [160] also developed a design algorithm integrated within CATIA V5® to model manufacturable fiber paths of structurally optimized composite laminates. The tool enables the automatic generation of continuous fiber paths for manufacturing, where each fiber path is modelled individually to match the optimal fiber angles while considering the maximum steering constraint, curve smoothness, gaps and overlaps, and course width.

Ensuring Manufacturability:

For the case of non-parallel fiber steering, the designer must realize that **gaps and overlaps** are a feature that will always occur unless tow dropping is used. Because tow-placed courses may overlap, this results in building ply thickness on the surface.

Manufacturing time, laminate structural response, and surface quality of a composite laminate is affected by this thickness buildup. To produce manufacturable laminates using fiber-steered paths, this thickness buildup should be minimized while still obtaining smooth fiber paths. Parallel fiber steering strategy may avoid having gaps and overlaps, but at specific locations it may activate the minimum turning radius constraint because the tows have a change in curvature [149]. In addition, parallel and shifted fiber steering methods do not precisely match the optimized fiber angle orientations, which in turn does not result in an optimal structure. Gaps are usually not desired, while small overlaps have resulted in performance improvements in certain applications where they act as structural reinforcements [14]. However, excessive overlaps may result in a non-manufacturable laminate and stress concentrations at tow drop locations might be significant [161].

The streamline analogy presented by Blom et al. helps in accounting for gaps and overlaps in the optimization process [159]. The formulation relates the thickness build-up within a ply with the optimal fiber orientation angle distribution obtained from the second optimization step. Moreover, it is usually not desired to leave gaps in a ply, and the designer has the capability of enforcing this as a constraint in the optimization problem. As a result, full control over the amount of gaps and overlaps is achieved while matching the optimal fiber angle distribution as close as possible, which helps in guaranteeing manufacturability of the designed laminate. To find optimal fiber courses, different optimization problems were formulated in terms of minimizing the maximum thickness build-up, maximizing fiber path smoothness, and a combined objective function.

Blom et al. [162] then developed a software tool capable of translating steered fiber laminates obtained from the streamline solution to AFP manufacturable steered laminates.

The software considers manufacturing constraints such as the minimum steering radius, minimum cut length, and fiber straightening due to steering. By optimizing the sequence of cutting and adding tows, overlaps that are obtained due to steering can be eliminated and a "near-constant" thickness steered ply can be obtained. Optimizing the direction of laying down a course also helps in avoiding fiber straightening due to steering. The software then generates the corresponding machine code for controlling a fiber placement machine to cut tows and lay down courses following the selections obtained from the optimization process to satisfy a no gap condition while minimizing overlaps and fiber straightening.

The automated tow placement algorithm documented by van Tooren et al. [43] may leave gaps or excessive overlaps within the domain, and a manual overlap-gap control post-processing step is required by the user to translate the design into a final manufacturable fiber path. The first step eliminates the excessive overlaps, and the second step fills up the gaps. Using successive iterations and restarting the tow placement algorithm, each ply is filled with fiber tows to match the optimal fiber orientation angles as close as possible. An example of feasible tow paths obtained using the tow placement algorithm is shown in Figure 2.16.

The design algorithm developed by Lozano et al. [160] utilizes the curve smoothing capability in CATIA V5® to comply with the minimum steering radius constraint. Maximum allowable gaps and overlaps are defined as input constraints between successive courses in the design process while the objective is to minimize the angle deviation between the fiber angle distribution and the obtained smooth fiber trajectories.

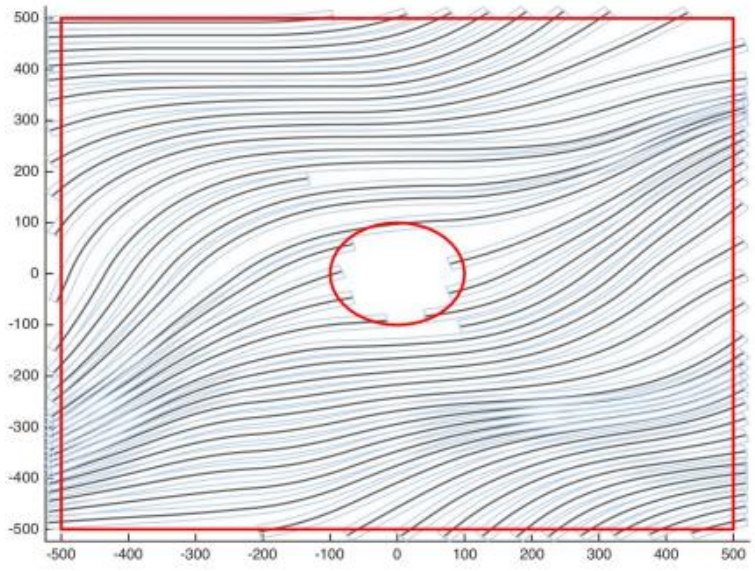

Figure 2.16 Tow paths obtained from tow placement algorithm [44]

However, it is noteworthy to mention that the design algorithms described above do not allow for course centerline intersections. This reduces the amount of tow-dropping that might take place, but it is more difficult to achieve highly non-linear fiber angle distributions. For structures with discontinuities, highly non-linear fiber angle distributions may be essential to achieve the desired load redistribution that would optimize the structure. If the fiber angle distribution is highly non-linear, then centerline intersections are necessary to achieve the desired fiber angles obtained from the second optimization step. The tow-dropping capability of the AFP machine can be utilized to obtain highly non-linear fiber angle distributions, which requires a design algorithm to allow for course centerline intersections between the different guide curves. This would generally result in additional discontinuities at tow-drop locations; hence, the designer must allow for a trade-off between the degree of allowable fiber steering and the amount of tow-dropping that is utilized in the third optimization step.

2.5 SUMMARY

The design optimization of nonconventional laminated composite is by no means a trivial task. The complexity of the optimization problem imposes the need for a multi-level optimization approach to achieve a global optimum design. In the first step, a theoretical optimum stiffness is achieved that accounts for optimum structural performance while maintaining smoothness and robustness. The fiber angle distribution is then obtained in the second step while accounting for the maximum curvature constraint as well as laminate design guidelines to attain manufacturability and feasibility. In the case of variable thickness variable stiffness laminates, blending constraints must be included in the design optimization process to guarantee structural continuity. In the case of curvilinear variable stiffness laminates, the fiber path should be constructed at the final stage to provide optimal fiber-steered paths for fiber placement machines while controlling gaps and overlaps.

Lamination parameters have been efficiently used for the design optimization of composite laminates to reduce the complexity of the design problem. Parametrizing the optimization problem in terms of lamination parameters retains the convex nature of the problem aiming to attain a global optimum design. Practical design problems require the use of both in-plane and flexural lamination parameters, where an efficient feasible region should be used. Although a challenging task to accomplish, formulating manufacturing constraints and laminate design guidelines in the lamination parameter space would result in a potentially improved structure because this reduces the discrepancies between the continuous design solution and the discrete stacking sequence design.

Given the achievable capacity of the composite manufacturing industry, it is significant to utilize nonconventional laminate designs because of the potential

performance gains that have been revealed by several researchers. It is also vital to include industry laminate design guidelines and manufacturing constraints in the optimization of nonconventional laminates to improve the robustness and guarantee manufacturability of the designed laminate. Each laminate design guideline and manufacturing constraint must be investigated to check its effect on the optimal response of the laminate. In addition, the realistic response of nonconventional laminates is not fully understood as good as conventional laminates. Hence, it is important to verify the optimal responses by using advanced analyses such as non-linear static response and progressive failure analysis. These are all major steps that demonstrate the structural improvements that can be obtained by utilizing nonconventional laminates. The goal is to harness the full capacity of nonconventional composite laminates while utilizing the experience gained by industry over the decades with conventional ones. This sets the path to produce optimal practical laminates that are “industry oriented”, which could serve as a major task towards industry adoption and certification of nonconventional laminates.

CHAPTER 3

MULTI-LEVEL OPTIMIZATION METHODOLOGY USING DESIGN-MANUFACTURING MESH

This chapter presents the proposed multi-level optimization methodology using a design-manufacturing mesh during each optimization step. The concept of including a design-manufacturing mesh is first introduced in Section 3.1. The presence of the design-manufacturing mesh and the use of proper distribution definitions for each optimization step improves the efficiency, manufacturability, and feasibility of the designed variable stiffness structure. The steps of the multi-level optimization framework are then detailed in the following sections. Section 3.2 demonstrates the benefits of using the design-manufacturing mesh by modelling the variable stiffness distribution continuously using a B-spline surface or NURBS surface. The design-manufacturing can be used in the second optimization step as shown in Section 3.3 to model the fiber angle distribution continuously. By utilizing a bilinear *sine* angle variation, smooth fiber angle distributions can be obtained, and a steering constraint can be applied as a manufacturing constraint. Section 3.4 also reveals the importance of including the design-manufacturing mesh by presenting a constant curvature arc solution for each element of the design-manufacturing mesh. A design-for-manufacturing tool was developed in Mathematica® for generating manufacturable fiber paths that match the designed fiber angle distributions from the second optimization step while satisfying AFP manufacturing constraints. Tow-by-tow

descriptions of the steered plies are then generated in the form of manufacturing boundaries for the AFP machine with optimized cut and restart positions. A summary of the multi-level optimization framework is presented in Section 3.5.

3.1 DESIGN-MANUFACTURING MESH

Using the multi-level optimization methodology presented in Section 2.4, variable stiffness laminates have been designed in the past by assigning the design variables to the nodes of the finite element model along with a reciprocal averaging scheme to guarantee the continuity of the spatial stiffness distribution [36]. This may suffer from an increasing number of design variables as the finite element analysis mesh may be well-refined. In addition, an optimal spatial stiffness distribution may not require the level of refinement as that of an analysis mesh. As a result, a design-manufacturing mesh can be used to solve the variable stiffness optimization problem using two decoupled but dependent meshes. The analysis mesh, which is a finer mesh, is used to evaluate the finite element solutions, whereas the design-manufacturing mesh is used to define the spatial stiffness distribution of the laminated structure by mapping the values of the design variables to the analysis mesh. The design-manufacturing mesh concept can be applied to any parametric surface by discretizing the parametric space of the surface into regions that are coarser than the analysis mesh. An example is shown in Figure 3.1 for a plate, a cylindrical shell, and a conical shell. The gray lines represent the finite element analysis mesh that is used in the structural analysis, and the thick red lines represent the design-manufacturing mesh that is used to define the spatial distribution of the design variables. The design variables in each optimization step are associated with the control points of the design-manufacturing mesh $P_{i,j}$, and then the distribution defined is mapped to the finite element analysis mesh.

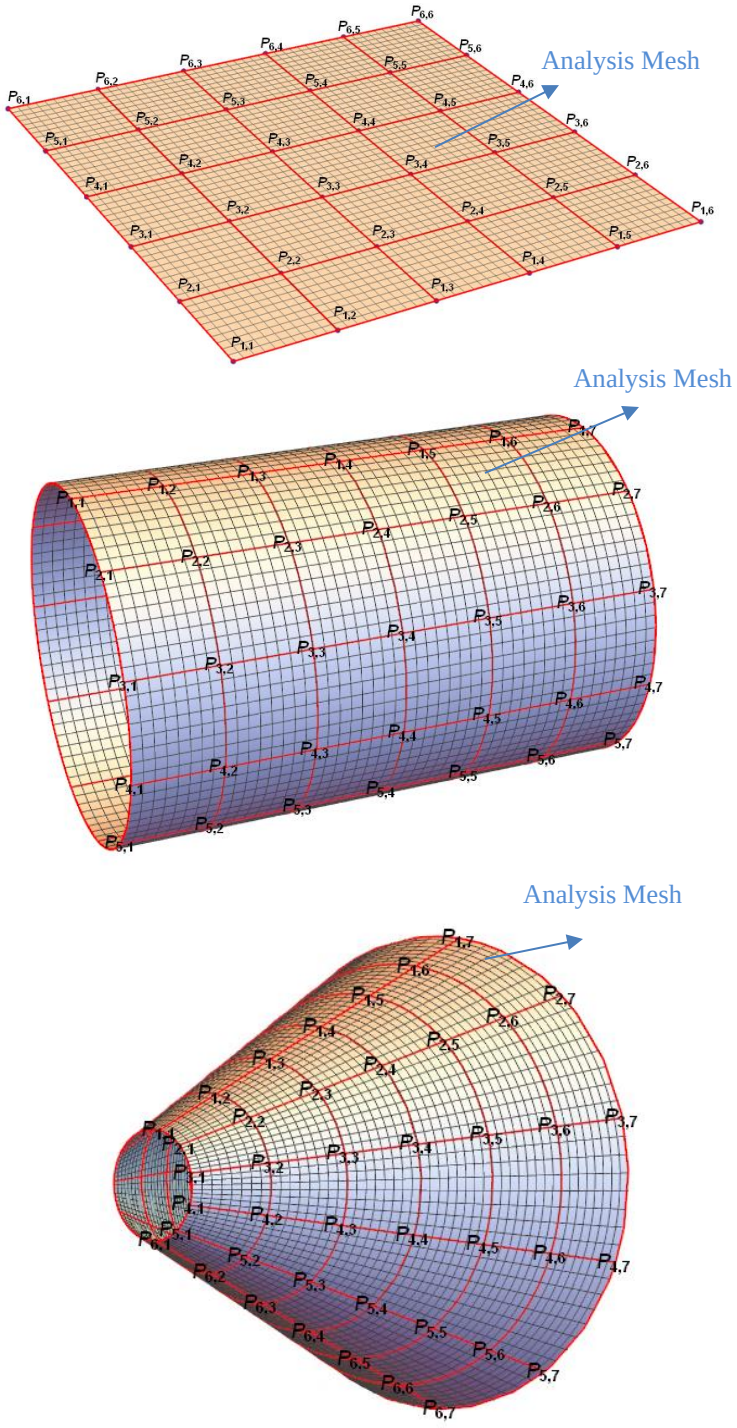

Figure 3.1: Design-manufacturing mesh example for discretizing design-manufacturing regions for a plate, a cylindrical shell, and a conical shell

Utilizing the design-manufacturing mesh concept in the multi-level optimization introduces benefits for each optimization step. It improves the efficiency of each optimization step and reduces the complexity by significantly lowering the number of design variables and allowing the spatial distribution of the design variables with the nodes of the design-manufacturing mesh serving as the control points.

In the first optimization step, reducing the number of design variables also reduces the computational expense of estimating the sensitivities of the responses with respect to the design variables. Utilizing a B-spline or NURBS surface definition also guarantees pointwise constraint satisfaction inherited from the strong convex hull property if the design variables at the control points satisfy the applied constraints in the optimization problem [105]. In addition, the design-manufacturing mesh improves the manufacturability of the variable stiffness structure in the second optimization step by imposing a steering constraint on the fiber angle distribution of each element within the design-manufacturing mesh. Moreover, a constant curvature arc solution can be obtained for each element within the design-manufacturing mesh to generate AFP manufacturable fiber paths that "locally" satisfy the minimum steering radius constraint in the third optimization step.

3.2 STIFFNESS OPTIMIZATION

The first optimization step in the multi-level optimization framework implements the direct stiffness modelling approach to optimize the performance of the laminated structure. Design drivers such as the stiffness properties, strength, buckling load, natural frequency and laminate weight can be considered in the first optimization step. Lamination parameters are used as intermediate design variables to reduce the number of design variables required as well as provide a convex design space, which allows efficient

gradient-based optimization algorithms to be used. The obtained optimal lamination parameter distribution offers the designer a theoretical stiffness variation that best satisfies the prescribed structural performance requirements. In addition, it provides valuable insight into the mechanisms that improve the laminate performance for a specific design problem.

3.2.1 B-Spline or NURBS Surface Spatial Distribution of Lamination Parameters

The design-manufacturing mesh discretizing the variable stiffness structure can be used to define the spatial variation of lamination parameters. It is important to consider a mathematical distribution that defines the spatial stiffness distribution while introducing benefits to the first step optimization problem. Because of its desirable properties, a B-spline surface representation can be used to model the stiffness variation of the laminated structure [105]. The utilization of the B-spline surface leads to a considerable reduction in the number of design variables by associating the lamination parameters with the control points of the design-manufacturing mesh. Using B-splines generally results in continuous and smooth distributions as well as having the benefit of local stiffness variation inside each patch of the design-manufacturing mesh due to the local support property. As a result, inherent smooth distributions can be obtained for the fiber orientation angles in the second optimization step. In addition, because of the strong convex hull property of the B-spline surface, the optimization constraints of the problem can be satisfied at the control points only; hence, the constraints are directly satisfied at each point of the structure domain leading to a significant reduction in the complexity of the optimization problem.

The distribution of four lamination parameters V_1, V_3, W_1, W_3 representing an orthotropic variable stiffness laminate configuration can be mathematically expressed in terms of the B-spline surface as:

$$S(\xi,\eta) = \sum_{i=0}^{n}\sum_{j=0}^{m} N_{i,p}(\xi)N_{j,q}(\eta)\boldsymbol{P}_{i,j}\,, \tag{3.1}$$

where $\boldsymbol{P}_{i,j}$ represent the bidirectional net of control points of the design-manufacturing mesh in the (ξ,η) parametric space of the shell structure being designed. The 1st and 2nd elements of $\boldsymbol{P}_{i,j}$ are associated with the u and v parametric coordinates of the control points and the 3rd element of $\boldsymbol{P}_{i,j}$ is associated with the value of the lamination parameter (V_1, V_3, W_1, W_3) at the corresponding location of the control point. $N_{i,p}$ and $N_{j,q}$ are the pth degree (along ξ) and qth degree (along η) B-spline basis functions defined on the non-periodic and non-uniform knot vectors Ξ and H, respectively [163]:

$$\begin{aligned} \Xi &= \left\{\underbrace{0,\ldots,0}_{p+1}, \xi_{p+1}, \ldots, \xi_{r-p-1}, \underbrace{1,\ldots,1}_{p+1}\right\}, \\ \mathrm{H} &= \left\{\underbrace{0,\ldots,0}_{q+1}, \xi_{q+1}, \ldots, \xi_{s-q-1}, \underbrace{1,\ldots,1}_{q+1}\right\}, \end{aligned} \tag{3.2}$$

where Ξ has r+1 knots and H has s+1 knots and r and s are defined as:

$$r = n + p + 1\,, \qquad\qquad s = m + q + 1\,, \tag{3.3}$$

We are interested in designing the 3rd element of the surface definition in Eq. (3.1) to define the spatial distribution of the lamination parameters on the surface of the structure. The lamination parameter spatial distribution in the (ξ,η) plane can thus be expressed as:

$$V_1(\xi,\eta) = \sum_{i=0}^{n}\sum_{j=0}^{m} N_{i,p}(\xi)N_{j,q}(\eta)V_1^{i,j}\,,$$

$$V_3(\xi,\eta) = \sum_{i=0}^{n}\sum_{j=0}^{m} N_{i,p}(\xi)N_{j,q}(\eta)V_3^{i,j}\,,$$

$$W_1(\xi,\eta) = \sum_{i=0}^{n}\sum_{j=0}^{m} N_{i,p}(\xi)N_{j,q}(\eta)W_1^{i,j}\,, \tag{3.4}$$

$$W_3(\xi,\eta) = \sum_{i=0}^{n}\sum_{j=0}^{m} N_{i,p}(\xi)N_{j,q}(\eta)W_3^{i,j}\,,$$

The design flexibility of the spatial stiffness distribution can be adjusted by altering the number and position of control points, the degrees p and q of the B-spline basis function $N_{i,p}$ and $N_{j,q}$, and the knot vectors associated with the B-spline basis functions Ξ and H, respectively.

By designing the values of the lamination parameters at the control points of the design-manufacturing mesh $V_{1,3}^{i,j}$ and $W_{1,3}^{i,j}$, the optimal stiffness distribution for the laminate is found in the (ξ,η) space. Considering a parametric surface defined by:

$$r(u,v) = \big(x(u,v), y(u,v), z(u,v)\big)\,,$$
$$u_{min} \le u \le u_{max}\,, \qquad v_{min} \le v \le v_{max}\,, \tag{3.5}$$

The dimensionless coordinates ξ and η are chosen to create the link between the B-spline parametric space and the physical space parametric coordinates u and v of the structure being designed. The relation between them can be expressed as:

$$\xi = \frac{u - u_{min}}{u_{max} - u_{min}}, \qquad \eta = \frac{v - v_{min}}{v_{max} - v_{min}}. \tag{3.6}$$

Some examples of parametric surfaces and the dimensionless coordinates ξ and η are shown in Table 3.1 for a plate, a cylindrical shell, and a conical shell with height along the z-axis.

Table 3.1 Relation between dimensionless coordinates in B-spline parametric space and surface parametric coordinates

Shell Structure	**Parametric Surface Equation** $\boldsymbol{r(u,v)}$	**Dimensionless coordinates** $\boldsymbol{(\xi,\eta)}$
Plate: a = Length b = Width	$x = \boldsymbol{u}$, $0 \le \boldsymbol{u} \le a$ $y = \boldsymbol{v}$, $0 \le \boldsymbol{v} \le b$ $z = C$,	$\boldsymbol{\xi} = {}^{\boldsymbol{u}}/_{a}$, $\boldsymbol{\eta} = {}^{\boldsymbol{v}}/_{b}$,
Cylindrical Shell: L = Length R = Radius	$x = R\cos\boldsymbol{\theta}$, $0 \le \boldsymbol{\theta} \le 2\pi$ $y = R\sin\boldsymbol{\theta}$, $0 \le \boldsymbol{z} \le L$ $z = \boldsymbol{z}$,	$\boldsymbol{\xi} = {}^{\boldsymbol{z}}/_{L}$, $\boldsymbol{\eta} = {}^{\boldsymbol{\theta}}/_{2\pi}$,
Conical Shell: $\boldsymbol{\alpha}$ = Cone Angle	$x = \boldsymbol{\rho}\sin\alpha\cos\boldsymbol{\theta}$, $0 \le \boldsymbol{\theta} \le 2\pi$ $y = \boldsymbol{\rho}\sin\alpha\sin\boldsymbol{\theta}$, $\frac{r_{min}}{\sin\alpha} \le \boldsymbol{\rho} \le \frac{r_{max}}{\sin\alpha}$ $z = \boldsymbol{\rho}\cos\alpha$,	$\boldsymbol{\xi} = \frac{\boldsymbol{\rho} - \rho_{min}}{\rho_{max} - \rho_{min}}$, $\boldsymbol{\eta} = {}^{\boldsymbol{\theta}}/_{2\pi}$,

In order to map the correct values of the lamination parameters for each element of the finite element mesh, and hence define the distribution in the physical Cartesian coordinate space (x, y, z), the following steps are required:

1. Construct the design-manufacturing mesh using iso-parametric curves of the surface, and define the location of the design control points $\boldsymbol{P}_{i,j}$ in (u, v) space
2. Construct the B-spline surface definition from the lamination parameters defined at the control points of the design-manufacturing mesh
3. For each element i in the finite element model, retrieve the Cartesian coordinates of the centroid $\left(x_C^i, y_C^i, z_C^i\right)$, calculate the parametric coordinates of the centroid $\left(u_C^i, v_C^i\right)$ using coordinate transformation, and then calculate the corresponding dimensionless coordinates $\left(\xi_C^i, \eta_C^i\right)$ according to Eq. (3.6)
4. Replace the dimensionless coordinates $\left(\xi_C^i, \eta_C^i\right)$ in the lamination parameter surface definition of Eq. (3.4) to obtain the values of the lamination parameters for each ith element and map these values to the corresponding element in the finite element mesh

An example of a B-spline surface distribution for $V_1(\xi, \eta)$ constructed using the design-manufacturing mesh of the plate in Figure 3.1 with 6 by 6 uniformly spaced control points in the parametric space and 2nd degree B-spline basis functions is shown in Figure 3.2

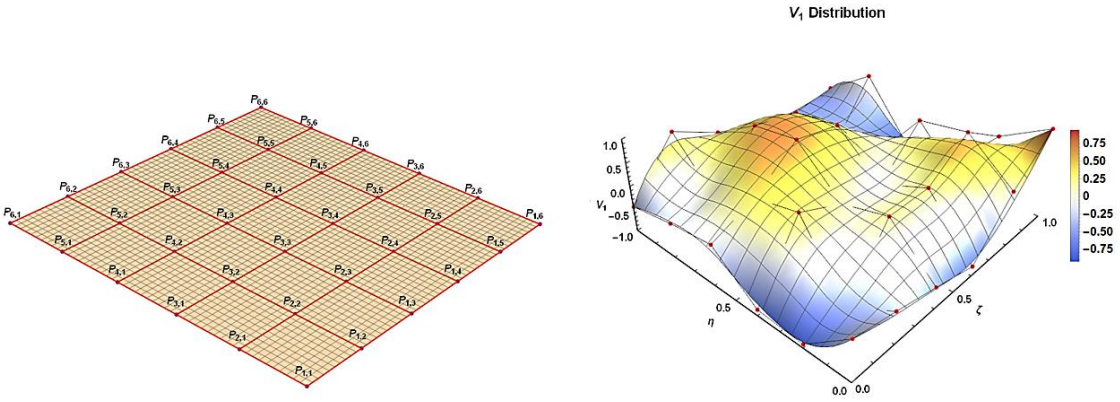

Figure 3.2: B-spline surface example for $V_1(\xi, \eta)$ distribution for plate

The spatial distribution of lamination parameters should also be matched by the fiber angle distribution definition at the second step and consequently the fiber paths at the third optimization step to guarantee that the manufactured laminate is as close as possible to the designed one. In this work, it is proposed that the *sine* of the fiber orientation angle varies bi-linearly over the domain of an element of the design-manufacturing mesh. The use of the *sine* function to define the spatial variation generates smooth fiber angle distributions, and a constant curvature arc solution can be found from the distribution definition to closely match the optimal fiber angle distribution defined by each element of the design-manufacturing mesh. For each element of the design-manufacturing mesh, a bilinear *sine* function variation for a $\{u,v\}$ domain can be defined as:

$$\sin \varphi_{uv} = a + b\,u + cv + d\,u\,v\,, \tag{3.7}$$

where the coefficients a, b, c, and d are defined from the fiber orientation angles obtained from the second optimization step at the corner nodes (control points) of each element. This represents a bilinear interpolation representing a surface of 2nd degree for each element of the design-manufacturing mesh. In order to define a feasible spatial lamination parameter distribution in the first optimization step, we can express the in-plane lamination parameters of the laminate as:

$$\begin{aligned} V_1(u,v) &= \sum_{k=1}^{N} v_k \cos 2\varphi_k(u,v)\,, \\ V_3(u,v) &= \sum_{k=1}^{N} v_k \cos 4\varphi_k(u,v)\,, \end{aligned} \tag{3.8}$$

Using the trigonometric formulas for double angles, we can express the in-plane lamination parameters as:

$$V_1(u,v) = \sum_{k=1}^{N} v_k(1 - 2\sin^2(\varphi_{uv})_k)\,,$$
$$V_3(u,v) = \sum_{k=1}^{N} v_k(1 - 8\sin^2(\varphi_{uv})_k + 8\sin^4(\varphi_{uv})_k)\,. \tag{3.9}$$

As a result, the distribution of $V_1(u,v)$ must be represented by a 4th degree surface (quartic) using bi-quadratic polynomials of 2nd degree, while that of $V_3(u,v)$ must be represented by an 8th degree surface using bi-quartic polynomials of 4th degree. Similar expressions can be obtained for the out-of-plane lamination parameters $W_1(u,v)$ and $W_3(u,v)$. The spatial lamination parameter distribution can be thus modified by specifying the degrees of the B-spline basis functions in the B-spline surface definition to obtain:

$$V_1(\xi,\eta) = \sum_{i=0}^{n}\sum_{j=0}^{m} N_{i,2}(\xi)N_{j,2}(\eta)V_1^{i,j}\,,$$
$$V_3(\xi,\eta) = \sum_{i=0}^{n}\sum_{j=0}^{m} N_{i,4}(\xi)N_{j,4}(\eta)V_3^{i,j}\,,$$
$$W_1(\xi,\eta) = \sum_{i=0}^{n}\sum_{j=0}^{m} N_{i,2}(\xi)N_{j,2}(\eta)W_1^{i,j}\,, \tag{3.10}$$
$$W_3(\xi,\eta) = \sum_{i=0}^{n}\sum_{j=0}^{m} N_{i,4}(\xi)N_{j,4}(\eta)W_3^{i,j}\,,$$

The polynomial components of $V_{1,3}(\xi,\eta)$ and $W_{1,3}(\xi,\eta)$ are defined piecewise on the sets $[\xi_i, \xi_{i+1}]$ x $[\eta_i, \eta_{i+1}]$. On each set, the polynomial surface definition is of degree $p + q$. It is noteworthy to mention that choosing 4th degree B-spline basis functions will modify the knot vectors over which they are defined on the B-spline surface. For a B-spline surface with basis function $N_{i,p}$ and $N_{j,q}$, the "patches" in the B-spline surface space (ξ,η)

are taken to be the non-zero knot spans, namely $[\xi_i, \xi_{i+1}]$ x $[\eta_i, \eta_{i+1}]$ where the knots in each vector are two *distinct* knot values [164]. As a result, the stiffness variations $V_3(\xi, \eta)$ and $W_3(\xi, \eta)$ using 4th degree B-spline basis functions, with the same control points, are defined over a smaller number of knot spans (or patches in B-spline surface space). For example, using 5 control points (n = 5, m = 5) along each direction ξ and η along with 4th degree B-spline basis functions, we obtain a Bezier surface distribution. To obtain a stiffness variation with the same knot spans as those defined by the $V_1(\xi, \eta)$ and $W_1(\xi, \eta)$, the number of control points must be increased by two along each direction ξ and η, which means an increase in the number of design variables (control points). However, when enough control points are present in the design-manufacturing mesh to explore the design space (n must be at least greater than $p + 1$), this is not necessary as the higher degree (4th degree) for each B-spline basis offers higher flexibility for the design of the stiffness variations $V_3(\xi, \eta)$ and $W_3(\xi, \eta)$ over suitable knot spans.

The discussion above considers the knot vectors to be uniform (knot values equally spaced) when defining the spatial stiffness distribution. For specific structural design problems with discontinuities or cutouts, the knot values may be chosen as non-uniform resulting in a nonuniform B-spline surface. Using a non-uniform B-spline surface introduces more design flexibility for local regions of the structure thus improving the spatial stiffness distribution. A further step can be taken by defining the stiffness distribution using nonuniform rational B-splines (NURBS). The weights in a NURBS representation can be used to account for design regions that have higher importance, thus basing the weights on the normalized sensitivities of the responses with respect to the design variables. In the case of NURBS, the stiffness variation takes the form of:

$$V_1(\xi,\eta) = \frac{\sum_{i=0}^{n}\sum_{j=0}^{m} N_{i,2}(\xi)N_{j,2}(\eta)\, w_{i,j}\, V_1^{i,j}}{\sum_{i=0}^{n}\sum_{j=0}^{m} N_{i,2}(\xi)N_{j,2}(\eta)\, w_{i,j}},$$

$$V_3(\xi,\eta) = \frac{\sum_{i=0}^{n}\sum_{j=0}^{m} N_{i,4}(\xi)N_{j,4}(\eta)\, w_{i,j}\, V_3^{i,j}}{\sum_{i=0}^{n}\sum_{j=0}^{m} N_{i,4}(\xi)N_{j,4}(\eta)\, w_{i,j}},$$

$$W_1(\xi,\eta) = \frac{\sum_{i=0}^{n}\sum_{j=0}^{m} N_{i,2}(\xi)N_{j,2}(\eta)\, w_{i,j}\, W_1^{i,j}}{\sum_{i=0}^{n}\sum_{j=0}^{m} N_{i,2}(\xi)N_{j,2}(\eta)\, w_{i,j}}, \quad (3.11)$$

$$W_3(\xi,\eta) = \frac{\sum_{i=0}^{n}\sum_{j=0}^{m} N_{i,4}(\xi)N_{j,4}(\eta)\, w_{i,j}\, W_3^{i,j}}{\sum_{i=0}^{n}\sum_{j=0}^{m} N_{i,4}(\xi)N_{j,4}(\eta)\, w_{i,j}},$$

where the weights $w_{i,j}$ (4^{th} dimensional) can be based on the importance of each control point with respect to the structural response $\tilde{f}$ and defined as: $w_{i,j} = {\partial \tilde{f}}/{\partial x_{i,j}}$, and $x_{i,j}$ is the design variable ($V_1^{i,j}$ - $W_3^{i,j}$) at the control point defining the surface distribution. If the NURBS surface definition was used with specified weights $w_{i,j}$ at each control point of the design-manufacturing mesh, the same weights must be applied to the surface definitions of the fiber orientation angles at the second and third optimization steps to closely match the designed stiffness distribution at the first optimization step.

3.2.2 Conservative Convex Separable Approximations

This subsection presents the structural approximations that can be used to optimally design the stiffness distribution of the structure by solving the approximate subproblem at each control point of the design-manufacturing mesh. The optimization complexity is highly influenced by the number of considered objectives, constraints, and design variables as well as their nature. By increasing the number of responses and design variables, the complexity of the first optimization step increases, and the type of algorithm used to solve the problem may be affected as well. If discrete design variables such as the number of

plies or the number and shape of stiffeners are considered, it would be incredibly difficult to solve the design problem using gradient-based optimization techniques. Since lamination parameters are used as continuous design variables, their convex space promotes the efficient use of sensitivity-based optimization algorithms. In addition, the nature of the response or how it can be expressed as function of the design variables (linear or non-linear) highly influences the optimization complexity. Gradient-based optimization techniques strictly depend on the starting point of the algorithm; hence it is necessary to guarantee the convexity of the design objective, constraints, and the design space to obtain a global optimum design. In addition, structural responses evaluated using finite element analysis require the most computational time in the algorithm. As a result, the use of suitable structural approximations to replace the analysis model that guarantee the convexity of the considered responses is a key element to obtain a global optimum design efficiently.

Successive approximation schemes are popular in efficient structural optimization because they reduce the number of structural analyses required to obtain an optimum design. In a successive approximation scheme, the optimization problem is solved by iteratively solving approximate subproblems, which are formulated in this work using the conservative convex separable approximations developed by Ijsselmuiden for the design of variable stiffness laminates [36]. The approximate subproblem with an objective function $\tilde{f}_0$, m individual constraints, $\tilde{f}_j$, and n design variables, x_i, with lower and upper bounds, x_i^L and x_i^U, takes the form:

$$\min_{\boldsymbol{x}} \tilde{f}_0(\boldsymbol{x})$$

$$\tilde{f}_j(\boldsymbol{x}) \leq 0 \qquad j = 1,2,\dots,m \tag{3.12}$$

$$x_i^L \leq x_i \leq x_i^U \qquad i = 1,2,\dots,n\,.$$

The constrained optimization subproblem is referred to as the primal problem. Since the considered structural approximations are convex and separable, the primal problem can be solved efficiently using the dual method presented by Fleury and Schmit [165]. The first step is to construct the Lagrangian of the primal convex subproblem as:

$$\mathcal{L}(\boldsymbol{\mu}, \boldsymbol{x}) = \tilde{f}_0(\boldsymbol{x}) + \sum_{j=1}^{m} \mu_j \tilde{f}_j(\boldsymbol{x})\,, \tag{3.13}$$

where μ_j are non-negative scalars known as the Lagrange multipliers, associated with the j^{th} response and $\boldsymbol{x}$ is the vector of design variables. The dual problem is then given by:

$$\max_{\boldsymbol{\mu}} \mathcal{L}_C(\boldsymbol{\mu}) \qquad \text{s.t.} \qquad \mu_j \geq 0\,, \tag{3.14}$$

where $\mathcal{L}_C$ is known as the complementary Lagrangian and is defined as the minimum of the Lagrangian $\mathcal{L}$ over all design variables as:

$$\mathcal{L}_C = \min_{\boldsymbol{x}} \mathcal{L}(\boldsymbol{x}(\boldsymbol{\mu})) \qquad \text{s.t.} \qquad \mu_j \geq 0\,, \tag{3.15}$$

where the Lagrange multipliers, $\boldsymbol{\mu}$, are fixed when solving for the optimal primal variables $\boldsymbol{x}$. For convex optimization problems, the duality gap is zero (optimal solution of the dual problem is the same as that of the primal) if the Karush-Kuhn-Tucker conditions are satisfied [28]. The dual formulation allows for separating the search for optimal primal and dual variables. The local optimization problem is solved to search for the optimal primal variables $\boldsymbol{x}$, then the global optimization problem is solved to search for the optimal dual variables $\boldsymbol{\mu}$.

The objective function $\tilde{f}_0$ and the constraints $\tilde{f}_j$ are constructed using the conservative convex structural approximations to minimize the number of finite element analysis required to converge to an optimum. Svanberg has demonstrated that these approximations are globally convergent, which guarantees that an optimum design will be found [133]. The framework expresses the structural response to be optimized as a Taylor series expansion in terms of stiffness matrices and their corresponding inverses obtained from the Classical Lamination Theory. The approximation of the response resembles the conservative structural approximation developed by Braibant and Fleury [28]. The conservative convex separable approximation of a structural response, $\tilde{f}_j$ (j = 0, 1,…,m), can be expressed as:

$$\tilde{f}_j = \sum_{i=1}^{N} (\breve{\Psi}_{i,j}^{m} : A_i + \breve{\Psi}_{i,j}^{b} : D_i + \breve{\Phi}_{i,j}^{m} : A_i^{-1} + \breve{\Phi}_{i,j}^{b} : D_i^{-1} + \breve{\alpha}_{i,j} h_i) + C_0 \,,$$
$$\Psi_{i,j}^{m} = \frac{\partial \tilde{f}_j}{\partial A_i} \,, \Psi_{i,j}^{b} = \frac{\partial \tilde{f}_j}{\partial D_i} \,, \Phi_{i,j}^{m} = \frac{\partial \tilde{f}_j}{\partial A_i^{-1}} \,, \Phi_{i,j}^{b} = \frac{\partial \tilde{f}_j}{\partial D_i^{-1}} \,, \alpha_{i,j} = \frac{\partial \tilde{f}_j}{\partial h_i} \,, \tag{3.16}$$

where $\breve{\Psi}_{i,j}^{m}$ and $\breve{\Psi}_{i,j}^{b}$ are the damped sensitivity matrices with elements representing the derivatives of the j^{th} response with respect to the elements of the in-plane and out-of-plane stiffness matrices, A_i and D_i, respectively, for the i^{th} control point including the convexifying terms obtained from damping. Similarly, $\breve{\Phi}_{i,j}^{m}$ and $\breve{\Phi}_{i,j}^{b}$ are the damped sensitivity matrices with elements representing the derivatives of the j^{th} response with respect to the elements of the inverse of the in-plane and out-of-plane stiffness matrices, A_i^{-1} and D_i^{-1}, respectively, for the i^{th} control point. The : operator represents a matrix inner product and can be calculated as the trace of the matrix product. For additional details about the damping terms that are added to ensure conservativenss and convexity of the

structural approximation, the reader is referred to [36]. A variable thickness design can also be obtained by including $\breve{\alpha}_{i,j}$ in the response approximation, which represents the derivatives of the response which depend explicitly on the laminate thickness, h_i. Including the thickness as a design variable requires an additional bound constraint in the optimization problem to obtain a bounded optimization problem. C_0 represents all remaining constant terms.

The linear terms of the stiffness matrices in the structural approximation are by definition convex, but convexity of the reciprocal parts is not always the case. For some structural responses such as strength, the approximation convexity cannot be always guaranteed, and if the damping terms added are not enough to ensure convexity of the response, a numerical algorithm is necessary to ensure struct convexity and guarantee a global optimum solution is obtained. To achieve strict convexity, the sensitivity matrices with elements representing the derivatives of the response with respect to the elements of the inverse of the in-plane and out-of-plane stiffness matrices $\breve{\Phi}_{i,j}^{m}$ and $\breve{\Phi}_{i,j}^{b}$ must be positivie semidefinite [15]. This can be achieved by mathematically separating the reciprocal sensitivity matrices (both membrane and bending) $\widetilde{\Phi}$ into two parts, a positive semi-definite part $\widetilde{\Phi}^{+}$ and a non-definite part $\widetilde{\Phi}^{-}$. Thus, the contribution of each reciprocal sensitivity matrix to the structural approximation is expressed as:

$$f_R = \widetilde{\Phi}^{+}\colon A^{-1} + \widetilde{\Phi}^{-}\colon A^{-1}\,, \tag{3.17}$$

A Taylor series expansion of the non-definite part $\widetilde{\Phi}^{-}$ in A around the approximation point, $A^{(k)}$, is performed to obtain:

$$f_R = \widetilde{\Phi}^{+}\colon A^{-1} + \widetilde{\Psi}^{-}\colon A + 2\,\widetilde{\Phi}^{-}\colon A^{(k)^{-1}}\,, \tag{3.18}$$

The homogeneity of the approximation terms can be maintained by the following constraint:

$$\widetilde{\Phi}^{-}\colon A^{(k)^{-1}} = 0\,, \tag{3.19}$$

Using the Cholesky decomoposition, $A^{(k)} = LL^T$, the constraint can be written as:

$$\mathrm{trace}(\widehat{\Phi}^{-}) = 0\,, \tag{3.20}$$

where $\widehat{\Phi}^{-} = L^{-1}\widetilde{\Phi}^{-}L^{-T}$. It is desirable to have only the semi-definite part in the approximation terms, so convexifying the approximation can be defined as an optimization problem as:

$$\min\left\|\widehat{\Phi}^{-}\right\|^2 \text{ subject to } \quad \mathrm{trace}\left(\widehat{\Phi}^{-}\right) = 0 \text{ and } \ \mathrm{eig}\left(\widehat{\Phi} - \widehat{\Phi}^{-}\right) \geq 0 \tag{3.21}$$

where $\widehat{\Phi} = L^{-1}\widetilde{\Phi}L^{-T}$. The solution guarantees that if $\widetilde{\Phi}$ is positive definite, then the non-definite part is zero. The optimization problem can be simplified using eigendecomposition where $\widehat{\Phi} = T^T D\, T$, where D is a diagonal matrix containing the eigenvalues d_i of $\widehat{\Phi}$. Similarly, $\widehat{\Phi}^{-} = T^T D^{-}\, T$, where D^{-} is a diagonal matrix containing the eigenvalues d_i^{-} of $\widehat{\Phi}^{-}$, and the optimization problem can be expressed as:

$$\min \frac{1}{2}\sum_{i=1}^{3}(d_i^{-})^2 \quad \text{subject to} \quad \sum_{i=1}^{3} d_i^{-} = 0 \quad \text{and} \quad d_i - d_i^{-} \geq 0 \tag{3.22}$$

The quadratic optimization problem is then solved to find the optimal d_i^{-}, hence $\widehat{\Phi}^{-}$ and finally $\widetilde{\Phi}^{-}$. The eigenvalues of the positive semi-definite part are found as $d_i^{+} = d_i - d_i^{-}$, which allows us to define $\widehat{\Phi}^{+}$, and finally $\widetilde{\Phi}^{+}$. The contribution of the reciprocal terms in the approximation thus becomes:

$$f_R = \widetilde{\Phi}^{+}\colon A^{-1} + \widetilde{\Psi}^{-}\colon A\,, \tag{3.23}$$

where $\tilde{\Psi}^{-} = -\mathrm{A}^{-1}\tilde{\Phi}^{-}\mathrm{A}^{-1}$. This guarantees the strict convexity of the structural approximation in terms of the laminate stiffness reciprocal matrices.

Because of the separability of the structural approximations, the local optimization problem can be conducted as N (N = number of control points in B-spline surface definition) independent local optimization problems to search for the optimal primal variables as:

$$\min_{x_i} \left(\breve{\Psi}_i^m : A_i + \breve{\Psi}_i^b : D_i + \breve{\Phi}_i^m : A_i^{-1} + \breve{\Phi}_i^b : D_i^{-1} + \breve{\alpha}_i h_i\right), \tag{3.24}$$

where x_i is the vector of design variables containing the lamination parameters and thickness of each control point subject to the constraints imposed on the design variables that include the lamination parameter feasible region as discussed in Section 2.3 and the thickness bound limits.

The dual variables μ_j are constant during the local optimization problem, so the sensitivities can be summed over all the responses m as:

$$\begin{aligned} &\breve{\Psi}_i^m = \sum_{j=0}^{m} \mu_j \breve{\Psi}_{i,j}^m, \qquad \breve{\Psi}_i^b = \sum_{j=0}^{m} \mu_j \breve{\Psi}_{i,j}^b, \qquad \breve{\Phi}_i^m = \sum_{j=0}^{m} \mu_j \breve{\Phi}_{i,j}^m, \\ &\breve{\Phi}_i^b = \sum_{j=0}^{m} \mu_j \breve{\Phi}_{i,j}^b, \qquad \breve{\alpha}_i = \sum_{j=0}^{m} \mu_j \breve{\alpha}_{i,j}, \qquad \mu_0 = 1. \end{aligned} \tag{3.25}$$

The separable nature of the local optimization problems facilitates parallel computing to reduce the computational time of the stiffness optimization step. The chosen structural approximation is separable and convex in terms of the elements of the laminate stiffness matrices, **[A]**, **[D]**, and their reciprocals. Since the stiffness matrix elements are interrelated, it is not practical to design in terms of the individual terms. The approximation is thus parameterized in terms of lamination parameters. Because the stiffness matrices are

linear functions of the lamination parameters, this helps in retaining all the required properties to achieve convexity when using lamination parameters as design variables. The local optimization problem can be solved using an efficient gradient-based optimization method such as sequential quadratic programming (SQP).

The global optimization problem is then solved to obtain the optimal dual variables. These are acquired by solving the dual problem of Eq. (3.14) where the sensitivities of the complementary Lagrangian, $\mathcal{L}_C$, with respect to the Lagrange multipliers, μ_j, is found as:

$$\frac{\partial \mathcal{L}_C}{\partial \mu_j} = -\mu_j , \tag{3.26}$$

The global optimization problem can also be efficiently solved using Sequential Quadratic Programming (SQP) with few responses, or an interior-point algorithm can be used to improve the convergence when a large number of constraint responses are considered [36].

Considering the conservative convex separable approximations, an improved convergence behavior is obtained when solving the first optimization step. These approximations constitute a replacement for the actual finite element analysis model to search for optimum stiffness distribution that minimizes the approximate objective function, thus accelerating the function evaluations that are required during the optimization.

3.2.3 Multi-Modal Problem Formulation

It is also important to consider the multi-modal nature of some responses such as buckling and natural frequency. Considering only the critical mode of a multi-modal response in optimization problems might result in unreliable solution convergence as mode switching can take place, which is a sudden change in the critical mode shape [166]. When

the structural design is modified, the critical mode shape might change, especially when there are global and local mode shapes present. If mode switching takes place, the new mode that will become critical might require a different structural solution than the initial one, and this might lead to continuous iteration between the different critical modes. Hence, the structural approximation must consider the multi-modal nature of the responses that are being optimized.

To account for multiple modes, the bound formulation presented by Olhoff can be used [134]. This is done by introducing an independent parameter, β, and reformulating the optimization problem as:

$$min\,\beta \quad s.t. \quad \tilde{f}_j \leq \beta\,, \tag{3.27}$$

with β being an upper-bound for the multi-modal response $\tilde{f}_j$ (j = 1, 2, ... M), which are the first M eigenvalues, and the largest value of $\tilde{f}_j$ corresponds to the critical mode (since the inverse of the responses are considered as $\tilde{f}_j$). Similarly, the problem can be subsequently solved using the dual method, where the Lagrangian can be expressed as:

$$\mathcal{L}(\boldsymbol{\mu}, \boldsymbol{x}) = \beta\left(1 - \sum_{j=1}^{M} \mu_j\right) + \sum_{j=1}^{M} \mu_j\, \tilde{f}_j(\boldsymbol{x})\,, \tag{3.28}$$

The dual problem is then given by:

$$\max_{\boldsymbol{\mu}} \mathcal{L}_C(\boldsymbol{\mu}) \qquad \text{s.t.} \qquad \mu_j \geq 0\,, \tag{3.29}$$

where $\mathcal{L}_C$ is known as the complementary Lagrangian and now results in two conditions:

$$\mathcal{L}_C = \min_{\boldsymbol{x}} \sum_{j=1}^{M} \mu_j\, \tilde{f}_j(\boldsymbol{x}) \qquad \text{s.t.} \qquad \sum_{j=1}^{M} \mu_j = 1\,, \tag{3.30}$$

The dual formulation for a multi-modal response is identical to the one formulated in equations (3.14) and (3.15) except an additional constraint to ensure that the Lagrange multipliers associated with the multi-modal responses sum to unity.

3.2.4 Stiffness Optimization Scheme

The steps of the Stiffness Optimization step are summarized in Figure 3.3, which is an extended design structure matrix (XDSM) diagram [167]. The XDSM diagram is often used in the Multidisciplinary Design Optimization (MDO) field, and it is utilized here to detail the optimization process flow. The diagram can be visualized as a matrix with the diagonal representing the main process components. A vertical data component along a column of the matrix is an input data to the main process components and a horizontal data component along a row of the matrix is an output from the main process components. Input data components below the diagonal component are feedback inputs, whereas input data components above the diagonal component are a priori input. The stack of process components indicates that the computation can be implemented in parallel.

Vertical data components that are not shaded (white) are initialization parameters that are introduced to the optimization process externally by the user. The input data to the first optimization step consist of the lamination parameters V_i^0, W_i^0, t_i^0 for each control point i and the feasible domain of lamination parameters along with any other constraints such as the 10% rule is incorporated in $D_{V,W}$. The damping parameter ρ^0 is initialized after running the finite element analysis (FEA) in the first optimization step iteration and later updated after the finite element analysis in each iteration to obtain the conservative convex separable approximations for each response in each iteration. The material properties Γ_i and the FEM model are also external input to the first optimization step.

Horizontal data components that are also not shaded (white) are output parameters that are requested by the user. The output parameters requested in the first optimization step are the optimum lamination parameter distribution V_i^*, W_i^*, t_i^*, the optimum stiffness properties A_i^*, D_i^*, t_i^*, and the optimum theoretical responses $\tilde{f}_{Theoretical}$. The Stiffness Optimization step consists of:

- Stiffness Optimizer: Solve the local (3.24) and global (3.14) optimization problems to obtain the optimum stiffness distribution defined by the lamination parameters V_i^*, W_i^* and thickness variables t_i^* at the control points of the design-manufacturing mesh subject to the feasible domain of lamination parameters (including robustness rules) and thickness bound constraints
- Sensitivity Analysis: Estimate the first order derivatives for each response $\tilde{f}$ with respect to each design variable defined at each control point i using finite difference technique coupled with finite element analysis
- Stiffness Distribution: Define the spatial stiffness distribution of the structure using the B-spline surface or NURBS surface formulation presented in Section 3.2.1 and map the values to the surface parametric space $\{u, v\}$
- Composite Parametrization: Evaluate the stiffness matrices at each element in the finite element model from the lamination parameter distribution and thickness using the linear relation between the stiffness matrices and the design variables
- Conservative Convex Separable Approximations: Approximate the responses $\tilde{f}$ using the first order derivatives with respect to the stiffness matrices and reciprocals with damping and reciprocal terms convexification to obtain conservative convex separable approximations as presented in Section 3.2.2

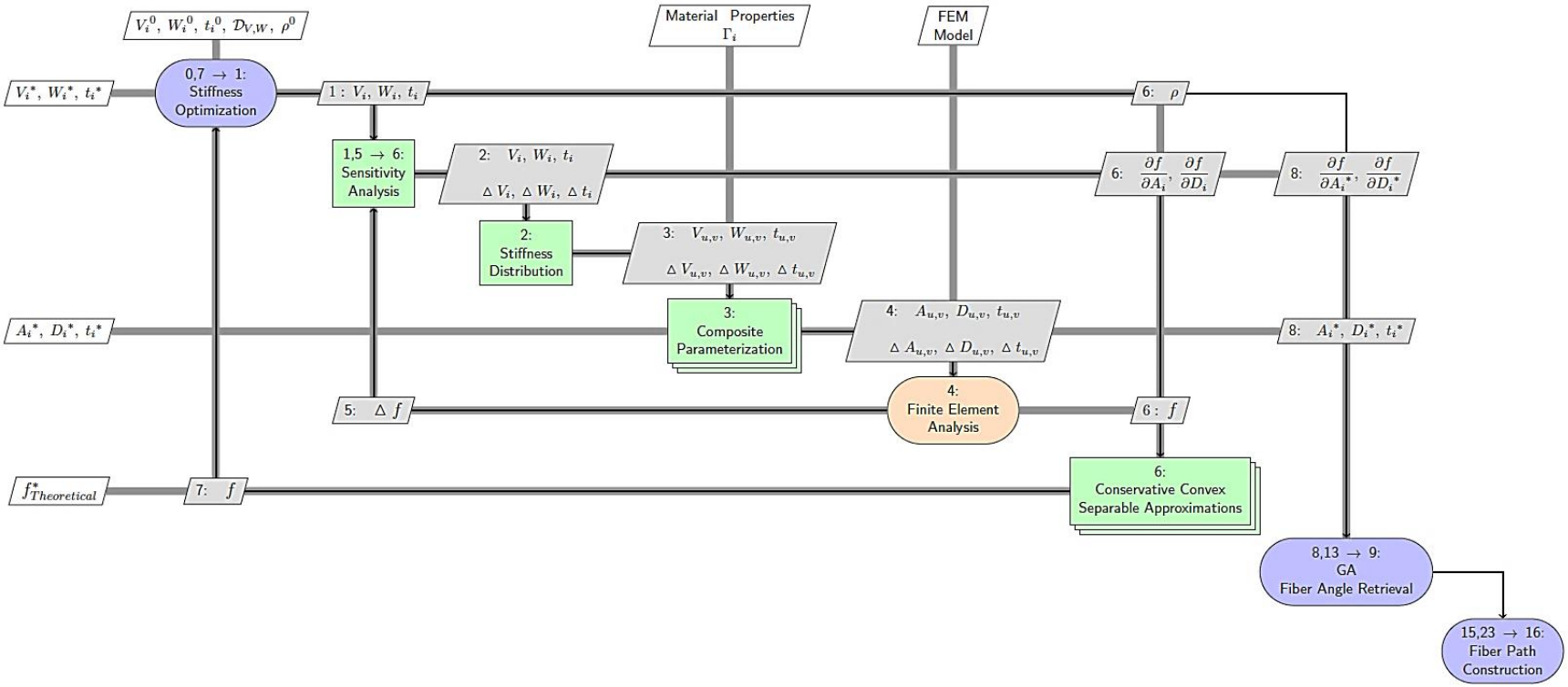

Figure 3.3 XDSM diagram for Stiffness Optimization Step

3.3 STACKING SEQUENCE RETRIEVAL

In the second optimization step, the fiber angle distributions that are required to match the optimum stiffness distributions from the first optimization step are sought. Using the design-manufacturing mesh, the next step aims to find the optimal fiber orientation angles at the control points that closely match the optimum stiffness properties. Since the B-spline surface distribution is not generally interpolatory at the control points, the optimum stiffness values are mapped to the control points in the physical domain space $\{u, v\}$ to be included in the second optimization step.

The second optimization step is termed as the inverse problem, and it is non-convex because it is posed in the space of layer fiber orientation angles. This step usually suffers from theoretical performance loss when additional design guidelines and manufacturing constraints are applied at the conversion process. This is because of the discrepancies between the continuous and the discrete optimization steps when applying additional constraints in the second optimization step. However, it is important to included laminate design guidelines in this step to improve robustness and feasibility for industrial applications. In addition, the minimum steering radius constraint can be applied at the second optimization step at the ply level to decrease the amount of course dropping that might be obtained for highly non-linear fiber angle distributions. Designers have usually applied this constraint as a measure of the rate of change of fiber angle, yet this might lead to overconstraining the design space when highly non-linear fiber angle variations are required. In this work, the maximum steering constraint in the second optimization step is considered as a general steering constraint that maintains a minimum degree of manufacturability of the fiber angle distributions. The actual AFP maximum steering

constraint is then defined locally along the manufacturable fiber-steered path using the solution developed in the third optimization step to avoid tow wrinkling as well as in-plane tow deformations.

3.3.1 Bilinear Spatial Interpolation of *Sine* of Fiber Orientation Angles

A bilinear variation of the *sine* of the fiber orientation angle over the domain of an element of the design-manufacturing mesh is proposed. The use of the *sine* function to define the spatial variation generates smooth fiber angle distributions while also allowing non-linear fiber angle variations, and a constant curvature arc solution can be found from the distribution definition in the third optimization step to closely match the optimal fiber angle distribution defined by each element of the design-manufacturing mesh. For each element of the design-manufacturing mesh, a bilinear *sine* function variation for a $\{u,v\}$ domain can be defined as:

$$\sin\varphi_{uv} = a + b\,u + cv + d\,u\,v\,, \tag{3.31}$$

where the coefficients a, b, c, and d are defined from the fiber orientation angles obtained from the second optimization step at the corner nodes (control points) of each element. An example showing a smooth fiber angle distribution defined by the bilinear *sine* variation is shown in Figure 3.4. By solving for the expressions of a, b, c, and d, the bilinear variation can be simplified as:

$$\begin{aligned}\sin\varphi_{uv} = {} & \frac{\sin[\varphi_{11}](u-u_0)(v-v_0)}{(u_1-u_0)(v_1-v_0)} + \frac{\sin[\varphi_{01}](u-u_1)(v_0-v)}{(u_1-u_0)(v_1-v_0)} \\ & + \frac{\sin[\varphi_{00}](u-u_1)(v-v_1)}{(u_1-u_0)(v_1-v_0)} + \frac{\sin[\varphi_{10}](u-u_0)(v_1-v)}{(u_1-u_0)(v_1-v_0)}\end{aligned} \tag{3.32}$$

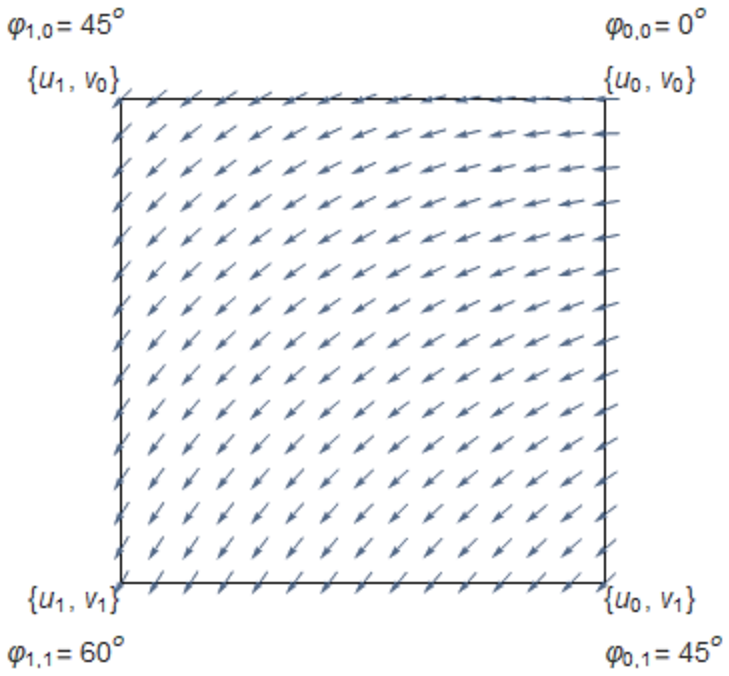

Figure 3.4: Bilinear *sine* angle variation example for single element of a design-manufacturing mesh in $\{u,v\}$ plane

The fiber angle distribution of each element depends on the position of the control points u_0, u_1, v_0, v_1, and the fiber orientation angle associated with each control point. The fiber angle distribution over the structural domain is thus defined by defining the spatial variation over all the connected design-manufacturing mesh elements. An example of a fiber angle distribution with φ_{uv} varying along the u direction over a plate domain is shown in Figure 3.5. The distribution over the structural domain can be represented as piecewise function of bilinear variations over the domain of each element. The orientation angles defined at the control nodes for each layer of the laminate are the design variables required in the second optimization step to match the optimum stiffness properties from the first optimization step.

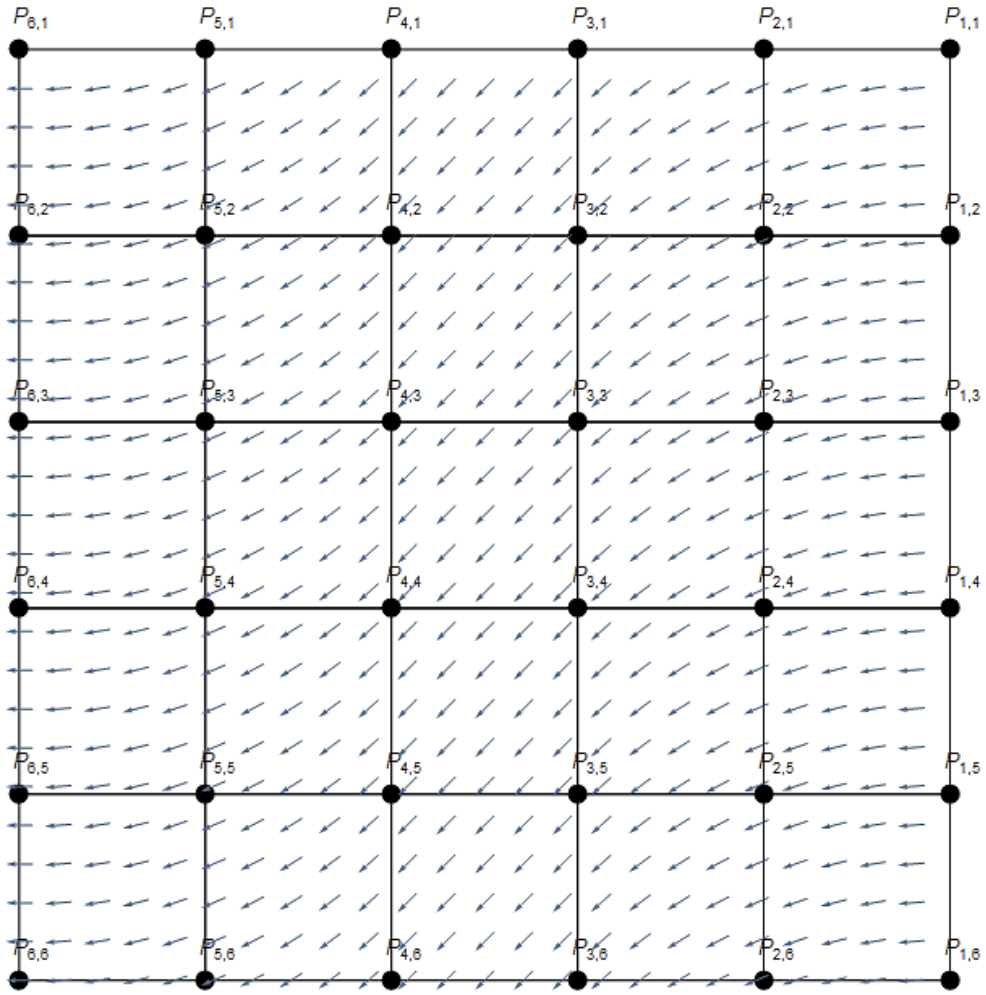

Figure 3.5: Bilinear *sine* angle variation example over plate domain with 6 by 6 control points defining the design-manufacturing mesh

By analyzing the fiber angle distribution in each element of the design-manufacturing mesh as a 2D vector field, a relationship between the tow-path curvature and the vector field curl can be developed [150,168]. This allows the designer to use the design-manufacturing mesh to mathematically define the curvature steering constraint at the ply level during the fiber angle retrieval step, thus improving the manufacturability of the designed variable stiffness structure. In addition, it also gives insight into how much steering is required by the AFP machine to match the optimal fiber orientation angles and hence the stiffness properties for a structural design problem. The use of an average

steering curvature constraint in the second step is an effective strategy in finding steered paths with a controlled amount of steering and reducing the possible number of course dropping in the third optimization step.

The relationship between the curl of the vector field and the curvature is valid for both developable (such as cylinder or cone) and non-developable surfaces (such as sphere). Considering a surface that is defined in a parametric form $r(u, v)$, where u and v are the surface curvilinear parametric coordinates, the vector field for each element of the design-manufacturing mesh can be written as a function of the surface unit vectors $\vec{e}_u$ and $\vec{e}_v$ as:

$$\vec{v} = \cos\varphi_{uv}\,\vec{e}_u + \sin\varphi_{uv}\,\vec{e}_v\,, \tag{3.33}$$

where $\sin\varphi_{uv}$ is defined as the bilinear *sine* angle variation along u and v surface directions. A curvilinear coordinate system is local since the direction of the unit vectors $\vec{e}_u$ and $\vec{e}_v$ change as a function of the location of the coordinates. The path curvature vector contains the geodesic curvature κ_g (in-plane) and the normal curvature κ_n (out-of-plane). For the maximum steering constraint on surfaces, the geodesic curvature κ_g (in-plane) determines the amount of steering that is required by the AFP head to follow a steered path. The geodesic curvature can be obtained by evaluating the curl of the vector field in the orthogonal parametric coordinate system and project it on to the local surface normal direction, $\vec{e}_w$. This would represent the circulation around the axis normal to the surface, which defines the in-plane curvature of the path. The curl for an orthogonal parametric coordinate system can be expressed as [168]:

$$\begin{aligned} &\kappa_g = (\nabla \times \vec{v}).\vec{e}_w = \frac{1}{h_u h_v}\left(\frac{\partial(h_v v_v)}{\partial u} - \frac{\partial(h_u v_u)}{\partial v}\right), \\ &h_u = \left\|\frac{\partial \vec{r}}{\partial u}\right\|, \qquad\qquad h_v = \left\|\frac{\partial \vec{r}}{\partial v}\right\|. \end{aligned} \tag{3.34}$$

The expression for the geodesic curvature in Eq. (3.34) can be simplified for different surfaces using the bilinear *sine* angle variation; the cases of a plate, a cylindrical shell, and a conical shell are considered here:

Plate:

The parametric equation for a plate can be expressed as:

$$x = \boldsymbol{u}\,, \qquad y = \boldsymbol{v}\,, \qquad z = C\,,$$

$$h_u = h_x = \sqrt{\left(\frac{\partial x}{\partial u}\right)^2 + \left(\frac{\partial y}{\partial u}\right)^2 + \left(\frac{\partial z}{\partial u}\right)^2} = 1 \tag{3.35}$$

$$h_v = h_y = \sqrt{\left(\frac{\partial x}{\partial v}\right)^2 + \left(\frac{\partial y}{\partial v}\right)^2 + \left(\frac{\partial z}{\partial v}\right)^2} = 1$$

The local coordinates $\{x, y\}$ can be used for the geodesic curvature definition on a plate. Considering the vector field for a plate as $\vec{v} = \underbrace{\cos\varphi_{xy}}_{v_u}\,\vec{\imath} + \underbrace{\sin\varphi_{xy}}_{v_v}\,\vec{\jmath}$, The curvature of the vector field can be calculated using Eq. (3.34) to obtain the magnitude of the circulation defining the curvature (along $\vec{k}$) as:

$$\kappa_{xy} = \underbrace{\frac{\partial\varphi_{xy}}{\partial x}\cos\varphi_{xy}}_{Axial\ Angle\ Variation} + \underbrace{\frac{\partial\varphi_{xy}}{\partial y}\sin\varphi_{xy}}_{Transverse\ Angle\ Variation}\,, \tag{3.36}$$

By taking the derivatives of φ_{xy} in Eq. (3.32) with respect to x and y, and replacing the values in Eq. (3.36) we obtain the curvature definition (easier to express in terms of a, b, c, and d) as:

$$\kappa_{xy} = b + dy + \frac{(c+dx)(a+bx+(c+dx)y)}{\sqrt{1-(a+bx+(c+dx)y)^2}}\,, \tag{3.37}$$

where each of the coefficients can be expressed as:

$$
\begin{aligned}
a &= \frac{x_1(\sin[\varphi_{00}]y_1 - \sin[\varphi_{01}]y_0) + x_0(\sin[\varphi_{11}]y_0 - \sin[\varphi_{10}]y_1)}{(x_1 - x_0)(y_1 - y_0)}, \\
b &= \frac{(\sin[\varphi_{01}] - \sin[\varphi_{11}])y_0 + (\sin[\varphi_{10}] - \sin[\varphi_{00}])y_1}{(x_1 - x_0)(y_1 - y_0)}, \\
c &= \frac{(\sin[\varphi_{10}] - \sin[\varphi_{11}])x_0 + (\sin[\varphi_{01}] - \sin[\varphi_{00}])x_1}{(x_1 - x_0)(y_1 - y_0)}, \\
d &= \frac{\sin[\varphi_{00}] - \sin[\varphi_{01}] - \sin[\varphi_{10}] + \sin[\varphi_{11}]}{(x_1 - x_0)(y_1 - y_0)},
\end{aligned}
\tag{3.38}
$$

Note that from Eq. (3.37), κ_{xy} is constant when both c and d are zero. By inspecting Eq. (3.42), this is achieved when $\sin[\varphi_{10}] = \sin[\varphi_{11}]$ and $\sin[\varphi_{01}] = \sin[\varphi_{00}]$, which satisfies the condition for having only an axial fiber angle variation (along u or x for the plate case), because of the definition of the bilinear *sine* angle variation. By analyzing the curvature of the vector fields of the plate example in Figure 3.5, a contour plot in Figure 3.6 shows that the curvature of each vector field in each element of the design-manufacturing mesh is constant. This is because only axial fiber angle variation was used when defining the fiber angles at the control points. This might be a beneficial aspect for simplifying some design problems, but generally this is not the case when the fiber angles at the control points are considered as design variables in the optimization problem, since the structure being designed might require fiber angle variations along both parametric coordinate directions to provide an improved load redistribution mechanism. The use of the bilinear *sine* angle variation allows the fiber angle variation to be a function of both parametric coordinates while still maintaining the smoothness of the fiber angle variation.

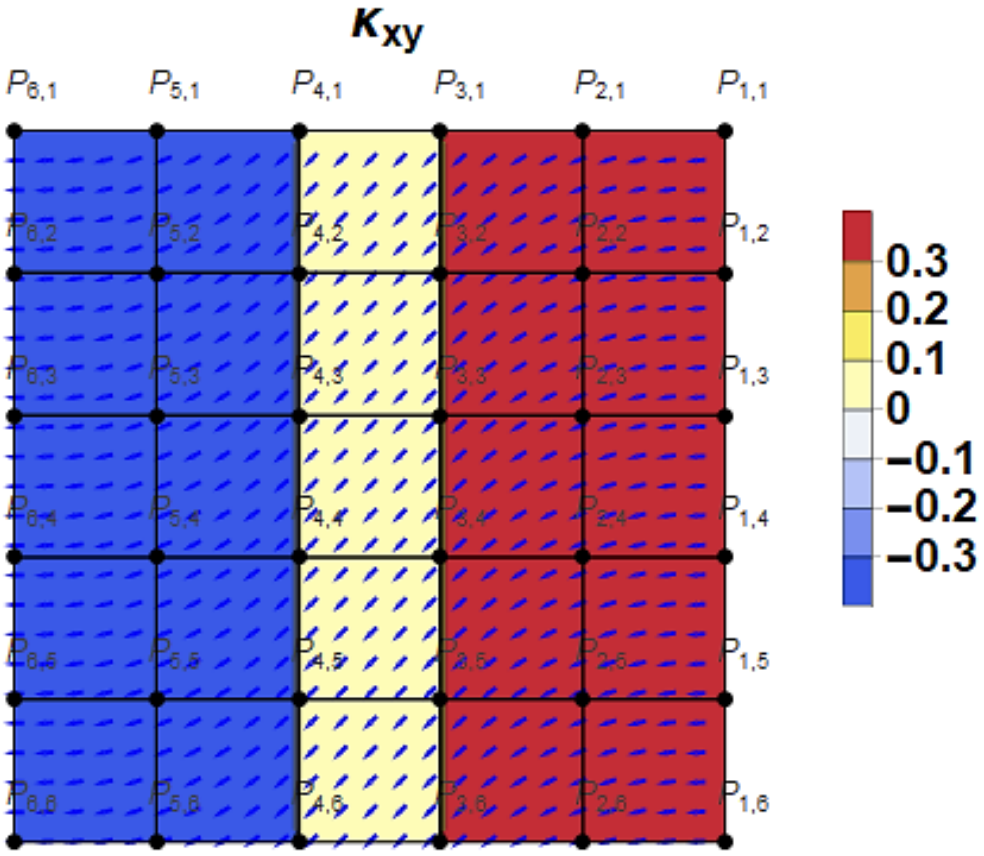

Figure 3.6: Curvature analysis of bilinear *sine* angle variation example with axial angle variation over plate domain

Cylindrical Shell:

The parametric equation for a cylinder can be expressed in Cylindrical coordinates, where R is the radius of the cylinder:

$$x = R\cos\boldsymbol{\theta}\,, \qquad y = R\,sin\,\boldsymbol{\theta}\,, \qquad z = \boldsymbol{z}\,,$$

$$h_u = h_z = \sqrt{\left(\frac{\partial x}{\partial z}\right)^2 + \left(\frac{\partial y}{\partial z}\right)^2 + \left(\frac{\partial z}{\partial z}\right)^2} = 1 \tag{3.39}$$

$$h_v = h_\theta = \sqrt{\left(\frac{\partial x}{\partial \theta}\right)^2 + \left(\frac{\partial y}{\partial \theta}\right)^2 + \left(\frac{\partial z}{\partial \theta}\right)^2} = R$$

The local coordinates $\{z, \theta\}$, which are the longitudinal and circumferential surface coordinates, can be used for the geodesic curvature definition on a cylindrical shell. Considering the vector field for a cylinder as $\vec{v} = \underbrace{\cos\varphi_{z\theta}}_{v_u}\vec{z} + \underbrace{\sin\varphi_{z\theta}}_{v_v}\vec{\theta}$, The curvature of the vector field can be calculated using Eq. (3.34) to obtain the magnitude of the circulation defining the curvature (along $\vec{r}$) as:

$$\kappa_{z\theta} = \underbrace{\frac{\partial\varphi_{z\theta}}{\partial z}\cos\varphi_{z\theta}}_{Axial\ Angle\ Variation} + \underbrace{\frac{\partial\varphi_{z\theta}}{R\,\partial\theta}\sin\varphi_{z\theta}}_{Circumferential\ Angle\ Variation}, \tag{3.40}$$

By taking the derivatives of $\varphi_{z\theta}$ in Eq. (3.32) with respect to z and θ, and replacing the values in Eq. (3.40) we obtain the curvature definition as:

$$\kappa_{z\theta} = b + d\theta + \frac{(c+dz)(a+bz+(c+dz)\theta)}{R\sqrt{1-(a+bz+(c+dz)\theta)^2}}, \tag{3.41}$$

where each of the coefficients can be expressed as:

$$\begin{aligned}
a &= \frac{z_1(\sin[\varphi_{00}]\theta_1 - \sin[\varphi_{01}]\theta_0) + z_0(\sin[\varphi_{11}]\theta_0 - \sin[\varphi_{10}]\theta_1)}{(z_1-z_0)(\theta_1-\theta_0)},\\
b &= \frac{(\sin[\varphi_{01}] - \sin[\varphi_{11}])\theta_0 + (\sin[\varphi_{10}] - \sin[\varphi_{00}])\theta_1}{(z_1-z_0)(\theta_1-\theta_0)},\\
c &= \frac{(\sin[\varphi_{10}] - \sin[\varphi_{11}])z_0 + (\sin[\varphi_{01}] - \sin[\varphi_{00}])z_1}{(z_1-z_0)(\theta_1-\theta_0)},\\
d &= \frac{\sin[\varphi_{00}] - \sin[\varphi_{01}] - \sin[\varphi_{10}] + \sin[\varphi_{11}]}{(z_1-z_0)(\theta_1-\theta_0)},
\end{aligned} \tag{3.42}$$

Since the cylinder can be developed to a flat plate in 2D (zero Gaussian curvature), the same expression can be obtained from the definition of the geodesic curvature for a plate by replacing the parametric coordinates with the expressions that maintain the same differential lengths between the unrolled cylinder and the cylindrical surface, which can be expressed as $dz = dx$ and $Rd\theta = dy$.

Conical Shell:

The parametric equation for a cone can be expressed in Spherical coordinates, where α is a constant representing the angle of the cone:

$$x = \boldsymbol{\rho} \sin\alpha \ cos\ \boldsymbol{\theta}, \qquad y = \boldsymbol{\rho} \sin\alpha \ sin\ \boldsymbol{\theta}, \qquad z = \boldsymbol{\rho} \cos\alpha,$$

$$h_u = h_\rho = \sqrt{\left(\frac{\partial x}{\partial \rho}\right)^2 + \left(\frac{\partial y}{\partial \rho}\right)^2 + \left(\frac{\partial z}{\partial \rho}\right)^2} = 1 \tag{3.43}$$

$$h_v = h_\theta = \sqrt{\left(\frac{\partial x}{\partial \theta}\right)^2 + \left(\frac{\partial y}{\partial \theta}\right)^2 + \left(\frac{\partial z}{\partial \theta}\right)^2} = \boldsymbol{\rho} \sin\alpha$$

The local coordinates $\{\rho, \theta\}$, which are the longitudinal and circumferential conical surface coordinates, can be used for the geodesic curvature definition on a conical shell. Considering the vector field for a conical shell as $\vec{v} = \underbrace{\cos\varphi_{\rho\theta}}_{v_u}\vec{\rho} + \underbrace{\sin\varphi_{\rho\theta}}_{v_v}\vec{\theta}$, The curvature of the vector field can be calculated using Eq. (3.34) to obtain the magnitude of the circulation defining the curvature (along $\vec{\phi}$) as:

$$\kappa_{\rho\theta} = \frac{\sin\varphi_{\rho\theta}}{\rho} + \frac{\partial\varphi_{\rho\theta}}{\partial\rho}\cos\varphi_{\rho\theta} + \frac{\partial\varphi_{\rho\theta}}{\partial\theta}\frac{\sin\varphi_{\rho\theta}}{\rho\sin\alpha}, \tag{3.44}$$

This is analogous to the curvature vector derived by Blom [169]. The ρ coordinate represents the conical longitudinal surface coordinate defined by the distance between the cone vertex to a point on the cone surface. The relationship between the cone radius and the spherical coordinate ρ is a function of the cone angle α:

$$\boldsymbol{\rho} = \frac{\boldsymbol{r}}{\sin\alpha}, \tag{3.45}$$

The curvature of the vector field along the can then be expressed as:

$$\kappa_{\rho\theta} = \underbrace{\frac{\sin\alpha \sin\varphi_{\rho\theta}}{r}}_{Cone\ Geometry} + \underbrace{\frac{\partial\varphi_{\rho\theta}}{\partial\rho}\cos\varphi_{\rho\theta}}_{Axial\ Angle\ Variation} + \underbrace{\frac{\partial\varphi_{\rho\theta}}{\partial\theta}\frac{\sin\varphi_{\rho\theta}}{r}}_{Circumferential\ Angle\ Variation}, \quad (3.46)$$

By taking the derivatives of $\varphi_{\rho\theta}$ in Eq. (3.32) with respect to ρ and θ, and replacing the values in Eq. (3.44) we obtain the curvature definition as:

$$\kappa_{\rho\theta} = b + d\theta + \frac{a + b\rho + c\theta + d\rho\theta}{\rho} + \frac{(c + d\rho)(a + b\rho + c\theta + d\rho\theta)}{\rho \sin\alpha \sqrt{1 - (a + b\rho + c\theta + d\rho\theta)^2}}, \quad (3.47)$$

where each of the coefficients can be expressed as:

$$\begin{aligned}
a &= \frac{\rho_1(\sin[\varphi_{00}]\theta_1 - \sin[\varphi_{01}]\theta_0) + \rho_0(\sin[\varphi_{11}]\theta_0 - \sin[\varphi_{10}]\theta_1)}{(\rho_1 - \rho_0)(\theta_1 - \theta_0)}, \\
b &= \frac{(\sin[\varphi_{01}] - \sin[\varphi_{11}])\theta_0 + (\sin[\varphi_{10}] - \sin[\varphi_{00}])\theta_1}{(\rho_1 - \rho_0)(\theta_1 - \theta_0)}, \\
c &= \frac{(\sin[\varphi_{10}] - \sin[\varphi_{11}])\rho_0 + (\sin[\varphi_{01}] - \sin[\varphi_{00}])\rho_1}{(\rho_1 - \rho_0)(\theta_1 - \theta_0)}, \\
d &= \frac{\sin[\varphi_{00}] - \sin[\varphi_{01}] - \sin[\varphi_{10}] + \sin[\varphi_{11}]}{(\rho_1 - \rho_0)(\theta_1 - \theta_0)},
\end{aligned} \quad (3.48)$$

Since the cone can also be developed in 2D, the same expression can be derived from the developed cone configuration, where the surface coordinates in 2D are the radial distance ρ, and the circumferential coordinate $\beta = \theta \sin\alpha$ [169]. The geodesic curvature of path on a cone's surface depends on the variation of the fiber orientation angle as well as the cone geometry.

The inclusion of the fiber steering constraint in the fiber angle retrieval step makes the fiber path construction an easier process. However, the steering constraint at the ply level should not correspond to the critical steering radius that is defined locally along the path of a steered fiber course. The steering constraint in the second optimization step does not account for the additional manufacturing capability of the AFP machine, which is the

possibility of course dropping. By defining the steering constraint locally in the third optimization step, optimal non-linear fiber angle variation can be matched closely although this might result in discontinuities between intersection fiber courses. The utilization of the steering constraint at the ply level helps in decreasing the number of course drops obtained at the third step, and hence generate smoother fiber discontinuities. Even if the steering constraint is not applied at the ply level, the paths generated in the fiber construction step should satisfy the steering constraint locally while matching the fiber orientation angles as close as possible.

3.3.2 Genetic Algorithms

The objective of the Stacking Sequence Retrieval step is to find the closest laminate stacking sequences that would generate the optimum lamination parameter or stiffness distribution that were obtained in the first optimization step. However, since the relationship between the lamination parameters and a stacking sequence is not unique, there are no closed-form solutions to obtain equal-thickness discrete layers from given lamination parameters. Hence, multiple stacking sequence designs may represent feasible solutions that closely match the optimum stiffness properties obtained from the first optimization step.

Obtaining the realistic stacking sequences that would match the optimum stiffness properties is designated as the inverse problem. The first optimization step is characterized by desirable properties such as the convexity of the design problem as discussed in Section 3.2.2. However, when retrieving the optimal stacking sequences, it is well known that the optimization problem is always non-convex in the space of fiber orientation angles because it is non-bijective. Gradient-based algorithms can only guarantee solution convergence to

a local optimum, which means a suitable initial stacking sequence must be used to ensure solutions are found to capture the performance gains of the theoretical stiffness optimum. In order to circumvent the problem of falling into local optima in the inverse problem, gradient-based algorithms were masked by direct stochastic search algorithms. Genetic algorithms (GAs) are by far the most popular stochastic methods dealing with stacking sequence design in terms of fiber angles [29]. Genetic algorithms are population-based search algorithms inspired by the application of Darwin's principle of survival of the fittest, and they mimic the process of natural selection and evolution found in nature. The principle of natural evolution can be transferred to structural laminate optimization problems by determining the optimal stacking sequences that generate the best performance or maximum fitness. The design space is explored by a group of individuals, where the better designs or the fittest individuals have a higher chance in transferring their superior genetic coding or design characteristics to subsequent generations.

The objective of laminate stacking sequence design is to determine the required number of layers in a laminate, each layer's fiber orientation angle that are chosen from a discrete set (constituent angles), and their ordering or stacking sequence. Because of the discrete nature of coding of a genetic algorithm, these features can be easily integrated. The discrete design variables involved may be encoded in the form of integer or binary encoding. Encoding designates a suitable format for the genetic algorithm to express the design variables. Once having decided how to encode the discrete design variables, they can be grouped together to form a *chromosomes* [170]. The characters in the string forming a chromosome are referred to as *genes*. The set of chromosomes involved is referred to as a *genotype*. A genetic algorithm is initiated with a population of individual genotypes,

where the individuals or stacking sequences are ranked based on their fitness function values. Designs with a better fitness function have a higher chance for being selected for the generation of new individuals. The new individuals are obtained using genetic operators such as crossover and mutation. The crossover operator randomly selects parts of the chromosomes of the two crossing genotypes for exchange, where as mutation randomly alters part of the chromosome in a single genotype to maintain diversity. The new generation is assembled to form a new generation of genotypes.

Evolutionary algorithms are the most widely used in the conversion step because of their discrete nature. A major benefit of using a genetic algorithm is that it does not require gradient information, and the population search can cover the full design space and may end up in near global optima in several cases. One drawback is that genetic algorithms require a huge number of function evaluations, hence the reason they are used in the second optimization step and are not coupled with finite element analyses. As a result, the fitness function used is essential to transition from the optimum stiffness properties to the stacking sequence design to maintain the efficiency of the optimization framework.

In the second optimization step, the stacking sequence design for each control point can be obtained using a genetic algorithm developed for stacking sequence design with arbitrary fiber orientation angles chosen as design variables. The genetic algorithm used in this work was developed by Dr. Brian Tatting based on previous research concerning stacking sequence optimization [23,171]. The genetic algorithm can be used with arbitrary user-defined fiber orientation angles and has the capability of including laminate design guidelines [151]. The elitist strategy is used, where a small number of individuals in the parent population are maintained through successive generations. These individuals have

the best fitness functions and are called elite individuals. Several genetic operators are used in the genetic algorithm to generate new individuals from the parent population, namely crossover, mutation, permutation, and ply swapping. For more details about stacking sequence optimization using genetic algorithms, the reader is also referred to [27,153,170,172].

3.3.3 Fitness functions for Stacking Sequence Retrieval

The selection process in genetic algorithms requires a fitness function to rank the individuals in the population and give the better designs a higher chance to breed and pass on their genetic coding to future generations. The fitness functions can be defined as the objective functions (for maximization) or minus the objective (for minimization). The fitness function defined in the second optimization step is important to obtain the optimal stacking sequences that match the optimal stiffness properties from the first optimization step. To retrieve the optimal stacking sequences, a homogeneous distance in stiffness space can be used as the fitness function to be minimized. The genetic algorithm is used to obtain the closest stacking sequence having the desired optimum stiffnesses obtained from the first optimization problem $[A_i^*]$ and $[D_i^*]$. The fitness function to be minimized at each control point i is presented as [147]:

$$
\begin{aligned}
d_{AD}^* &= 2\sqrt{M_1 M_2} - M_3 \,, \\
M_1 &= \frac{1}{6}\left(A_i : A_i^{*-1}\right) + \frac{1}{54}\left(D_i : D_i^{*-1}\right) \,, \\
M_2 &= \frac{1}{6}\left(A_i^{-1} : A_i^*\right) + \frac{1}{54}\left(D_i^{-1} : D_i^*\right) \,, \\
M_3 &= \frac{10}{9} \,,
\end{aligned}
\tag{3.49}
$$

where 1/6 and 1/54 scaling terms take into consideration the linear and cubic dependency of the membrane and bending stiffness matrices on the laminate thickness, respectively; d_{AD}^{*} approaches zero when the optimal stacking sequence identically represents the stiffness matrices A_i^* and D_i^*. The laminates with the minimum distance and closest stiffness values would represent the optimal stacking sequences for this fitness function.

By using the homogeneous distance measure in stiffness space, it is assumed that each lamination parameter contributes equally to the design objective in the first optimization step and that the optimum stiffness matrices obtained from the first optimization step are the global optimum values. The homogeneous distance in stiffness space can be described as a blind fiber angle retrieval formulation, which means that it is a post-processing step that does not consider the structural design objective function that is used in the first optimization step. To improve the fitness function, the sensitivities of the structural response with respect to the design variables (lamination parameters) must be included in the fitness function. This provides a guarantee that, at least in the close vicinity of the design point that is obtained from the first optimization step, the obtained stacking sequence has a directional distance in the stiffness space that provides a better structural response than a blind closest distance. In the space of lamination parameters, an improved fitness function applied at each control point can be expressed as:

$$f_{GA} = \left(\sum_{i=1}^{4} \frac{\left(\frac{\partial f_s}{\partial V_i}\right)^*}{f_s{}^*} (V_i - V_i^*) + \frac{\left(\frac{\partial f_s}{\partial W_i}\right)^*}{f_s{}^*} (W_i - W_i^*) \right)^2 , \tag{3.50}$$

where f_s is the structural response under consideration in the first optimization step, $f_s{}^*$ is the optimal response at the final design point, and $\left(\frac{\partial f_s}{\partial V_i}\right)^*$ are the values of the sensitivities

of the response with respect to the lamination parameters evaluated at the final design point (V_{1-4}^{*}, W_{1-4}^{*}). The sensitivities distinguish the relative importance of each design variable on the structural response to find a stacking sequence that better matches the structural response at the final design point. In addition, the sign of each design sensitivity considers the effect of the directionality on the structural response, which is a beneficial property of gradient-based optimization. The sensitivities of the response with respect to V_2, V_4, W_2, W_4 are included to make sure the extension-shear coupling and bending-twisting coupling terms are minimal if they have a significant effect on the structural response (or in other cases closest to the optimum lamination parameters that include shear and twisting properties). As a result, the fitness function favors stacking sequences that generate an optimal structural response even if the distance to the optimum lamination parameters is greater. If all the lamination parameters of the retrieved stacking sequence match the optimum lamination parameters, the fitness function reduces to zero and the stacking sequence obtained yields the optimum stiffness properties.

The manufacturability of the obtained fiber distribution must be also considered in the second optimization step to guarantee a certain level of fiber angle manufacturability for the third optimization step. The ply steering constraint as described in Section 3.3.1 can be included in the fitness function of the genetic algorithm by using a penalty approach [145]. The ply steering constraint g is first normalized with the allowable steering constraint defined by the user κ_{all} as:

$$g = \frac{\kappa_{uv}}{\kappa_{all}} - 1 \ , \tag{3.51}$$

The critical steering constraint g_{max} can then be included in the improved fitness function using an augmented objective function. However, when the steering constraint is

applied in the second optimization step, the inverse problem cannot be solved independently at each control point. The fitness function for the genetic algorithm must include the summation of the individual f_{GA} at each control point as well. The augmented fitness function is therefore expressed as:

$$\Psi_{GA} = \begin{cases} \frac{1}{N}\sum_{i}^{N} {f_{GA}}^{i} + \alpha g_{max} \quad if \;\; g_{max} \leq 0 \\ \frac{1}{N}\sum_{i}^{N} {f_{GA}}^{i} + \beta g_{max} \;\; if \;\; g_{max} > 0 \end{cases}, \tag{3.52}$$

where Ψ_{GA} is minimized to obtain the optimal stacking sequences at each control point i for N control points of the design-manufacturing mesh, α is a bonus factor that is very small and β is a penalty factor that is large to penalize the violation of the steering constraint.

3.3.4 Fiber Angle Retrieval Scheme

The steps of the Stacking Sequence Retrieval step are summarized in Figure 3.7. Design guidelines and manufacturing constraints are required for genetic algorithm along with a random seed to generate random individuals in the second optimization step. The diagram is kept for general purpose, so that a genetic algorithm may use different material properties $\Gamma_{i,j}$ to match the optimum stiffness properties. The second optimization step outputs the optimal fiber angle distribution ${\theta_{k_i}}^{*}$ for the Fiber Path Construction i.e. the stacking sequence at each control point i, and the actual response f_{Actual}, which usually show a reduction in the performance improvements compared to the theoretical responses $f_{Theoretical}$. The ultimate failure load can also be obtained from detailed analysis of the retrieved stacking sequences and corresponding fiber angle distribution defined by the

bilinear *sine* angle variation. The Fiber Angle Retrieval step contains the following components:

- Genetic Algorithm: Obtain the optimal fiber angle distribution matching the optimum stiffness properties subject to industry design guidelines and manufacturing constraints. A random seed is used to ensure a random stacking sequence is generated for the population
- Fiber Angle Distribution: Define the spatial fiber angle distribution using the bilinear *sine* angle variations and obtain the curvatures of the vector fields κ_{uv}
- Fitness Evaluation: Evaluate the fitness of each individual in the population using the augmented fitness function to identify the elite laminate designs. The elitist strategy is used, where a few optimal stacking sequences are maintained between successive iterations
- Selection Mechanism: Rank the individuals in the population to give a higher chance for selecting the optimal laminate designs that match the stiffness properties while satisfying the laminate design rules and manufacturing constraints
- Genetic Operators: Crossover, mutate, interchange, permute, and swap individuals in the population to generate new individuals and eventually converge to the optimal laminate fiber angle distributions. The probabilities of each genetic operator can be fine-tuned to obtain the optimal laminate designs
- Finite Element Analysis: The retrieved optimal stacking sequences with variable fiber angle variations are then analyzed using detailed linear analyses and non-linear analysis with progressive failure analysis to predict the actual responses, and the ultimate failure load of the laminate

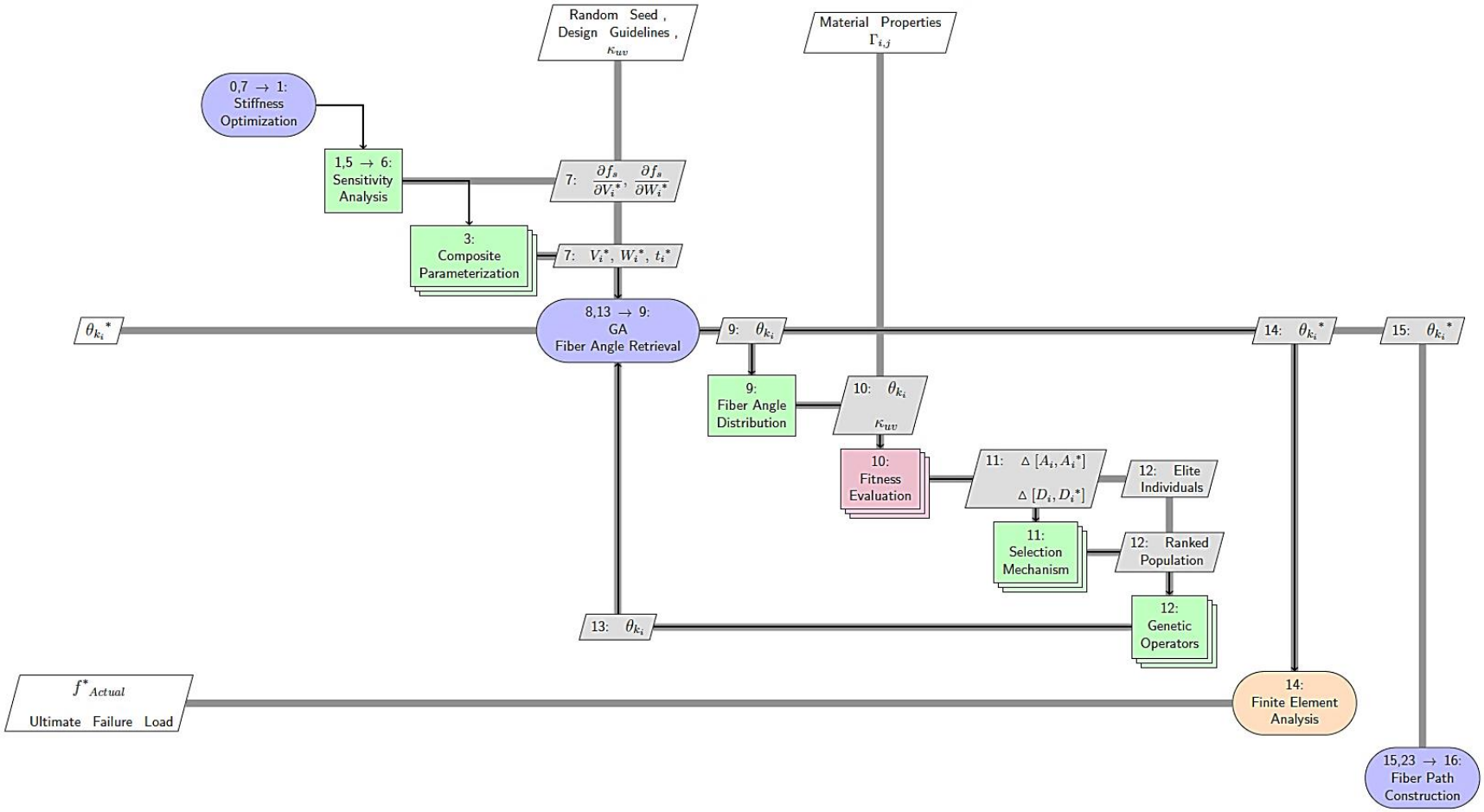

Figure 3.7 XDSM diagram for Stacking Sequence Retrieval

3.4 FIBER PATH CONSTRUCTION

In the third optimization step, the goal is to construct the continuous manufacturable fiber paths from the retrieved fiber angle distributions obtained from the second optimization step. The difficulty in this step lies in matching the optimal fiber orientation angles while satisfying the manufacturing constraints imposed by the AFP machine. The constructed fiber paths can then be supplied to the fiber placement machine for manufacturing. To generate a fiber-steered layup, multiple tows are required to be placed adjacently. Two well-known layup strategies for a fiber-steered layup are the parallel and shifted layup strategies, where the adjacent steered tows are derived from one reference curve. However, using a parallel or shifted fiber layup strategy does not necessarily match the optimal fiber angle distributions obtained from the second optimization step. In general, the optimal fiber angle distributions can only be matched by considering several independent reference curves, also called guide curves.

The use of the bilinear *sine* angle variations in each element of the design-manufacturing mesh introduces an important benefit for the third optimization step, where a constant curvature arc solution for each element can be obtained to closely match the optimal fiber orientation angles. The construction of a manufacturable fiber path is then represented through an assembly of piecewise constant curvature arcs that allow local tailoring in each element of the design-manufacturing mesh.

A design-for-manufacturing tool was developed in Mathematica® for generating manufacturable fiber paths that match the designed fiber angle distributions of the design-manufacturing mesh while satisfying AFP manufacturing constraints. The developed methodology for the tool in this work can be used with developable surfaces (isometric),

since the preservation of the differential lengths between the 3D surface and the developed configuration in 2D is required to maintain the same geodesic curvature of the designed fiber paths. However, the concept can also be extended for general 3D surfaces. The maximum steering constraint is applied locally for each fiber path to guarantee the manufacturability, while allowing course centerline intersections to match highly non-linear fiber angle distributions. If a steering constraint is not applied at the second optimization step (ply level), the fiber angle can be matched at an expense of having fiber angle discontinuities between some fiber paths because of the tow-dropping capability that is included in the design-for-manufacturing tool. Each individual course is modeled as an independent guide curve to match the optimal fiber angle distribution from the second optimization step while accounting for AFP manufacturing constraints. Tow-by-tow descriptions of the steered plies can then be generated in the form of manufacturing boundaries for the AFP machine with optimized cut and restart positions.

3.4.1 Constant Curvature Arc Solution and Maximum Curvature Constraint

The design-manufacturing mesh is an important element that is used to make the transition from the fiber angle distribution to the manufacturable fiber paths. The bilinear *sine* angle variation distribution is used to obtain a constant curvature arc solution that matches the optimal fiber orientation angle at the edge of each element starting from an arbitrary point and initial angle within the domain of each element. Using the geometry of a constant curvature arc and the bounds of each element of the design-manufacturing mesh as shown in Figure 3.8, a constant curvature arc solution can be obtained within each element of the design-manufacturing mesh.

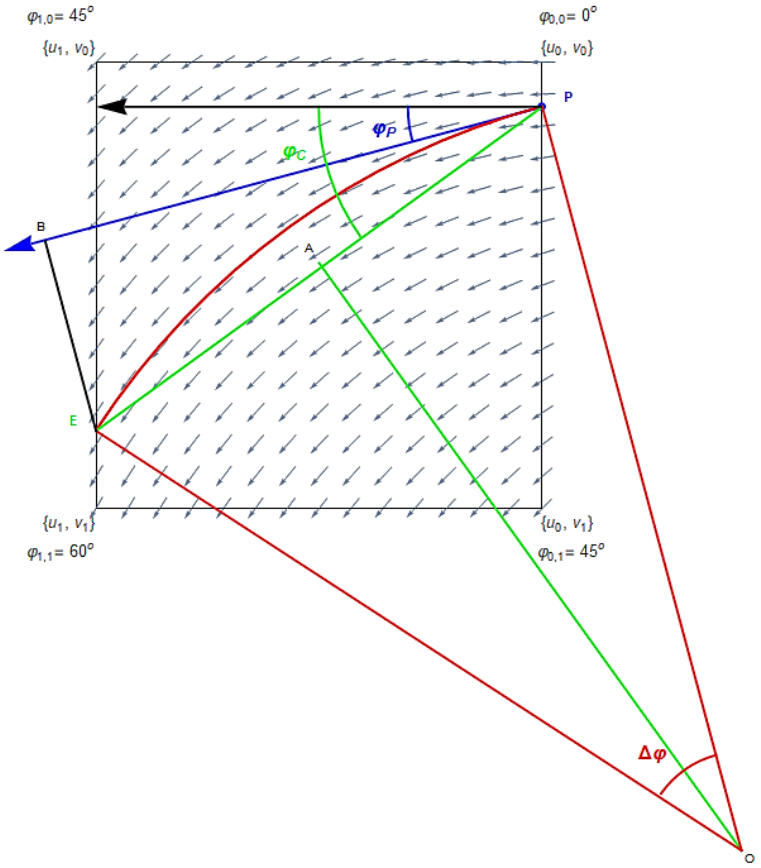

Figure 3.8: Constant curvature arc example for an element of design-manufacturing mesh

A non-linear solution can be found to match the angles at the edges of an element defined by the bilinear *sine* angle variation presented in Section 3.3.1, which is repeated here for convenience:

$$\sin\varphi_{uv} = \frac{\sin[\varphi_{11}](u-u_0)(v-v_0)}{(u_1-u_0)(v_1-v_0)} + \frac{\sin[\varphi_{01}](u-u_1)(v_0-v)}{(u_1-u_0)(v_1-v_0)} + \frac{\sin[\varphi_{00}](u-u_1)(v-v_1)}{(u_1-u_0)(v_1-v_0)} + \frac{\sin[\varphi_{10}](u-u_0)(v_1-v)}{(u_1-u_0)(v_1-v_0)} \tag{3.53}$$

The green line from P to E represents the chord for the given circular arc, which starts from an arbitrary starting point P with a given initial angle φ_P to match the fiber orientation angle φ_E at point E. The use of the chord including the calculations for its length C and orientation φ_C with respect to the u axis enable a reasonably straightforward

non-linear solution to find the correct value of the arc curvature that matches the angle φ_E at point E with coordinates $\{u_E, v_E\}$. The curvature of the arc is $\kappa = {}^{1}/_{\rho}$, where ρ is the radius of the circle with center O outside the domain of the element. The angle subtended by the arc is defined by $\Delta\varphi$.

The constant curvature arc solution is intended to find the value of κ that would satisfy the edge angle requirements as described above. The non-linear solution that would match the fiber orientation angle at the edge can be expressed in terms of the bilinear *sine* angle variation in Eq. (3.53) as:

$$\sin[\varphi_{\mathrm{uv}}(u_E, v_E)] - \sin[\varphi_P + \Delta\varphi] = 0 \tag{3.54}$$

Using the geometry in Figure 3.8, the chord length C can be expressed as a function of $\Delta\varphi$ and the arc curvature κ as:

$$C = \frac{2\sin\left[{}^{\Delta\varphi}/_{2}\right]}{\kappa}\ , \tag{3.55}$$

To find the root of Eq. (3.54), the intermediate variables can be expressed as functions of the chord length C, and the input variables which are defined by the position of point P as $\{u_P, v_P\}$ and the initial angle φ_P. The solution depends on the fiber orientation angles defined at the control points of the element of the design-manufacturing as well as the initial starting point and angle defining the constant curvature arc. For example, two solutions exist for two edges of the element considered if point P starts at an arbitrary point within the domain (not at the edges). The solution corresponding to the example given in Figure 3.8 is presented here for a rectangular domain, and the solution for the remaining edges can be derived in a similar manner.

The chord line can be parameterized as a straight line to find the coordinate values of point E at the edge as:

$$\begin{aligned} u_E &= u_P + C\cos[\varphi_C] \ , \\ v_E &= v_P + C\sin[\varphi_C] \ , \end{aligned} \tag{3.56}$$

The cosine of the chord angle φ_C for a chord intersecting with the left edge of the element can be determined by replacing u_E with u_1 to obtain:

$$\cos[\varphi_C] = \frac{u_1 - u_P}{C} \ , \tag{3.57}$$

Using the trigonometric identity, we can obtain the sine of the chord angle φ_C as:

$$\sin[\varphi_C] = \frac{\sqrt{C^2 - (u_1 - u_P)^2}}{C} \ , \tag{3.58}$$

For the solution of the left edge, we can then express the coordinates of point E as:

$$\begin{aligned} u_E &= u_1 \ , \\ v_E &= v_P + \sqrt{C^2 - (u_1 - u_P)^2} \ , \end{aligned} \tag{3.59}$$

By replacing the coordinates of point E in the bilinear *sine* angle variation defined in Eq. (3.53), we can obtain the angle variation of the left edge of the element as:

$$\begin{aligned} \sin[\varphi_{\mathrm{uv}}(u_E, v_E)] = {} & \frac{\sin[\varphi_{11}]\left(v_P + \sqrt{C^2 - (u_1 - u_P)^2} \ - v_0\right)}{(v_1 - v_0)} \\ & + \frac{\sin[\varphi_{10}](v_1 - v_P - \sqrt{C^2 - (u_1 - u_P)^2} \ )}{(v_1 - v_0)} \end{aligned} \tag{3.60}$$

The second term in Eq. (3.54) can be obtained from the geometry in Figure 3.8, where we have the following relation:

$$\Delta\varphi = 2(\varphi_C - \varphi_P) \ , \tag{3.61}$$

As a result, we can express the second term as:

$$\sin[\varphi_P + \Delta\varphi] = \sin[\varphi_E] = \sin[2\varphi_C - \varphi_P]\,, \tag{3.62}$$

Using trigonometric formulations and replacing the expressions of equations (3.57) and (3.58) into Eq. (3.62), the second term can be simplified as:

$$\begin{aligned}\mathrm{Sin}[\varphi_P + \Delta\varphi] = &\frac{2\sqrt{C^2 - (u_1 - u_P)^2}\,(u_1 - u_P)\cos\varphi_P}{C^2} \\ &+ \frac{(C^2 - 2(u_1 - u_P)^2)\sin\varphi_P}{C^2}\,,\end{aligned} \tag{3.63}$$

As a result, the only variable to solve for in Eq. (3.54) is the chord length C, since the initial arbitrary point variables $\{u_P, v_P, \varphi_P\}$ are considered given or correspond to the design variables of each manufacturable fiber path. The domain of the element is defined by the design-manufacturing mesh used. A certain value of the chord length must be found to match the fiber orientation angles at the edges of the element while constraining the chord length to a positive value in the domain starting from point P. In addition, for a positive ply defined by positive fiber orientation angles $0^o \leq \varphi \leq \pi/2$ at the control points of the element, the chord angle φ_C is bounded between $\varphi_P/2$ and $\pi/2$. The solution can be used to obtain constant curvature solutions with both positive and negative values of curvatures depending on the starting point and the optimal fiber orientation angles at the control nodes. After obtaining the chord length that matches the fiber orientation angle at the edge, we can obtain all the other variables $\{v_E, \varphi_C, \Delta\varphi, \varphi_E\}$, and the curvature of the arc is obtained using Eq. (3.55).

The constant curvature arc solution defined above provides the optimal constant curvature arc without regard for the maximum allowable curvature. If a steering constraint is applied at the second optimization step (ply level), then the solution presented is sufficient to match the optimal fiber orientation angles. However, if the obtained curvature,

that matches the angle at the edge point E, is higher in absolute value than the maximum allowable steering curvature, then the equation is back-solved again using the maximum allowable curvature value κ_{max} to obtain an approximate solution that best matches the angle at the edge using Eq. (3.64):

$$\frac{2\sin(\varphi_C - \varphi_P)}{C} = sign[\kappa] * \kappa_{max}\,, \qquad \varphi_C = \tan^{-1}\left(\frac{u_E - u_P}{v_E - v_P}\right), \tag{3.64}$$

where $sign[\kappa]$ is defined by the positive or negative sign of the curvature κ obtained when solving the problem without the steering constraint. This presents the solution for one element of the design-manufacturing mesh. The solution can be used for arbitrary fiber angle distributions defined by the control points that are obtained from the fiber angle retrieval step. An example is shown for constructing constant curvature paths with different curvature constraints in Figure 3.9.

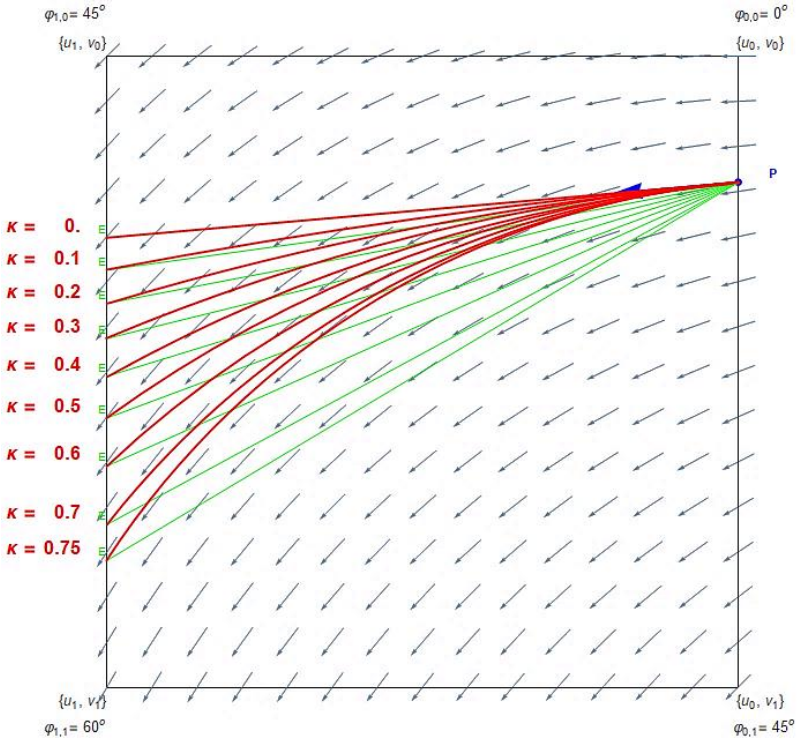

Figure 3.9: Constrained constant curvature arc example for an element of design-manufacturing mesh

As the difference between the absolute value of the ideal curvature κ obtained from solving Eq. (3.54) and κ_{max} increases, the angle deviation between the angles obtained from the designed manufacturable fiber paths and the optimal fiber angles obtained from the second optimization step increases.

In addition, applying a steering constraint κ_{max} might modify the solution obtained from Eq. (3.54) from the bottom edge of the element for example to the left edge since the solution is constrained within the domain of the element. The constant curvature arc is then represented by a circular arc with the center O, radius defined as the inverse of the curvature, and the arc is bounded between the angles θ_1 and θ_2 given by:

$$\begin{gathered} u_O = u_P - \frac{\sin\varphi_P}{\kappa}, \\ v_O = v_P + \frac{\cos\varphi_P}{\kappa}, \\ \rho = \frac{1}{|\kappa|}, \\ \theta_1 = \varphi_P - sign[\kappa]\frac{\pi}{2}, \qquad \theta_2 = \varphi_P + sign[\kappa]\left(\Delta\varphi - \frac{\pi}{2}\right), \end{gathered} \tag{3.65}$$

The constant curvature arc solution developed in this work assumes the surface to be developable or isometric, such that the Gaussian curvature of the surface is zero. For an isometric surface, the mapping between the 3D surface and its development in 2D preserves lengths and angles, thus the curvature of a fiber path defined in the 2D element of a design-manufacturing mesh is the same as the geodesic curvature of the transformed fiber path in 3D.

3.4.2 Generation of Manufacturable Fiber Paths

The solution presented in Section 3.4.1 defines a constant curvature arc which corresponds to one segment within the steered fiber path. To extend a single constant curvature arc over the whole domain, the design-manufacturing mesh is used where several elements are aligned with each other with optimized fiber orientation angles defined at the control points. Choosing a starting point P $\{u_P, v_P, \varphi_P\}$ within one element, the resulting edge values corresponding to point E $\{u_E, v_E, \varphi_E\}$ are used to generate the consecutive constant curvature arc for the adjacent connected element of the design-manufacturing mesh starting from the same edge where point E ended. The new constant curvature arc is generated to match the fiber orientation angles by solving the constant curvature arc solution. This is done iteratively until the end of the parametric domain $\{u, v\}$ of the structure is reached. The angle at the starting point φ_P does not have to conform with the fiber orientation angles defined by the bilinear *sine* angle variation, rather it is a design variable that modifies the whole path and provides extra freedom to satisfy other manufacturing constraints such as controlling the amount of gaps and overlaps obtained between successive courses placed. An example is shown in Figure 3.10 for the plate structure considered in Section 3.3.1 for different starting points P_1 to P_5. If a point starts somewhere within the domain of the structure, constant curvature arcs in both directions are generated with the opposite side having $\varphi_P + \pi$. Notice that P_1, P_2, and P_3 are chosen so that φ_P is the same as the fiber orientation angle defined by the spatial distribution, whereas P_4 and P_5 are chosen to have $\varphi_P = 0$ (huge difference with respect to $\varphi_P = 45^o$ defined by the spatial angle distribution). Changing the starting angle φ_P introduces an error between the fiber angle of the fiber path and the angle obtained from the second

optimization step near the starting point, but the error gradually decreases at points far away from the starting point. In addition, modifying φ_P provides extra freedom in the optimization problem to satisfy the applied constraints related to gaps and overlaps. No steering constraints are applied for the paths generated starting with P_1 to P_4, but the last fiber path generated at P_5 has an additional steering constraint κ_{max} to reduce the amount of steering and the fiber angle deviation (error) increases for each constant curvature arc generated to construct the manufacturable fiber path. Each constant curvature arc in each path is given a different color to show how the piecewise constant curvature path is constructed.

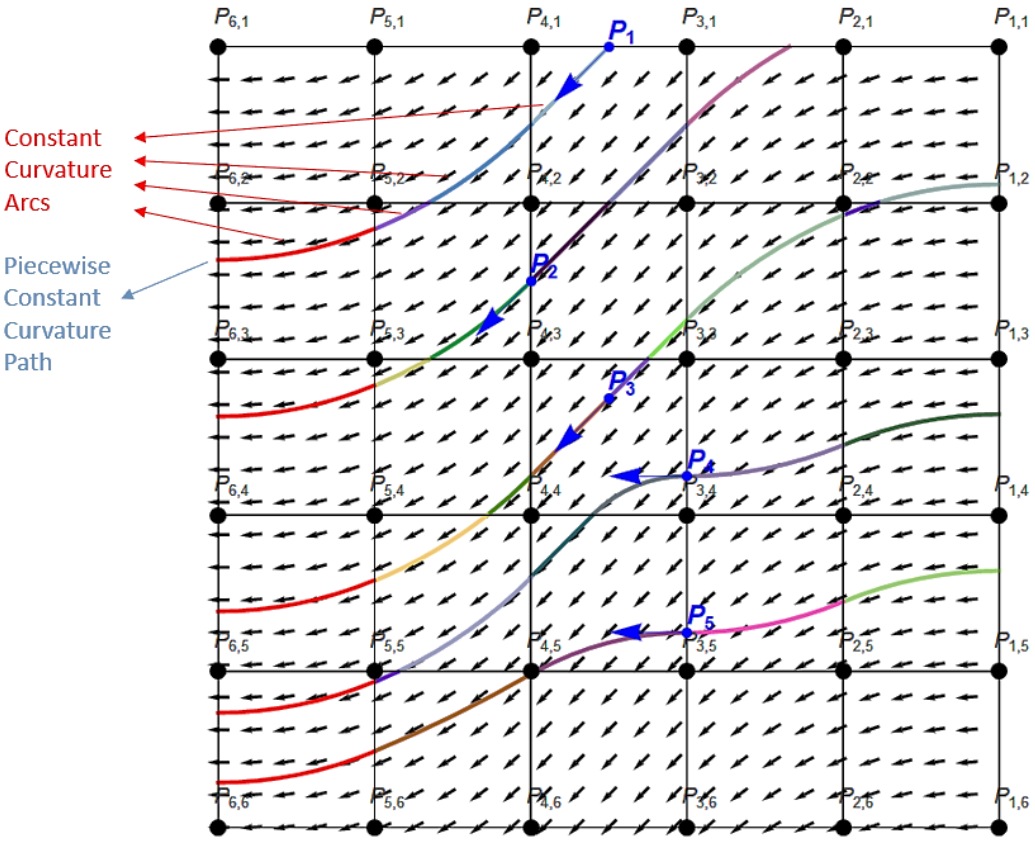

Figure 3.10: Example of fiber paths constructed from constant curvature arcs over a plate domain with 6 by 6 control points

Note that the path generated will be C^1 continuous (continuous and smooth) by having the same tangents defined by the fiber orientation angles at the linking points, but the second derivatives (curvatures) will be piecewise continuous by providing different curvature values obtained from the solutions to match the optimal fiber orientation angles at the edges of each element. As a result, the manufacturable fiber path is defined as a continuous path with piecewise constant curvature arcs satisfying locally the minimum steering radius constraint.

Each generated manufacturable fiber path defines one course centerline. Using the constant curvature arc solution, the course centerlines are generated numerically. To transform the fiber paths to actual courses, the numerical solution is then parameterized to generate parallel paths from the centerline. If the curvature of the arc is zero, then it can simply be parameterized as a straight line joining the starting point P and the ending point E. If the curvature is not zero, each constant curvature arc constructing the fiber path can be parameterized with respect to a parameter t ($0 \leq t \leq 1$) as:

$$u(t) = \left(u_P - \frac{\sin\varphi_P}{\kappa}\right) + \frac{1}{|\kappa|}\cos[t\,(\theta_2 - \theta_1) + \theta_1]\,,$$

$$v(t) = \left(v_P + \frac{\cos\varphi_P}{\kappa}\right) + \frac{1}{|\kappa|}\sin[t\,(\theta_2 - \theta_1) + \theta_1]\,, \tag{3.66}$$

$$\theta_1 = \varphi_P - sign[\kappa]\frac{\pi}{2}\,, \qquad \theta_2 = \varphi_P + sign[\kappa]\left(\Delta\varphi - \frac{\pi}{2}\right)\,,$$

The parametric equation can then be used to generate the parallel curves to each constant curvature arc constructing the fiber path. The parametric representation of the parallel curves can be expressed as:

$$u_d(t) = u(t) + \frac{d\, v'(t)}{\sqrt{u'(t)^2 + v'(t)^2}},$$
$$v_d(t) = v(t) - \frac{d\, u'(t)}{\sqrt{u'(t)^2 + v'(t)^2}}\ , \tag{3.67}$$

where d represents the perpendicular distance between the centerline curve and the parallel curve generated, which can be defined based on the course width w and the number of tows N_{Tows} constructing the fiber course. The boundaries of the course can be obtained by the parallel curves at distances $\{w/2, -w/2\}$ from the centerline. In addition, we can express the parallel curves defining the detailed tow information of the course by choosing a vector d with successive increments of w/N_{Tows} as:

$$d = [-\frac{w}{2}, -\frac{w}{2} + \frac{w}{N_{Tows}}, \dots, -\frac{w}{2} + \frac{w(N_{Tows} - 1)}{N_{Tows}}, \frac{w}{2}]\,, \tag{3.68}$$

An example is shown in Figure 3.11 for generating courses (that are shifted in the domain) with different course widths w and number of tows N_{Tows} from a centerline obtained at point P_3 from Figure 3.10.

For the design-for-manufacturing tool developed in this work, geometric region functions in Mathematica® were used to evaluate the gaps and overlaps between the successive courses. Hence, an additional step was taken to define convex hull regions for each set of parallel constant curvature arcs. Instead of expressing the parametric curves symbolically, the numerical implementation of the convex hull makes the algorithm much faster in creating the detailed course information and consequently measuring the required gaps and overlaps efficiently.

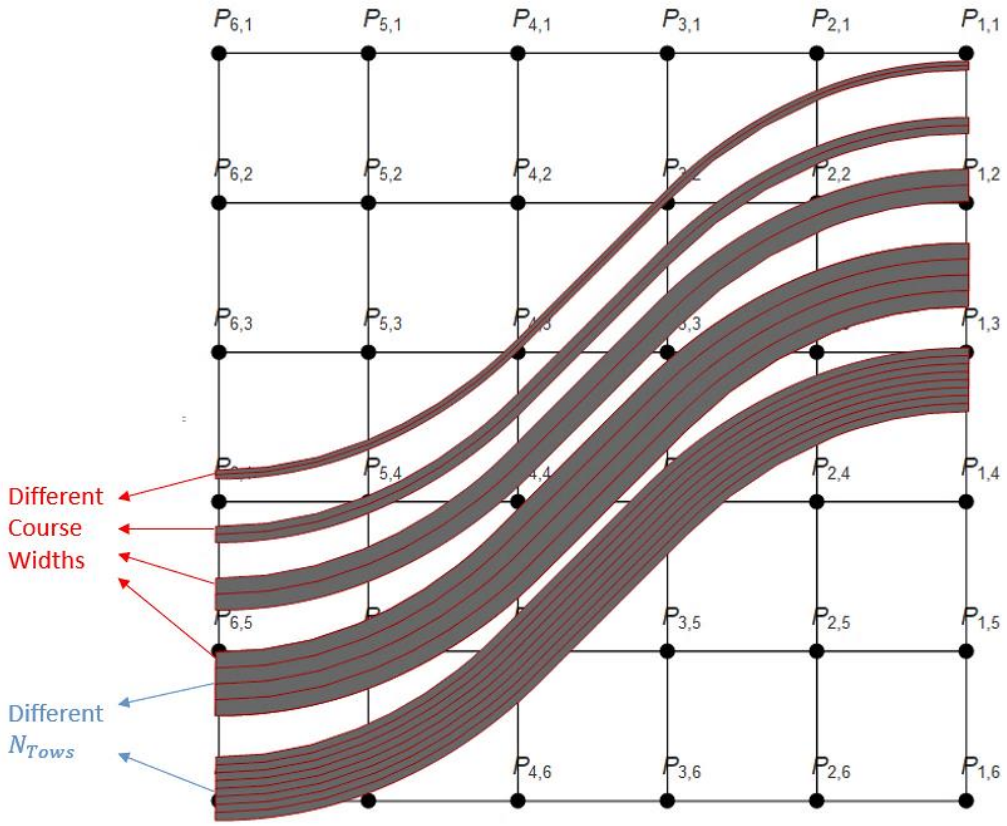

Figure 3.11: Example of courses constructed from using different course widths and number of tows

3.4.3 Analysis of Fiber Angle Deviation and Gaps and Overlaps

The objective of the third optimization step is to match the optimal fiber orientation angles while satisfying manufacturing constraints such as the maximum steering curvature, zero-gap constraint, and minimal overlaps to obtain full coverage of the steered ply with a near constant thickness. As a result, for each fiber course that is placed by the algorithm, a measure of the fiber angle deviation or error with respect to the fiber orientation angles of the second step is required, and an accurate representation of the gaps and overlaps that are obtained between adjacent courses is also essential.

The error or fiber angle deviation is measured along the arc length of each fiber path that is constructed using the constant curvature arcs. The numerical solution of the

constant curvature arcs provides the errors at the edges of the elements of the design-manufacturing mesh, but the errors within the domain can also be evaluated using the parametric equation defining the centerline of each placed course. The fiber angle deviation at each point along a constant curvature arc can be expressed as:

$$\Delta\varphi = \int_{t=0}^{t=1} \left|\varphi_{uv}(t)^{Actual} - \varphi_{uv}(t)^{Desired}\right| dt \,,$$
$$\varphi_{uv}(t)^{Actual} = \tan^{-1}\left(\frac{v'(t)}{u'(t)}\right) \,, \tag{3.69}$$

where $\varphi_{uv}(t)^{Actual}$ is defined by the fiber orientation angle at the course centerline along a constant curvature arc, and $\varphi_{uv}(t)^{Desired}$ is defined by the bilinear *sine* angle variation obtained from the second optimization step which is a function of the fiber orientation angles at the control points and the location within the domain. The total fiber angle deviation along the fiber path constructed can be defined as:

$$\Delta\varphi_{Path} = \frac{\sum_{i=1}^{N_C} \Delta\varphi * s_i}{s} \tag{3.70}$$

where s_i is the arc length of each constant curvature arc in the fiber path, s is the total arc length of the path, and N_C is the number of constant curvature arcs defining the path. This defines the local objective function of the optimization problem in the third step during the placement of each fiber course.

Gaps are measured as areas of difference using geometric regions, while overlaps are measured as areas of intersection between consecutive courses generated. These are obtained using geometric region functions in Mathematica®. The overlap region can be easily evaluated as an area of intersection between the adjacent courses. However, the gap uses the outer boundaries of the courses to define two regions, one defined as a region

below the lower boundary of Course 1, and the other region is defined above the upper boundary of Course 2, and the intersection of these two regions defines the area of the gap. These measures can also be obtained mathematically using numerical integration of the areas defined by the equations corresponding to the outer boundaries of each course. An example of the measurement of gaps and overlaps as an area is shown in Figure 3.12

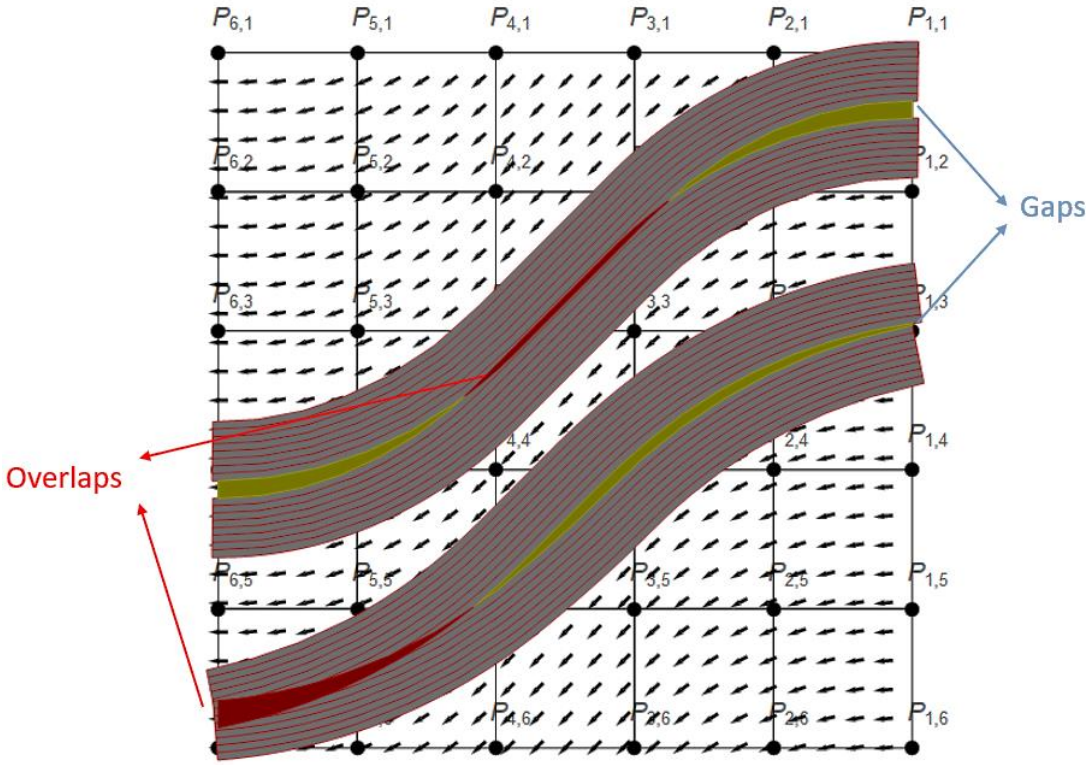

Figure 3.12: Example of gaps and overlaps measured between successive courses

The individual cut and restart capability of the AFP machine is also utilized in the design-for-manufacturing tool developed to be able to match highly non-linear fiber orientation angle distributions. As a result, the algorithm allows course centerline intersections between successive courses, which necessitates the definition of new boundaries during placement for proper measurements of the error, gaps, and overlaps of the courses that will be placed.

Considering a case where the optimal fiber orientation angle distribution is shown in Figure 3.13, a non-linear fiber angle variation is now present around the middle of the plate domain (by increasing the value of the orientation angles at $P_{3,i}$ and $P_{4,i}$). The orientation angles can be matched using the constant curvature arc solution, but this will usually violate the maximum steering curvature constraint.

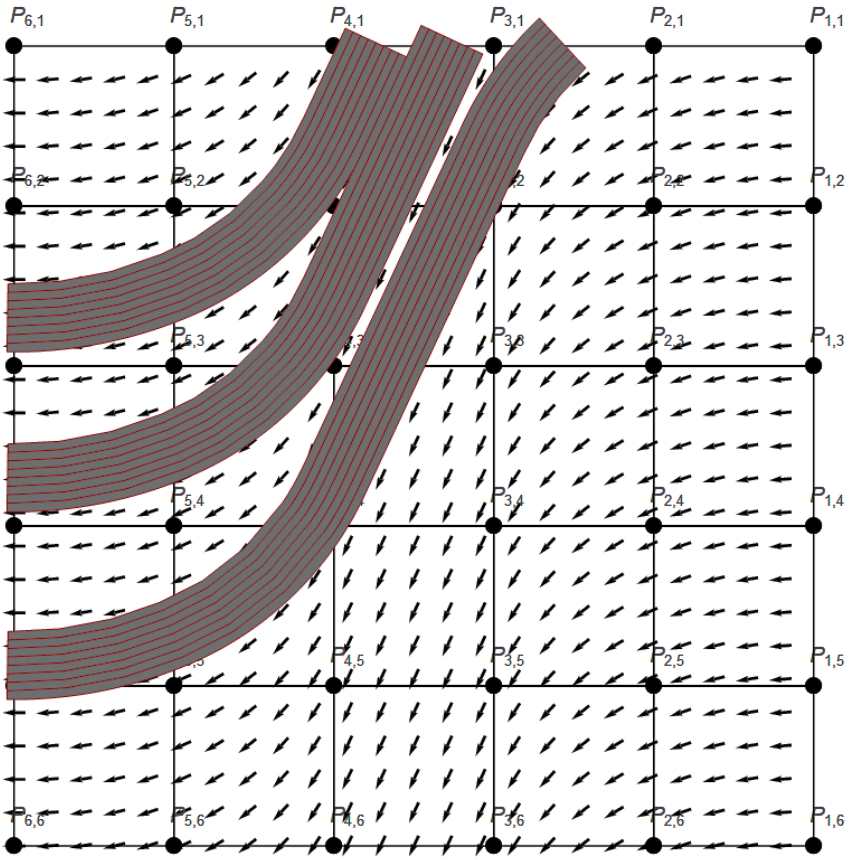

Figure 3.13: Example of a highly non-linear fiber angle variation violating maximum curvature constraint

The presence of highly non-linear fiber orientation angles can be closely matched while satisfying the maximum curvature constraint by allowing for course centerline intersections, where the portion of the new course that is overlapping the already placed courses is then removed using the tow-dropping capability. An example showing courses satisfying a maximum steering curvature is shown in Figure 3.14.

For Course 2 to closely match the fiber orientation angles while satisfying a zero-gap constraint, an intersection between the two adjacent courses must be allowed. The starting point and angle (seed point) of Course 2 must be optimized to match the fiber orientation angles as closely as possible while satisfying a zero-gap constraint. The overlaps that are obtained are then removed using the tow-dropping capability to obtain a near constant thickness layup. Notice that the fiber orientation angles of Course 2 are closely matching the fiber orientation angle distribution defined by the control points, and the measurements of the error along the path ends at the intersection of the centerline with Course 1. Using the intersection point, an updated boundary is then generated from the constant curvature arcs of both fiber Courses 1 and 2. This new updated boundary is then used for the measurements of the new area of gap and overlap when placing a successive Course 3.

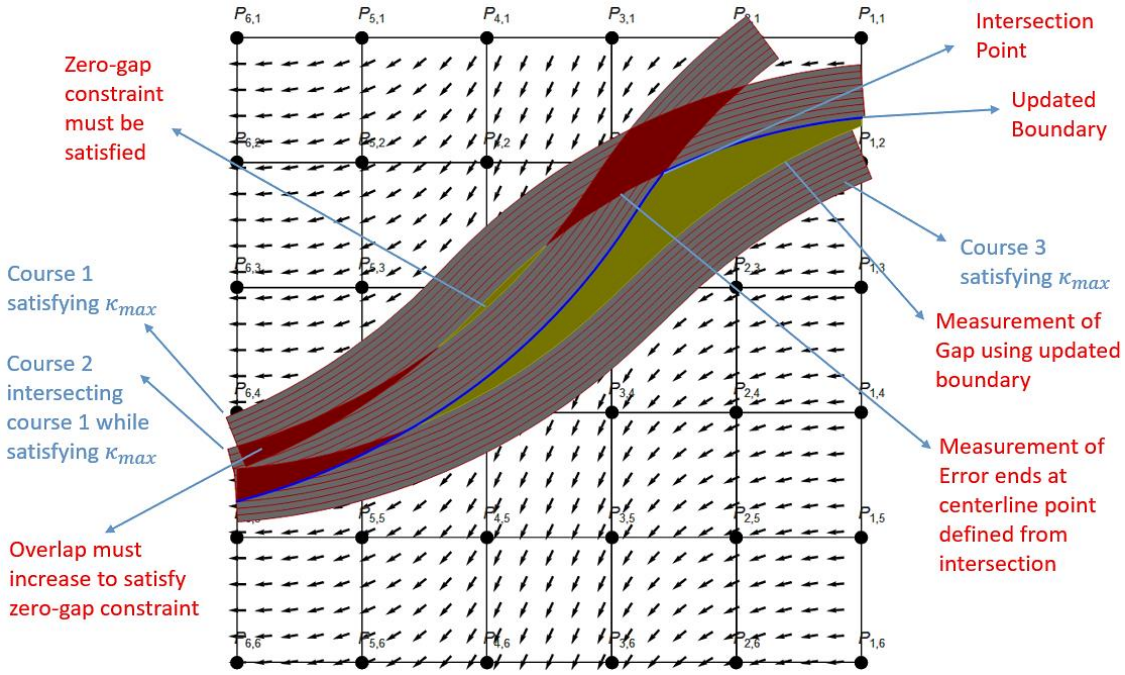

Figure 3.14: Example of a highly non-linear fiber angle variation with courses closely matching fiber orientation angles while satisfying maximum curvature constraint

3.4.4 Sequential Course Placement

The fiber path constructions step aims to find the optimal starting points (seed points) for each path that achieves the minimum fiber angle deviation or error with respect to the desired angles while generating zero gaps between successive courses. Sequential placement of the fiber courses was utilized in the design-for-manufacturing tool, where the third optimization step can be expressed as a set of local optimization problems that are solved for each manufacturable fiber path placed. The local optimization problem in the can be expressed as:

$$\min_{\{\boldsymbol{u_P},\boldsymbol{v_P},\boldsymbol{\varphi_P}\}} \Delta\varphi_{Path} \ , \qquad Gap = 0 \ , \qquad |\kappa_{local}| \leq \kappa_{max} \ , \tag{3.71}$$

where $\{u_P, v_{P,}\varphi_P\}$ are the design variables for each manufacturable fiber path being placed. The gap constraint is satisfied locally, hence full coverage of the domain is obtained globally, and the constant curvature arcs generated locally satisfy κ_{max}. The overlaps obtained are left to be minimized during the tow-dropping algorithm. The design algorithm for fiber course placement utilizes Sequential Linear Optimization (SLP) to solve the local optimization problem for each fiber path. The first seed point defining the first course in the structure is arbitrarily chosen, although this may affect the global optimization problem because it is solved locally.

It is then important to consider feasible starting points for the algorithm to efficiently converge to local optimal design points. The starting points of the adjacent courses are chosen to be generated along the parallel path to the initial course as shown in Figure 3.15 while choosing:

$$\varphi_P = \varphi_{uv}{}^{Desired}(u_P, v_P) \tag{3.72}$$

where $\{u_P, v_P\}$ are the locations of the starting points on the parallel path generated at a distance equal to the course width w from the centerline of the initial course.

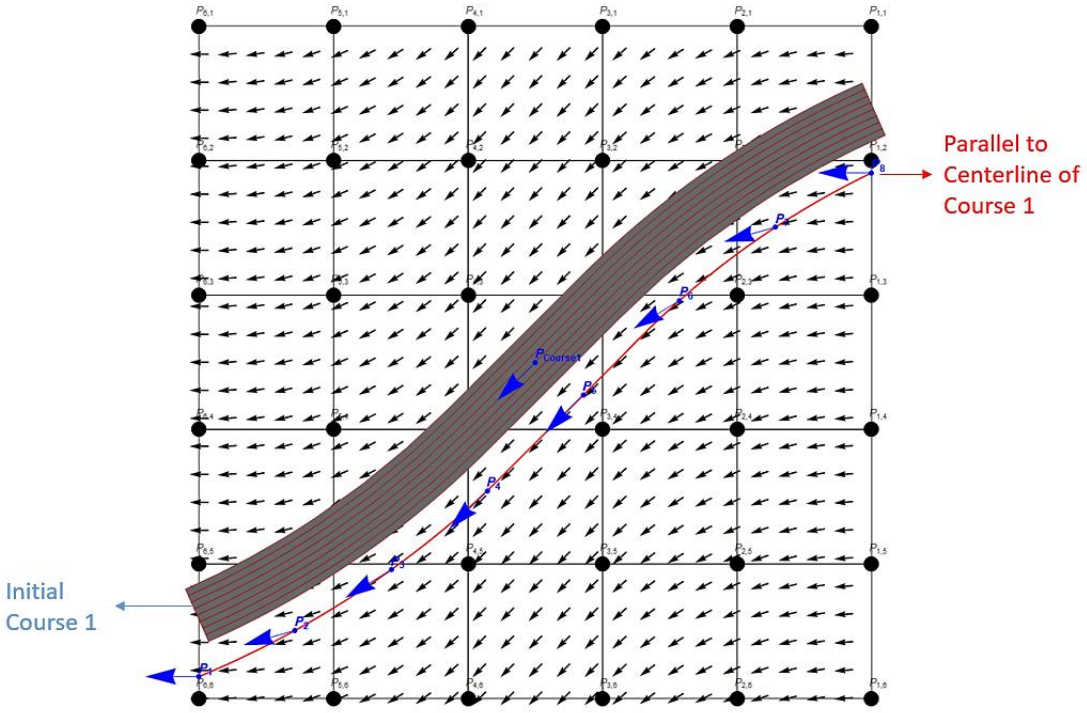

Figure 3.15: Example showing generation of initial path starting points from an initial Course

For each of the multiple initial design points (P_1-P_n), the manufacturable fiber paths satisfying the local curvature constraint κ_{max} are generated; then the courses are constructed and the fiber angle deviation and gaps are measured to choose a best candidate for the SLP algorithm. This can be parallelized easily, so the computational time is the same as the time taken to generate one fiber course. The seed point having the minimum of a multi-objective function with normalized objectives (error and gap) is then chosen as the initial candidate. From the chosen initial design point P_i, the sensitivities of the error and gap with respect to the normalized design variables are estimated using central finite

difference technique, and then conservative convex approximations are used to approximate the objective (error) and constraints (gap) as [28]:

$$f_C(\boldsymbol{x_i}) = f(\boldsymbol{x_0}) + \sum_{i=1}^{n} F_i\,(\boldsymbol{x_i} - \boldsymbol{x_{0i}})\left(\frac{\partial f}{\partial \boldsymbol{x_i}}\right)_{\boldsymbol{x_0}},$$

$$F_i = \begin{cases} \boldsymbol{x_{0i}}/\boldsymbol{x_i} & \text{if } \boldsymbol{x_{0i}}\left(\dfrac{\partial f}{\partial \boldsymbol{x_i}}\right) < 0 \\ 1 & \text{otherwise} \end{cases} \tag{3.73}$$

where $\boldsymbol{x_0}$ is the initial design point defining the generated fiber path, and $\left(\frac{\partial f}{\partial \boldsymbol{x_i}}\right)$ are the sensitivities of the error and gap with respect to the design variables $\{u_P, v_{P,}\varphi_P\}$ that are estimated using finite difference technique. The approximate optimization problem is then solved to minimize the error while constraining the approximation of the gap to be equal to zero to generate a new design point $\{u_P, v_{P,}\, \varphi_P\}$, which is used to generate a new approximation until the algorithm converges to an optimal design point $\{u_P{}^*, v_P{}^*,\ \varphi_P{}^*\}$.

Suitable move limits must also be used for the SLP algorithm. The move limits of $\{u_P, v_P, \varphi_P\}$ in the developed algorithm were chosen to be damped by the amount of gap between the adjacent fiber courses, such that higher move limits were used when the gaps were larger, and near the vicinity of an optimal design point the move limit is much smaller. An example for optimizing the seed point using SLP corresponding to the adjacent Course 2 from Figure 3.15 is shown in Figure 3.16. Notice that $P_{Optimized}$ changes location as well as the angle φ_P to satisfy the zero-gap constraint while minimizing the error between the fiber orientation angles of the path and those obtained from the desired fiber angle distribution. The overlap obtained between the successive courses is then minimized using the tow-dropping algorithm.

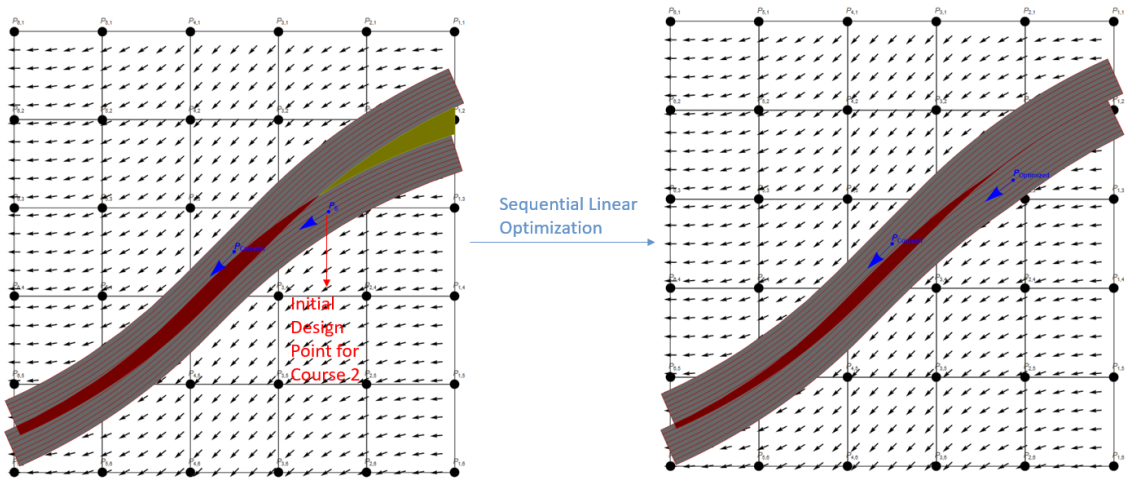

Figure 3.16: Example for optimizing seed point of Course 2 using SLP

After choosing the first seed point defining the first course in the structure, the remaining courses are then sequentially placed by solving the local optimization problem for each consecutive course being placed. The optimal starting points for each consecutive course must satisfy the zero-gap constraint while minimizing the fiber angle deviation with respect to the desired angles. An example of a full ply generation for the plate example of Figure 3.10 is shown in Figure 3.17. Each course placed satisfies the zero-gap constraint while matching the optimal fiber orientation angles. However, each course placed ends when the centerline of the course reaches the structural domain boundaries. If the course is not perpendicular to the domain boundaries at the ending point, triangular gaps will be obtained as shown at the top and bottom sides of the plate. In addition, an inter-band gap may be obtained at the end of the sequential placement algorithm as shown in the bottom right region of the plate, because there is not enough coverage to place an additional course.

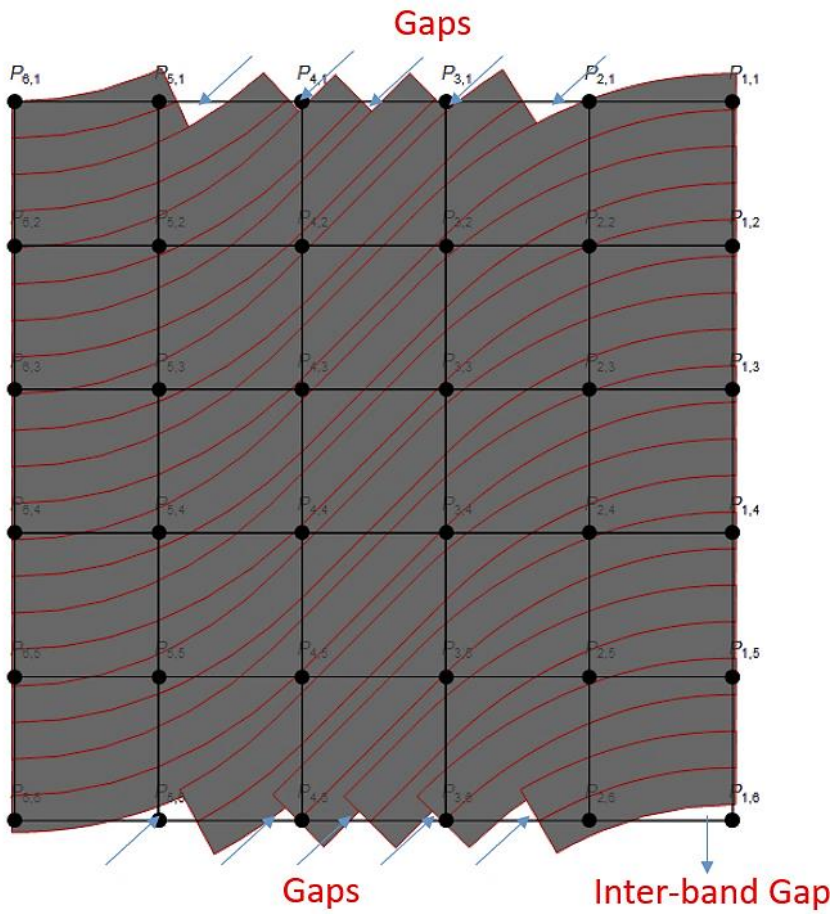

Figure 3.17: Example for full ply generation using sequential course placement

The inter-band gap can be removed by optimizing the sequential course placement and modifying the local optimization problem as:

$$\min_{\{\boldsymbol{u_P},\boldsymbol{v_P},\boldsymbol{\varphi_P}\}} \Delta\varphi_{Path} \ , \qquad (3.74)$$

$$Gap = Interband\ Gap/N_{Courses} \ , \qquad |\kappa_{local}| \leq \kappa_{max} \ ,$$

where the area of the inter-band gap is divided by the number of courses $N_{Courses}$ placed initially with the zero-gap constraint. This divides the obtained inter-band gap area into negligible inter-band offsets between the consecutive courses that were placed. An example is shown in Figure 3.18.

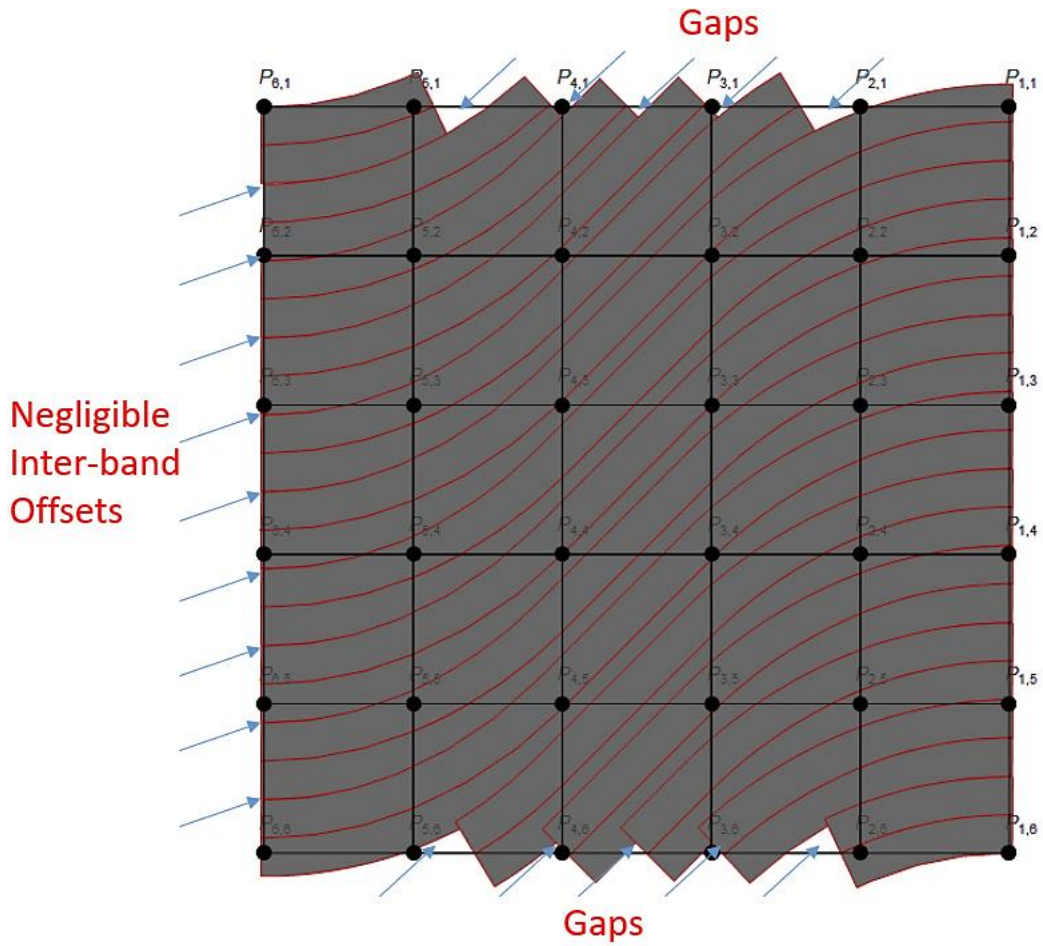

Figure 3.18: Example for full ply generation while accounting for inter-band offsets

An additional manufacturing constraint of the AFP machine is the minimum cut length. The minimum cut length depends on the machine configuration used and is defined as the minimum tow length that must be laid by an AFP machine before a tow can be cut after it has been fed. There is no control over the path of a tow by the guiding rollers once it is cut, so the tow will follow a geodesic path on a curved surface leading to fiber straightening [169]. As a result, ply boundaries are extended from each side of the part boundary to generate the extended manufacturing boundaries of the steered ply, where the fiber courses are extended with linear portions at the ends equal to the minimum cut length to minimize fiber straightening obtained due to steering and satisfy minimum cut length

issues that may arise near boundary edges. An example is shown in Figure 3.19 for the full ply generated in Figure 3.18. This guarantees that the minimum cut length constraint is satisfied for each course being placed, removes the gaps that are obtained at the part boundaries, and guarantees that during manufacturing the desired angles are obtained for each course within the part boundary (no fiber straightening at the edges).

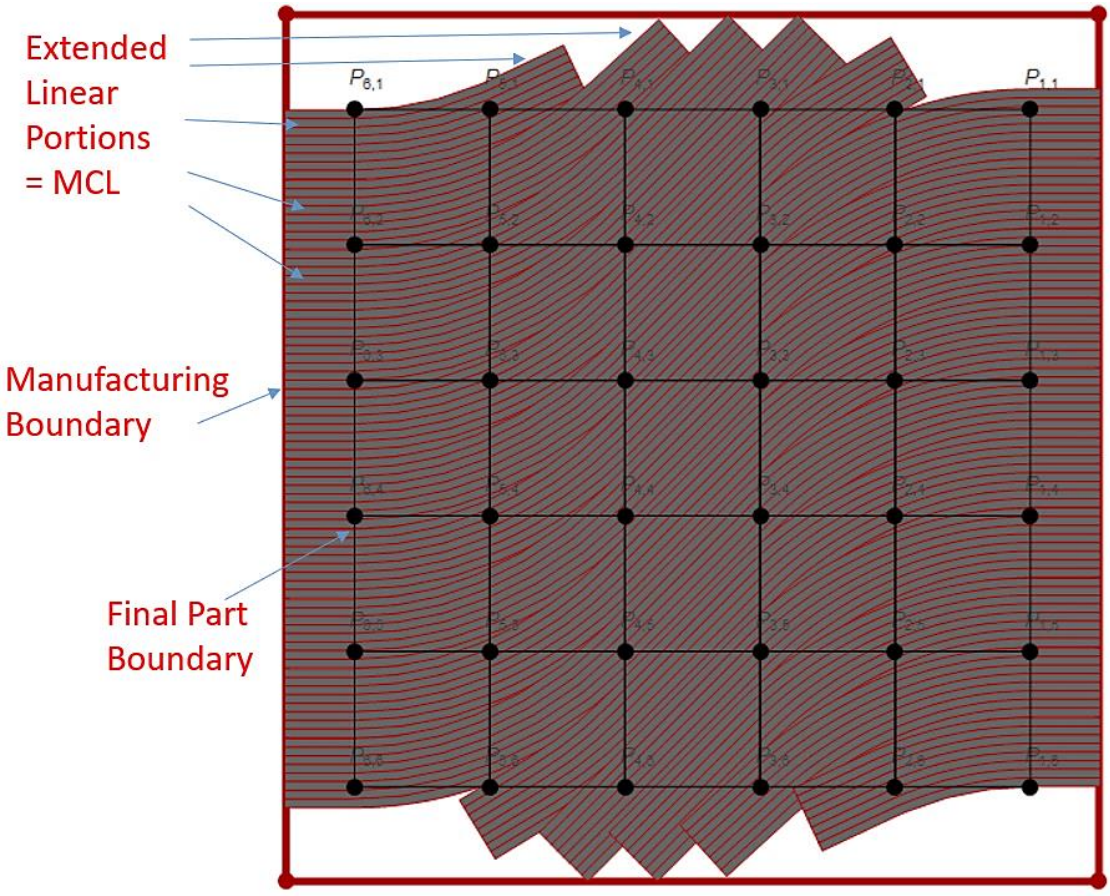

Figure 3.19: Example for full ply generation with extended manufacturing boundary

Periodic conditions at boundaries (for a cylinder circumference for example) can be solved by generating a continuous fiber path at the periodic boundary. However, because fiber orientation angles are only defined within the structural domain, the endpoint of the fiber path that is generated must be translated by the maximum value of the parametric coordinate that corresponds to the periodic condition, such as v_{max}. The continuous fiber

path that is generated within the domain is then translated to an extended manufacturing domain where it ended to perform the same measurements of the error, gaps, and overlaps of a continuous course. For the case of a cylinder, ply boundaries are only extended along the length of the cylinder (right and left edges of structural domain).

In the previous example, there were no course intersections, which are defined here as the intersection of the lower boundary of Course 2 with the lower boundary of Course 1. Generally, this also occurs if an intersection occurs between the course centerlines, and an updated boundary must be taken as an output for the adjacent fiber course that will be placed to measure the new objectives and constraints correctly. The boundaries are also updated after each placement of a new fiber course by finding new intersections. Course drop locations are identified for intersecting fiber paths, and the measurement of fiber angle deviations ends at the drop location that is shifted to the centerline of the course being dropped. The algorithm must also distinguish from which direction the course is dropped in addition to identifying cut and restart courses or add and drop courses (more than one intersection point). Course drop locations and the updated boundaries are then exported for the tow-dropping algorithm.

3.4.5 Tow-Dropping and AFP Manufacturing Boundaries Generation

After completing the sequential placement of the fiber courses, the tow-level information and the boundaries are exported for the tow-dropping algorithm that uses the cut and restart capability of the AFP machine to minimize the overlaps to small triangular gaps and overlaps. This helps in obtaining a near constant thickness for the laminate which is consistent with the corresponding theoretical constant thickness laminate designed.

Using tow boundaries, intersections are found to identify drop locations. A coverage parameter, also called boundary lap/gap, is included to provide extra freedom for satisfying the minimum cut length constraint within the structural domain and reducing the triangular gap and overlap areas. An example is shown in Figure 3.20 for dropping tows using a 0% coverage parameter. For a 0% coverage parameter, the tows are dropped at the first intersection of a boundary defining the tow.

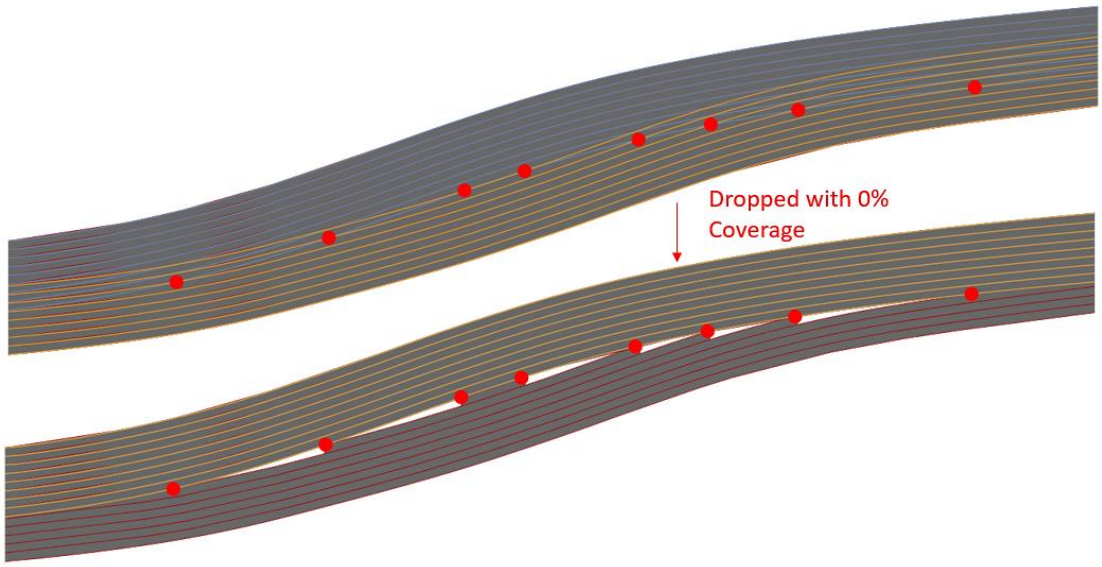

Figure 3.20: Example for tow-dropping using 0% coverage

The first dropped tow of Course 2 in Figure 3.20 violates the minimum cut length constraint of an AFP machine. The minimum cut length is an important constraint that must be considered for each tow during the tow-dropping algorithm to satisfy the condition for placing it during manufacturing. The coverage parameter can be used to extend the tows to satisfy the minimum cut length constraint. An example is shown for the same tow-dropping configuration using a 50% coverage in Figure 3.21. For a 50% coverage, the tow-drop locations are defined at the midpoint between the intersections of the edges of a tow with the boundary. In addition, using a 0% coverage results in larger areas of gaps which are

undesirable because they are considered stress risers. In some cases, a 50% coverage may not satisfy the minimum cut length constraint; thus, the tow violating the constraint must be extended in the algorithm with a coverage parameter greater than 50%.

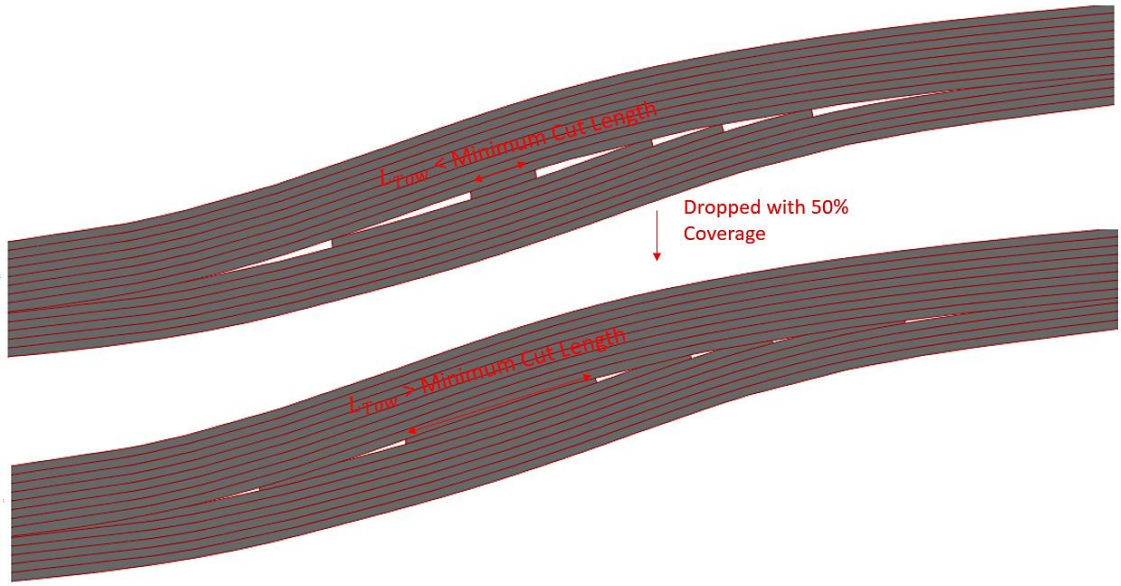

Figure 3.21: Example for tow-dropping using 50% coverage satisfying minimum cut length constraint

Dropping is performed sequentially by finding the intersections between adjacent courses that are placed. The coverage parameter and the minimum cut length are provided as input to the algorithm to generate the final dropped ply. An example is shown in Figure 3.22 for a 0% coverage of the full ply generated in Figure 3.19. A dropped ply with a 50% coverage is also shown in Figure 3.23, where the areas of the gaps are much smaller compared to dropped ply using 0% coverage. Using a 100% coverage parameter will cover all the gaps at the drop locations, but this may also result in thickness build-ups if several steered plies are present in the laminate. As a result, a 50% coverage offers a good compromise between small gap areas as well as minimal thickness build-ups.

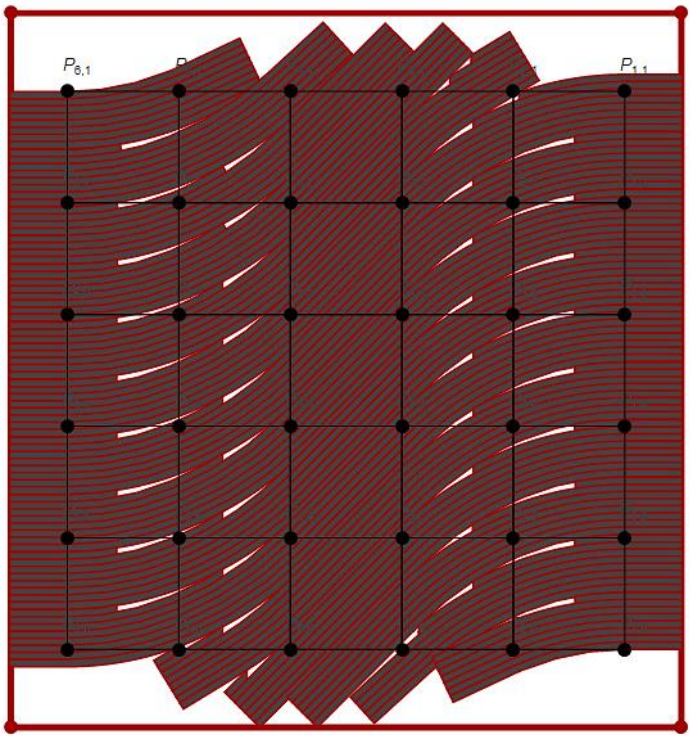

Figure 3.22: Example for tow-dropped ply with 0% coverage

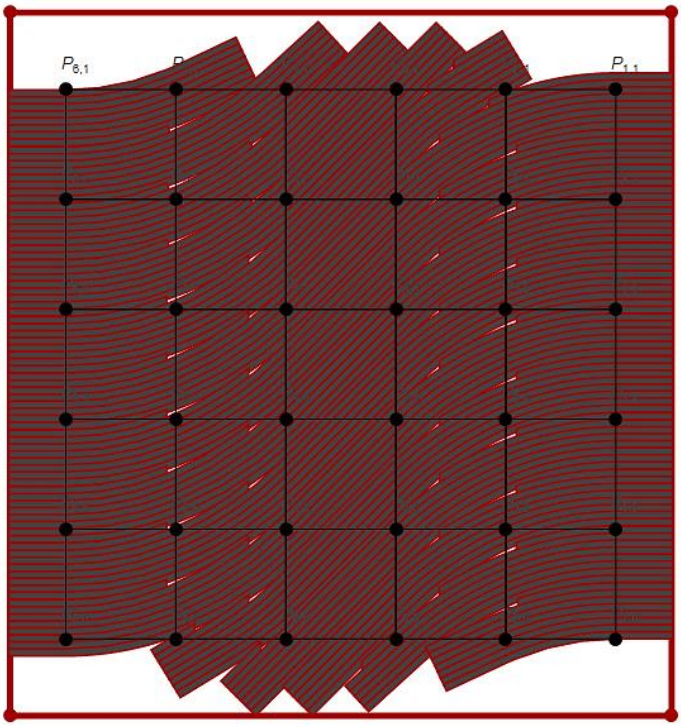

Figure 3.23: Example for tow-dropped ply with 50% coverage

The balancing ply $-\varphi$ can then be generated by constructing the mirror image of the positive ply $+\varphi$ with respect to the right boundary $u = u_{min}$ as shown in Figure 3.24. However, for completely independent guide curves without symmetry, the balancing condition is not guaranteed at all points in the structure.

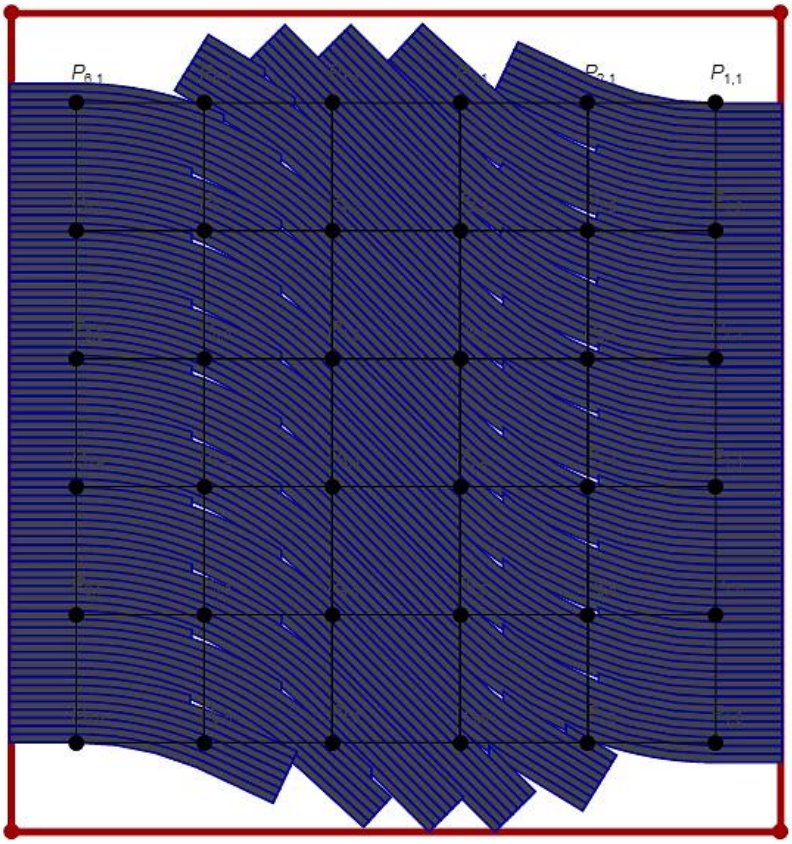

Figure 3.24: Example for generating $-\varphi$ ply using mirror image of $+\varphi$ ply

Since the algorithm also allows for centerline intersections, some courses placed will intersect several other courses. In this case, only the course that is intersecting the other ones is dropped by using the updated boundary corresponding to the intersection that is exported from the sequential placement algorithm. An example is shown in Figure 3.25, where Course 2 below the updated boundary is dropped from both sides, and an add-drop mechanism is obtained. The drop locations are identified, and the boundaries of the tow

are discretized between tow-drop locations along the boundaries defining each tow. From the discretized points defining the tow-drop locations, AFP manufacturing boundaries are then generated to export for the AFP machine.

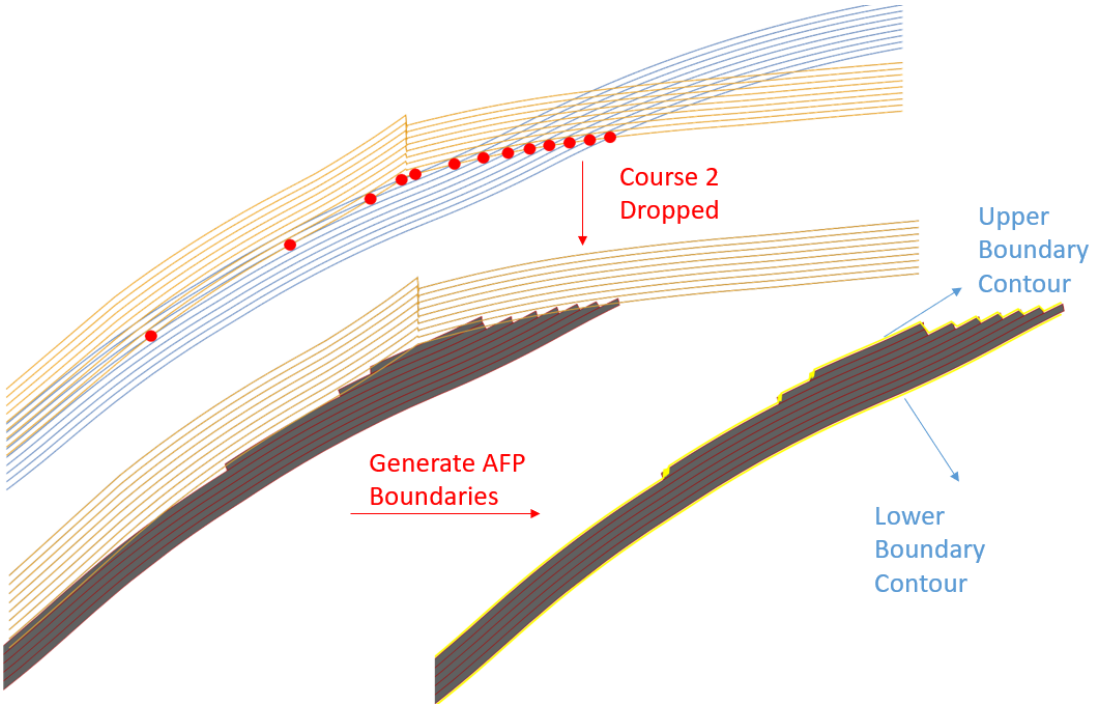

Figure 3.25: Example for tow-dropping Course 2 from both sides defining add-drop locations and generation of AFP boundaries

However, if two adjacent courses do not completely intersect, then the tows are dropped dynamically from both courses to keep the tows having less fiber angle deviation by comparing the fiber orientation angles at the tow-intersection locations to the ones obtained from the second optimization step. An example showing both courses being dropped is shown in Figure 3.26, where tows in this case will be dropped based on the error between the orientation angles of the tows of each course and the desired fiber orientation angles at the intersection points. Dropping tows dynamically between both courses can also be chosen to reduce the areas of the gaps that are obtained due to tow-dropping. Manufacturing boundaries defining the drop locations for each course are then generated

for the AFP machine. To account for manufacturing tolerances, the boundaries of each course can be shifted by a small measure away from the course to make sure the tows are programmed as designed within the computer aided software used.

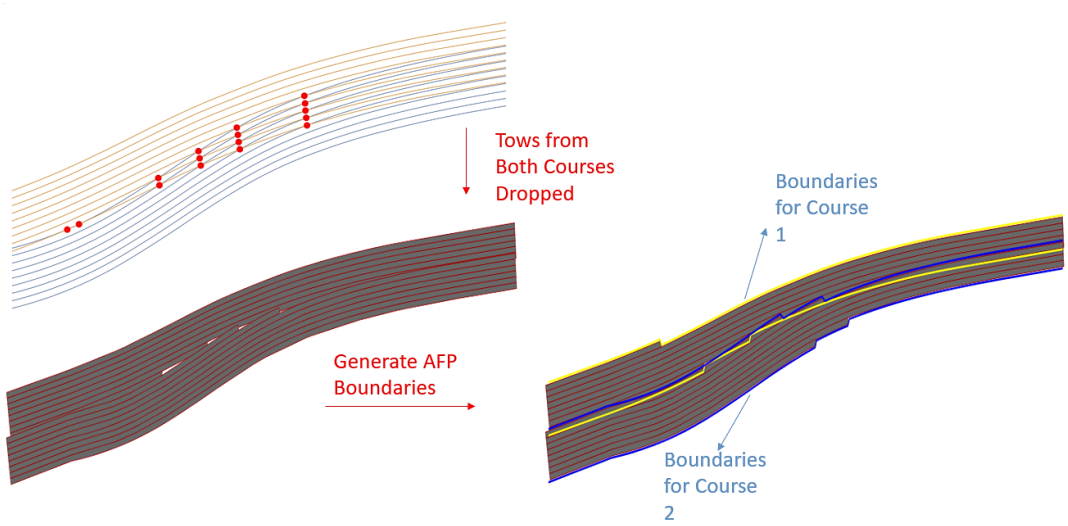

Figure 3.26: Example for tow-dropping both courses dynamically to keep tows with fiber orientation angles closer to the desired fiber orientation angles

3.4.6 Fiber Orientation Angle Retrieval from Manufactured Fiber Paths

After generating the manufacturable fiber courses, and dropping the overlapping tows between the successive courses, the fiber orientation angles at the control points of the design-manufacturing mesh are obtained from the fiber tows remaining within the structure. The tow-level details defined by the parallel paths of each course are used to consider the fiber angle deviation between the course centerline and the parallel paths. For each node of the design-manufacturing mesh, the shortest distance between the node and all the tows that remain within the structure is evaluated, and the nearest point on the edge of the closest tow to each control point is then identified. The orientation angle at this nearest point can be obtained using the parametric equations defining the boundary of the tow. The fiber orientation angles at the control points are then updated using the angles

obtained from the manufacturable fiber tows, and these fiber orientation angles can be used to re-define the fiber angle distribution for the finite element analysis of the structure. An example is shown in Figure 3.27 for identifying each tow that is associated to the fiber orientation angle defining the angle at the control points. It is noteworthy to mention that if there are several intersections (centerline) between courses that are placed for a steered ply, it is reasonable at this level to include a more refined design-manufacturing mesh to obtain a better accurate representation of the fiber orientation angle distribution within the structure.

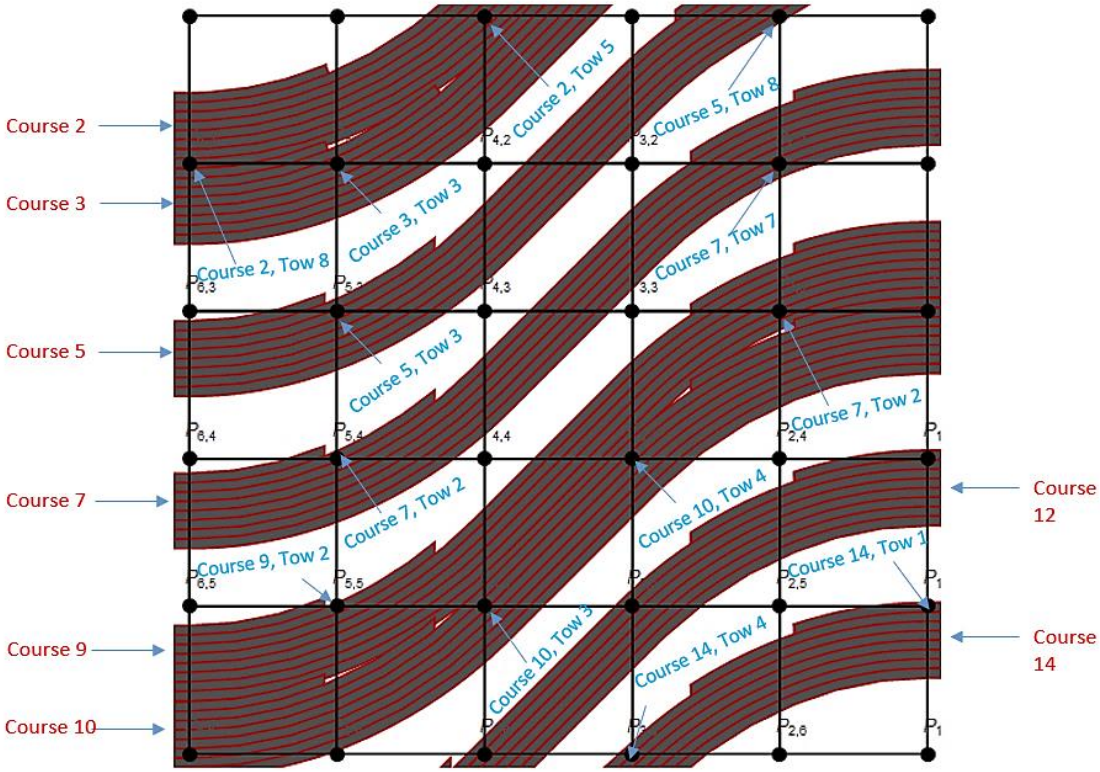

Figure 3.27: Example for tow-dropping both courses dynamically to keep tows with fiber orientation angles closer to the desired fiber orientation angles

3.4.7 Methodology for AFP Design-For-Manufacturing Tool

The steps of the Fiber Path Construction step are summarized in Figure 3.28. Manufacturing constraints including the maximum steering constraint and the minimum

cut length are required for the third optimization step along with the boundary lap/gap percentage used and the FEM model. The fiber path construction step outputs the optimal fiber paths along with the manufacturing boundaries for AFP manufacturing. The final obtained design is then analyzed using linear and non-linear analyses to obtain the ultimate failure load of the variable stiffness structure that will be manufactured. The Fiber Path Construction contains the following components:

- Generate Adjacent Course: Starting from an initial design point of a course, this module generates a near-optimal adjacent course that has minimal gap and error along the parallel to the initial starting course or boundary
- Sequential Linear Optimization: Sequentially optimizes the adjacent course placed to satisfy a zero-gap constraint while minimizing the error between the desired angles and the angles of the course satisfying the maximum steering constraint
- Parameterize and Create Tows: The course centerline is parameterized and the parallel boundaries representing the tows are created to define the geometric entity of each tow
- Find Intersections: This module finds the intersections between the initial course and the one being optimized to update the boundary that is used for measuring the amount of gap between the successive adjacent courses
- Evaluate Error and Gap: Upon placing the adjacent course, the objective (error between desired and obtained fiber angles) and constraint (zero-gap) are evaluated at the starting design point and the perturbed design points

- Conservative Approximation: The objective and constraint are approximated using the evaluation module to create a conservative approximation for the sequential linear optimization
- Tow-Dropping: After obtaining the optimal fiber courses, this tool constructs the dropped tows and the manufacturing boundaries that are used for AFP manufacturing and analysis of the manufactured structure
- Boundary Intersections: The intersections of adjacent courses are obtained to generate the drop locations to minimize the overlap between the courses placed
- Generate Dropped Tows: Using the drop locations obtained and the minimum cut length manufacturing constraint, the dropped tows are generated along with the manufacturing boundaries defining each course
- Extract Fiber Angle Distributions: After the tow-dropping is done, the course centerlines are updated using the manufacturing boundaries and the closest fiber orientation angles on the boundaries of the nearest tows are used to define the fiber orientation angles at the control points of the design-manufacturing mesh
- Finite Element Analysis: Once the optimal stacking sequences are retrieved from the manufactured variable stiffness structure, linear and non-linear analyses are performed to predict the ultimate failure load of the manufactured steered laminate

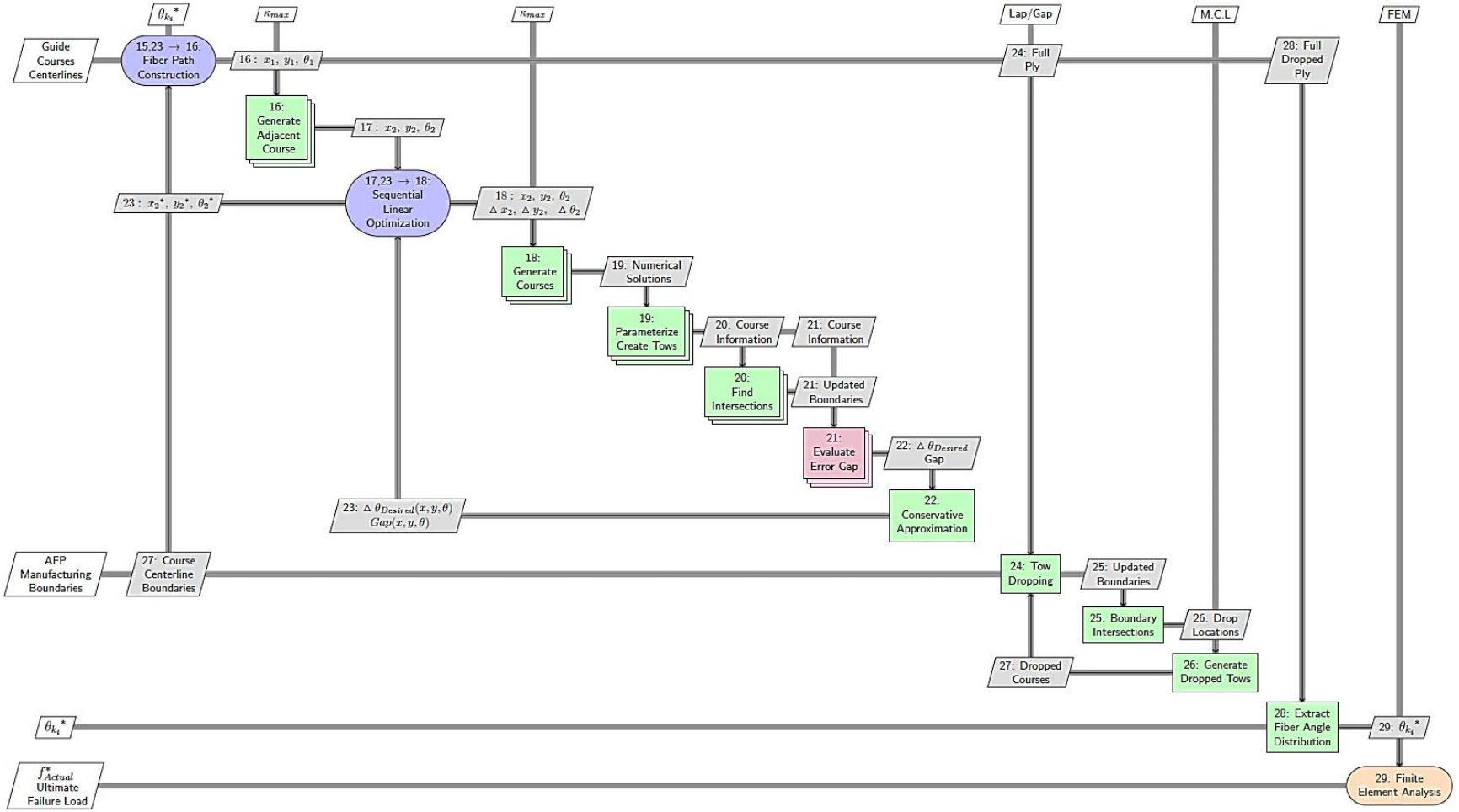

Figure 3.28 XDSM diagram for Fiber Path Construction

3.5 SUMMARY AND CONCLUSIONS

The complexity of the optimization problem imposes the need for an efficient multi-level optimization approach to achieve a global optimum design. In this chapter, the importance of including a design-manufacturing mesh is demonstrated in each optimization step of the multi-level optimization framework.

In the first step, a theoretical optimum stiffness is achieved that accounts for optimum structural performance while maintaining smoothness and robustness. The design-manufacturing mesh allows the spatial stiffness distribution to be expressed as a B-spline or NURBS surface defined by the control points of the design-manufacturing mesh. This introduces several benefits to the optimization problem, by significantly reducing the number of design variables while achieving local tailoring of the stiffness distribution as well as smoothness and point-wise constraint feasibility.

The fiber angle distribution is then obtained in the second step to match the optimum stiffness properties from the first optimization step while accounting for the maximum steering constraint and laminate design guidelines to attain manufacturability and feasibility. A bilinear *sine* angle variation is presented to obtain smooth fiber angle distributions, and the maximum steering constraint to guarantee a minimum degree of manufacturability at the second optimization step (ply level) is derived for different surfaces using the curl of the vector field.

Using the design-manufacturing mesh, a constant curvature arc solution is developed in the third optimization step to generate manufacturable fiber paths with piecewise constant curvature arcs that match the optimal fiber orientation angles from the second optimization step. A design-for-manufacturing tool has been developed to consider

the maximum steering constraint locally in the third optimization step while accounting for gaps and overlaps to obtain a near constant thickness variable stiffness structure. Sequential course placement can be used to solve the third optimization step locally considering each fiber course to closely match the optimal fiber orientation angles. Finally, detailed tow-level information in the form of manufacturing boundaries are then exported to the AFP machine with optimized cut and restart positions.

Chapter 4

DESIGN APPLICATION: OPTIMIZATION OF CYLINDRICAL SHELL WITH CUTOUTS UNDER BENDING USING VARIABLE STIFFNESS LAMINATE

The purpose of this chapter is to utilize the multi-level optimization methodology discussed in Chapter 3 to obtain a variable stiffness laminate design of a cylindrical shell with cutouts under bending. The cylindrical shell with cutouts to be designed is introduced in Section 4.1. Lamination parameters are used as intermediate design variables at the first optimization step to achieve a convex optimum laminate stiffness design in Section 4.2. A design-manufacturing mesh is then introduced to model the spatial stiffness variation of the cylinder in ABAQUS®. Circumferential and longitudinal stiffness variations are considered globally and locally around the holes to study their effect on the buckling load. A well-discretized optimum lamination parameter distribution alters the local buckling modes and shows an 83% increase in linear buckling load of the variable stiffness cylinder compared to an optimized traditional laminate, which turned out to be a quasi-isotropic laminate. The optimal fiber orientation angle distributions matching the optimum stiffness properties are then retrieved at the second optimization step in Section 4.3 using a genetic algorithm, while satisfying laminate design guidelines. A steering constraint is not applied at the ply level in the second step to see if the developed design-for-manufacturing tool in the third optimization step can match optimal fiber angle variations with highly non-linear

fiber angle variations. The optimal fiber angle distribution is then transformed to optimal fiber paths using the Fiber Path Construction tool developed with details included in Section 4.4. After obtaining the manufacturable variable stiffness cylinder, the final fiber angle distributions are retrieved from the final tow-by-tow configuration. Detailed analyses are performed for each optimization step in each section to predict the non-linear buckling load as well as the ultimate failure load of the designed cylinder. Section 4.5 concludes this chapter with important observations.

4.1 PROBLEM STATEMENT

This chapter presents a design application for a practical aerospace application, which is the design of a variable stiffness cylindrical shell with a cutout. A cylindrical shell with a circular cutout resembles a section of the aircraft fuselage with multiple door and window cutouts. The presence of the cutouts introduces local stress concentrations, global load redistribution, and locally buckled regions. Cutouts thus compromise the structural integrity and airworthiness of the fuselage section. The effects of the cutouts must be accounted for by reinforcing the regions around the cutouts. However, the designer also has the capability of tailoring the laminate aiming to reduce the stress concentrations and improve the ultimate failure load or decrease the weight to obtain an efficient light-weight fuselage section. In this design application, the thickness (weight) of the laminate is assumed to be constant, whereas the goal is to design the laminate to improve the ultimate failure load using nonconventional variable stiffness laminates. A variable stiffness laminate allows the designer to harness the full potential of composite laminates by providing the largest possible design space. Thus, variable stiffness laminates provide more

efficient structures than constant stiffness laminates by utilizing the strong directional properties of fiber-reinforced composites.

Tatting was the first to investigate the design of variable stiffness cylindrical shells to identify possible areas of improvement that may be accomplished with fiber-steered laminates [173]. The first design problem had an axial stiffness variation to tailor the cylindrical shell against axial compression, pressure, and torsion. It was found that little improvement over traditional laminates can be achieved because of the presence of a weak link area within the stiffness variation. The second design problem consisted of circumferential stiffness variation to tailor the cylindrical shell against axial compression, pressure, torsion, bending, and transverse shear forces. Significant improvements in load carrying capability was obtained for loads that vary along the circumference of the cylindrical shell, such as bending and shear forces. A linear membrane solution was used along with linear angle variation within segments of the cylinder circumference. The optimal fiber orientation angles were optimized using a genetic algorithm. The improvements were explained by stress redistribution to minimize stress concentrations, and by the presence of a relatively stiff region that modifies the buckling behavior of the structure.

After that, it has been demonstrated by Blom et al. [65] that circumferential tailoring can increase the buckling load of cylindrical shells under bending while subjected to the Tsai-Wu strength constraint. The fiber paths were optimized using a surrogate model with multiple-segment constant curvature fiber angle variation to efficiently account for the manufacturing curvature constraint in the design process. The optimal circumferential variation shows a stiffer tension side and a softer compression side of the cylinder. This is

achieved by changing the fiber orientation angles from near 0° at the tension side to higher fiber orientation angles at the compression side. This circumferential variation helps in redistributing the load from the buckling critical compression side to the tension side and modifies the buckling modes.

Khani et al. then utilized circumferential stiffness tailoring to maximize the buckling load of general cross section cylinders under axial compression and bending with strength constraints [127]. A multi-step optimization framework was used to obtain the optimum lamination parameters in the first step, the optimal stacking sequences in the second step, and the optimal fiber-steered paths in each layer in the third step. Buckling load improvements were obtained for a circular cylinder under bending and elliptical cylinder under axial compression. Improvements were explained by stress redistribution and the presence of a relatively stiff region that modifies the buckling behavior of the structure. Sun et al. also improved the buckling loads of elliptical cylinders in pure compression using a circumferential stiffness variation [174]. In addition, considerable improvements in axial buckling capacity of isotropic elliptical shells have been achieved by circumferential thickness variation as demonstrated by Paschero et al. [175].

The presence of holes in a structure introduces severe stress concentrations that affect the material failure as well as the buckling capacity. By examining the stress resultant contours around a plate with a circular hole, Hyer et al. demonstrate that steered fibers provide a load redistribution mechanism that move the loads away from the unsupported hole region to the supported edges, thus improving the tensile and buckling capacity [40]. For the design application in hand, the presence of the cutout at the compression side of the cylindrical shell under bending imposes severe stress concentrations that lead to an

interactive failure mode instigated by both local buckling and material failure around the cutout. This necessitates the use of variable stiffness laminates to redistribute the stress and obtain a structurally optimal design. Because the presence of the cutout modifies the stress distributions compared to a "pristine" cylindrical shell, both circumferential and longitudinal stiffness variations are considered to tailor the laminate aiming to improve the load carrying capability of the cylindrical structure. The buckling optimization of the cylindrical shell will be presented in this chapter. The aim is to prove that significant improvements can be achieved by using variable stiffness laminates for realistic design problems, which can be a major task towards their industry adoption and certification in the future.

The geometry chosen is based on the cylindrical shell manufactured and tested by Blom [169], such that the same test fixture can be used to experimentally test the optimized cylindrical shells. The cutout size and location are selected after a parametric study of the effects of size and location of a circular cutout on buckling and failure of the cylindrical shell [176]. A brief summary of the study is explained next.

4.1.1 Effect of Size and Location of a Circular Cutout on Response of Cylindrical Shell in Bending

Celebi et al. [176] investigated the effects of the cutout size and position on the progressive failure characteristics of CFRP cylindrical shells under pure bending. The manufactured cylindrical shells were designed by Blom [169] without a cutout, and they were chosen to introduce different cutout configurations to perform a parametric design study by using different cutout configurations. The parametric study was performed for a

fixed geometry cylindrical shell by varying both the location and size of the cutout, and the ultimate failure loads were identified with several observed failure modes.

The cutout location was allowed to vary circumferentially from the top $\beta = 0°$ to the bottom $\beta = 180°$ of the cylinder, with a symmetric cutout on the opposite side of the shell to maintain left/right symmetry as shown in Figure 4.1. The circumferential locations were spaced at 15° intervals, without the locations near the top and bottom because of the overlapping of the symmetric cutouts on the opposite sides. The cutout size was represented as a fraction of the radius of the cylinder $r = iR$ with $i = \{0.1,0.3,0.5\}$.

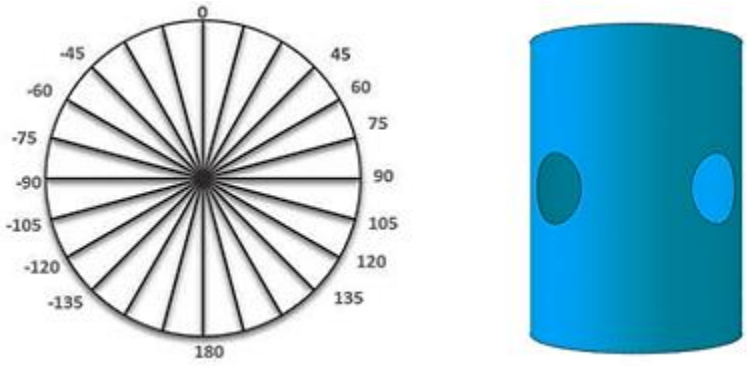

Figure 4.1 Cutout configuration possibilities [133]

The analysis was done using ABAQUS®, and the cylinder was modelled using S4R shell elements, which represents a general purpose, reduced integration, finite-membrane-strain shell element with four nodes and one integration point. A specific failure mode is preferred that is dominated by both local buckling around the cutout leading to local deformation and material failure progression. The finite element model for each cutout configuration was generated using Python® scripts integrated with the ABAQUS® environment for rapid model generation.

The response of each generated model was then analyzed using four different types of analyses in ABAQUS®. These types involve linear static analysis, linear buckling

analysis, and non-linear static analysis with and without progressive failure analysis [176]. Each analysis type is discussed briefly here, because they will be utilized after obtaining the optimal steered laminate design to verify the potential improvements that can be achieved using nonconventional variable stiffness laminates compared to conventional ones.

Linear Static Analysis:

Linear static analysis uses Hashin criterion to determine whether material failure has occurred or not. Hashin criteria investigates the stress state within each layer of the laminate for every element in the structure and determines if the stress values surpass the material failure thresholds. The failure load calculated using this analysis type is referred to as "first ply fiber failure", in which the failure corresponds to the load level at which fiber failure is first encountered. In most problems, first ply fiber failure is instigated after matrix failure happens which does not represent the collapse of the structure. The linear static analysis serves as a baseline for more accurate progressive failure analysis using the non-linear static response by identifying the onset of failure and the contribution of the stress concentration leading to material failure due to the presence of the cutout.

Linear Buckling Analysis:

Linear buckling analysis is used to calculate the critical eigenvalues and mode shapes for a shell under a specified loading. For pure bending case, the compressive bottom half is the region of interest where the cutout is also located. The linear buckling analysis assumes a perfect structure without any imperfections present and neglects any material or geometric imperfections (non-linearity). However, the eigenvalue analysis is extremely useful in determining the underlying causes of the collapse. This analysis also provides the

mode shapes that are used in the non-linear analysis to include a theoretical imperfection. The lowest five eigenvalues and their associated mode shapes are calculated using the Lanczos solver option within ABAQUS®.

Non-linear Analysis without Progressive Failure Analysis:

Non-linear static analysis is generally required for thin shells undergoing compressive loading because these structures highly depend on geometric non-linearity resulting from initial shape imperfections. The non-linear analysis tends to follow the linear buckling solution without the introduction of imperfections until an unstable eigenvalue is reached and the structure deforms into a post-buckled state. Thin-walled structures under compression often attain a much lower maximum load because of the triggering of post-buckled mode shapes with the presence of initial shape imperfections. A Riks analysis is used to follow these non-linear paths into the post-buckled range. To complete this non-linear analysis, the linear buckling solution is found in the usual manner and the mode shapes of the first five eigenvalues are preserved. The non-linear solution defines the imperfection as a small factor of the critical buckling mode or as a linear combination of the calculated modes. A theoretical 10% imperfection of the total shell thickness is used. The response is computed along the non-linear load path, and the maximum load that is attained is recorded.

Non-linear Analysis with Progressive Failure Analysis:

Anisotropic damage of fiber-reinforced composites can also be modeled in ABAQUS®. Hashin initiation criterion is used to predict the onset of damage, and the damage evolution law is based on the energy dissipated during the damage process and linear material softening. In the ABAQUS® progressive damage model, the material

stiffness is gradually reduced as deformation continues to accumulate after first ply fiber failure. This type of instantaneous, discrete stiffness reduction can pose severe convergence difficulties for finite element codes. As a result, the commercial Helius Progressive Failure Analysis (PFA) tool to monitor this aspect of the solution was used to provide more consistent numerical convergence as compared to the ABAQUS® progressive damage model. Helius PFA is composed of a set of software modules and a composite material library that integrates with the ABAQUS®/Standard finite element analysis, providing material modeling capability for unidirectional and woven fiber-reinforced composite materials. Helius PFA utilizes a form of multiscale material modeling that is based on Multi-Continuum Theory (MCT). In traditional continuum mechanics approach, the physical quantities such as stress and strain are averaged over the entire heterogeneous microstructure of the composite material. In contrast, MCT retains the properties of the fiber and matrix constituents within the microstructure. Consequently, the physical quantities of interest are averaged over each individual constituent. During an ABAQUS® finite element analysis of a composite structure, Helius PFA decomposes the composite average stress/strain field into constituent average stress/stain fields. The constituent average stress states are used by Helius PFA to predict damage evolution and material failure individually for each of the fiber and matrix in the structure. It is generally difficult to achieve good convergence in a progressive failure simulation of a composite structure. In fact, many progressive failure analyses terminate before global structural failure due to the inability of the finite element code to obtain a converged solution at a certain load increment. Helius PFA significantly improves the overall convergence rate and robustness of finite element simulations of progressive failure of composite structures. Progressive

failure analysis (PFA) can also be assessed during the non-linear Riks analysis, which provides the best overall estimate of the response of the cylindrical shell.

These analyses types were then used to assess the performance of each model with different cutout configuration. A summary of the obtained results is presented in Figure 4.2.

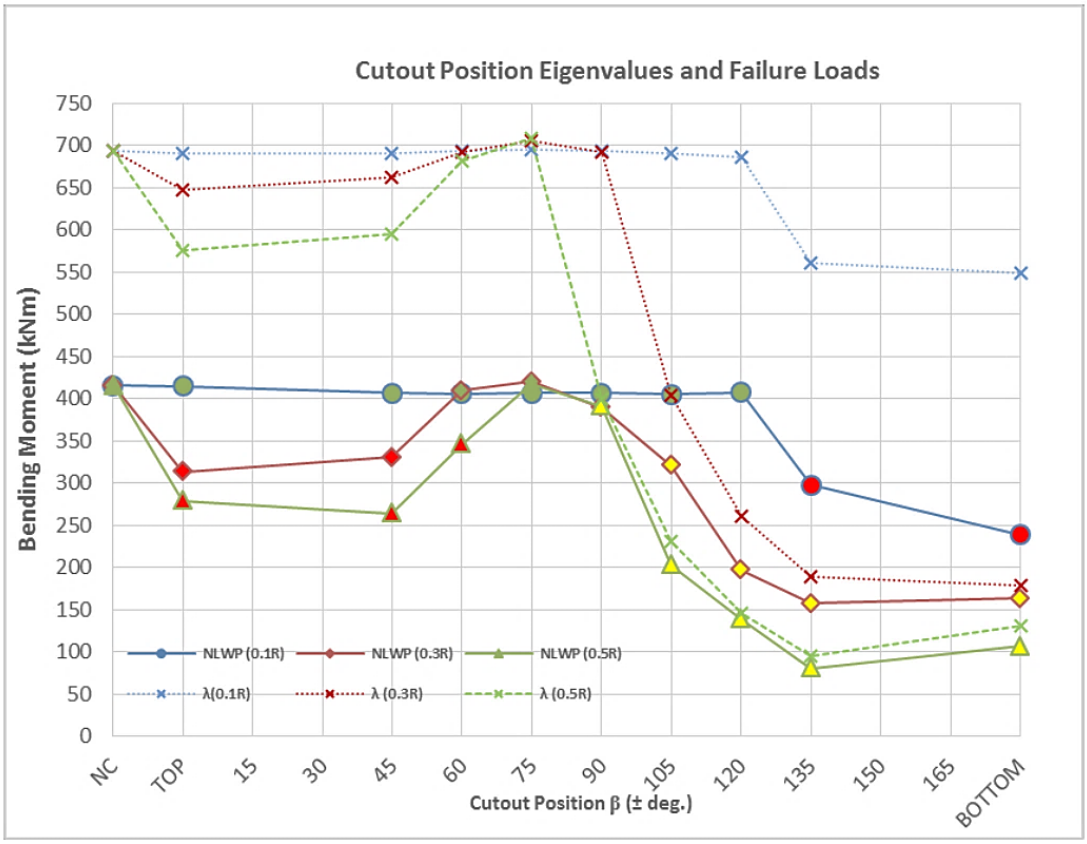

Figure 4.2 Failure loads as a function of cutout position β for different cutout sizes [176]

Several observations were made concerning the effects of the cutout size and location. Smaller cutouts have little effect on the buckling of the structure except if they are situated in the compressive area of the cylindrical shell ($\beta \geq 120°$). The stress concentrations are also higher because the material failure is initiated at a considerably lower level. For medium to large cutouts at the top of the cylinder, the cylindrical shell exhibits similar buckling modes and knockdown factors as the classical global shell

collapse mode of failure. However, at the lower half of the cylinder ($\beta \geq 90°$), a huge drop is shown in the linear buckling load signifying that local buckling initiates around the cutout. In addition, stress concentrations around the cutout highly reduce the ultimate failure load. As a result, the collapse of the cylinder is assumed to be instigated by a combination of material failure and buckling deformation leading to an "interactive local and global failure mode". The cutout size $r = 0.3R$ and $\beta = 120°$ was chosen for the design application to tailor the performance of the cylindrical shell to optimize the buckling performance of the cylindrical shell.

4.1.2 Cylindrical Model for Design Application

Cylindrical Shell Geometry:

The cylindrical shell shown in Figure 4.3 has a circular cross section with a radius *R* of 304.5 mm (12 in), a length *L* of 813 mm (32 in), and an overall shell thickness of 4.392 mm (0.173 in) with 24 plies. A pure bending moment about the x-axis is introduced at each end of the cylinder leading to compression at the bottom of the cylinder, $\beta = 180°$, and tension at the top, $\beta = 0°$.

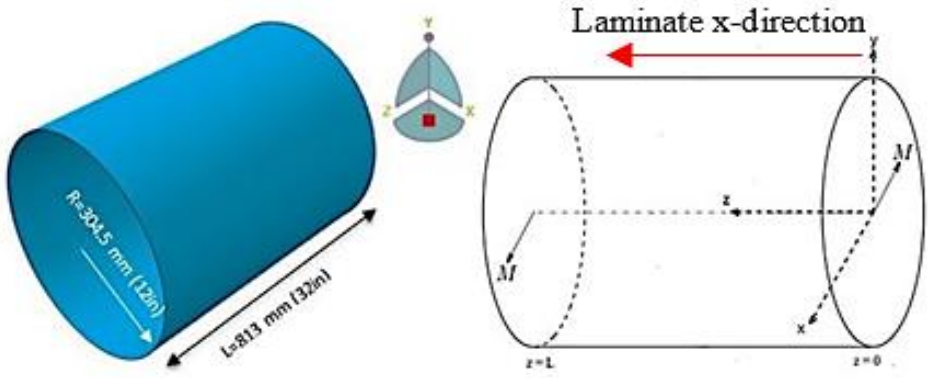

Figure 4.3 Cylinder geometry

The initial stacking sequence of the composite shell is given as $[\pm 45/0_2/90_2/0/\pm 45_2/90]_s$, which is an optimized conventional laminate for the cylindrical shell without a cutout [169]. Results for an optimized cylindrical shell with a cutout presented later will be compared to this baseline conventional laminate design, which happens to be a quasi-isotropic stacking sequence.

Specified Cutout Configuration:

The cutout configuration chosen is shown in Figure 4.4. The cutout has a circular cross section and is centered longitudinally at the mid-length of the cylindrical shell. The cutout is located at an angle $\beta = 120°$ measured circumferentially from the top of the cylinder with a similar cutout also placed at $\beta = -120°$ to maintain left/right symmetry. The cutout size is $r = 0.3R$ where R is the total radius of the cylinder. As explained before, the cutout location and size were chosen based on the parametric design study to obtain a failure mode that reflects interaction of both local buckling and stress concentrations around the cutout.

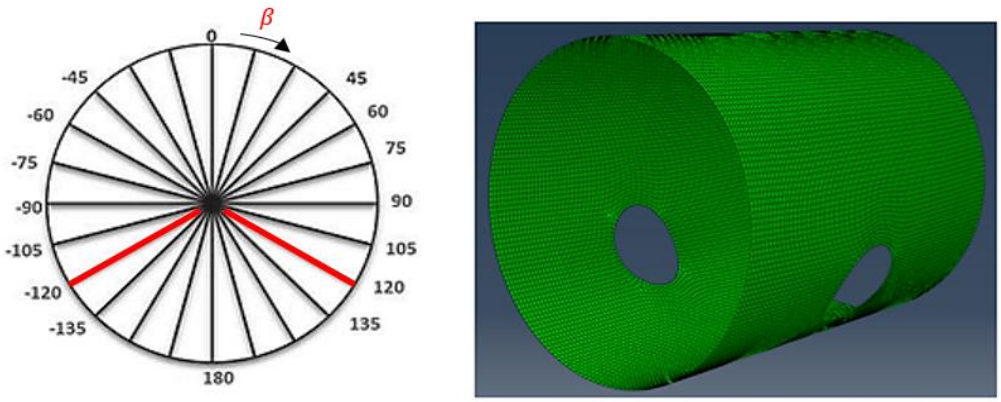

Figure 4.4 Cutout configuration $r = 0.3R$, $\beta = 120°$

Material Properties:

IM7/8552 material is used for design and analysis which is a typical material used in aerospace applications [176]. The material properties are provided in Table 4.1.

Table 4.1 IM7/8552 (1290 g/mm^2) Lamina Mechanical Properties

t_{ply}	0.183 mm (0.0072 in)	ρ	1580 kg/m^3 (0.057 lb/in^3)
E_1	158.5 GPa (23.0 Msi)	X_t	2500.7 MPa (362.7 ksi)
E_2	8.963 GPa (1.3 Msi)	X_c	1716.4 MPa (248.9 ksi)
ν_{12}	0.316	Y_t	64.05 MPa (9.29 ksi)
G_{12},G_{13}	4.688 GPa (0.680 Msi)	Y_c	285.7 MPa (41.44 ksi)
G_{23}	3.9735 GPa (0.444 Msi)	S	91.15 MPa (13.22 ksi)

A design-manufacturing mesh is introduced to model the stiffness variation to reduce the computational expense in evaluating the sensitivity of the responses with respect to the design variables (lamination parameters). The design variables are then extrapolated to the nodes after the optimum results are obtained. The design-manufacturing mesh is generated using a Python® script integrated with the ABAQUS® environment for rapid model generation. The variable stiffness distribution is mapped to the design-manufacturing mesh in ABAQUS® using distribution tables over element sets. The variable stiffness design problem is then solved using two decoupled but dependent meshes. The analysis mesh, which is a finer mesh, is used to evaluate the buckling finite element solutions, whereas the design-manufacturing mesh is used to design the laminated structure by mapping the values of the design variables to the analysis mesh considering several

design regions with different stiffness properties. A global stiffness variation with 8 circumferential by 4 longitudinal design regions is shown in Figure 4.5. All the area of the cylinder is used to discretize the design-manufacturing mesh with uniform circumferential and longitudinal divided regions as specified by the user. However, the presence of the cutout imposes severe stress concentrations around its area. As a result, it may require additional local stiffness variation around the cutout to capture an optimal stiffness distribution. A global-local stiffness variation is shown in Figure 4.6, where the local area around the cutout is also divided into longitudinal and circumferential regions to further tailor the stiffness properties around the hole.

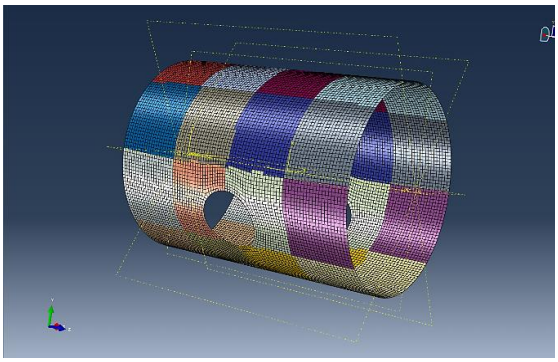

Figure 4.5 Global stiffness variation of cylindrical shell

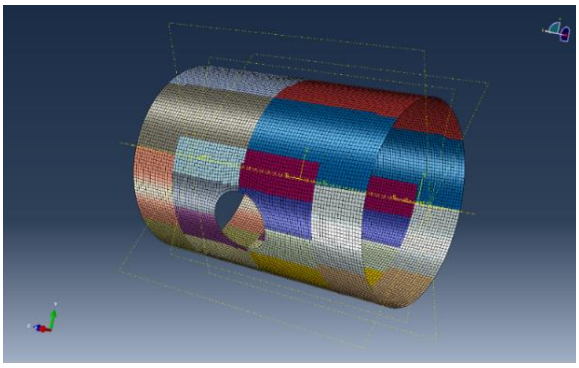

Figure 4.6 Global-local stiffness variation of cylindrical shell

The B-spline surface spatial distribution of the lamination parameters described in Section 3.2.1 has not been considered in this application because it was interesting to study the separate effect of the axial and circumferential stiffness variations as well as the importance of including a locally refined design-manufacturing mesh around the region of the cutout. To account for locally refined design-manufacturing mesh distribution around the hole, a non-uniform B-spline surface must be utilized.

4.2 CONCEPTUAL STIFFNESS OPTIMIZATION

The first optimization step lies in obtaining the optimum lamination parameters that would result in the optimum stiffness requirements for the considered structural performance. Following the conservative convex separable approximations as discussed in Section 3.2.2, the optimization formulation for maximizing the buckling load will be presented in this section.

4.2.1 Conservative Convex Separable Approximations

Successive approximations of the response are extensively used in structural optimization, mainly to improve the computational efficiency by reducing large number of repetitive exact analysis. In addition, the separable nature of the approximations can facilitate parallel computing to further reduce the computational flow time. The response to be optimized is expressed as an approximation, and the optimization problem is implemented on the conservative convex separable approximations. The approximations are then updated at the new design points, and this is repeated until convergence is achieved. The successive approximations are expressed directly in terms of the laminate stiffness matrices that are linear functions of the lamination parameters. As a result, the parameterization scheme used in this approach retains the convex nature of the design space yielding a unique optimum stiffness. A homogenous convex approximation that is a hybrid formulation of linear and reciprocal approximations, is utilized for approximating r_b, which is defined as the inverse of the buckling load. The response is expanded using a Taylor series in terms of in-plane and out-of-plane stiffness matrices and their reciprocals.

The optimization problem is formulated as a minimization of the buckling load factor r_b in order to maximize the buckling load of the cylindrical shell. The effect of stiffness on r_b is divided into two parts to achieve a convex approximation. The first part of the responses is expanded linearly in terms of the stiffness matrices while the second part is expanded reciprocally in terms of the inverse of the stiffness matrices. The approximation thus can be expressed as:

$$r_b = \sum_{i=1}^{N} (\breve{\Psi}_i^m : A_i + \breve{\Psi}_i^b : D_i + \breve{\Phi}_i^m : A_i^{-1} + \breve{\Phi}_i^b : D_i^{-1}) \,,$$
$$\Psi^m = \frac{\partial r_b}{\partial A} \,, \Psi^b = \frac{\partial r_b}{\partial D} \,, \Phi^m = \frac{\partial r_b}{\partial A^{-1}} \,, \Phi^b = \frac{\partial r_b}{\partial D^{-1}} \,, \tag{4.1}$$

where $\breve{\Psi}_i^m$ and $\breve{\Psi}_i^b$ are the damped sensitivity matrices with elements representing the derivatives of r_b with respect to the elements of the in-plane and out-of-plane stiffness matrices, A_i and D_i, respectively, for the i^{th} design region in the design-manufacturing mesh including the convexifying terms obtained from damping [36]. Similarly, $\breve{\Phi}_i^m$ and $\breve{\Phi}_i^b$ are the damped sensitivity matrices with elements representing the derivatives of r_b with respect to the elements of the inverse of the in-plane and out-of-plane stiffness matrices, A_i^{-1} and D_i^{-1}, respectively, for the i^{th} design region in the design-manufacturing mesh. Because of the separability of the structural approximation, the optimization problem can be conducted as N independent local optimization problems as:

$$\min_{x_i} \; (\breve{\Psi}_i^m : A_i + \breve{\Psi}_i^b : D_i + \breve{\Phi}_i^m : A_i^{-1} + \breve{\Phi}_i^b : D_i^{-1}) \tag{4.2}$$

where x_i is the vector of design variables containing the lamination parameters $V_{1,3}$ and $W_{1,3}$ of each design region i subject to the constraints of the feasible regions.

Multiple buckling modes must be considered to make sure mode-switching does not take place while the cylindrical shell is optimized. For this case, five mode shapes are considered for buckling. The optimization problem can be formulated as minimizing the maximum response subject to the feasible region of lamination parameters [102]:

$$\min(\max(r_{bi})) \qquad \text{subject to } (V, W) \text{ feasible domain }, \tag{4.3}$$

where r_{bi} (for i = 1,…,5) is the value of the inverse of the buckling load factor for mode number i. A 16% rule is also applied to each design region i in the design-manufacturing mesh to ensure the lamination parameters obtained satisfy the 10% robustness rule [136]. A 16% rule is used instead of 10% to obtain at least four 90° layers out of 24 plies. Because a 24-ply symmetric laminate is to be obtained, having only two 90° layers does not satisfy the 10% rule and using 4 plies would then represent 16.67% of the laminate.

This multi-response optimization problem can be solved using the bound formulation proposed by Olhoff, by introducing a new variable β and reformulating the optimization problem:

$$min\,\beta \quad subject\ to \quad r_{bi} \leq \beta\,, \tag{4.4}$$

with β being an upper-bound for r_{bi}. The problem can be subsequently solved using the dual method [135], which can be expressed as:

$$\max\min(\sum_{i=1}^{5}(\mu_b r_b)) \qquad subject\ to \sum_{i=1}^{5}\mu_b = 1\,, \tag{4.5}$$

where $\mu_{b,s}$ are the Lagrange multipliers for the different buckling modes r_b (for i = 1,…,5). Solving the optimization problem of Eq. (4.5) leads to maximizing the buckling load, hence the problem is a stiffness tailoring problem. The numerical results of each stiffness variation are summarized below for optimizing the buckling load of the cylindrical shell.

4.2.2 Global Stiffness Variation Results

In the global stiffness variation, the whole area of the cylinder is uniformly divided along the length or circumference. The cylindrical model under bending is symmetric around the two vertical symmetry planes. The 0-degree direction of the laminate is defined along the longitudinal coordinate z of the cylinder. It is expected that the circumferential variation along the circumferential coordinate β (β = 0º at top of cylinder) will provide the most significant improvements in the load carrying capability of the cylinder [65,127,173]. To demonstrate that, the cylinder is discretized into 16 circumferential regions as shown in Figure 4.7.

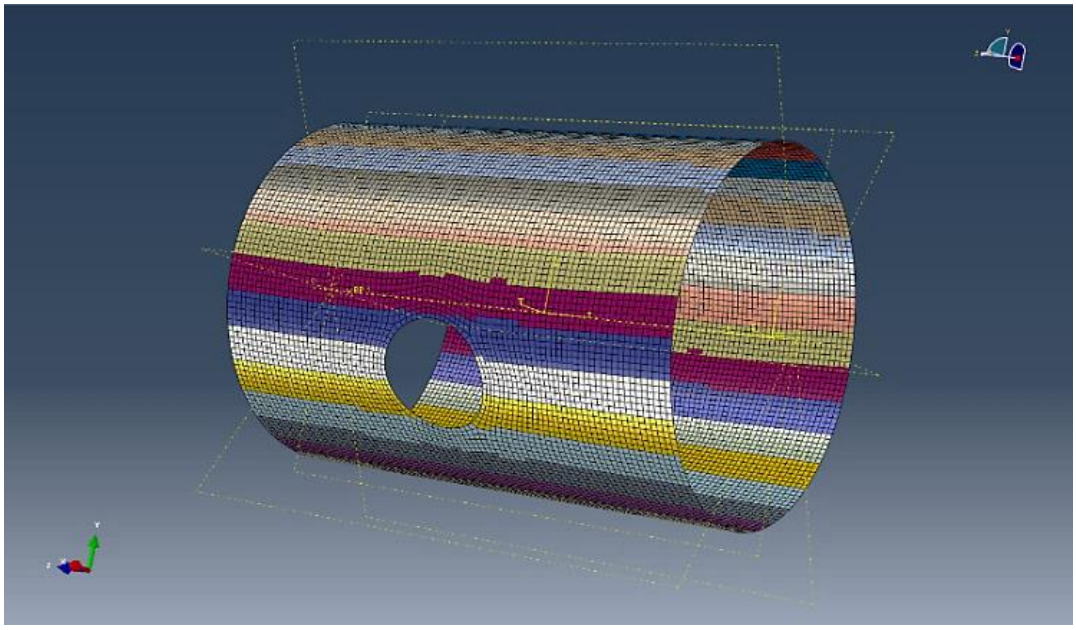

Figure 4.7 Global circumferential stiffness variation with 16 circumferential regions

After solving the optimization problem, the critical buckling load λ increases from 267 kN.m to 459 kN.m, which is a 72% increase compared to the initial quasi-isotropic design. This demonstrates that circumferential tailoring has indeed significant improvements on the critical buckling load of the cylindrical shell with a cutout under

bending. To visualize the optimum circumferential stiffness variation, the cylinder surface is developed on a flat plane in Figure 4.8, and contour plots of the equivalent axial in-plane stiffness E_x, and out-of-plane axial stiffness D_x are shown (in GPa). As a reference, E_x = 59.65 GPa and D_x = 70.91 GPa for the quasi-isotropic laminate. The equivalent laminate stiffnesses are obtained from the inverse of the **[ABD]** matrix. The contour plot resembles a cylindrical shell with longitudinal stiffeners that modify the stiffness properties around the circumference.

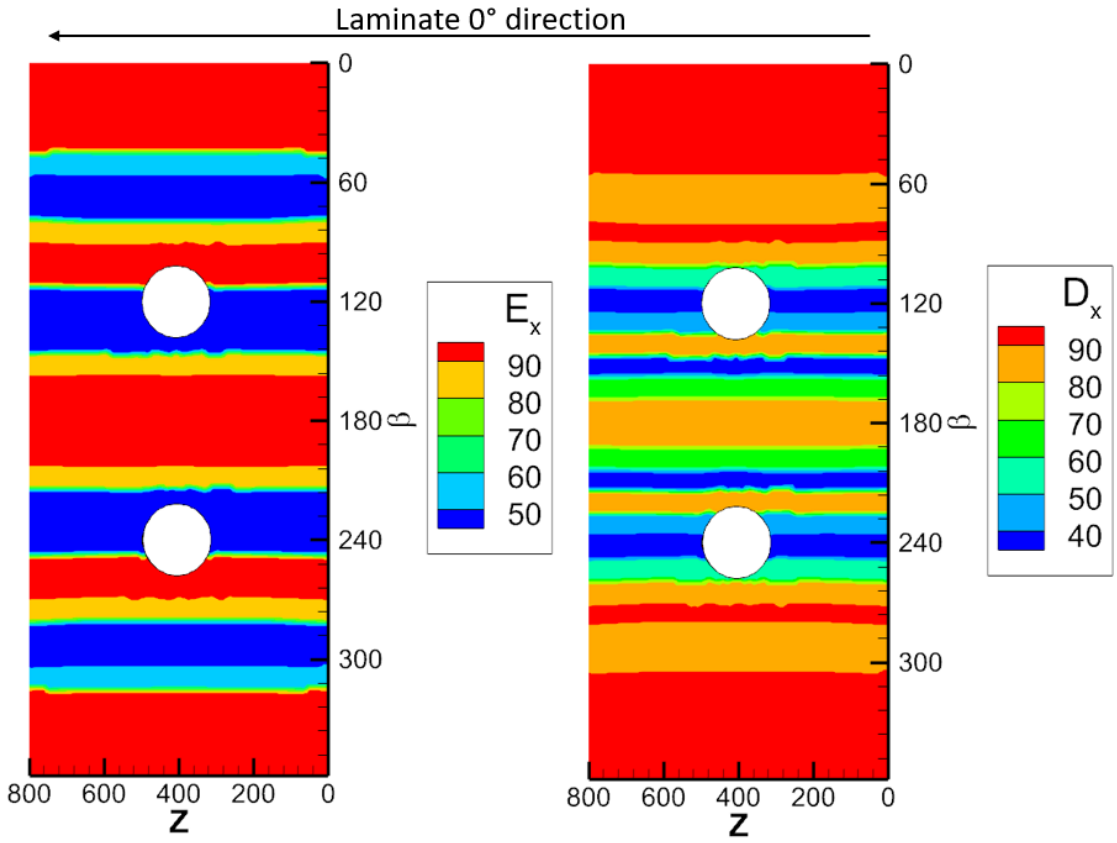

Figure 4.8 Equivalent axial stiffnesses of cylinder with circumferential variation

Since the stiffness variations are along the circumferential direction β only, the effective axial in-plane stiffness E_x and the effective circumferential in-plane stiffness E_β

are normalized with respect to the in-plane stiffness of the quasi-isotropic laminate and shown in Figure 4.9.

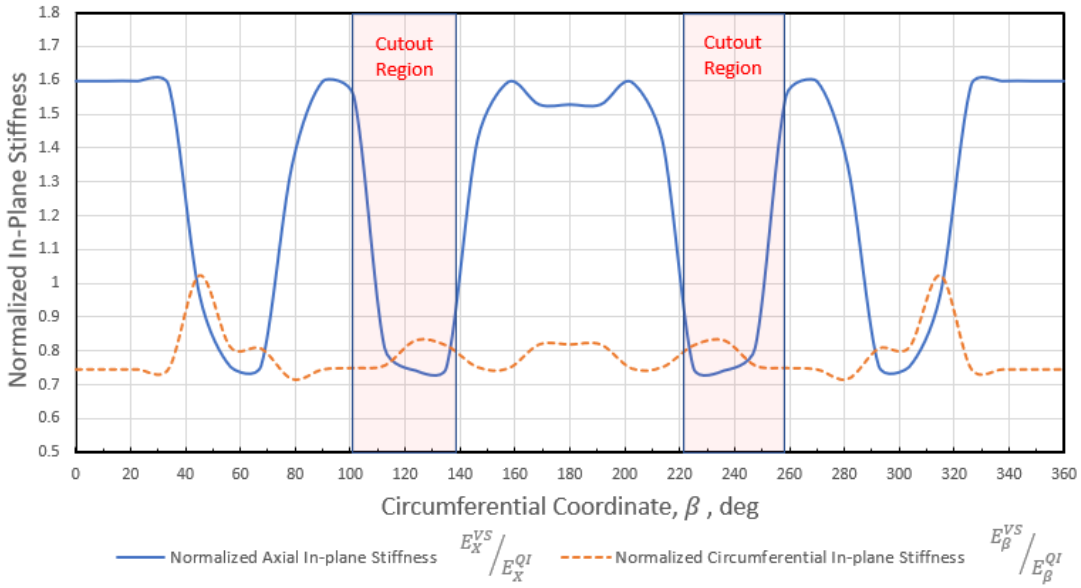

Figure 4.9 Normalized circumferential in-plane stiffness variation

The maximum axial in-plane stiffnesses (with values of 1.6 times the axial stiffness of the quasi-isotropic laminate) are at the top region ($0° \leq \beta \leq 40°$), just above the cutout location ($90° \leq \beta \leq 100°$), and right below the cutout at the bottom region ($150° \leq \beta \leq 180°$) of the cylindrical shell. The axial stiffnesses at the cutout region ($100° \leq \beta \leq 140°$) have relatively much lower values, which indicates that the cutout region is carrying a relatively lower in-plane load N_x ($N_x \approx E_x \varepsilon_x t$) and the load is redistributed to the stiffer regions right above and below the cutout region. There is also a transition region above the cutout ($40° \leq \beta \leq 80°$) with relatively much lower axial stiffness that also helps in redistributing the loads from the cutout region to the stiffened region at the top of the cylinder. The higher values of the circumferential stiffness E_β at this transition region indicates that it carries slightly higher circumferential loads N_β.

Similarly, the normalized effective axial out-of-plane stiffness D_x and effective circumferential out-of-plane stiffness D_β are plotted in Figure 4.10.

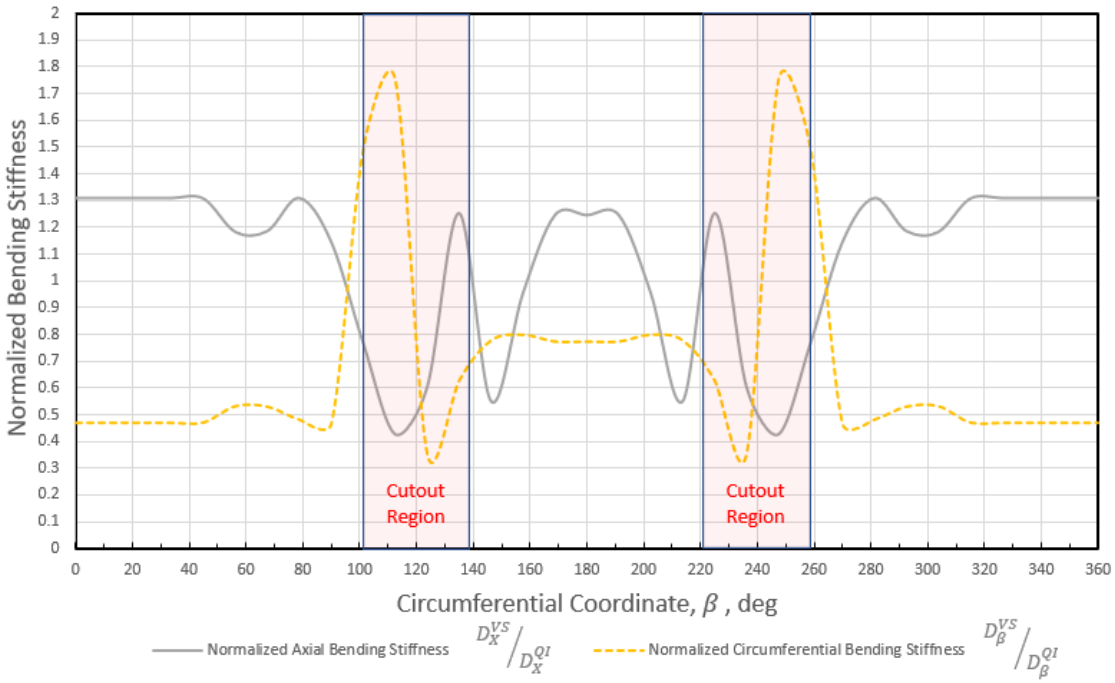

Figure 4.10 Normalized circumferential out-of-plane stiffness variation

The out-of-plane equivalent axial stiffnesses show that the stiffness variations are important around the cutout region and at the compression side of the cylinder ranging from $80° \leq \beta \leq 180°$, because this area is loaded in compression. However, the top region of the cylinder ($0° \leq \beta \leq 80°$) is insensitive to out-of-plane stiffness because it is loaded in tension. This can be clearly shown by plotting the axial strain distribution ε_x as shown in Figure 4.11. The presence of the cutout in the cylinder shifts the neutral axis from the 90° circumferential location by almost 1°, and the region above the neutral axis location is subjected to tension loads, which are insensitive to out-of-plane stiffnesses. The circumferential stiffness variation further shifts the neutral axis to $\beta = 84°$, and the compressive strains obtained were thus larger than the quasi-isotropic cylinder while the

tensile strains were smaller. The fluctuations in the equivalent out-of-plane stiffness near the cutout indicate the importance of locally reinforcing the regions around the cutout, where the maximum axial bending stiffnesses are at the cutout region ($120° \leq \beta \leq 140°$) and at the bottom compression side of the cylinder ($160° \leq \beta \leq 180°$). The circumferential bending stiffness also plays a significant role in increasing the circumferential moment resultants M_β to decrease the axial moment resultants M_x at the cutout region ($100° \leq \beta \leq 120°$).

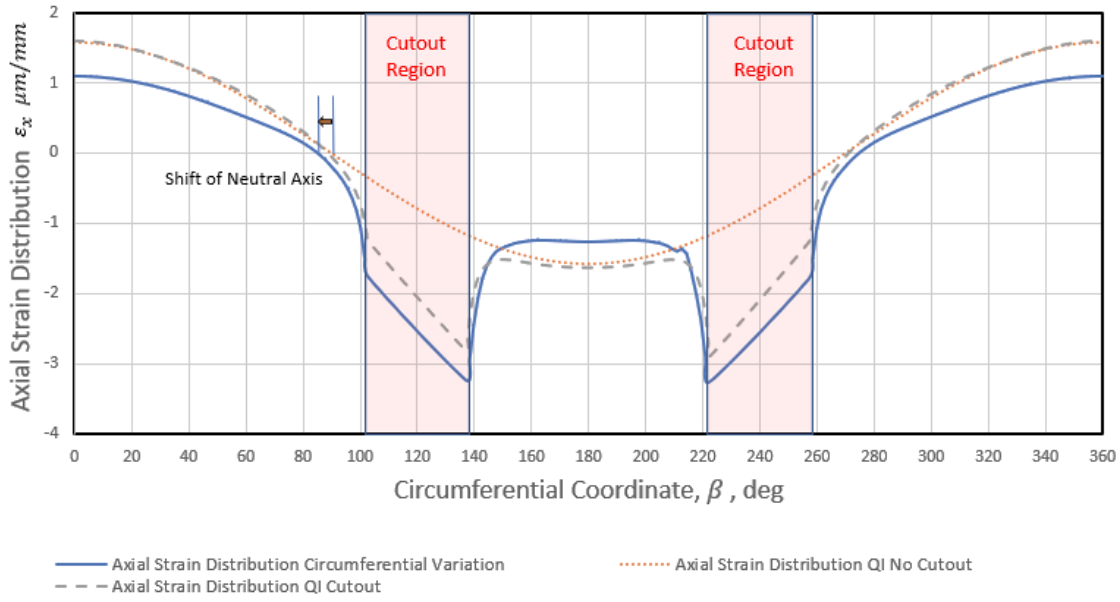

Figure 4.11 Axial strain distribution for circumferential variation

To gain more insight into the effects of the circumferential variation on the structural performance, the distribution of the in-plane axial force resultant N_x and the axial moment resultant M_x are obtained by extracting the values from the ABAQUS® output database along the circumferential path shown in Figure 4.12. A pre-buckling moment of 120 kN.m is applied. The distributions depend on both the stiffness distributions and the laminate mid-plane strain and curvature distributions along the circumferential coordinate.

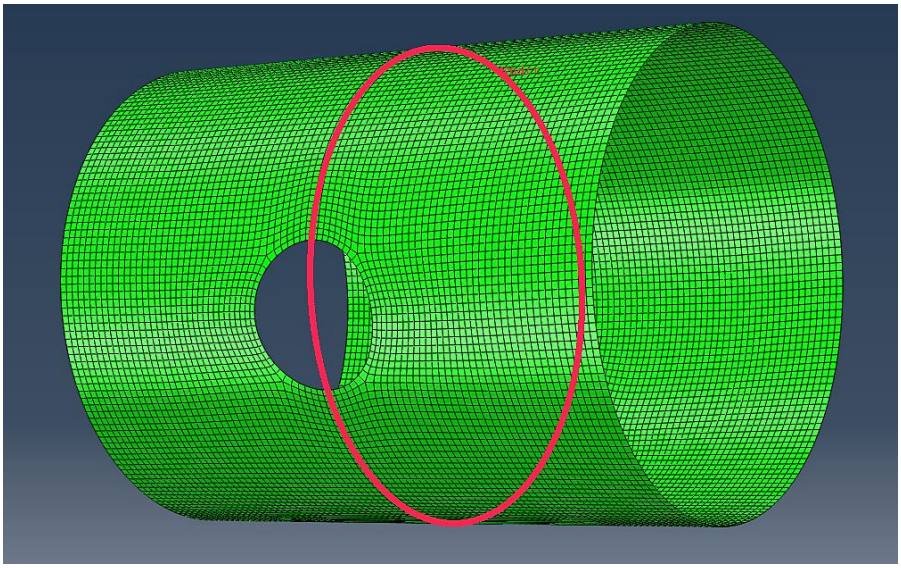

Figure 4.12 Circumferential path at mid-length of cylinder

The axial load and moment variations are shown in Figure 4.13 and Figure 4.14, respectively. The tensile loads carried by the variable stiffness cylinder were higher at the top of the cylinder ($0° \leq \beta \leq 40°$) and lower at the transition region ($40° \leq \beta \leq 80°$) , which demonstrates the load distribution at the tension side of the cylinder. At the compression side, the presence of the cutout results in a huge increase of the compression loads at the bottom side of the cutout region $\beta = 140°$, while the circumferential stiffness variation results in much lower compressive loads of almost 50% smaller that the quasi-isotropic case. The compressive loads at ($150° \leq \beta \leq 180°$) are also higher compared to the quasi-isotropic case which also indicates the load distribution mechanism from the cutout region to the stiffened region at the bottom of the cylinder.

A similar observation is found by comparing the axial moment distribution, but the mechanism resulting in an improved buckling load is the local reinforcement and variation of the bending stiffnesses at the cutout region, since the axial moments are reduced at every point along the circumferential path. The presence of the cutout induces a huge axial

moment increase compared to a cylinder without a cutout, and the circumferential stiffness variation reduces the maximum axial moment at the cutout region to almost 10%. The axial moments at the compression side below the cutout ($150° \leq \beta \leq 180°$) are also almost reduced to zero, thus highly improving the buckling load capacity.

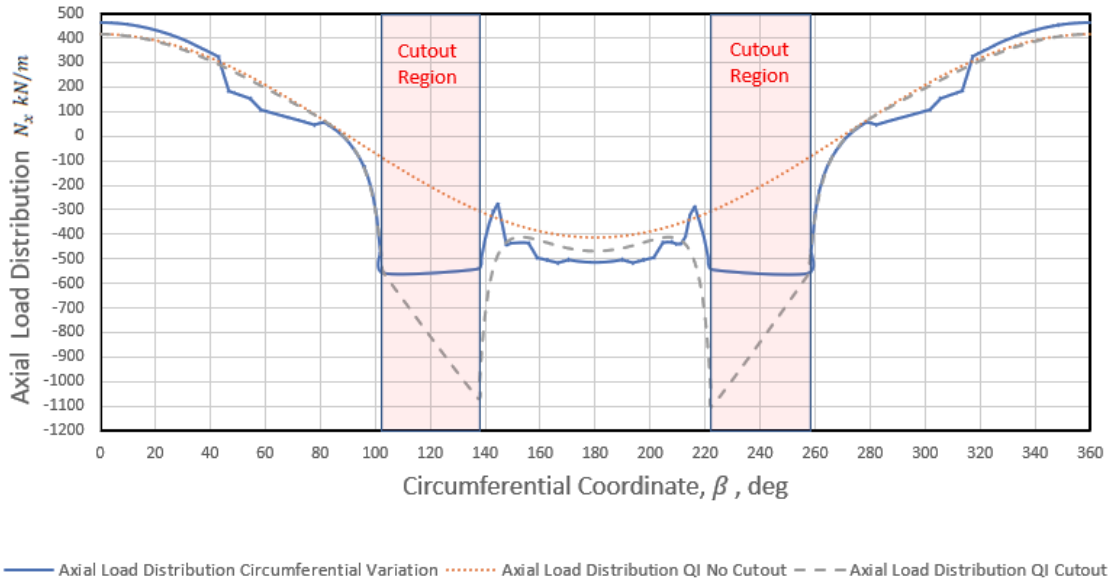

Figure 4.13 Axial load distribution for circumferential variation

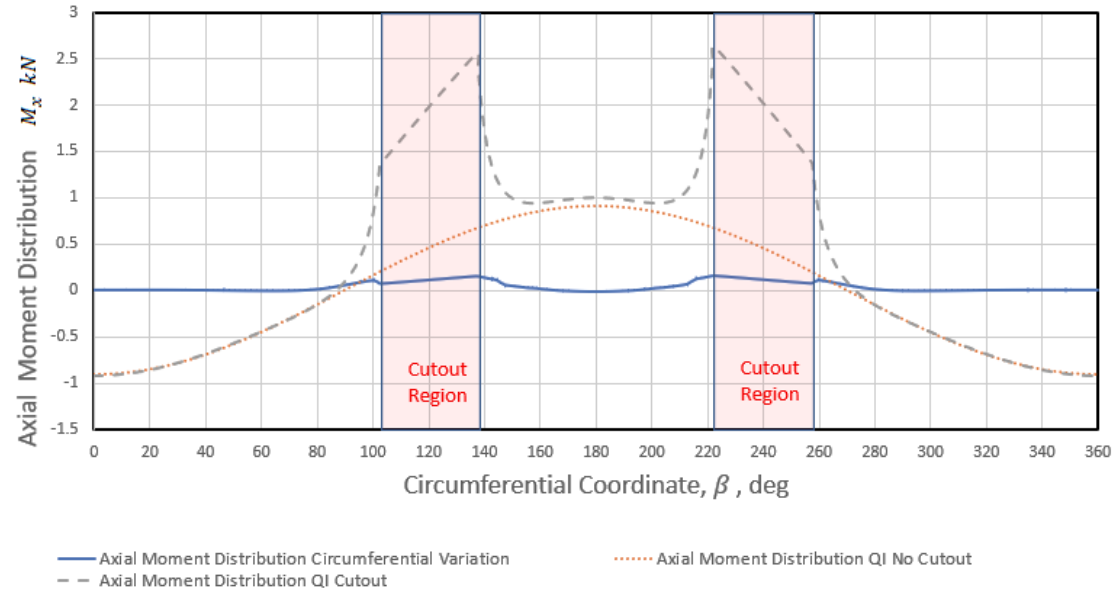

Figure 4.14 Axial moment distribution for circumferential variation

As for longitudinal stiffness variation, the cylindrical shell with a hole is discretized into 16 longitudinal regions as shown in Figure 4.15.

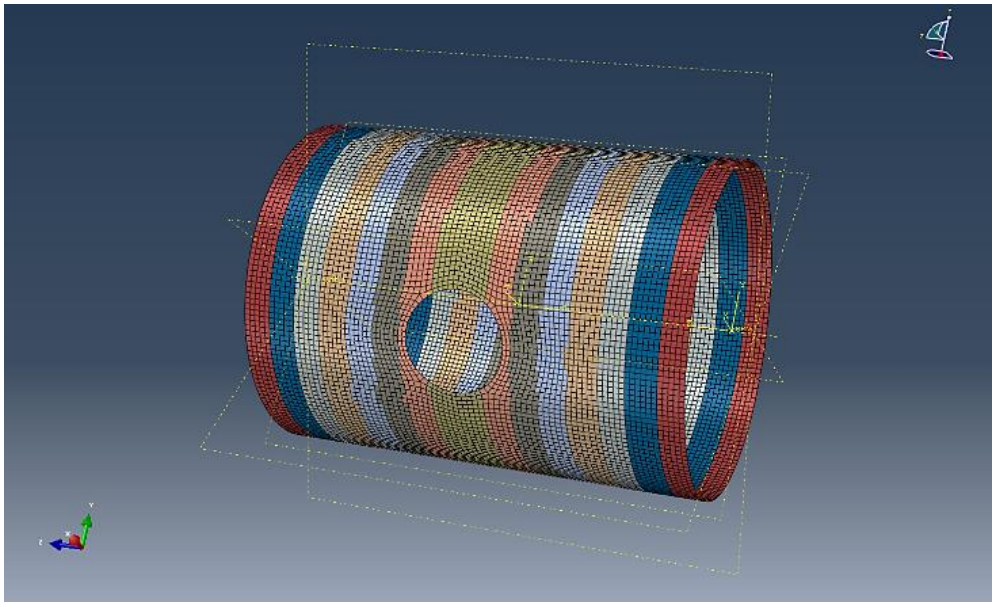

Figure 4.15 Global longitudinal stiffness variation with 16 longitudinal regions

After solving the optimization problem, the critical buckling load increases from 267 kN.m to 321 kN.m, which is a 20% increase compared to the initial quasi-isotropic design. Although this is a smaller increase compared to the circumferential stiffness tailoring, it is still a significant improvement that increases the load carrying capability of the cylindrical shell. The cylinder surface is also developed on a flat plane to visualize the optimum axial stiffness properties in Figure 4.16, and contour plots of the equivalent axial in-plane stiffness E_x, and out-of-plane axial stiffness D_x are shown (in GPa). As a reference, E_x = 59.65 GPa and D_x = 70.91 GPa for the quasi-isotropic laminate. The contour plot resembles a cylindrical shell with ring stiffeners that modify the stiffness properties around the length of the cylinder.

Since the stiffness variations are along the longitudinal direction z only, the effective axial in-plane stiffness E_x and the effective circumferential in-plane stiffness E_β

are normalized with respect to the in-plane stiffness of the quasi-isotropic laminate and shown in Figure 4.17.

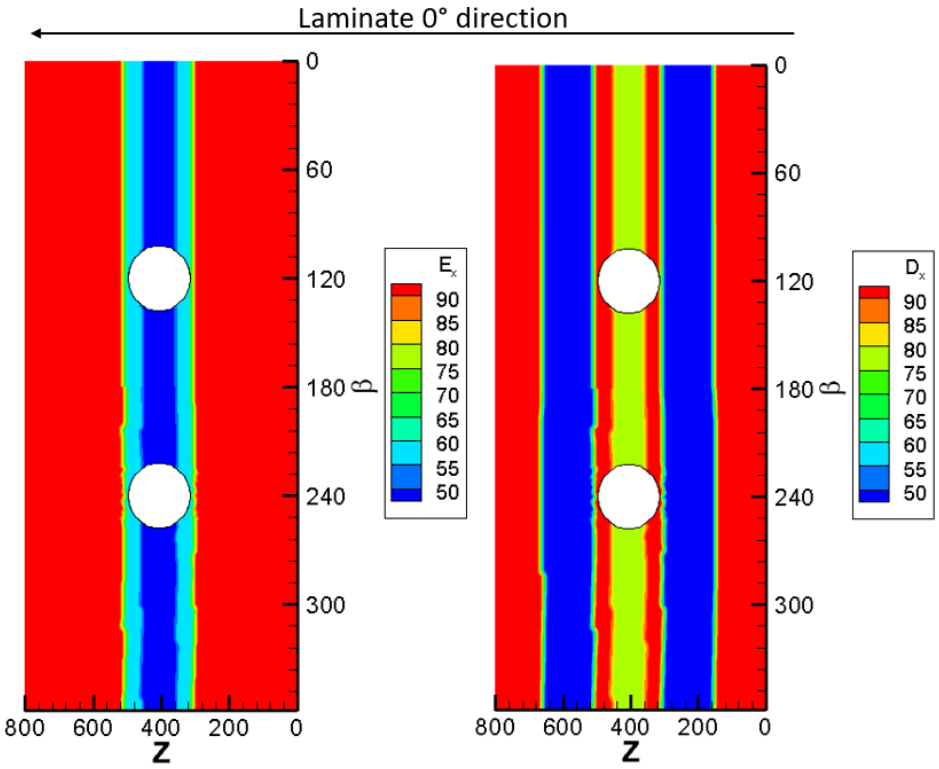

Figure 4.16 Equivalent axial stiffnesses of cylinder with longitudinal variation

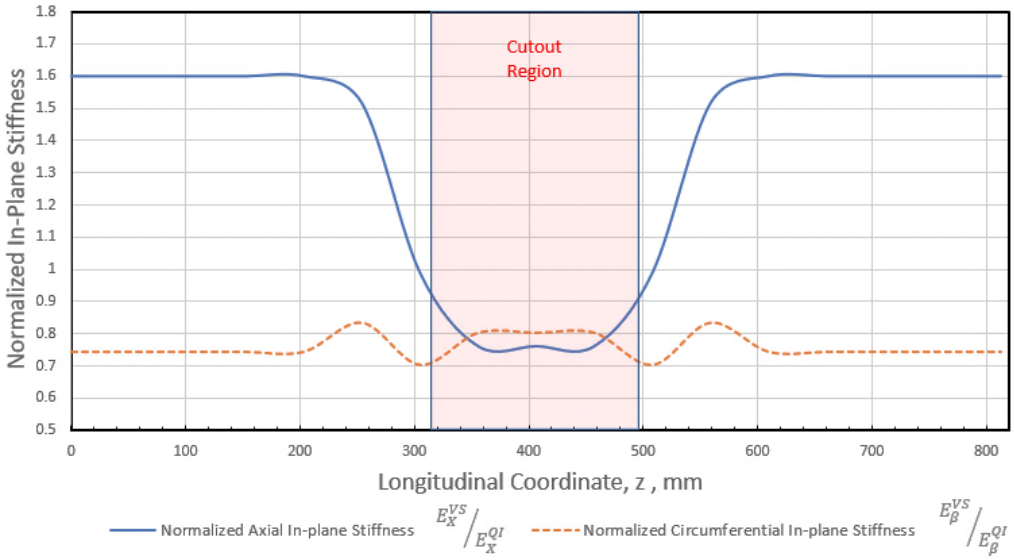

Figure 4.17 Normalized longitudinal in-plane stiffness variation

The maximum axial in-plane stiffnesses are at the ends of the cylinder away from the cutout ($0 \leq z \leq 200\ mm$), and the axial stiffness at the cutout region is relatively much smaller signifying that the axial load at the cutout region is smaller. The lower values of circumferential in-plane stiffness E_β are important in reducing the circumferential load resultants N_β around the cutout. Similarly, the normalized effective axial out-of-plane stiffness D_x and effective circumferential out-of-plane stiffness D_β along with the normalized Poisson's ratio are plotted in Figure 4.18. Since the cutout is in the bottom region of the cylinder under compression, the variation of the out-of-plane stiffnesses is important to reinforce to region around the cutout and improve the buckling load. The maximum axial bending stiffnesses are on the right and left sides of the cutout region $z \approx 316$ and $z \approx 496$, and away from the cutout at the edges of the cylinder. The variation of D_x is very similar to the variation of the Poisson's ratio around the region of the cutout. The higher values of D_x (higher values of D_{11}, D_{12} due to the Poisson's ratio, and relatively lower values of D_{22}) at the cutout region help in preventing the cutout edge from buckling, but also the lower values of circumferential bending stiffness D_β are important in reducing the circumferential moment resultants M_β around the cutout.

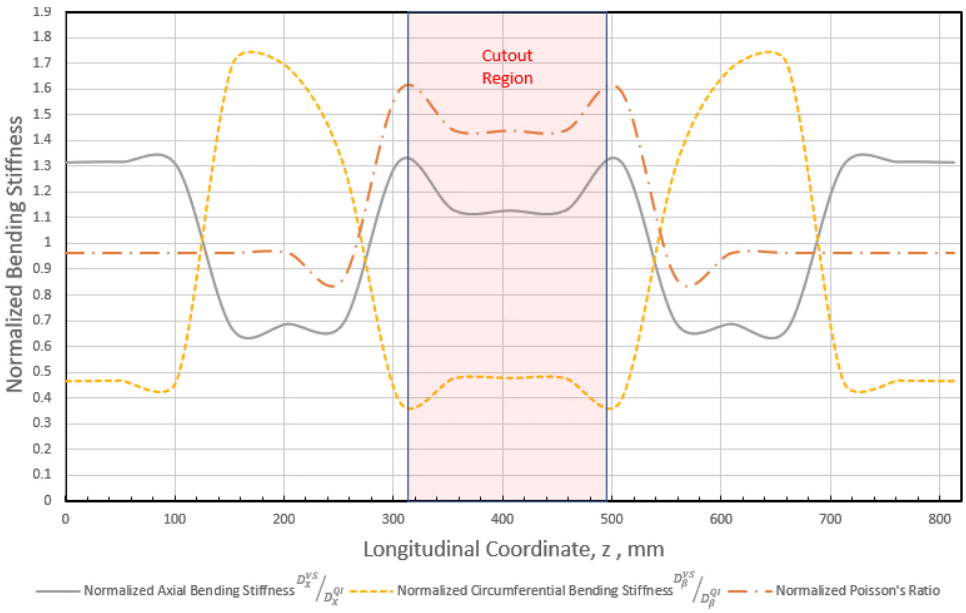

Figure 4.18 Normalized longitudinal out-of-plane stiffness variation

To gain more insight into the effects of the longitudinal variation on the structural performance, the distribution of the in-plane axial and circumferential force resultants N_x, N_β, and the axial and circumferential moment resultants M_x, M_β are obtained by extracting the values from the ABAQUS® output database along the longitudinal path shown in Figure 4.19. A pre-buckling moment of 120 kN.m is applied. The distributions depend on both the stiffness distributions and the laminate mid-plane strain and curvature distributions.

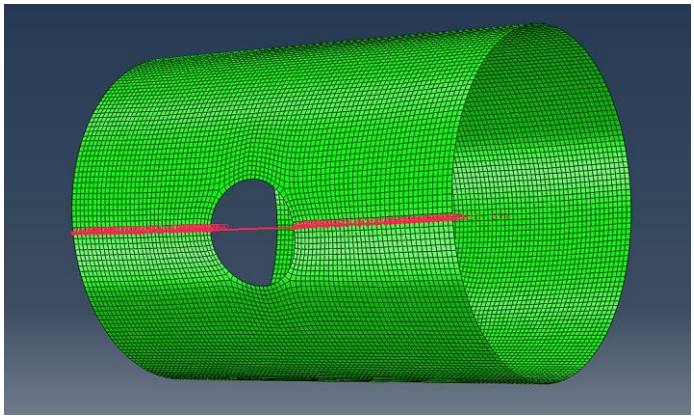

Figure 4.19 Longitudinal path at cutout location $\beta = 120°$

The axial load and moment variations are shown in Figure 4.20 and Figure 4.21, respectively. There is no effective load redistribution mechanism that transfers the loads from the cutout region to the regions away from the cutout, but rather a reinforcement mechanism that reduced the load and moment resultants slightly around the region of the cutout and close to the edges of the cylinder. The axial load and moment resultant are much smaller compared to the cylinder without a cutout, hence the modification of the axial stiffness properties is not the main reason behind the increase of the buckling load.

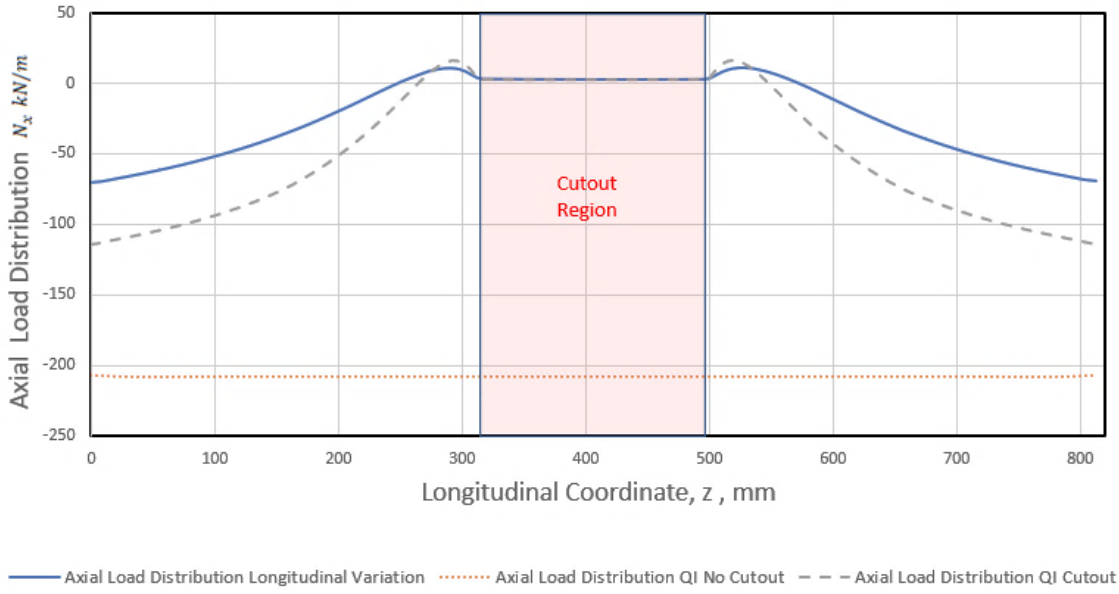

Figure 4.20 Axial load distribution for longitudinal variation

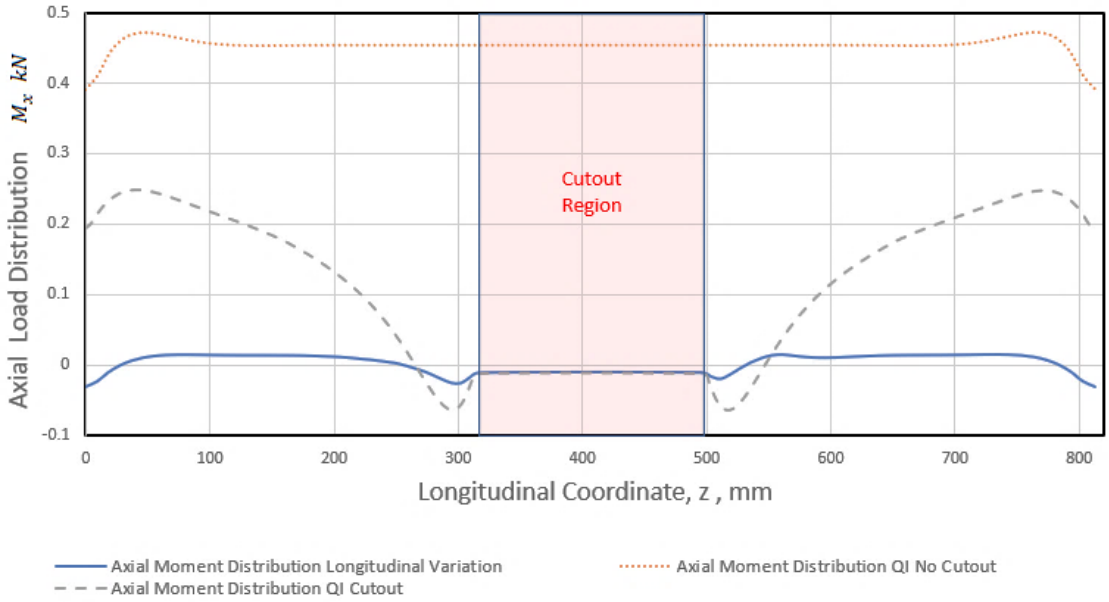

Figure 4.21 Axial moment distribution for longitudinal variation

However, the increase in the buckling load can be explained by the circumferential load and moment variations as shown in Figure 4.22 and Figure 4.23, respectively. The presence of the cutout in the cylinder results in an increase in the circumferential load and moment resultants compared to the "pristine" cylinder. The longitudinal stiffness variation thus decreases the circumferential load (around 50%) and moment resultants (around 75%) at the cutout region yielding a higher buckling capacity. The reduction of the load and moment resultants can be explained by the Poisson's ratio effect as well as the modification of the stiffness and strain distributions. The axial strains were mostly compressive strains around the cutout region, while the circumferential strains where tensile. Hence, the Poisson's ratio helps in reducing the loads and moments by cancelling the positive and negative terms.

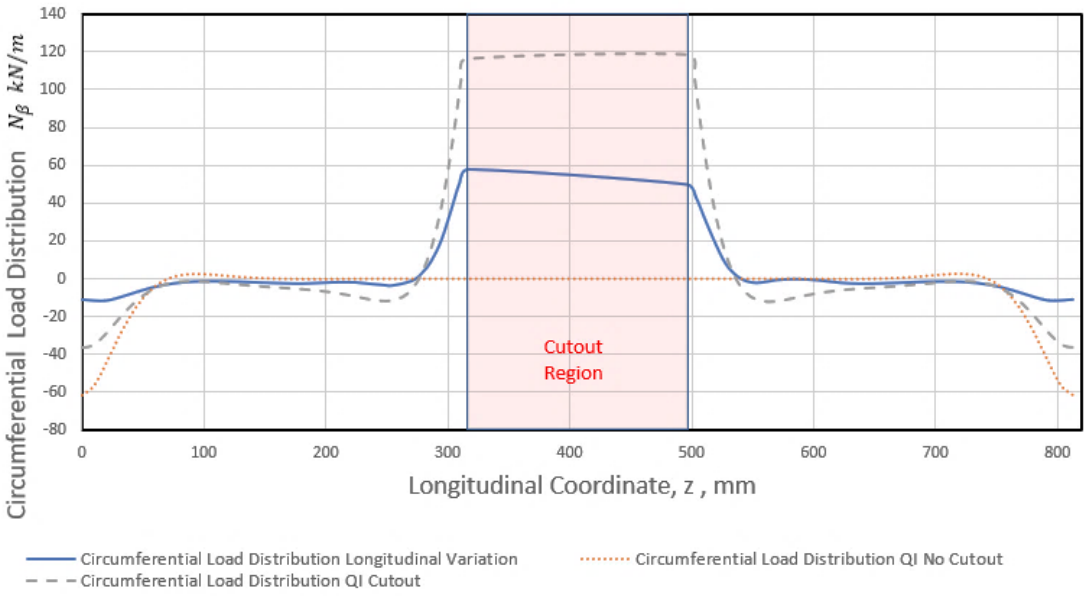

Figure 4.22 Circumferential load distribution for longitudinal variation

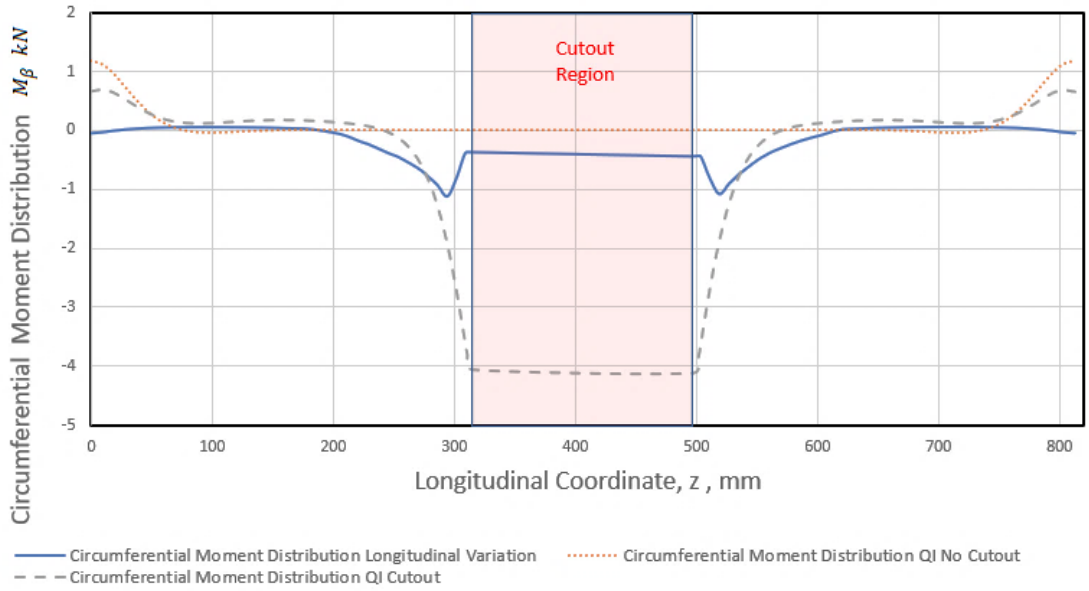

Figure 4.23 Circumferential moment distribution for longitudinal variation

4.2.3 Global-Local Stiffness Variation Results

After investigating the importance of both circumferential and longitudinal stiffness variations to tailor the stiffness properties of the cylindrical shell, it was clear that the presence of the cutout necessitates the presence of a local discretized region to capture

the optimum stiffness variation in more detail. As a result, the cylindrical shell is now discretized using a global-local design-manufacturing mesh. The buckling loads were optimized for several models with different combinations of global and local circumferential and longitudinal stiffness variations. In the following, only the case providing the optimum stiffness properties and the highest improvement in buckling load is presented, shown in Figure 4.24. The model considers that circumferential variation is much more important that longitudinal variation. As a result, the global area is discretized to 64 circumferential regions by 8 longitudinal regions. In addition, the local area is also discretized to 64 circumferential regions by 8 longitudinal regions. The results of the buckling optimization are presented in Figure 4.25.

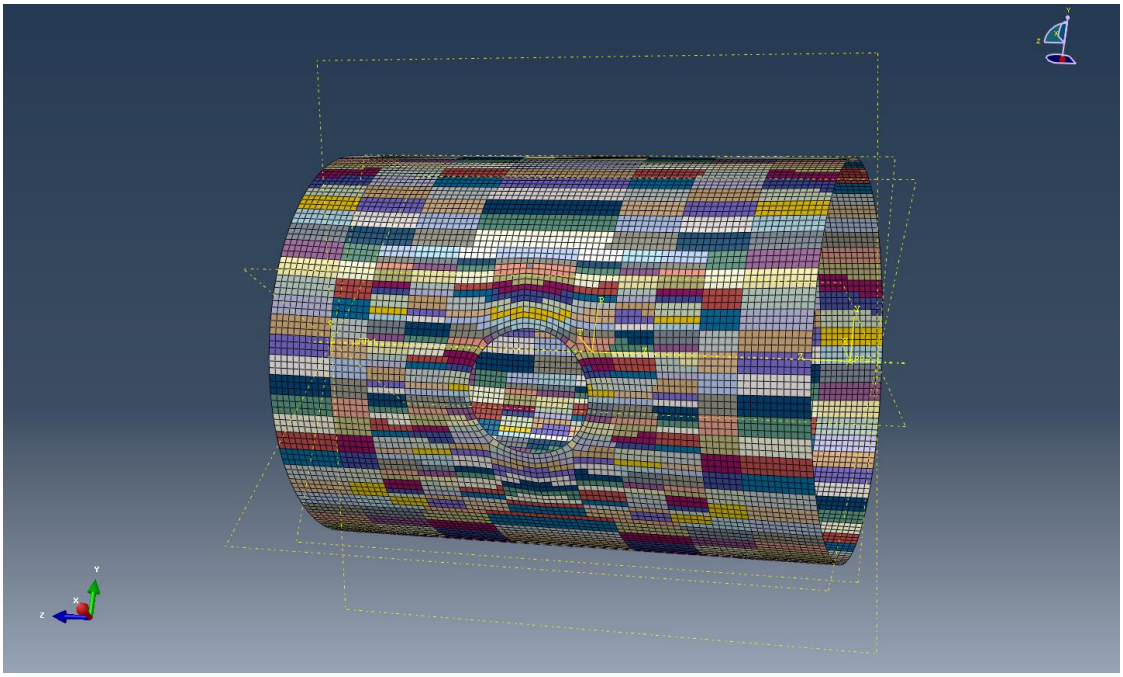

Figure 4.24 Well discretized cylindrical shell with global-local stiffness variation

The critical buckling load of the cylindrical shell increases from 267 kN.m to 489 kN.m, which is an 83% increase compared to the initial quasi-isotropic design. The mechanisms behind the increased buckling capacity can be explained as a combination of

both circumferential and longitudinal stiffness variations. This demonstrates the importance of the combined circumferential and longitudinal stiffness variation over the area of the cylindrical shell and locally around the cutout. The stiffness tailoring provides a significant improvement in the critical buckling load of the cylindrical shell. The buckling loads of the other non-critical modes are also plotted to identify if mode switching took place. The buckling loads of the different modes considered converged to close values, hence emphasizing the importance of accounting for multiple buckling modes in the design process.

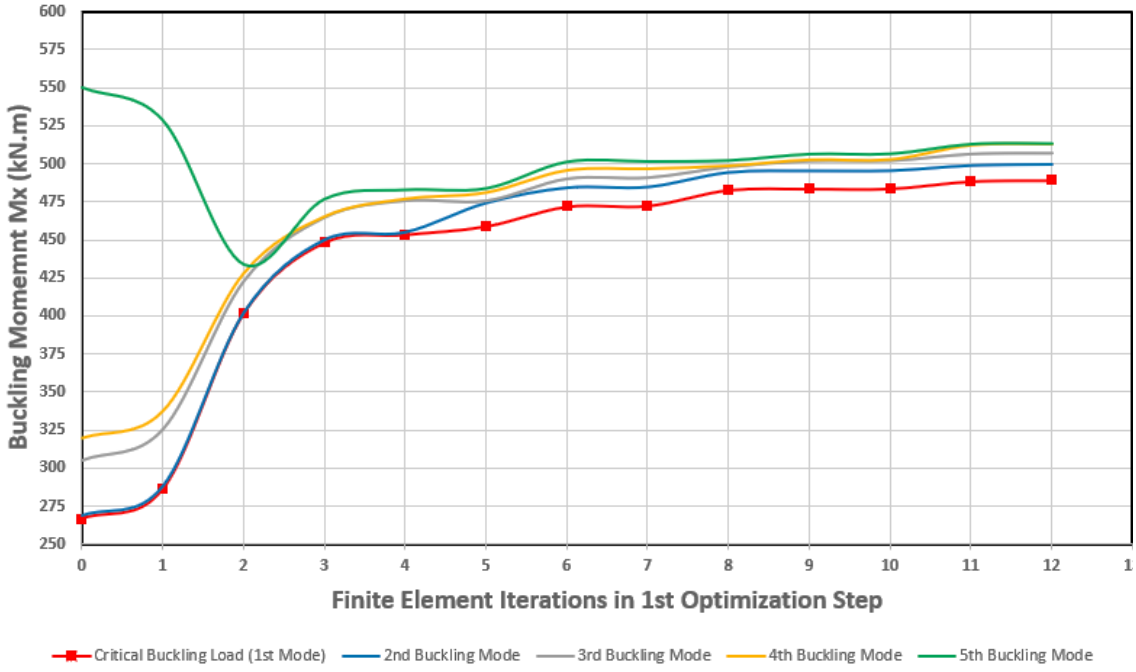

Figure 4.25 Buckling load optimization results for cylindrical shell in Figure 4.24

To visualize the variable stiffness distribution, the in-plane lamination parameters V_1, V_3 and the out-of-plane lamination parameters W_1 and W_3 are shown in Figure 4.26 and Figure 4.27, respectively.

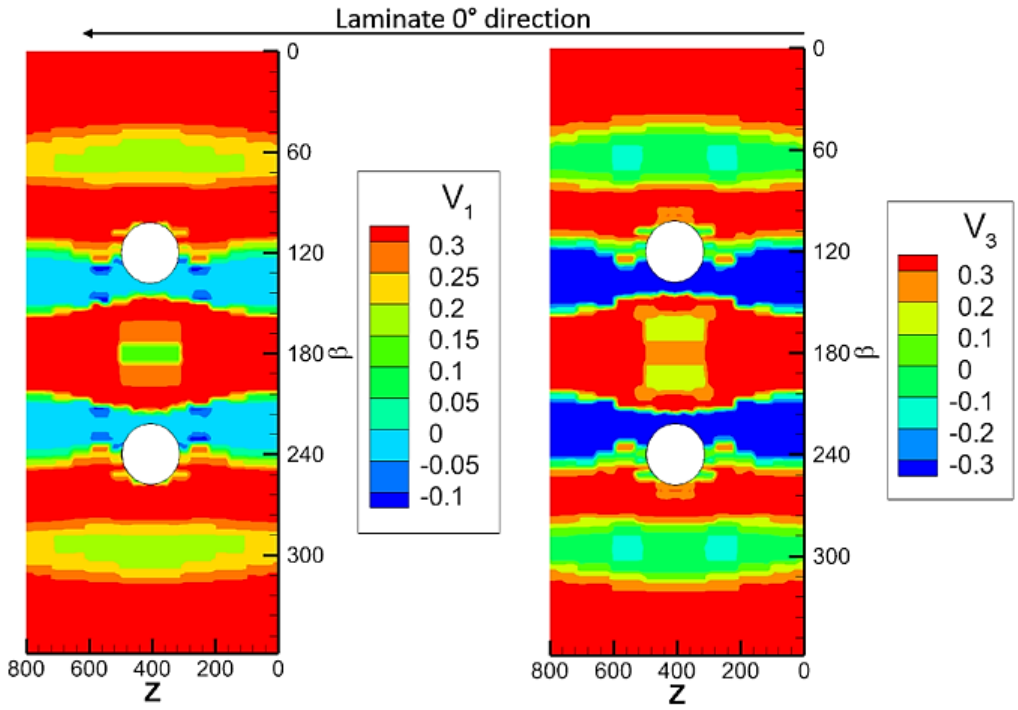

Figure 4.26 Optimal in-plane lamination parameter distribution for buckling optimization of cylindrical shell with cutout under bending

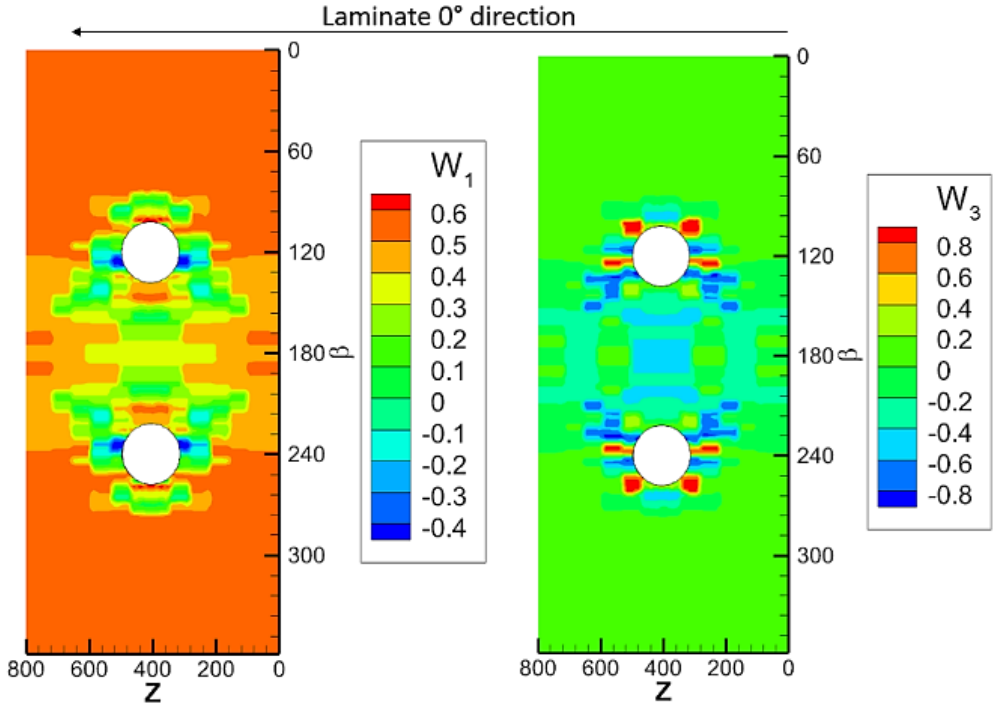

Figure 4.27 Optimal out-of-plane lamination parameter distribution for buckling optimization of cylindrical shell with cutout under bending

The in-plane lamination parameters are almost bound between -0.3 and 0.3 because the 16% rule is applied at each design region. The in-plane stiffness distribution demonstrates that the combination of global-local circumferential and longitudinal variation yields an efficient load redistribution to minimize stress concentrations around the cutout by transferring the stresses to the relatively stiffer regions. The stiffened regions can be identified as the top side of the cylinder $\beta = 0°$, just above the cutout $\beta = 90°$, and the bottom side $\beta = 180°$. The out-of-plane lamination parameter distribution demonstrates that tailoring the bending stiffnesses locally around the hole is much more important than regions away from the hole. The area of the cylinder above the hole $0° < \beta < 90°$ does not require much of an out-of-plane stiffness variation, because it is loaded in tension, which is insensitive to out-of-plane stiffness. The bending stiffness does reinforce the regions around the cutout and at the compression side of the cylinder because buckling is driven by out-of-plane behavior. As a result, the stiffness variation at the compression side below the cutout $120° \leq \beta \leq 180°$ plays a significant role in the stiffness tailoring leading to an improved buckling load.

The optimum stiffness variation also leads to altering the buckling modes of the cylindrical shell. The location and size of the specified cutout initiates local buckling around the cutout, thus leading to a drastic decrease in the buckling load compared to the classical global buckling of a cylindrical shell. The local buckling phenomena is shown in Figure 4.28 for the first two buckling modes of the constant stiffness design. Local buckling dominates the buckling failure, and the constant stiffness design does not utilize the material efficiently to redistribute the stress to stiffer regions with a higher load carrying

capability. However, the variable stiffness cylindrical shell shows nearly a global-local buckling mode shape, as presented in Figure 4.29.

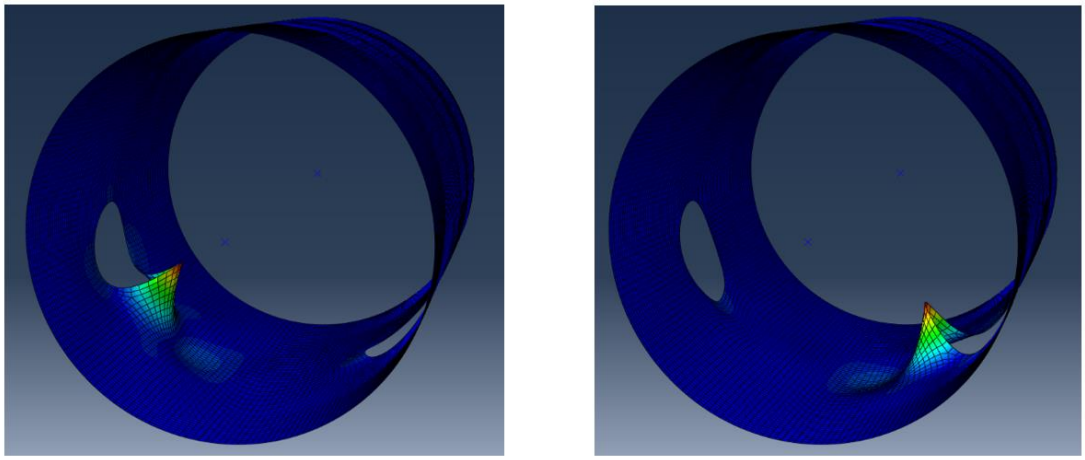

Figure 4.28 1st and 2nd buckling modes of the optimum quasi-isotropic design

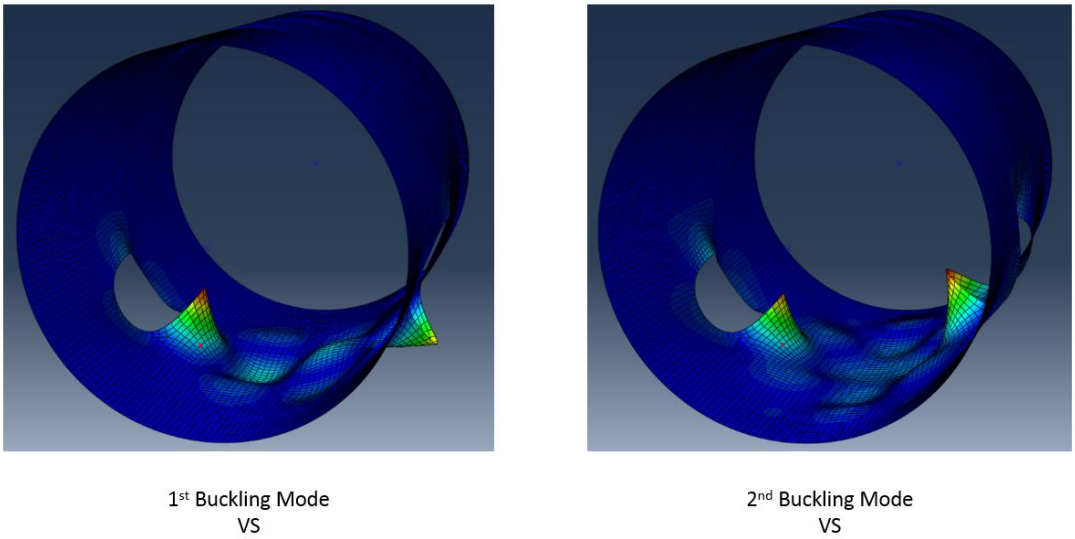

Figure 4.29 1st and 2nd buckling modes of the optimum variable stiffness design

The cylindrical shell still fails due to local buckling around the cutout while showing large displacements at the stiffened compression side of the cylinder. This modification leads to an improved buckling load, where the stiffened material at the bottom side of the cylinder is now used efficiently to carry the loads before the region around the

cutout fails. Thus, the stresses are redistributed to other stiffer regions (in-plane), and the regions around the cutouts are now reinforced (out-of-plane), requiring a higher load to induce buckling.

The results presented above were focused on increasing the buckling performance of the cylindrical shell, hence no considerations for manufacturability as well as stiffness variation continuity was imposed in the first optimization step. The continuity of the stiffness variation can be achieved by using the NURBS surface distribution to model the stiffness variation from the optimized design variables at the control points, or by using a reciprocal averaging scheme to obtain the stiffness properties at the nodes. The obtained optimal stiffness distribution yields a buckling load that denotes a theoretical optimum that might be achieved, but when retrieving the fiber angle distribution and consequently the optimal fiber paths, a reduction in the theoretical performance is observed when additional manufacturing constraints and industry design guidelines are applied.

It is also interesting to do a more detailed analysis of the designed variable stiffness cylinder using non-linear buckling analysis to study the sensitivity of the shell to geometric imperfections introduced in the model. It is well known that the theoretical predictions of geometrically perfect structures overpredicts the buckling loads of inherently imperfect real structures, such as cylindrical shells [177–179]. Thin-walled structures under compression or bending often attain a much lower failure load because of the triggering of post-buckled mode shapes with the presence of initial shape imperfections. For a cylindrical shell under compression, the buckling loads of different modes are very close to each other, hence they are more sensitive to geometric imperfections. For the design application at hand, the alteration of the buckling mode from a local one to a local-global

one also shows that the eigenvalues converge to very close values. Hence, it may be more sensitive to imperfections than the quasi-isotropic initial design. The non-linear solution used in ABAQUS® defines the imperfections as a small factor of the critical buckling mode or a linear combination of the calculated modes. A theoretical 10% imperfection of the total shell thickness was assumed for the first two buckling mode shapes in the analysis. The analysis results are shown in Figure 4.30, where both the designed variable stiffness cylinder and the quasi-isotropic design are compared. It is observed that assuming 10% imperfection for the local buckling mode shapes does not induce global failure of the cylinder, and the load still increases beyond local buckling until the general non-linear collapse is obtained. This phenomenon was observed by Starnes [180], where the local buckling mode is characterized by a stable buckling state, and after local buckling had occurred, it was still possible to increase the loading of the cylinder until the shell buckled into the general collapse state. This is because the eigenvalues of the quasi-isotropic laminate corresponding to local buckling are obtained at much lower buckling loads than the ones that correspond to global mode shapes. However, it will be shown in the later stages of the optimization that considering progressive failure analysis with non-linear analysis results in an ultimate failure load lower than the linear buckling load. As for the variable stiffness cylinder, the presence of a global-local buckling phenomenon indeed reduced the linear buckling load significantly, which means that the variable stiffness cylindrical shell at the first optimization step is very sensitive to geometric imperfections yielding a 25% reduction in the buckling load (365 kN.m) obtained using non-linear analysis compared to the linear buckling load. This can possibly be remedied by imposing

a mode spacing constraint in the dual formulation of the first optimization step [37], which can be useful when modal interaction may lead to unstable post-buckling behavior.

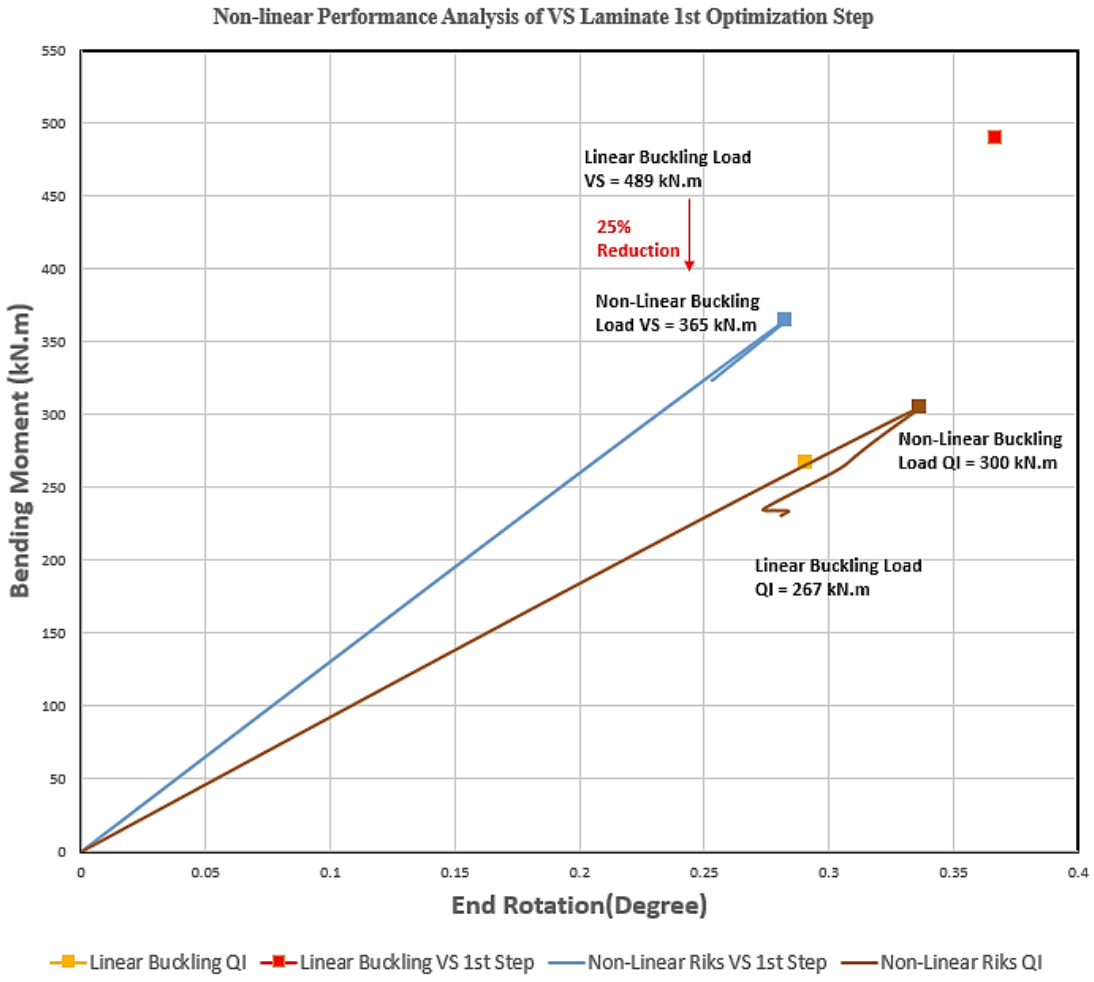

Figure 4.30 Non-linear analysis results for designed VS cylindrical shell 1st Step

4.3 STACKING SEQUENCE RETRIEVAL

Obtaining realistic stacking sequences that match the optimum stiffness properties is designated as the 2nd optimization step. The 1st optimization step is characterized by desired properties such as the convexity of the optimization problem in terms of lamination parameters. However, when retrieving the stacking sequences, this is no longer the case. In order to circumvent the problem of falling into local optima in the inverse problem, a

genetic algorithm is employed for stacking sequence optimization with arbitrary fiber angles to define the laminate. The genetic algorithm used in this work was developed by Dr. Brian Tatting based on previous research concerning stacking sequence optimization [23,171]. Increments of 5° angles were used for the arbitrary fiber orientation angles. To retrieve the optimal stacking sequences, a homogeneous distance in stiffness space was used as the fitness function. The genetic algorithm is used to obtain the stacking sequences having the optimum stiffnesses obtained from the 1st optimization step A^* and D^*. The fitness function to be minimized is presented in Section 3.3.3:

$$d_{AD}^* = 2\sqrt{M_1 M_2} - M_3 \,,$$
$$M_1 = \frac{1}{6}(A : A^{*-1}) + \frac{1}{54}(D : D^{*-1}) \,, \tag{4.6}$$
$$M_2 = \frac{1}{6}(A^{-1} : A^*) + \frac{1}{54}(D^{-1} : D^*)$$
$$M_3 = \frac{10}{9}$$

where 1/6 and 1/54 scaling terms take into consideration the linear and cubic dependency of the membrane and bending stiffness matrices on the laminate thickness, respectively; d_{AD}^* approaches zero when the optimal stacking sequence identically represents the stiffness matrices A^* and D^*. The fitness function is minimized for each control point i of the design-manufacturing mesh to obtain the fiber orientation angle distributions that match the optimum stiffness distributions. The laminates with the minimum distances and closest stiffness values would represent the optimal stacking sequences, while obeying laminate design guidelines. However, in implementation, a variable α for matching A^* and (1-α) for matching D^* was included in the distance function to identify the important stiffness parameters that were contributing to the increase in buckling load from the sensitivity

analysis at the final design point. The following stacking sequence was chosen $[\pm 45/0_2/\pm\varphi_1/\pm\varphi_2/-\varphi_3/90/\varphi_3/90]_s$ to compare the performance of a robust variable stiffness laminate satisfying industry design guidelines with the quasi-isotropic laminate, where φ_i are defined as layers with a variable fiber angle distribution. The following laminate design guidelines are applied:

- Maximum 2 consecutive plies of the same orientation to decrease the chance of delamination and residual stresses
- Minimum ply count percentage for 0°, ±45°, and 90° already satisfied with chosen stacking sequence to avoid micro-cracking and ensure robustness against secondary loading that is not modeled during the design process
- Adding ±45° degree layers on the surface of the laminate to increase damage tolerance, which is satisfied with the chosen stacking sequence
- Mid-plane symmetric and balanced laminate satisfied

The minimum and maximum angle jump constraints [151] are not imposed at each design region as they may significantly reduce the design space with the chosen stacking sequence and limit the ability of in-plane steering to redistribute the stresses efficiently. The retrieved stacking sequences would not match the optimum stiffness properties, resulting in significant performance loss due to the retrieval process.

The results of the second optimization step are exported to Tecplot® to visualize the optimal fiber angle distribution in each layer φ_i, after retrieving the optimal stacking sequence for each control point i. The optimal fiber orientation angle distributions for φ_1, φ_2, and φ_3 are shown in Figure 4.31, Figure 4.32, and Figure 4.33, respectively, for the developed cylinder on a flat plane.

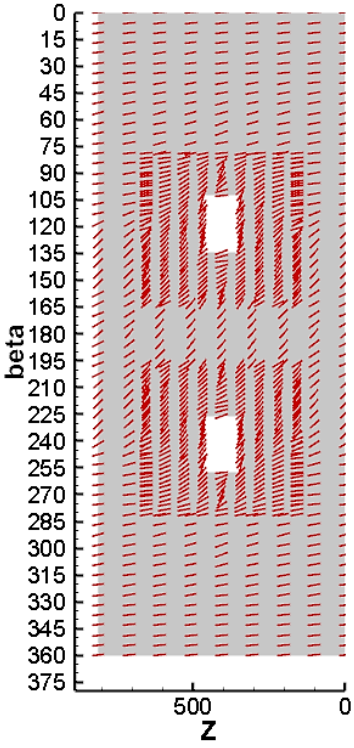

Figure 4.31 Optimal φ_1 distribution

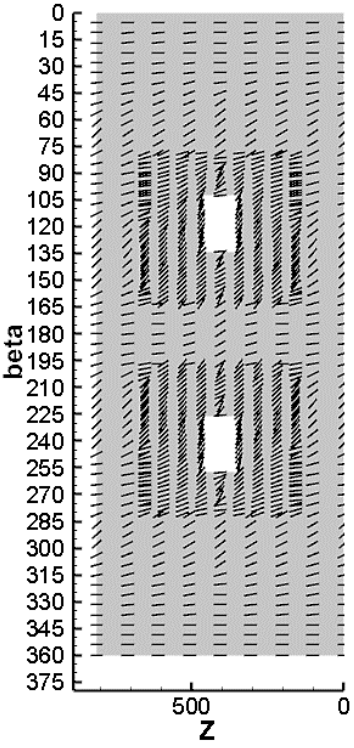

Figure 4.32 Optimal φ_2 distribution

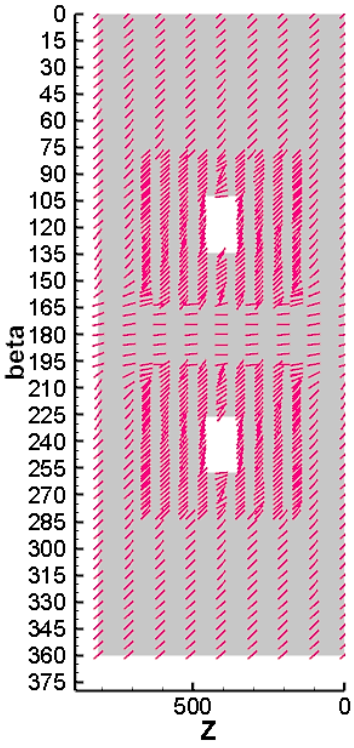

Figure 4.33 Optimal φ_3 distribution

The fiber-steered layers φ_1 and φ_2 show smaller fiber orientation angles at the top side resulting in higher in-plane stiffness in the loading direction. Plies φ_2 and φ_3 result in a stiffer region at the compression side of the cylinder. There is a transition region above the location of the cutout with relatively larger fiber orientation angles to create a region that helps in redistributing the stresses from the weak regions around the hole to the relatively stiffer regions away from the hole. As a result, fiber-steered laminates improve the load carrying capability by two important mechanisms. The first one is evident in each of the fiber-steered layers φ_i aiming to efficiently utilize the anisotropic properties of the material to redistribute the stresses, thus reducing the stress concentrations around the cutout to avoid local buckling phenomena. The second mechanism is related to reinforcing the regions of the cutout with variable bending stiffness properties. The second mechanism

can be better explained by noticing the optimal bending stiffness distribution in the first optimization step, which is a property of the stacked laminate and not of the separate fiber-steered layers.

After obtaining the optimal fiber angle distributions, detailed analyses were used to predict the actual buckling and non-linear buckling loads of the designed cylindrical shell obtained from the 2nd optimization step. The results of the analyses are shown in Figure 4.34. The results show that the buckling load of the steered cylindrical shell after the retrieval step decreases by 23% (489 to 376 kN.m), due to the application of the industry design guidelines in the 2nd optimization step as well as the laminate configuration that was chosen to satisfy these guidelines. In addition, using the chosen laminate configuration, we are trying to match 4 lamination parameters V_1, V_3, W_1, W_3 (as well as 2 inherent out-of-plane lamination parameters W_2 and W_4 in the fitness function to minimize bending-twisting coupling) using only 3 fiber-steered plies. This makes the inverse problem an overdetermined system, which means that the ideal stiffness distributions would not be matched exactly. Comparing the linear buckling load of the variable stiffness cylinder in the 2nd optimization step to the quasi-isotropic laminate, a 41% increase is achieved. It is also interesting to note that the non-linear buckling of the variable stiffness cylinder in the 2nd optimization step is not sensitive to imperfections as the variable stiffness design in the 1st optimization step, because the retrieved laminate with a reduced critical linear buckling load is associated with a local buckling mode shape as shown in Figure 4.35. The non-linear buckling load of the variable stiffness cylindrical shell at the 2nd optimization step is almost the same as that from the 1st optimization step (365 to 362 kN.m).

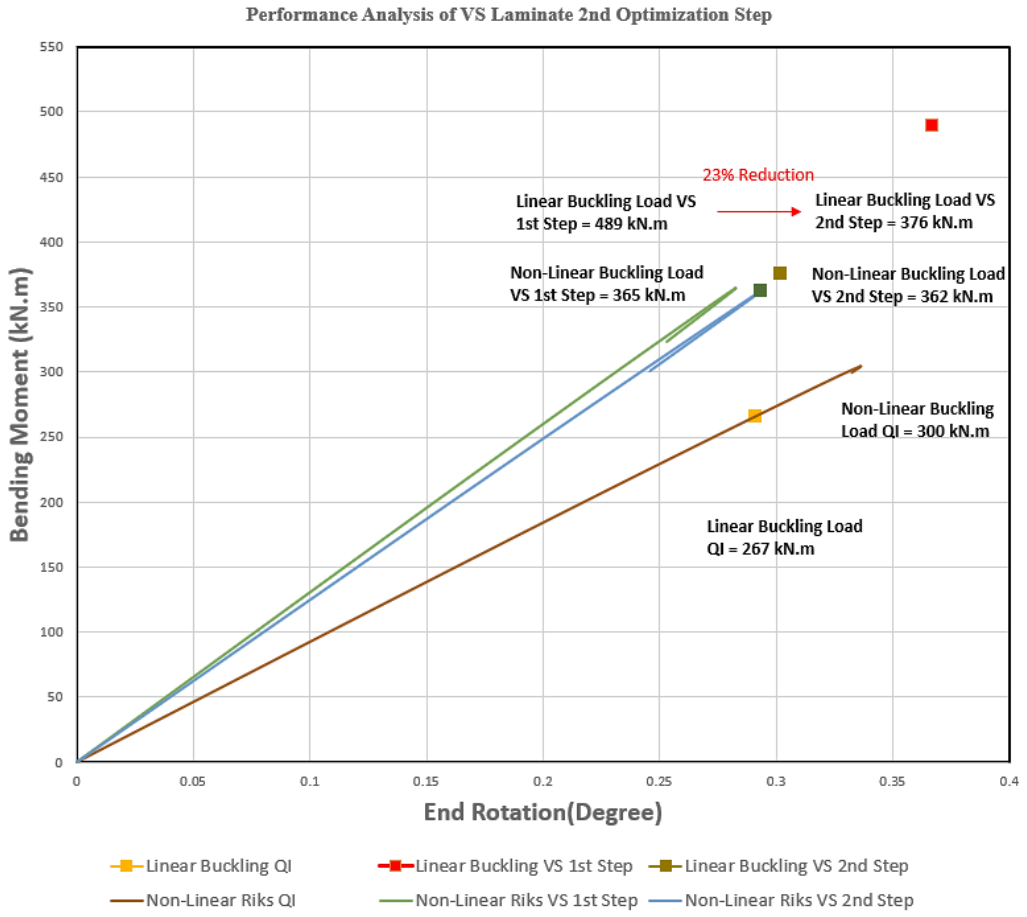

Figure 4.34 Non-linear analysis results for designed VS cylindrical shell 2nd Step

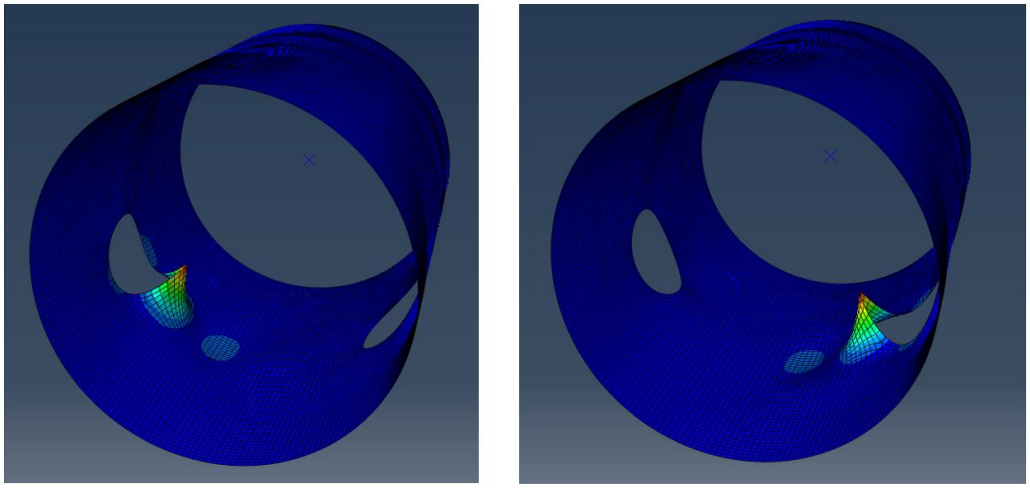

1st Buckling Mode VS 2nd Step

2nd Buckling Mode VS 2nd Step

Figure 4.35 1st and 2nd buckling mode shapes of the designed cylindrical shell 2nd optimization step

It is noteworthy to mention that a manufacturing steering constraint was not applied at the second optimization step as discussed in 3.3.1, as it was observed that the steering constraint at the ply level may reduce the non-linearity of the fiber angle distribution and result in further performance loss to guarantee manufacturability [181]. Peeters et al. demonstrated that for a minimum steering radius of 1000 mm ($\approx$40 in), a significant reduction in the buckling load was obtained for a plate design after the fiber angle retrieval process (50% reduction). The authors then use an additional fiber angle optimization procedure to obtain a 39% reduction for the same minimum steering radius. As the maximum steering constraint was relaxed, the buckling load obtained from the fiber angle distribution is increased and the performance loss between the 1st and 2nd optimization steps was reduced. As a result, the goal was to develop a design-for-manufacturing tool at the third optimization step that would utilize the steering constraint locally for each fiber path to guarantee manufacturability while matching non-linear fiber angle distributions as close as possible. By applying this methodology, the fiber angle distributions are not overconstrained at the second optimization step, at the expense of having fiber angle discontinuities between some fiber paths because of the tow-dropping capability that was included in the design-for-manufacturing tool which allows for fiber path intersections. However, applying a non-conservative steering constraint at the second optimization step is beneficial to guarantee a certain degree of manufacturability, to simplify the generation of fiber paths that match the fiber angle distributions, and to reduce the amount of fiber angle discontinuity that may be obtained due to excessive tow-dropping.

4.4 FIBER PATH CONSTRUCTION

The last step of the multi-level optimization for variable stiffness steered-fiber laminates is to construct the fiber path that can be supplied to the fiber placement machine for manufacturing. The fiber path must match the optimal fiber orientation angle distribution in each ply as well as satisfy the manufacturing constraints. First, an analysis was performed on the curvature of the vector field of steered ply φ_1 defined by the fiber orientation angles from the second optimization step, as shown in Figure 4.36. The fiber orientation angle distribution is highly non-linear because of the presence of the cutout, which requires local stiffness tailoring to achieve the desirable performance improvements as explained in the first optimization step. The maximum curvature is around 0.012 mm^{-1}, which corresponds to a radius of steering of around 3.3 in. This is considered as a significant amount of steering that is required by the AFP machine, which will inevitably result in a huge number of out-of-plane and in-plane deformations that will generate undesirable defects such as wrinkling, folding, in-plane waviness and bunching [182,183]. It would have been extremely beneficial to apply a non-conservative constraint (such as a 20 in minimum steering radius) in the second optimization step to maintain a certain degree of manufacturability globally in the ply as well as reduce the number of tow-dropping that was required to closely match the optimal fiber orientation angles. For the AFP machine that will be used for manufacturing the fiber-steered cylindrical shell, the minimum steering radius was constrained to be a 40 in radius to obtain a reasonable amount of steering while maintaining a suitable layup quality for each steered ply.

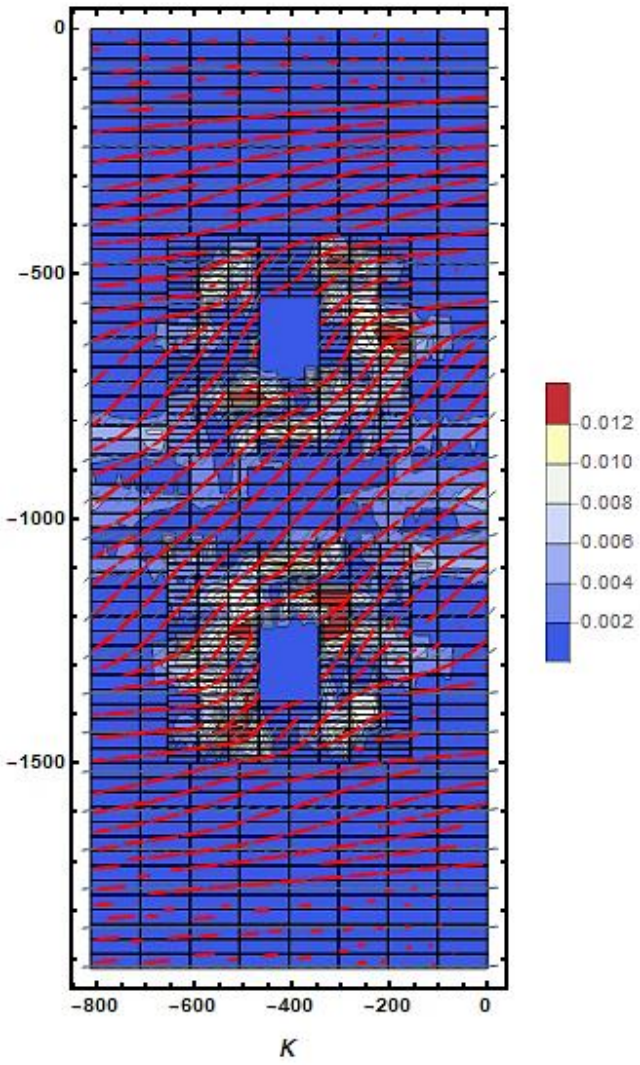

Figure 4.36 Curvature of vector field of steered ply φ_1

Following the methodology developed for the design-for-manufacturing tool as explained in Section 3.4, the manufacturable fiber-steered layers φ_1, φ_2, and φ_3 were obtained as shown in Figure 4.37, Figure 4.39, and Figure 4.41, respectively. The global-local design-manufacturing mesh was used to generate the fiber paths. A minimum steering radius around 40 in (maximum curvature of 0.001 mm^{-1}) was used to generate locally the constant curvature arcs that construct each piecewise constant curvature manufacturable fiber path with a course width of 2 in and 8 number of tows. Each course is sequentially

placed while minimizing the error with respect to the desired fiber orientation angles subject to a zero-gap constraint. Using a 40 in radius for each fiber path, it was very difficult to match the optimal fiber orientation angles that were obtained from the second optimization step without having centerline intersections. Because of the highly non-linear fiber angle variations obtained from the stacking sequence retrieval, a huge number of course dropping during the sequential placement algorithm was required to closely match the optimal fiber orientation angles. This is achieved at the expense of having more tow-drops and fiber angle discontinuities between fiber paths at the regions near the hole and the compression side of the cylinder. After the fiber courses are placed, the tow-dropping algorithm developed generates the dropped tows and the manufacturing boundaries for the AFP machine. A coverage parameter of 50% was used for the tow-dropping and additional coverage was added for tows that were violating the minimum cut length constraint of 4 in defined by the AFP machine configuration used. The fiber-steered layers -φ_1, $-\varphi_2$, and $-\varphi_3$ were then generated using a mirror image of the positive steered ply with respect to the circumferential coordinate axis β (z = 0). In addition, since every guide curve is independent from the other, the balancing condition obtained using the mirror image is not satisfied at all positions within the laminate. This is because no symmetry was considered when generating the fiber courses for each layer, as this will further increase the number of courses and affect the reliability of the manufacturing process afterwards. To obtain a better balancing condition, the fiber courses of the negative steered plies can be independently generated in the third optimization step while using the negative values of the retrieved fiber orientation angles of the positive steered plies as the desired fiber orientation angles for the optimization process. In addition, changing the initial starting

point of the algorithm might generate a better symmetric steered layer. During the generation of each fiber-steered ply, the first arbitrary fiber path was generated at the top of the cylinder. Other feasible starting points might be at important locations in the cylindrical shell such as near the hole location or at the compression side of the cylinder.

Figure 4.37 Steered ply φ_1

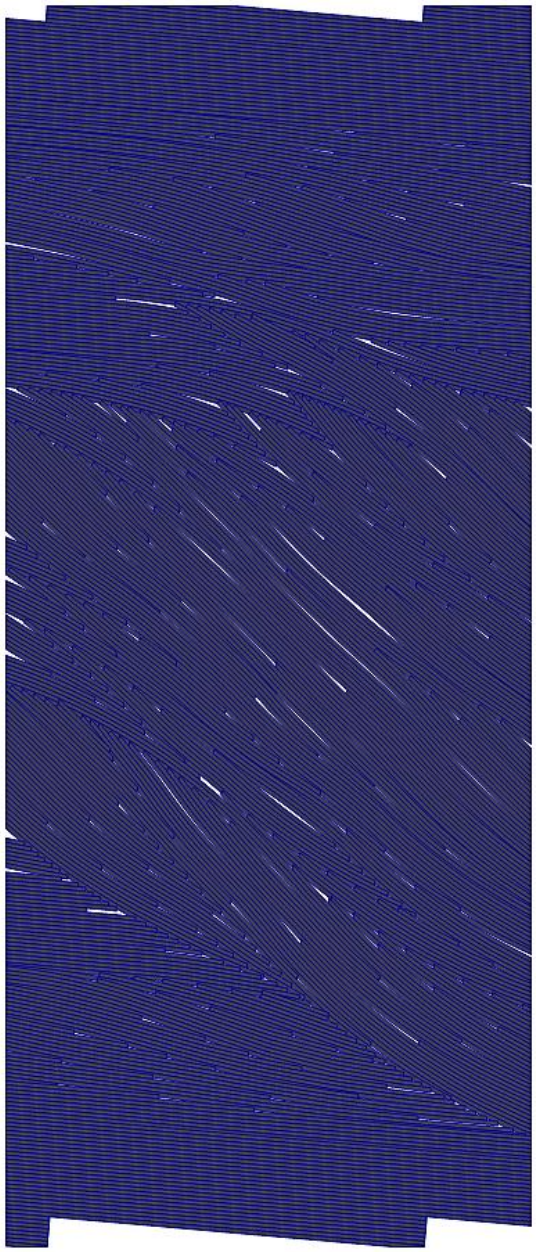

Figure 4.38 Steered ply $-\varphi_1$

Figure 4.39 Steered ply φ_2

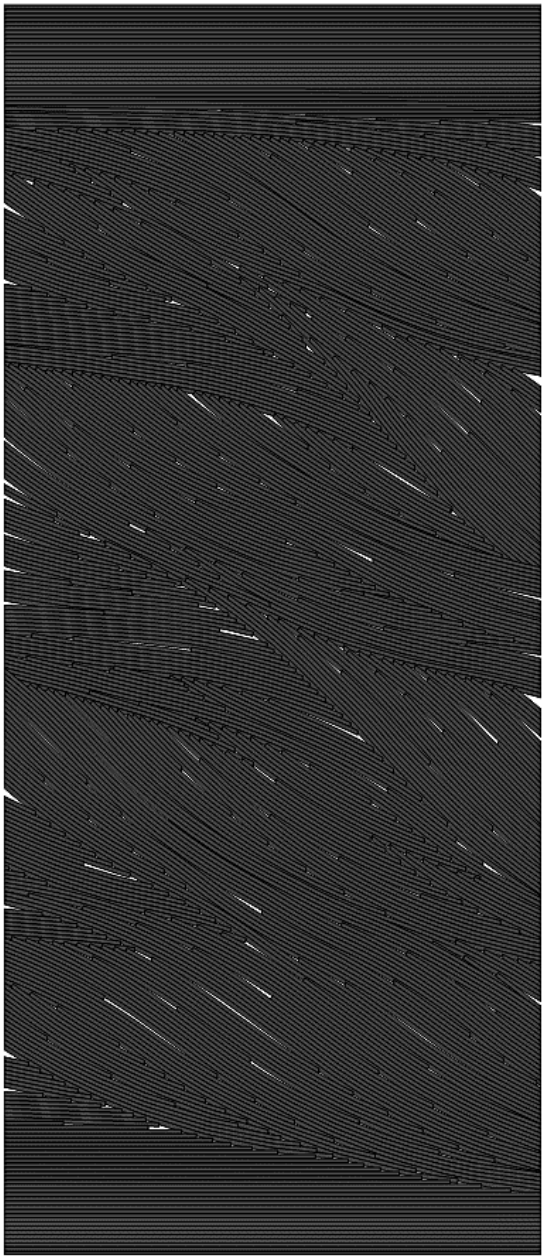

Figure 4.40 Steered ply $-\varphi_2$

Figure 4.41 Steered ply φ_3

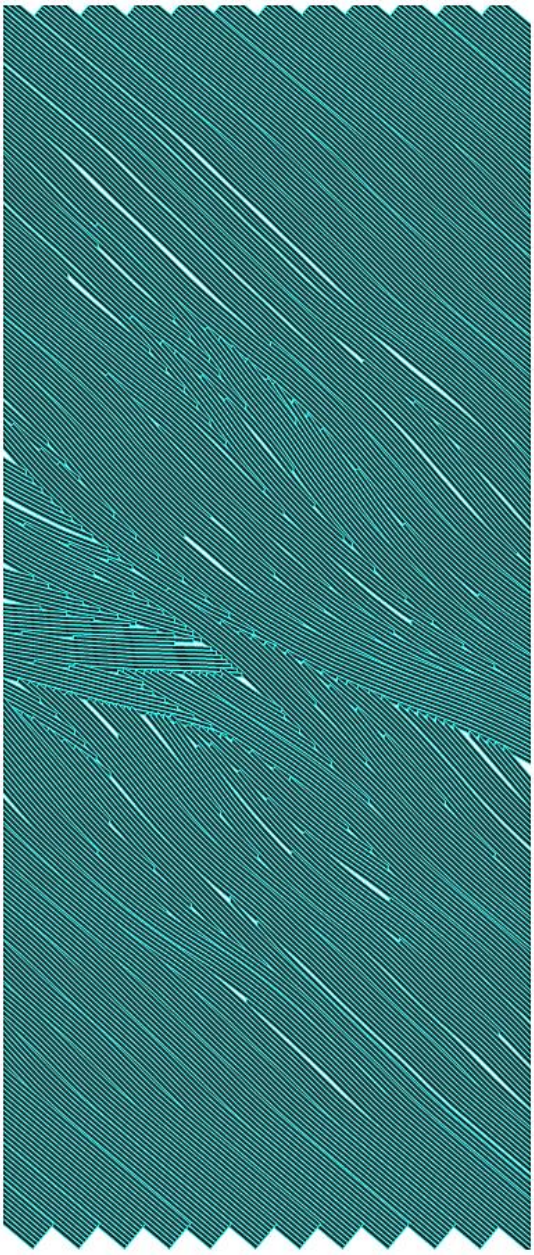

Figure 4.42 Steered ply $-\varphi_3$

After obtaining the manufacturable fiber-steered layers with tow-level detail, the fiber orientation angles at the control points of the design-manufacturing mesh were retrieved by finding the closest tows for each control point and obtaining the fiber orientation angles from the parametric equations of the boundaries defining the tows as shown in Figure 4.43-Figure 4.45.

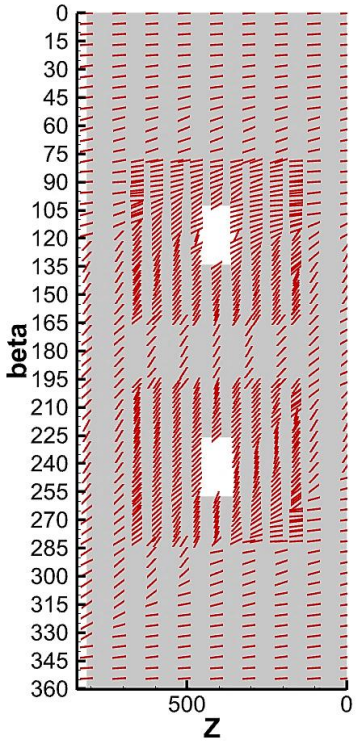

Figure 4.43 Optimal φ_1 distribution 3rd Step

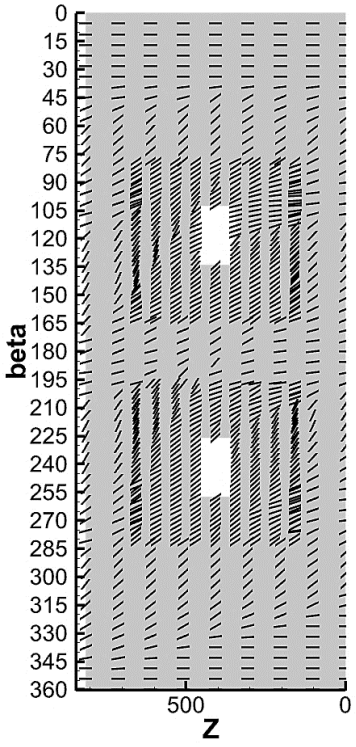

Figure 4.44 Optimal φ_2 distribution 3rd Step

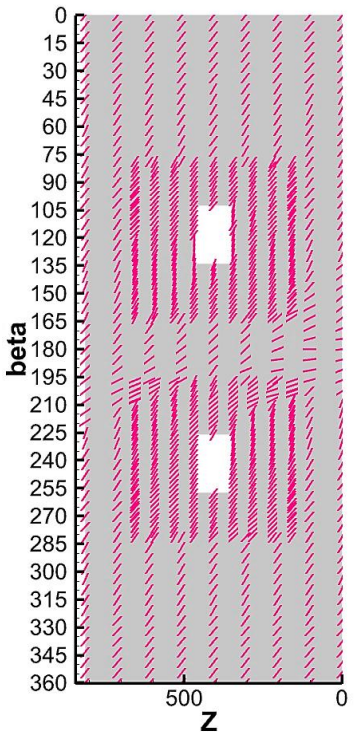

Figure 4.45 Optimal φ_3 distribution 3rd Step

After obtaining the optimal fiber angle distributions, detailed analyses were used to predict the actual buckling and non-linear buckling loads of the designed cylindrical shell obtained from the 3rd optimization step. The results of the analyses are shown in Figure 4.46. The results show that the linear buckling load of the steered cylindrical shell after the fiber path construction step decreases by 9% (376 to 341 kN.m), due to the application of the maximum steering constraint as well as the balancing condition that was not satisfied at each point in the laminate. Comparing the linear buckling load of the manufacturable variable stiffness cylinder in the 3rd optimization step to the quasi-isotropic laminate, a 28% increase is achieved. It is also interesting to note that the non-linear buckling of the variable stiffness cylinder in the 3rd optimization step is also not very sensitive to imperfections as the variable stiffness design in the 1st optimization step, because the retrieved laminate with

a reduced critical linear buckling load is associated with a local buckling mode shape similar to the laminate obtained in the 2nd optimization step. The reduction in the non-linear buckling load of the variable stiffness cylindrical shell at the 3rd optimization step is almost the same as the reduction of the linear buckling load compared to the 2nd optimization step.

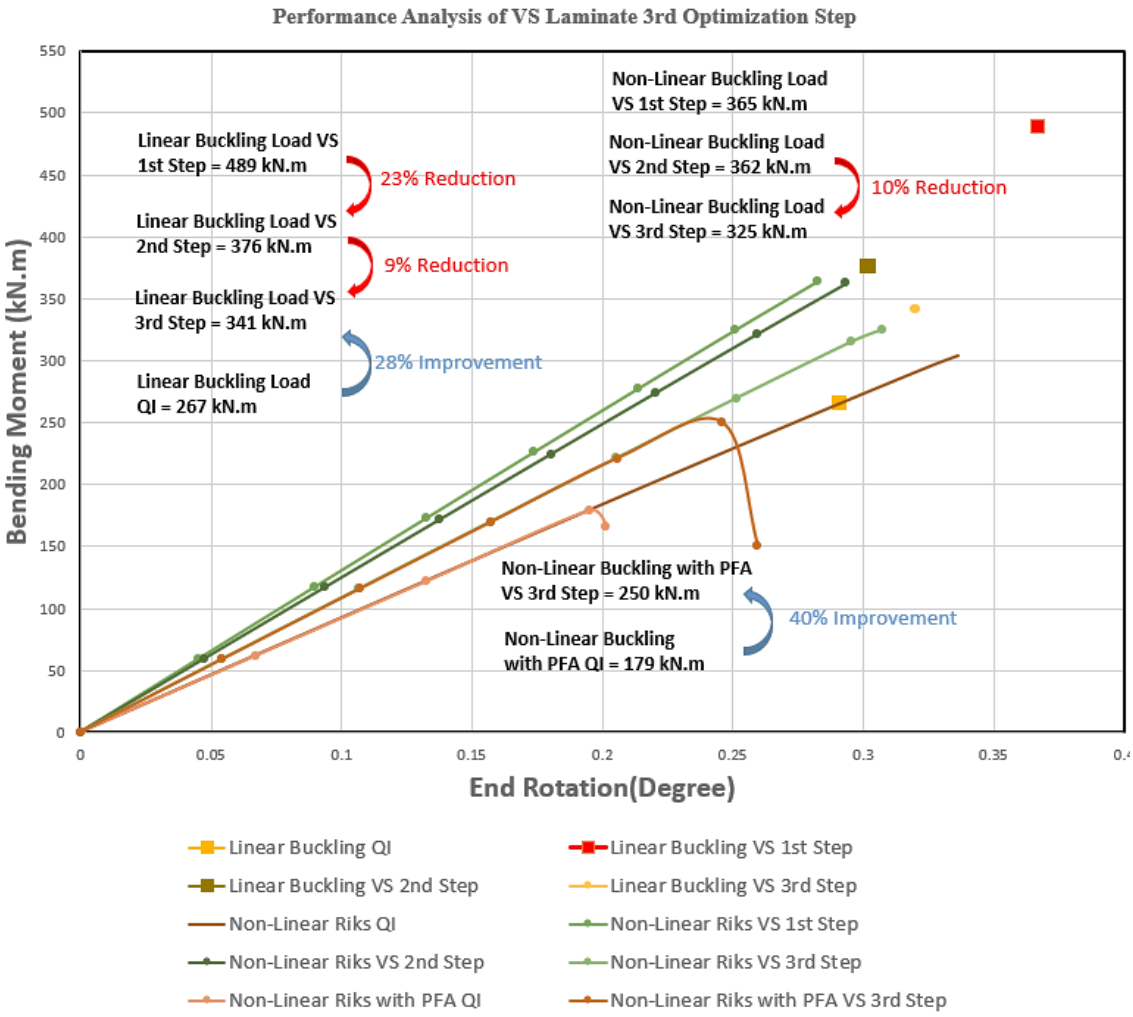

Figure 4.46 Detailed analyses results for designed VS cylindrical shell 3rd Step

Even though the cylinder was not designed for strength, non-linear analysis with progressive failure analysis was also performed as described in Section 4.1.1. The ultimate failure load of the manufacturable steered fiber laminate is around 250 kN.m which is a 40% improvement compared to the ultimate failure load of the quasi-isotropic laminate

which is 179 kN.m. Further improvements might be achieved by considering the strength as a response during the 1st optimization step. This demonstrates that manufacturable variable stiffness laminates provide significant performance improvements compared to traditional conventional laminate designs.

4.5 SUMMARY AND CONCLUSIONS

In conclusion, the buckling load of a cylindrical shell with a cutout under bending was optimized using nonconventional variable stiffness laminates. An efficient multi-level optimization approach was used to demonstrate the potential improvements of variable stiffness laminates while satisfying manufacturing constraints and laminate design guidelines.

Lamination parameters were used as intermediate design variables in the first optimization step to achieve convexity and reduce the design complexity. The use of conservative convex separable approximations for the approximation of the inverse of the buckling load was proved to be efficient in obtaining the optimum stiffness requirements of the cylindrical shell. A design-manufacturing mesh was introduced to perform the buckling load optimization, where both circumferential and longitudinal stiffness variations were considered to physically understand the importance of the stiffness tailoring mechanism in efficient load redistribution and local reinforcements around the regions of the cutouts. Based on the optimum lamination parameter distribution obtained, the theoretical linear buckling load improved by 83% compared to the initial quasi-isotropic design.

An optimal laminate with fiber-steered layers is then designed to match the optimum stiffness requirements using a genetic algorithm. The linear buckling load shows

a 23% reduction compared to the linear buckling load of the variable stiffness cylinder in the 1st optimization step, and a 41% increase compared to the quasi-isotropic laminate. The fiber paths are then constructed using the developed design-for-manufacturing tool and the manufacturing boundaries are generated for the AFP machine. The final manufacturable variable stiffness laminate results in a 30% reduction compared to the variable stiffness laminate obtained in the 1st optimization step, a 9% reduction compared to the 2nd optimization step, and a 28% increase compared to the quasi-isotropic laminate, while satisfying locally the maximum steering constraint at the 3rd optimization step and industry design guidelines in the 2nd optimization step.

Even though significant buckling load improvements based on the stiffness variations were obtained, the design problem has not been completely solved. The first issue is the significance of stress concentrations around the cutout that may lead to material strength failure before the buckling load is attained. It has been shown that the ultimate failure load increases by 40% as obtained using the final steered laminate obtained from the buckling design solution, yet further improvements can be achieved by considering the strength response as well in the first optimization step as a multi-objective function to improve the ultimate failure load of the cylindrical shell. It is also essential to consider the effect of the gaps and overlaps obtained on the structural analysis, which may result in additional performance reduction. In addition, a non-conservative steering constraint can be applied at the second optimization step at the ply level to reduce the fiber angle discontinuities and the amount of tow-dropping that are obtained in the third optimization step.

Chapter 5

MANUFACTURING ASSESMENT OF DESIGNED VARIABLE STIFFNESS CYLINDRICAL SHELL

The purpose of this chapter is to demonstrate the applicability of the design-for-manufacturing tool that was developed for obtaining an optimal variable stiffness laminate design. Section 5.1 introduces an experimental investigation that was undertaken at McNAIR Center to study the effect of different combinations of process parameters such as temperature, feed-rate, and compaction pressure on the layup quality with constant curvature steered fiber courses on a 48 inch cylindrical shell. After choosing a suitable combination of processing parameters for the designed cylindrical shell, the designed fiber paths were imported into CATIA V5® and prepared for AFP manufacturing in Section 5.2. Section 5.3 then introduces the stages required using iCPS® (Ingersoll Composite Programming System) to program the imported fiber paths and generate the manufacturing program for the AFP machine. A brief summary regarding the manufacturing of steered fiber laminates is then presented in Section 5.4.

5.1 EFFECT OF AFP PROCESS PARAMETERS ON LAYUP QUALITY OF STEERED FIBER COURSES ON CYLINDER

In this section, two steering radii are considered for steered fiber paths on a 48 in cylindrical shell. Constant curvature courses having 1-inch width (4 tows, each one 0.25 in) were placed on the cylindrical shell with radii of 50 in and 25 in. The experiment was conducted as a team collaboration at McNAIR Center to study the effect of AFP process parameters such as temperature, feed-rate, and compaction pressure on the layup quality of the steered fiber courses. To assess the quality, the fiber-steered courses are analyzed using an automated inspection system that detects defects such as wrinkle formations, gaps, and overlaps that are obtained because of the minimum steering radius used as well as the chosen manufacturing process parameters.

5.1.1 Introduction

A major manufacturing constraint for fiber-steered variable stiffness laminates is the minimum steering radius. When the tows are steered, the inner edges are subjected to compressive forces, which may lead to fiber wrinkling. The laminate quality is directly affected by the resulting out-of-plane undulations that are undesirable. Therefore, a limit on the steering radius should be imposed to minimize the presence of wrinkled tows. This experimental investigation was conducted to find a critical steering radius for the design application in Chapter 4 based on the quality of the steered courses obtained along with an optimal set of process parameters to achieve a suitable layup quality during the manufacturing of the variable stiffness cylinder. The process parameters were monitored during the placement of each fiber course, and the scanned layups were then analyzed for defects using image analysis.

During AFP production of even straight fiber layups, several defects may arise such as gaps, overlaps, twists, wrinkles, and wandering tows [184]. In addition, fiber-steered paths may induce additional defects depending on the steering radius and AFP processing parameters. Tow deformations that may occurs during steering can be separated into strain deformations (tensile, compressive, shear), large in-plane deformations (waviness and bunching), and large out-of-plane deformations (wrinkling and folding) [182,183]. However, the appearance of steering-induced defects can be minimized by optimizing the manufacturing process parameters such as temperature, feed-rate, and compaction pressure. Other processing parameters such as tow tension, ambient conditions, and compaction roller type are also important but were not considered in this experimental study.

5.1.2 Experimentation

For the steering experiment on the cylinder, two constant curvature arcs with radii of 50 and 25 in were used. The arcs were created on a developed surface and then transformed to 3D using the parametric equations for a cylinder, because the geodesic curvature of the arcs on the cylindrical surface is the same as the 2D curvature. Each arc was discretized and exported to CATIA as a cloud of points, then the steered paths were reconstructed and projected on the tool surface to make sure the 3D is exactly on the surface. Linear portions were added tangentially to the constant curvature arcs on each sided and extended to cover the boundaries of the cylinder. A total of 9 courses were programmed for each curved arc. The courses were spaced by using the rotation functions in CATIA so that the surface was covered without any overlap between the courses as shown in Figure 5.1.

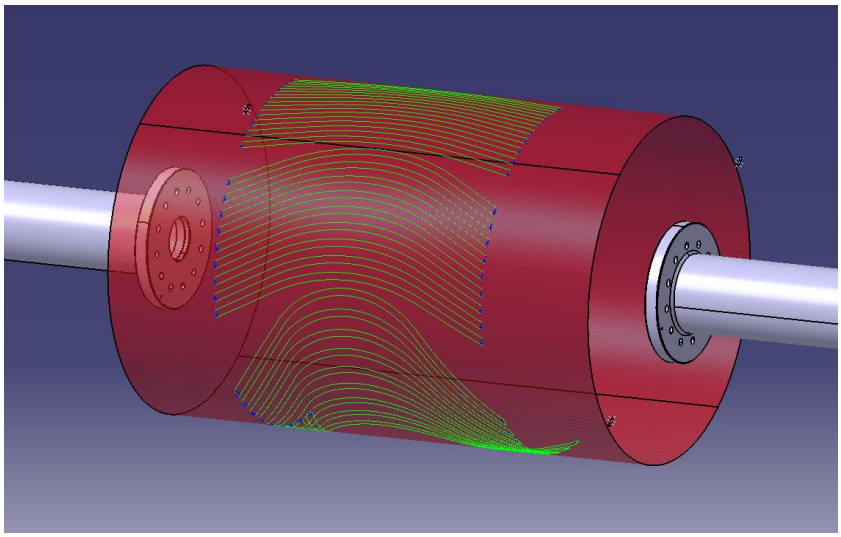

Figure 5.1 Constant curvature arcs projected on cylindrical tool

For each arc, a set of process parameters (temperature, feed-rate, compaction pressure) was chosen to study their effect on the course quality in terms of in-plane and out-of-plane deflections. Each of these parameters was varied within a specified range and the effect of their interactions was observed on the layup quality. The importance of each process parameter considered is briefly explained here:

Temperature:

Choosing a suitable temperature for the layup process is a crucial element to obtain proper quality of layup and bonding of layers. The increase in heat results in an increase of the tackiness of the tows allowing a better adhesion of subsequent layers during layup. However, excessive temperatures may result in partially localized curing of the layup which may affect its mechanical properties. In addition, a decrease in temperature may result in insufficient consolidation.

Feed-rate:

Feed-rate determines the speed at which the tows are deposited onto the tool surface or substrate. Higher feed-rate result in higher productivity rate, which is desirable for

industry. However, it is difficult to ensure a suitable quality of the layup while maintaining high deposition rates. A lower feed-rate increases adhesion and laminate bonding. As the feed-rate increases, the layup process is more prone to the presence of defects due to the vibrations and dynamic behavior of the tows entering the machine head as well as the risk of incomplete adhesion. Hence, a tradeoff occurs between layup quality and production rate. For steered layups, a consistent layup quality can be achieved by using lower speeds than straight fiber layups. The layup speed also impacts other processing parameters, where a slow layup indicates an additional exposure to the heat source and thus higher processing temperatures during layup.

Compaction pressure:

Compaction is essential to the proper adhesion of each layer to the previous one. Compaction is applied to the placed tows by means of a roller when they the material is deposited onto the tool surface or substrate. Sufficient pressure must be applied to ensure the layers properly adhere to each other during layup. Compaction also plays an important role in increasing the surface area of contact between the layers to obtain a better quality of the part. Without proper compaction forces, layups may have weak adhesion, higher void content, and higher out-of-plane deformations such as wrinkling for steered fiber courses.

For the temperature, a xenon light heater HUMM3 attached to the AFP head was used where the voltage, frequency, and pulse duration of the light source can be changed to control the layup temperature. The frequency and pulse duration were kept constant at 60 Hz and 2000 μs, but the voltage was chosen from the following levels: 150, 170, 180, and 190 Volts (V). For the feed-rate, the layup speed at five different levels was

investigated: 10, 20, 40, 60, and 100% of the programmed speed of 25000 mm/min. In addition, the compaction force of the roller was chosen from the following set: 178, 300, 445, 600, and 750N. The set of parameters are summarized in Table 5.1.

Table 5.1 Process parameters and discrete values chosen for the experiment

Parameters	Discrete Values				
Heater Voltage (V)	150	170	180	190	
Feed Rate (%)	10	20	30	50	100
Compaction Force (N)	178	300	445	600	750

A baseline for each parameter that yields a successful layup with minimum desirable quality is required. A random grid search was used here. The separate parameters were modified while fixing the others one at a time to note how the layup is affected and to distinguish the effects of each parameter. The steering experiments were carried individually for each course by modifying the combination of the process parameters. The investigated combination of parameters for each course are summarized in Table 5.2. The temperature is measured at 4 locations using 4 thermocouples along the length of the paths. Since the layup speed was not controlled during the process, the layup speed was recorded for each course to capture any discrepancy between the actual feed-rate of the course and the programmed one. The compaction pressure was not monitored using any instrumentation, it was solely programmed in the machine parameters. For more details concerning the instrumentation measurements of the substrate temperature and the feed-rate, the reader is referred to [185].

Table 5.2 Course descriptions and set of process parameters

Course#	Radius (in)	T(V)	S(%)	P(N)	Course#	Radius (in)	T(V)	S(%)	P(N)
130	50	150	30	600	139	25	170	30	600
131	50	170	50	445	140	25	170	20	600
132	50	150	100	445	141	25	170	10	600
133	50	170	50	445	142	25	150	10	600
134	50	170	100	300	143	25	170	10	750
135	50	170	100	600	144	25	170	20	750
136	50	170	20	600	145	25	190	50	750
137	50	170	20	750	146	25	180	30	750
138	50	170	20	445	147	25	190	100	750

To assess the effects of the parameters on the quality of each course placed, linear profilometry scans of the layup are captured using the ACSIS system developed by IMT as shown in Figure 5.2. The linear profilometry scans are visualized in black and white images. An image is generated for each of the 4 profilometers mounted on the robotic arms.

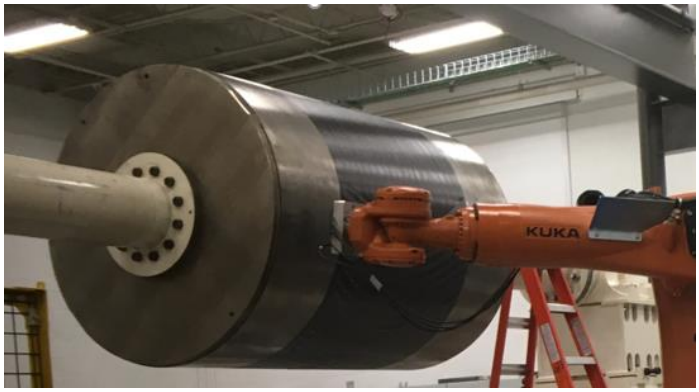

Figure 5.2 Profilometry scanning of steered layup using ACSIS system

The images are later stitched together to reconstruct the developed surface of the layup.

The stitches scans for the placed courses are shown in Figure 5.3 and Figure 5.4.

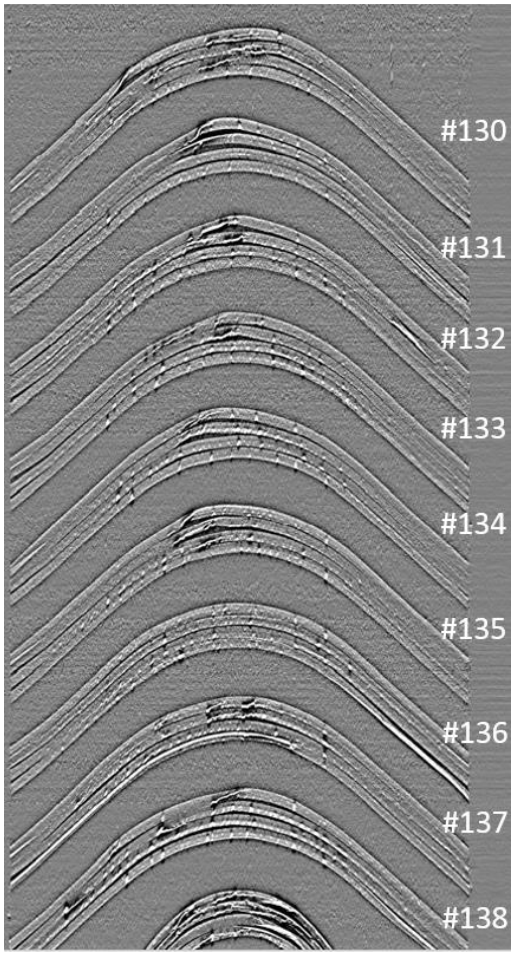

Figure 5.3 Stitched scans for R50

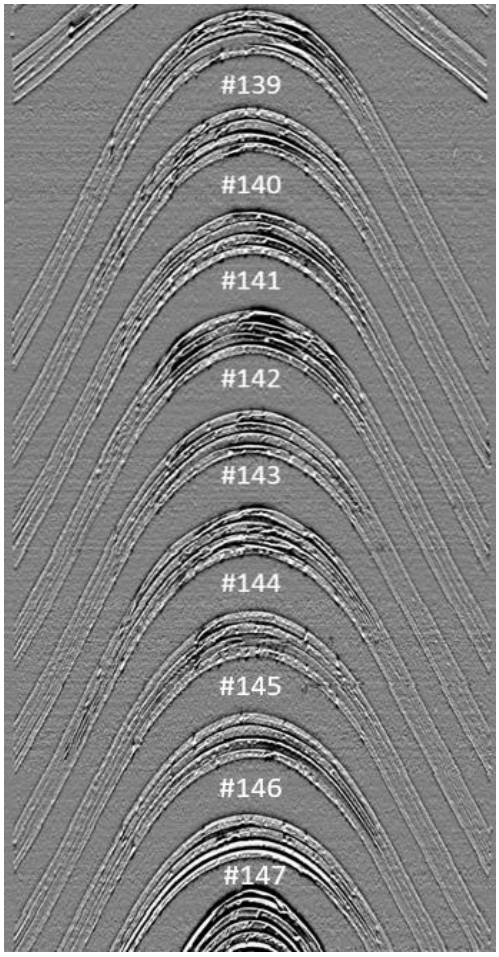

Figure 5.4 Stitched scans for R25

5.1.3 Results

To quantify the defects obtained during the layup and assess the influence of the process parameters, the stitches images are then analyzed using a high-low filter [185]. The analyses of these images are shown in Figure 5.5 for R50 courses and Figure 5.6 for R25 courses. Out-of-plane deformations are identified by the white shades in the scanned images and highlighted in orange resulting from folds and wrinkles. In-plane deformations are identified by the darker shades and highlighted in green. To assess the influence of the process parameters on the steering induced defects, only the curved portions of the steered paths are considered for analysis. A percentage of the total area of the courses including defects can be obtained, which is summarized in

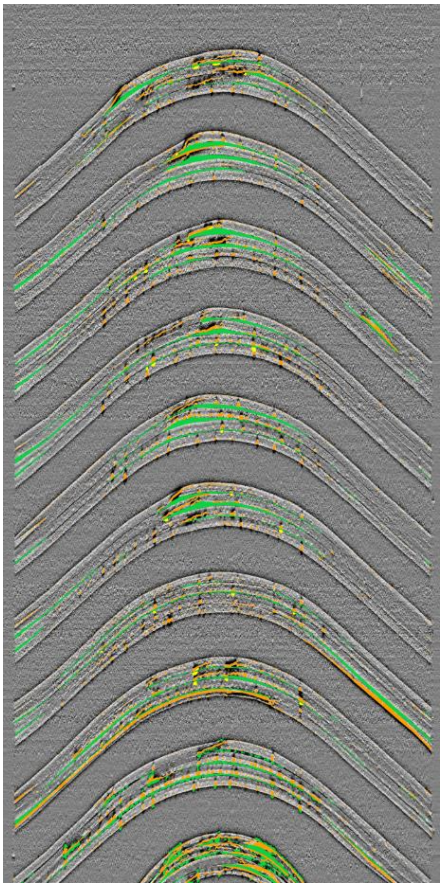

Figure 5.5 Defect analyses for R50

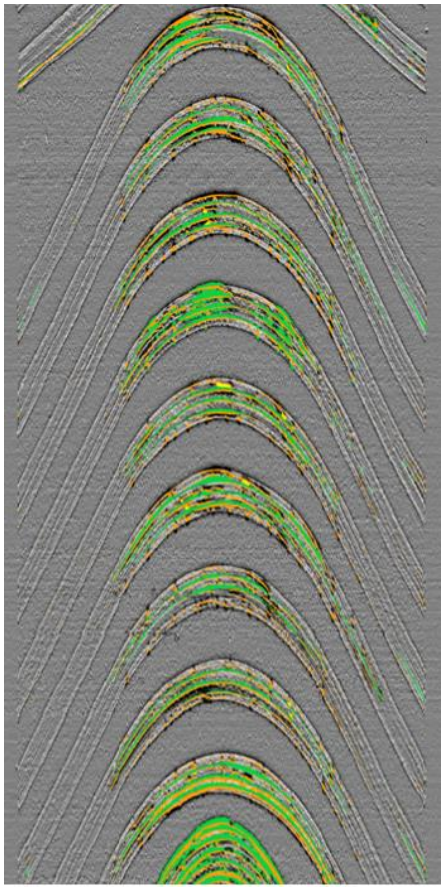

Figure 5.6 Defect analyses for R25

Table 5.3 Percentage of defects for steered portion of R50 courses

Course	Out-of-plane defects (%)	In-plane defects (%)	Total defects (%)
130	6.37	7.44	14.29
131	3.60	12.32	15.98
132	5.73	10.45	16.49
133	5.60	6.30	12.52
134	4.96	11.08	16.11
135	5.15	10.08	15.51
136	5.37	4.46	10.06
137	10.07	8.33	18.99
138	7.45	9.88	17.75

Table 5.4 Percentage of defects for steered portion of R50 courses

Course	Out-of-plane defects (%)	In-plane defects (%)	Total defects (%)
139	14.12	10.13	24.32
140	12.66	10.79	23.50
141	11.68	11.37	23.36
142	18.65	8.85	27.67
143	10.19	10.66	21.46
144	16.20	12.96	29.56
145	7.049	9.14	16.20
146	9.83	8.97	19.02
147	21.01	12.54	33.62

Course # 136 from the family of R50 courses had the lowest percentage of defects while having the voltage set to 170V, layup speed around 5000mm/min, and 600N compaction force. Since a 50 in steering radius is very limiting for the design of a 24 inch variable stiffness cylinder, a critical steering radius of 40 in was chosen for the cylinder design application in Chapter 4 based on the quality of the steered courses obtained for the optimal set of process parameters found in this experiment.

5.2 TRANSFORMING DESIGNED COURSES TO CATIA V5®

Since the cylinder is a developable surface with zero Gaussian curvature, the mapping between the 3D surface and its development in 2D preserves lengths and angles, thus the curvature of a fiber path defined in the 2D element of a design-manufacturing mesh is the same as the geodesic curvature of the transformed fiber path in 3D. The designed fiber paths obtained from the design-for-manufacturing tool are discretized in the 2D domain, and parametric equations of the cylinder can be used to transform the 2D fiber paths to 3D paths on the cylindrical surface.

For each steered ply, the course centerline and AFP manufacturing boundaries are discretized in the 3D coordinate system. A macro is then used to import the points into CATIA V5® and the spline function is used to generate the centerline paths and boundaries. A geometric set is then created for each course within a steered ply, and the corresponding boundary contours and course centerline are projected to the cylindrical surface to make sure the curves are exactly lying on the surface for the composite design programming phase. The transformed AFP manufacturing boundaries are shown for steered plies φ_1, φ_2, and φ_3 in Figure 5.7, Figure 5.8, and Figure 5.9, respectively.

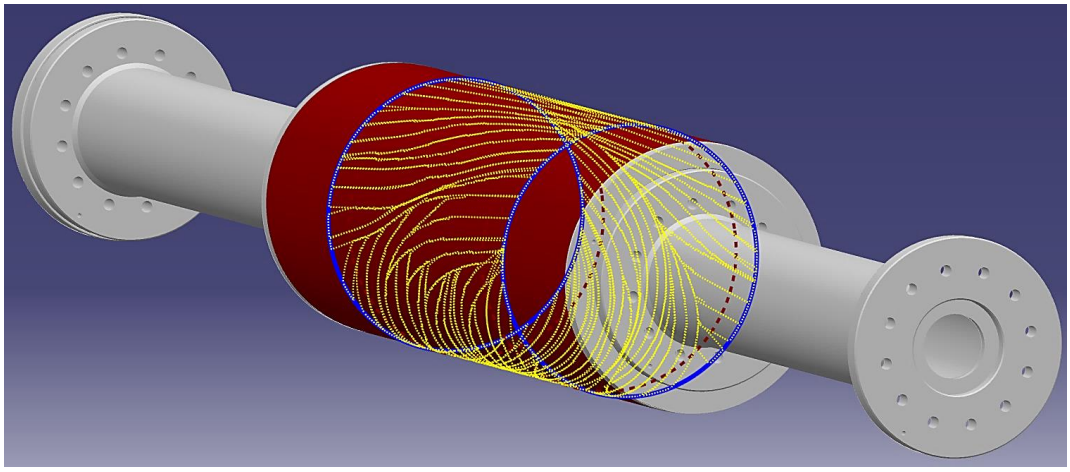

Figure 5.7 Steered ply φ_1 imported to CATIA V5®

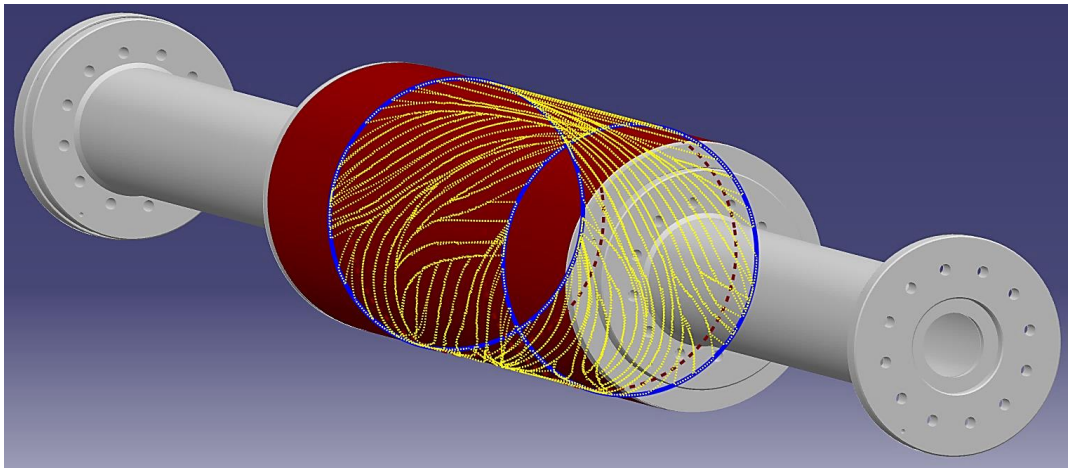

Figure 5.8 Steered ply φ_2 imported to CATIA V5®

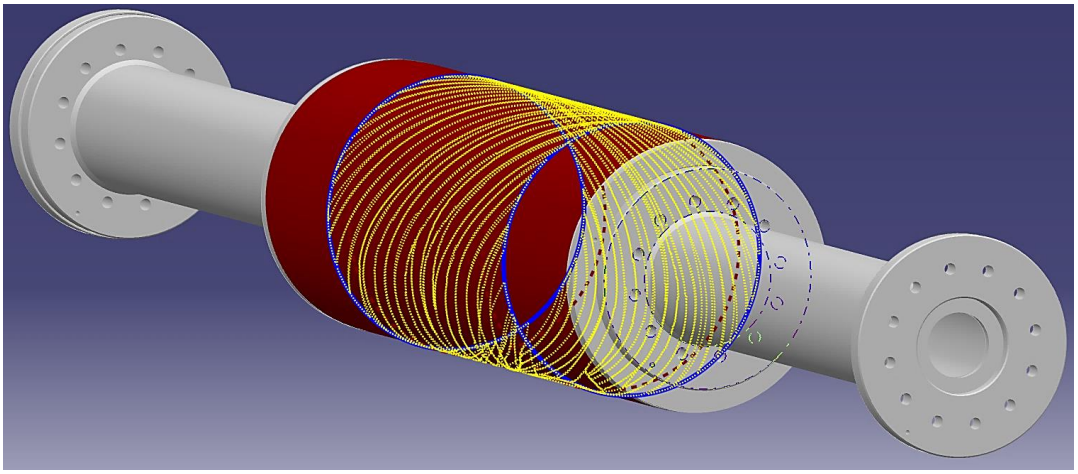

Figure 5.9 Steered ply φ_3 imported to CATIA V5®

5.3 COMPOSITE DESIGN PROGRAMMING

After importing all the required geometric elements to the CAD model in CATIA V5®, the iCPS® (Ingersoll Composite Programming System) software was used to program the manufacturing of the cylindrical composite part [186]. The composite design programming steps required can be summarized in the flow chart shown in Figure 5.10. The flow chart contains the following three major components:

1. Composite Design (CATIA V5®): The composite design module in CATIA V5® provides process-oriented tools for preliminary and detailed designing of composite parts. It can be used along with other modules in CATIA V5® to model the geometry of the composite part, the stacking sequence design, and independent guide curves for steered plies. In addition, iCPS® is integrated within the composite design module to optimize the layup of the composite part. The general steps required to program a composite part are:

- Generative Shape Design: This module is used to model the geometry of the tool surface, importing the guide curves if a steered ply is being designed, generating the manufacturing boundaries of the composite part, and creating the safety plane for controlling the off-part motion in the manufacturing simulation.
- Composite Parameters: This module is used for specifying the material that is used during manufacturing, specifying the Rosette axis system for the part, and defining the constant angle ply orientations that are used to obtain the designed laminate.
- Stacking Sequence: The stacking (engineering) module is used to create the stacking sequence design within CATIA V5® and preparing the laminate design for automated manufacturing using the AFP machine. The ply groups are

specified by the user, where a layup method (constant ply angle or guide curves for steered) must be specified along with the fiber layup strategy parameters. For the constant angle plies, the coverage parameter, inter-band offsets, and the staggering are provided by the user to reduce the gaps obtained between successive courses and to obtain a uniform thickness laminate. For the designed steered plies, these are already accounted for in the design-for-manufacturing tool and a 0% coverage is used.

- Surface Simplification and Skin Swapping: After the stacking sequence design for the laminate is programmed, a continuous parametric surface definition is generated using the integrated iCPS® module and a skin swapping is performed to prepare the design for manufacturing.

2. Computer Aided Manufacturing (iCPS®): Ingersoll Composite Programming System provides a solution for automating the manufacturing process of composite parts. From the designed composite part that is programmed within the CATIA V5® environment, iCPS® allows the user to generate the ply details and analyze the manufacturability of the part. The NC data is then generated for the simulation software to post-process the designed part and inspect for any errors before manufacturing. The general steps required for programming the manufacturing of the part are:

- Composite Part Operation: This module defines the machine set-up for AFP processing of the part. The composite design file is imported, and the safety plane is specified for the off-part motion during manufacturing.
- Ply Operation Definition: This module defines the manufacturing operations and layup parameters for each designed ply. The global process parameters that

are used during manufacturing are also specified, and the off-part motion can be optimized to reduce the time taken during manufacturing.

- Path Computation: After the ply operation is defined for each ply, the tool path computation generates the tow-by-tow descriptions for each designed ply (constant angle or steered guide curve). The tool path information can be analyzed to check off-part motion, laying motion, and in-plane steering curvature. The tool path parameters can be optimized for steered tool paths to avoid fiber straightening that appear at the tow-drop locations. For example, if a tow is cut while it is being steered, it will follow a geodesic path on a curved surface. As a result, the layup direction can be reversed to drop at the extended linear portions of the steered fiber courses.
- Generate NC Code: The NC data is generated to import into the simulation software and visualize the manufacturing process for each designed ply.

3. Process Simulation: Ingersoll Gen2 software is used to simulate the programmed composite part manufacturing and inspect for any errors before exporting the programmed tool paths to the AFP machine. The general steps for the simulation are:
    - Simulation Configuration: This module imports the AFP machine file that will be used for manufacturing. The composite part file is also imported, and the default axis limits (range of motion) of the machine are specified.
    - Post-Processing: The post-processor takes the NC data that was generated to generate a simulation for each course within each ply. The post-processing and machine kinematics depend on the specified axis limits, so these are debugged and modified to obtain a successful post-processing of the ply courses.

- Simulation: The courses that are loaded into the simulation are further post-processed to create a ply display within the simulation for visual inspection. The tool paths are then simulated course-by-course to inspect for any errors such as irregular AFP head motion and possible collisions.
- Export to AFP Machine: The programmed fiber courses are exported for the AFP machine for final manufacturing of the designed composite part.

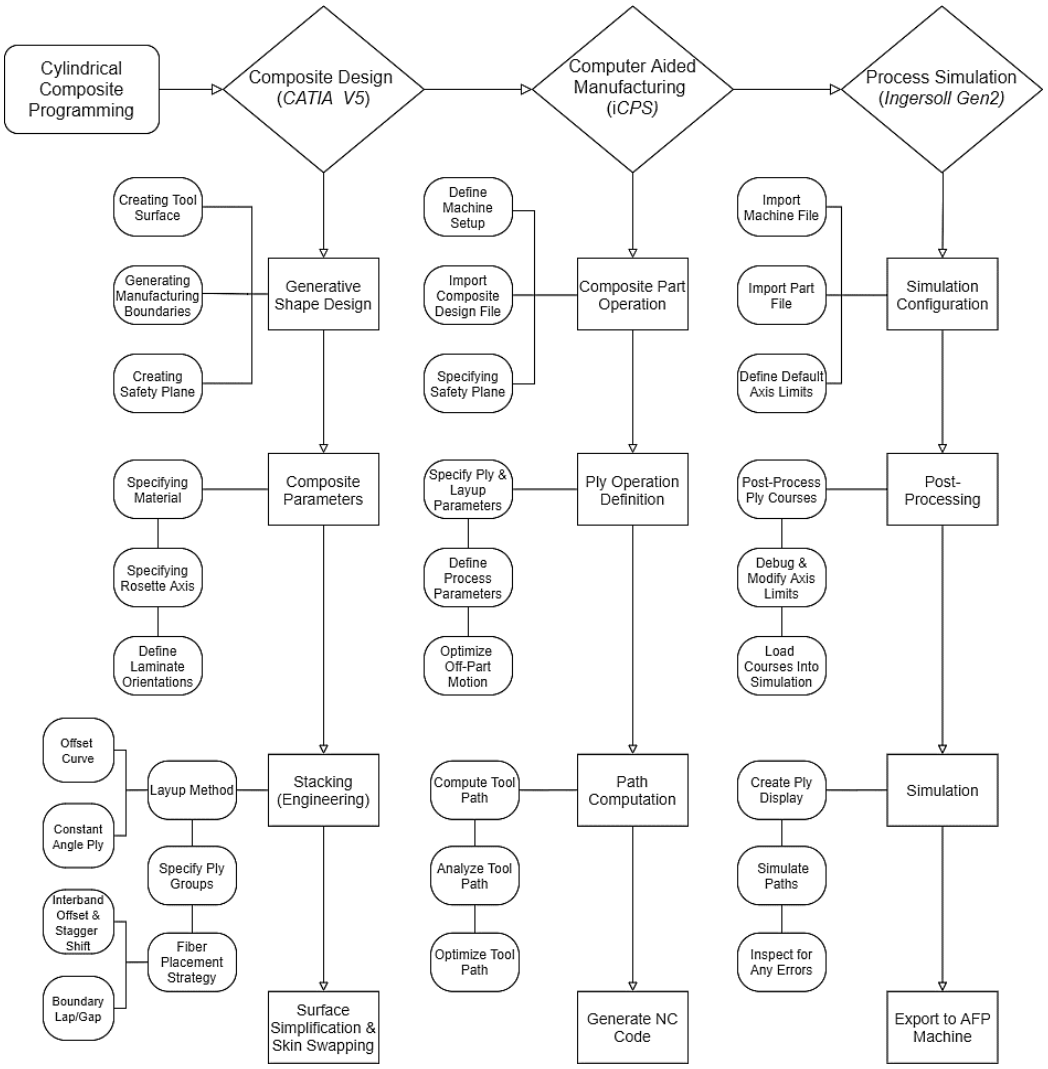

Figure 5.10 Composite design programming flow chart

5.4 SUMMARY AND CONLUSIONS

In conclusion, this chapter demonstrates the applicability of the design-for-manufacturing tool developed to generate optimal variable stiffness steered fiber laminates. The designed fiber-steered laminate is transformed to the surface of the cylinder and imported into CATIA V5® and programmed using iCPS® for manufacturing. The stages required using iCPS® to program the imported fiber paths and generate the manufacturing program for the AFP machine are also presented briefly. Unfortunately, the manufacturing of the designed cylinder is not presented in this work because of time constraints.

The importance of including the maximum steering constraint in the design process is demonstrated by presenting the results of an experimental study that was undertaken to study the effect of process parameters on the layup quality of steered paths on a cylinder. For different materials and steered-fiber path designs, a different optimal set of process parameters is needed to achieve a suitable layup quality with minimal wrinkles, gaps, and overlaps. If the maximum steering constraint is relaxed, a higher maximum curvature constraint can be used during the design step, hence better local tailoring can be achieved as well as less course centerline intersections which lead to fiber angle discontinuities.

Chapter 6

CONCLUSIONS AND FUTURE WORK

Since their introduction and initial development, advanced fiber-reinforced composite materials have earned a widespread acceptance for different structural applications. The ability to tailor the material properties of composites to achieve high specific stiffness and high specific strength has promoted them as ideal candidates for constructing efficient light-weight structures. However, despite their increased usage, the potential improvements that can be achieved by composite laminates have not been fully exploited. With the introduction of new manufacturing technologies such as advanced fiber placement, engineers now have the capability to harness the benefits of composite laminates. This represents a remarkable step in the development of efficient light-weight structures that are energy-efficient. As a result, this thesis aims to abandon the traditional usage of composite laminates in the favor of exploring the structural improvements that can be achieved by nonconventional variable stiffness laminates. However, the structural enhancements come at the expense of an increased design complexity. The presence of appropriate design tools that can help unlock the advancements achieved by nonconventional laminates is an essential step in the certification of such structures. Therefore, the purpose is to adopt an efficient design optimization methodology to realize the full capacity of steered fiber laminated composite structures, subject to industry design guidelines and manufacturing constraints.

The complexity of the optimization problem imposes the need for an efficient multi-level optimization approach to achieve a global optimum design. In this work, the importance of including a design-manufacturing mesh is demonstrated in each optimization step of the multi-level optimization framework. In the first optimization step, a theoretical optimum stiffness is achieved that accounts for optimum structural performance while maintaining smoothness and robustness. The design-manufacturing mesh allows the spatial stiffness distribution to be defines as a B-spline or NURBS surface defined by the control points of the design-manufacturing mesh. This introduces several benefits to the optimization problem, by significantly reducing the number of design variables while achieving local tailoring of the stiffness distribution as well as smoothness and point-wise constraint feasibility. The fiber angle distribution is then obtained in the second step to match the optimum stiffness properties from the first optimization step while accounting for the maximum steering constraint and laminate design guidelines to attain manufacturability and feasibility. A bilinear *sine* angle variation is presented to obtain smooth fiber angle distributions, and the maximum steering constraint to guarantee a minimum degree of manufacturability at the second optimization step (ply level) is derived for different surfaces using the curl of the vector field. Using the design-manufacturing mesh, a constant curvature arc solution is developed in the third optimization step to generate manufacturable fiber paths with piecewise constant curvature arcs that match the optimal fiber orientation angles from the second optimization step. A design-for-manufacturing tool has been developed to consider the maximum steering constraint locally in the third optimization step while accounting for gaps and overlaps to obtain a near constant thickness variable stiffness structure. Sequential course placement can be

used to solve the third optimization step locally considering each fiber course to closely match the optimal fiber orientation angles. Finally, detailed tow-level information in the form of manufacturing boundaries are then exported to the AFP machine with optimized cut and restart positions.

An aerospace application of a cylindrical shell with a cutout under bending was chosen to demonstrate the potential improvements of using nonconventional variable stiffness laminates compared to traditional laminate designs. An efficient multi-level optimization approach was used to demonstrate the potential improvements of variable stiffness laminates while satisfying manufacturing constraints and laminate design guidelines. Lamination parameters were used as intermediate design variables to achieve convexity and reduce the design complexity. The use of conservative convex separable approximations for the approximation of the inverse of the buckling load was proved to be efficient in obtaining the optimum stiffness requirements of the cylindrical shell. A design-manufacturing mesh was introduced to perform the buckling load optimization, where both circumferential and longitudinal stiffness variations were considered to physically understand the importance of the stiffness tailoring mechanism in efficient load redistribution and local reinforcements around the regions of the cutouts. Based on the optimum lamination parameter distribution obtained, the theoretical linear buckling load improved by 83% compared to the initial quasi-isotropic design. An optimal laminate with fiber-steered layers is then designed to match the optimum stiffness requirements using a genetic algorithm. The linear buckling load shows a 23% reduction compared to the linear buckling load of the variable stiffness cylinder in the 1st optimization step, and a 41% increase compared to the quasi-isotropic laminate. The fiber paths are then constructed

using the developed design-for-manufacturing tool and the manufacturing boundaries are generated for the AFP machine. The final manufacturable variable stiffness laminate results in a 30% reduction compared to the variable stiffness laminate obtained in the 1st optimization step, a 9% reduction compared to the 2nd optimization step, and a 28% increase compared to the quasi-isotropic laminate, while satisfying locally the maximum steering constraint at the 3rd optimization step and industry design guidelines in the 2nd optimization step.

Even though significant buckling load improvements based on the stiffness variations were obtained, the design problem has not been completely solved. The first issue is the significance of stress concentrations around the cutout that may lead to material strength failure before the buckling load is attained. It has been shown that the ultimate failure load increases by 40% as obtained using the final steered laminate obtained from the buckling design solution, yet further improvements can be achieved by considering the strength response as well in the first optimization step as a multi-objective function to improve the ultimate failure load of the cylindrical shell. It is also essential to consider the effect of the gaps and overlaps obtained on the structural analysis, which may result in additional performance reduction. In addition, a non-conservative steering constraint can be applied at the second optimization step at the ply level to reduce the fiber discontinuities and the amount of tow-dropping that are obtained in the third optimization step

It is also important to address the design of more realistic fuselage structures including stiffening elements using nonconventional laminates. This aims to prove that reliable structural improvements can be achieved by using nonconventional laminates for

realistic design problems, which can be a major task towards their industry adoption and certification in the future.

In addition, the considered design problem was limited to pure bending; in the future, it will be interesting to investigate design of cylindrical shell under combined loadings such as transverse shear and internal pressure. In that case, the orthotropic assumption must be negated, and bending-twisting coupling must be taken into consideration to obtain the optimal design of the structure. When shear loads are present, bending-twisting coupling can help improve the optimal response of the cylindrical shell to introduce further improvements in structural performance.

Moreover, the cylindrical shell was optimized with constant thickness throughout the laminate. A potential future work would be to design the cylindrical shell with variable thickness that would act as reinforcements around the hole to further optimize the structural performance. It is well known that the regions around the cutouts are usually reinforced to minimize the stress concentrations and improve the structural performance. However, this reinforcement can also be achieved by designing the structure with variable thicknesses that further tailor the stiffness properties to induce improved load carrying capabilities. The presence of overlaps around the cutout in a variable stiffness design can also be investigated to study the effect of reinforcing the region with thickness build-ups. This enables the designer to embrace the features that are obtained with fiber-steered laminates, rather than trying to eliminate them.

An additional indispensable problem to address is designing the manufacturing process for variable stiffness laminates. In terms of industrial utilization, the minimization of production time while ensuring an optimal quality of the manufactured part is a crucial

requirement to reduce labor costs, minimize waste of material, and the number of rejected parts. In general, manufacturing costs strongly depend on manufacturing time, so increasing the production rate is significant for industrial manufacturing. However, increasing the machine deposition rates sacrifices the quality of the manufactured part, hence efficient path planning must be considered by optimizing the machine and process parameters during the layup process. This helps in achieving a cost-effective AFP manufacturing process to obtain the optimal structural part quality with an optimized manufacturing time.

In conclusion, the development of composite materials is following an evolutionary phase rather than a revolutionary one. The reason for that is that the overly conservative utilization of composite materials has not been abandoned yet by industry. Even though significant improvements have been obtained using nonconventional laminates in structural applications both theoretically and experimentally, certification of nonconventional laminates is still a hurdle that must be confronted to allow their usage in aerospace applications. As a result, design practicality should be considered to satisfy industrial feasibility to set the path for industry certification in the future. Traditionally, certification of composite laminates is done based on allowables databases, which are generated through a set of extensive test programs. However, for nonconventional laminates, perhaps a different approach must be taken, because it is impossible to build databases that cover all the different possible stacking sequences that can be generated. In addition, nonconventional laminates might possess different failure mechanisms than conventional laminates. As a result, accurate analysis models (virtual testing) should be utilized for reliable failure prediction of manufactured nonconventional laminates.

Moreover, damage propagation and failure mechanisms have to be investigated for understanding the effect of different defects associated with nonconventional laminates for different structural applications, as presented by Lopes [187]. Consequently, the presence of accurate analysis models that might include the effect of these defects for reliable failure prediction of nonconventional laminates is essential. Certification of nonconventional laminates may be initiated through accurate analysis models, and then validated through experimental test results. Throughout this thesis work, non-linear static analysis with progressive failure analysis using Helius PFA is utilized to predict the realistic ultimate failure loads of the designed cylindrical shell without accounting for defects. In the future, the cylindrical shells might still be manufactured for experimental testing and validation of the obtained results. This would hopefully contribute to support the research community by providing reliable analysis capabilities that can match experimental test results and verify that structural improvements can be achieved by using nonconventional variable stiffness laminated composite structures.

REFERENCES

[1] Herakovich CT. Mechanics of fibrous composites. Wiley; 1998.

[2] Beukers A, Hinte E van. Lightness : the inevitable renaissance of minimum energy structures. 010 Publishers; 1999.

[3] Beukers A, Hinte E van. Flying lightness : promises for structural elegance. Rotterdam: 010 Publishers; 2005.

[4] Licewicz LB, Smith PJ, Horton RE. ADVANCED COMPOSITE FUSELAGE TECHNOLOGY. n.d.

[5] Roeseler WG, Sarh B, Kismarton MU. 6 TH INTERNATIONAL CONFERENCE ON COMPOSITE MATERIALS COMPOSITE STRUCTURES: THE FIRST 100 YEARS. n.d.

[6] Hale J. Boeing 787: From the Ground Up. Aero Mag 2006:17–23.

[7] Subramanian S, Lesko JJ, Reifsnider KL, Stinchcomb WW. Characterization of the Fiber-Matrix Interphase and its Influence on Mechanical Properties of Unidirectional Composites. J Compos Mater 1996;30:309–32. https://doi.org/10.1177/002199839603000302.

[8] COMPOSITES 101 | Quartus Engineering n.d. https://www.quartus.com/resources/composites-101/ (accessed June 19, 2018).

[9] Muzzy JD, Kays AO. Thermoplastic vs. thermosetting structural composites. Polym Compos 1984;5:169–72. https://doi.org/10.1002/pc.750050302.

[10] Holmes LR, Wolbert JP, Gardner JM. A processing method for high fiber volume fraction composites. Fort Belvoir, VA: 2012.

[11] Upadhya AR, Dayananda GN, Kamalakannan GM, Ramaswamy Setty J, Daniel JC. Autoclaves for Aerospace Applications: Issues and Challenges. Int J Aerosp Eng 2011;2011:11. https://doi.org/10.1155/2011/985871.

[12] Lukaszewicz DHJA, Ward C, Potter KD. The engineering aspects of automated prepreg layup: History, present and future. Compos Part B Eng 2012;43:997–1009. https://doi.org/10.1016/j.compositesb.2011.12.003.

[13] Marsh G. Automating aerospace composites production with fibre placement. Reinf Plast 2011;55:32–7. https://doi.org/10.1016/S0034-3617(11)70075-3.

[14] Lozano GG, Tiwari A, Turner C, Astwood S. A review on design for manufacture of variable stiffness composite laminates. Proc Inst Mech Eng Part B J Eng Manuf 2016;230:981–92. https://doi.org/10.1177/0954405415600012.

[15] Khani A. Optimum Design of Steered Fibre Composite Cylinders with Arbitrary Cross-Sections. 2013.

[16] Peeters D, Abdalla M. Design Guidelines in Nonconventional Composite Laminate Optimization. J Aircr 2017;54:1454–64. https://doi.org/10.2514/1.C034087.

[17] Diaconu CG, Sekine H. Layup Optimization for Buckling of Laminated Composite Shells with Restricted Layer Angles. AIAA J 2004;42:2153–63. https://doi.org/10.2514/1.931.

[18] Bloomfield M, Herencia J, Weaver P. Optimisation of Anisotropic Composite Plates Incorporating Non-Conventional Ply Orientations. 49th AIAA/ASME/ASCE/AHS/ASC Struct Struct Dyn Mater Conf
 16th AIAA/ASME/AHS Adapt Struct Conf 10t 2008:1–15. https://doi.org/10.2514/6.2008-1918.

[19] Albazzan MA, Harik R, Tatting BF, Gürdal Z, Blom-Schieber AW, Rassaian M, et al. Optimization of cylinders with holes under bending using nonconventional laminates. AIAA/ASCE/AHS/ASC Struct. Struct. Dyn. Mater. Conf. 2018, 2018. https://doi.org/10.2514/6.2018-1377.

[20] Sabido A, Bahamonde L, Harik R, van Tooren MJL. Maturity assessment of the laminate variable stiffness design process. Compos Struct 2017;160:804–12. https://doi.org/10.1016/j.compstruct.2016.10.081.

[21] Wu K, Gürdal Z. Thermal testing of tow-placed, variable stiffness panels. 19th AIAA Appl Aerodyn Conf 2001. https://doi.org/10.2514/6.2001-1190.

[22] Blom AW, Rassaian M, Stickler PB, Gürdal Z. Bending test of a variable-stiffness fiber-reinforced composite cylinder. Collect Tech Pap - AIAA/ASME/ASCE/AHS/ASC Struct Struct Dyn Mater Conf 2010:12–5.

[23] Tatting BF, Gürdal Z. Design and manufacture of elastically tailored tow placed plates. Nasa/Cr 2002- 211919 2002:1–14.

[24] Khani A, Abdalla MM, Gürdal Z, Sinke J, Buitenhuis A, Van Tooren MJL. Design, manufacturing and testing of a fibre steered panel with a large cut-out. Compos Struct 2017;180:821–30. https://doi.org/10.1016/j.compstruct.2017.07.086.

[25] Albazzan M, Tatting B, Harik R, Gürdal Z, Blom-Schieber A, Rassaian M, et al. Design of Variable Stiffness Cylinder with Holes Under Bending for Maximum Buckling Load Using Lamination Parameters. SAMPE 2019 - Charlotte, NC 2019:1–18. https://doi.org/10.33599/nasampe/s.19.1378.

[26] Albazzan MA, Harik R, Tatting BF, Gürdal Z. Efficient design optimization of nonconventional laminated composites using lamination parameters : A state of the art. Compos Struct 2019;209:362–74. https://doi.org/10.1016/j.compstruct.2018.10.095.

[27] Gürdal Z, Haftka RT, Hajela P. Design and Optimization of Laminated Composite Materials. 1999.

[28] Haftka RT, Gürdal Z. Elements of Structural Optimization. vol. 11. Kluwer Academic Publishers; 1992. https://doi.org/10.1002/nme.2403.

[29] Ghiasi H, Pasini D, Lessard L. Optimum stacking sequence design of composite materials Part I: Constant stiffness design. Compos Struct 2009;90:1–11. https://doi.org/10.1016/j.compstruct.2009.01.006.

[30] Ghiasi H, Fayazbakhsh K, Pasini D, Lessard L. Optimum stacking sequence design of composite materials Part II: Variable stiffness design. Compos Struct 2010;93:1–13. https://doi.org/10.1016/j.compstruct.2010.06.001.

[31] Venkataraman S, Haftka RT. Optimization of composite panels- A review. Am Soc Compos Tech Conf 14 Th, Fairborn, OH 1999:479–88.

[32] Zabinsky ZB, Tuttle ME, Khompatraporn C. A Case Study: Composite Structure Design Optimization. Glob. Optim., Springer US; n.d., p. 507–28. https://doi.org/10.1007/0-387-30927-6_21.

[33] Gürdal Z, IJsselmuiden S, van Campen J. Composite Laminate Optimization with Discrete Variables. Encycl Aerosp Eng 2010;9:43–90. https://doi.org/10.1002/9780470686652.eae499.

[34] Verchery G. Design rules for the laminate stiffness. Mech Compos Mater 2011;47:47–58. https://doi.org/10.1007/s11029-011-9186-x.

[35] Albazzan MA, Harik R, Gürdal Z, Hartzell J. 43-SOME QUASI-ISOTROPIC LAMINATES ARE MORE ISOTROPIC THAN OTHERS. 2018.

[36] Ijsselmuiden ST. Optimal design of variable stiffness composite structures using lamination parameters. 2011.

[37] Setoodeh S, Abdalla MM, IJsselmuiden ST, Gürdal Z. Design of variable-stiffness composite panels for maximum buckling load. Compos Struct 2009;87:109–17. https://doi.org/10.1016/j.compstruct.2008.01.008.

[38] Setoodeh S, Gürdal Z, Watson LT. Design of variable-stiffness composite layers using cellular automata. Comput Methods Appl Mech Eng 2006;195:836–51. https://doi.org/10.1016/j.cma.2005.03.005.

[39] Hyer MW, Charrette RF. Use of Curvilinear FIber Format in Composite Structure Design. AIAA J 1991;29:1011–5.

[40] Hyer MW, Lee HH. The use of curvilinear fiber format to improve buckling resistance of composite plates with central circular holes. Compos Struct 1991;18:239–61. https://doi.org/10.1016/0263-8223(91)90035-W.

[41] Katz Y, Haftka RT, Altus E. Optimization of Fiber Directions for Increasing the Failure Load if a Plate with a Hole. ASC Tech. Conf. Vol. 4, 1989, p. 62–71.

[42] Setoodeh S, Gürdal Z, Abdalla M, Watson L. Design of Variable Stiffness Composite Laminates For Maximum Bending Stiffness. 10th AIAA/ISSMO Multidiscip. Anal. Optim. Conf., Reston, Virigina: American Institute of Aeronautics and Astronautics; 2004. https://doi.org/10.2514/6.2004-4528.

[43] Tooren MJ Van, Jahangir I, Elham A. Optimization of variable stiffness composite plates with cut-outs subjected to compression, tension and shear using an adjoint formulation. 57th AIAA/ASCE/AHS/ASC Struct. Struct. Dyn. Mater. Conf., Reston, Virginia: American Institute of Aeronautics and Astronautics; 2016, p. 1–17. https://doi.org/doi:10.2514/6.2016-1970.

[44] Barazanchy D. A new framework for optimization of variable stiffness plates. 58th AIAA/ASCE/AHS/ASC Struct Struct Dyn Mater Conf 2017:1–16. https://doi.org/10.2514/6.2017-0894.

[45] Tauchert TR, Adibhatla S. Design of Laminated Plates for Maximum Stiffness. J Compos Mater 1984;18:58–69. https://doi.org/10.1177/002199838401800105.

[46] Topal U, Uzman Ü. Maximization of buckling load of laminated composite plates with central circular holes using MFD method. Struct Multidiscip Optim 2008;35:131–9. https://doi.org/10.1007/s00158-007-0119-1.

[47] Huang J, Haftka RT. Optimization of fiber orientations near a hole for increased load-carrying capacity of composite laminates. Struct Multidiscip Optim 2005;30:335–41. https://doi.org/10.1007/s00158-005-0519-z.

[48] Narita Y. Layerwise optimization for the maximum fundamental frequency of laminated composite plates. J Sound Vib 2003;263:1005–16. https://doi.org/10.1016/S0022-460X(03)00270-0.

[49] Nagendra S, Jestin D, Gürdal Z, Haftka RT, Watson LT. Improved genetic algorithm for the design of stiffened composite panels. Comput Struct 1996;58:543–55. https://doi.org/http://dx.doi.org/10.1016/0045-7949(95)00160-I.

[50] Todoroki A, Haftka RT. Stacking sequence optimization by a genetic algorithm with a new recessive gene like repair strategy. Compos Part B Eng 1998;29:277–85. https://doi.org/10.1016/S1359-8368(97)00030-9.

[51] Liu B, T. Haftka R, A. Akgun M, Todoroki A. Permutation genetic algorithm for stacking sequence design of composite laminates. Comput Methods Appl Mech Eng 2000;186:357–72. https://doi.org/10.1016/S0045-7825(99)90391-2.

[52] Muc A, Gurba W. Genetic algorithms and finite element analysis in optimization of composite structures. Compos Struct 2001;54:275–81.

[53] Almeida FS, Awruch AM. Design optimization of composite laminated structures using genetic algorithms and finite element analysis. Compos Struct 2009;88:443–54. https://doi.org/10.1016/j.compstruct.2008.05.004.

[54] Gürdal Z, Olmedo R. In-plane response of laminates with spatially varying fiber orientations - Variable stiffness concept. AIAA J 1993;31:751–8. https://doi.org/10.2514/3.11613.

[55] Gürdal Z, Tatting BF, Wu CK. Variable stiffness composite panels: Effects of stiffness variation on the in-plane and buckling response. Compos Part A Appl Sci Manuf 2008;39:911–22. https://doi.org/10.1016/j.compositesa.2007.11.015.

[56] Alhajahmad A, Abdalla MM, Gürdal Z. Optimal Design of a Pressurized Fuselage Panel with a Cutout Using Tow-Placed Steered Fibers. Optimization 2008:01–5.

[57] Lopes C. Tailoring for Strength of Steered-Fibre Composite Panels with Cutouts. 51st AIAA/ASME/ASCE/AHS/ASC Struct Struct Dyn Mater Conf 2010:8. https://doi.org/10.2514/6.2010-2946.

[58] Abdalla MM, Gürdal Z, Abdelal GF. Thermomechanical Response of Variable Stiffness Composite Panels. J Therm Stress 2008;32:187–208. https://doi.org/10.1080/01495730802540916.

[59] Alhajahmad A, Abdalla MM, Gürdal Z. Optimal Design of Tow-Placed Fuselage Panels for Maximum Strength with Buckling Considerations. J Aircr 2010;47:775–82. https://doi.org/10.2514/1.40357.

[60] Nagendra S, Kodiyalam S, Davis JE, Parthasarthy VN. Optimization of tow fiber paths for composite design. Am. Inst. Aeronaut. Astronaut., vol. 36, Reston, Virigina: American Institute of Aeronautics and Astronautics; 1995, p. 1031–41. https://doi.org/10.2514/6.1995-1275.

[61] Setoodeh S, Blom A, Abdalla M, Gürdal Z. Generating Curvilinear Fiber Paths from Lamination Parameters Distribution. 47th AIAA/ASME/ASCE/AHS/ASC Struct Struct Dyn Mater Conf 14th AIAA/ASME/AHS Adapt Struct Conf 7th 2006;5:3440–52. https://doi.org/10.2514/6.2006-1875.

[62] Alhajahmad A, Abdalla MM, Gürdal Z. Design Tailoring for Pressure Pillowing Using Tow-Placed Steered Fibers. J Aircr 2008;45:630–40. https://doi.org/10.2514/1.32676.

[63] Blom AW, Tatting BF, Hol JMAM, Gürdal Z. Fiber path definitions for elastically tailored conical shells. Compos Part B Eng 2009;40:77–84. https://doi.org/10.1016/j.compositesb.2008.03.011.

[64] Blom AW, Setoodeh S, Hol JMAM, Gürdal Z. Design of variable-stiffness conical shells for maximum fundamental eigenfrequency. Comput Struct 2008;86:870–8. https://doi.org/10.1016/j.compstruc.2007.04.020.

[65] Blom AW, Stickler PB, Gürdal Z. Optimization of a composite cylinder under bending by tailoring stiffness properties in circumferential direction. Compos Part B Eng 2010;41:157–65. https://doi.org/10.1016/j.compositesb.2009.10.004.

[66] Vannucci P, Verchery G. Stiffness design of laminates using the polar method 2001;38.

[67] Montemurro M. An extension of the polar method to the first-order shear deformation theory of laminates. Compos Struct 2015;127:328–39. https://doi.org/10.1016/j.compstruct.2015.03.025.

[68] Vannucci P, Verchery G. A special class of uncoupled and quasi-homogeneous laminates. Compos Sci Technol 2001;61:1465–73. https://doi.org/10.1016/S0266-3538(01)00039-2.

[69] Garulli T, Catapano A, Montemurro M, Jumel J, Fanteria D. Quasi-trivial stacking sequences for the design of thick laminates. Compos Struct 2018;200:614–23. https://doi.org/10.1016/j.compstruct.2018.05.120.

[70] Montemurro M. Corrigendum to “An extension of the polar method to the First-order Shear Deformation Theory of laminates” [Compos. Struct. 127 (2015) 328–339]. Compos Struct 2015;131:1143–4. https://doi.org/10.1016/J.COMPSTRUCT.2015.06.002.

[71] Montemurro M. The polar analysis of the Third-order Shear Deformation Theory of laminates. Compos Struct 2015;131:775–89. https://doi.org/10.1016/j.compstruct.2015.06.016.

[72] Catapano A, Desmorat B, Vannucci P. Invariant formulation of phenomenological failure criteria for orthotropic sheets and optimisation of their strength. Math Methods Appl Sci 2012;35:1842–58. https://doi.org/10.1002/mma.2530.

[73] Catapano A, Montemurro M. On the correlation between stiffness and strength properties of anisotropic laminates. Mech Adv Mater Struct 2018:1–10. https://doi.org/10.1080/15376494.2017.1410906.

[74] Montemurro M, Pagani A, Fiordilino GA, Pailhès J, Carrera E. A general multi-scale two-level optimisation strategy for designing composite stiffened panels. Compos Struct 2018;201:968–79. https://doi.org/10.1016/j.compstruct.2018.06.119.

[75] Montemurro M, Vincenti A, Vannucci P. A Two-Level Procedure for the Global Optimum Design of Composite Modular Structures—Application to the Design of an Aircraft Wing. J Optim Theory Appl 2012;155:1–23. https://doi.org/10.1007/s10957-012-0067-9.

[76] Montemurro M, Catapano A, Doroszewski D. A multi-scale approach for the simultaneous shape and material optimisation of sandwich panels with cellular core. Compos Part B Eng 2016;91:458–72. https://doi.org/10.1016/J.COMPOSITESB.2016.01.030.

[77] Montemurro M, Vincenti A, Vannucci P. A Two-Level Procedure for the Global Optimum Design of Composite Modular Structures—Application to the Design of an Aircraft Wing. J Optim Theory Appl 2012;155:24–53. https://doi.org/10.1007/s10957-012-0070-1.

[78] Montemurro M, Vincenti A, Koutsawa Y, Vannucci P. A two-level procedure for the global optimization of the damping behavior of composite laminated plates with elastomer patches. J Vib Control 2015;21:1778–800. https://doi.org/10.1177/1077546313503358.

[79] Montemurro M, Catapano A. On the effective integration of manufacturability constraints within the multi-scale methodology for designing variable angle-tow laminates. Compos Struct 2017. https://doi.org/10.1016/j.compstruct.2016.11.018.

[80] Catapano A, Montemurro M. A multi-scale approach for the optimum design of sandwich plates with honeycomb core. Part I: homogenisation of core properties. Compos Struct 2014;118:664–76. https://doi.org/10.1016/J.COMPSTRUCT.2014.07.057.

[81] Catapano A, Montemurro M. A multi-scale approach for the optimum design of sandwich plates with honeycomb core. Part II: the optimisation strategy. Compos Struct 2014;118:677–90. https://doi.org/10.1016/J.COMPSTRUCT.2014.07.058.

[82] Montemurro M, Catapano A. A New Paradigm for the Optimum Design of Variable Angle Tow Laminates, Springer, Cham; 2016, p. 375–400. https://doi.org/10.1007/978-3-319-45680-5_14.

[83] Catapano A, Desmorat B, Vannucci P. Stiffness and Strength Optimization of the Anisotropy Distribution for Laminated Structures. J Optim Theory Appl 2015;167:118–46. https://doi.org/10.1007/s10957-014-0693-5.

[84] Tsai SW, Pagano NJ. Invariant properties of composite materials. Ft. Belvoir: Defense Technical Information Center; 1968.

[85] Tsai SW, Hahn HT. Introduction to composite materials. Technomic Pub; 1980.

[86] Grenestedt JL, Gudmundson P. Lay-up optimisation of composite material structures. Optim Des with Adv Mater 1993;The Frithi:311–36.

[87] Miki M. Material Design of Composite Laminates with Required In-Plane Elastic Properties. Prog Sci Eng Compos 1982.

[88] Miki M. Design of Laminated Fibrous Connposite Plates with Required Flexural Stiffness. Recent Adv. Compos. United States Japan, 100 Barr Harbor Drive, PO Box C700, West Conshohocken, PA 19428-2959: ASTM International; 1985, p. 387–400. https://doi.org/10.1520/STP32802S.

[89] Miki M, Murotsu Y. Optimum Design of Laminated Composite Plates Using Lamination Parameters. AIAA J 1993;31:921–2. https://doi.org/10.2514/3.49033.

[90] Grenestedt JL. Layup optimization against buckling of shear panels. Struct Optim 1991;3:115–20. https://doi.org/10.1007/BF01743281.

[91] Fukunaga H, Sekine H. Stiffness design method of symmetric laminates using lamination parameters. AIAA J 1992;30:2791–3. https://doi.org/10.2514/3.11304.

[92] Fukunaga H, Sekine H. A Laminate Design for Elastic Properties of Symmetric Laminates with Extension- Shear or Bending-Twisting Coupling. J Compos Mater 1994;28:708–31.

[93] Hammer VB, Bendsøe MP, Lipton R, Pedersen P. Parametrization in laminate design for optimal compliance. Int J Solids Struct 1997;34:415–34. https://doi.org/10.1016/S0020-7683(96)00023-6.

[94] Setoodeh S. Optimal Design of Variable-Stiffness Fiber-Reinforced Composites Using Cellular Automata. 2005.

[95] van Campen J, Gürdal Z. Retrieving Variable Stiffness Laminates from Lamination Parameters Distribution. 50th AIAA/ASME/ASCE/AHS/ASC Struct Struct Dyn Mater Conf 2009:4–7. https://doi.org/10.2514/6.2009-2183.

[96] Fukunaga H, Vanderplaatsj GN. Stiffness Optimization of Orthotropic Laminated Composites Using Lamination Parameters. AIAA J 1991;29:641–6. https://doi.org/10.2514/3.59931.

[97] Diaconu CG, Sato M, Sekine H. Feasible Region in General Design Space of Lamination Parameters for Laminated Composites. AIAA J 2002;40:559–65. https://doi.org/10.2514/2.1683.

[98] Diaconu CG, Sato M, Sekine H. Layup optimization of symmetrically laminated thick plates for fundamental frequencies using lamination parameters. Struct Multidiscip Optim 2002;24:302–11. https://doi.org/10.1007/s00158-002-0241-z.

[99] Liu B, Haftka RT, Trompette P. Maximization of buckling loads of composite panels using flexural lamination parameters. Struct Multidiscip Optim 2004;26:28–36. https://doi.org/10.1007/s00158-003-0314-7.

[100] Diaconu CG, Sekine H. Layup Optimization for Buckling of Laminated Composite Shells with Restricted Layer Angles. AIAA J 2004;42:2153–63. https://doi.org/10.2514/1.931.

[101] Liu D, Toropov V V. A lamination parameter-based strategy for solving an integer-continuous problem arising in composite optimization. Comput Struct 2013;128:170–4. https://doi.org/10.1016/j.compstruc.2013.06.003.

[102] Setoodeh S, Abdalla MM, Gürdal Z. Approximate feasible regions for lamination parameters. {Collection Tech. Pap. - 11th AIAA/ISSMO Multidiscip. Anal. Optim. Conf., vol. 2, Reston, Virigina: American Institute of Aeronautics and Astronautics; 2006, p. 814–22. https://doi.org/10.1016/j.compositesb.2005.12.001.

[103] Bloomfield M., Diaconu C., Weaver P. On feasible regions of lamination parameters for lay-up optimization of laminated composites. Proc R Soc A Math Phys Eng Sci 2009;465:1123–43. https://doi.org/10.1098/rspa.2008.0380.

[104] Wu Z, Raju G, Weaver PM. Feasible Region of Lamination Parameters for optimization of Variable Angle Tow (VAT) Composite Plates. 54th AIAA/ASME/ASCE/AHS/ASC Struct. Struct. Dyn. Mater. Conf., Reston, Virginia: American Institute of Aeronautics and Astronautics; 2013, p. 1–10. https://doi.org/10.2514/6.2013-1481.

[105] Wu Z, Raju G, Weaver PM. Framework for the Buckling Optimization of Variable-Angle Tow Composite Plates. AIAA J 2015;53:3788–804. https://doi.org/10.2514/1.J054029.

[106] Raju G, Wu Z, Weaver P. On Further Developments of the Feasible Region of Lamination Parameters for Composite Laminates. 55th AIAA/ASME/ASCE/AHS/ASC Struct. Struct. Dyn. Mater. Conf., Reston, Virginia: American Institute of Aeronautics and Astronautics; 2014, p. 1–13. https://doi.org/10.2514/6.2014-1374.

[107] Ijsselmuiden ST, Abdalla MM, Gürdal Z. Implementation of Strength-Based Failure Criteria in the Lamination Parameter Design Space. AIAA J 2008;46:1826–34. https://doi.org/10.2514/1.35565.

[108] Khani A, Ijsselmuiden ST, Abdalla MM, Gürdal Z. Design of variable stiffness panels for maximum strength using lamination parameters. Compos Part B Eng 2011;42:546–52. https://doi.org/10.1016/j.compositesb.2010.11.005.

[109] Foldager JP, Hansen JS, Olhoff N. A general approach forcing convexity of ply angle optimization in composite laminates. Struct Optim 1998;16:201–11. https://doi.org/10.1007/BF01202831.

[110] Fukunaga H, Ishikawa T, Sato M, Sekine H. Thermoelastic design of symmetric laminates using lamination parameters. JSME Int Journal, Ser A Mech Mater Eng 1997;40:389–97. https://doi.org/10.1299/jsmea.40.389.

[111] MIKI M, MUROTSU Y, MURAYAMA N, TANAKA T. Application of lamination parameters to reliability-based stiffness design of composites. AIAA J 1993;31:1938–45. https://doi.org/10.2514/3.11870.

[112] Kogiso N, Nakagawa S, Murotsu Y. Lamination Parameters Applied to Reliability-Based In-Plane Strength Design of Composites. AIAA J 2003;41:2200–7. https://doi.org/10.2514/2.6812.

[113] Kameyama M, Fukunaga H. Optimum design of composite plate wings for aeroelastic characteristics using lamination parameters. Comput Struct 2007;85:213–24. https://doi.org/10.1016/j.compstruc.2006.08.051.

[114] Kameyama M, Takahashi A. Damping Optimization of Symmetrically Laminated Plates with Shear Deformation using Lamination Parameters. 57th AIAA/ASCE/AHS/ASC Struct. Struct. Dyn. Mater. Conf., Reston, Virginia: American Institute of Aeronautics and Astronautics; 2016, p. 1–8. https://doi.org/10.2514/6.2016-1968.

[115] Thuwis GAA, De Breuker R, Abdalla MM, Gürdal Z. Aeroelastic tailoring using lamination parameters :Drag reduction of a Formula One rear wing. Struct Multidiscip Optim 2010;41:637–46. https://doi.org/10.1007/s00158-009-0437-6.

[116] Stanford B, Wieseman CD, Jutte C. Aeroelastic Tailoring of Transport Wings Including Transonic Flutter Constraints. 56th AIAA/ASCE/AHS/ASC Struct Struct Dyn Mater Conf 2015:1–22. https://doi.org/10.2514/6.2015-1127.

[117] Stanford BK, Jutte C V., Wieseman CD. Trim and Structural Optimization of Subsonic Transport Wings Using Nonconventional Aeroelastic Tailoring. AIAA J 2016;54:293–309. https://doi.org/10.2514/1.J054244.

[118] Wu Z, Raju G, White S, Weaver PM. Optimal Design of Postbuckling Behaviour of Laminated Composite Plates using Lamination Parameters. 55th AIAA/ASME/ASCE/AHS/ASC Struct Struct Dyn Mater Conf 2014:1–15. https://doi.org/10.2514/6.2014-1376.

[119] Dutra TA, de Almeida SFM. Composite plate stiffness multicriteria optimization using lamination parameters. Compos Struct 2015;133:166–77. https://doi.org/10.1016/j.compstruct.2015.07.029.

[120] Liu D, Toropov V, Zhou M, Barton D, Querin O. Optimization of Blended Composite Wing Panels Using Smeared Stiffness Technique and Lamination Parameters. 51st AIAA/ASME/ASCE/AHS/ASC Struct Struct Dyn Mater Conf 18th AIAA/ASME/AHS Adapt Struct Conf 12th 2010. https://doi.org/10.2514/6.2010-3079.

[121] Macquart T, Bordogna MT, Lancelot P, De Breuker R. Derivation and application of blending constraints in lamination parameter space for composite optimisation. Compos Struct 2016;135:224–35. https://doi.org/10.1016/j.compstruct.2015.09.016.

[122] Macquart T, Werter N, De Breuker R. Aeroelastic Design of Blended Composite Structures Using Lamination Parameters. J Aircr 2017;54:561–71. https://doi.org/10.2514/1.C033859.

[123] Abdalla MM, Setoodeh S, Gürdal Z. Design of variable stiffness composite panels for maximum fundamental frequency using lamination parameters. Compos Struct 2007;81:283–91. https://doi.org/10.1016/j.compstruct.2006.08.018.

[124] Ijsselmuiden ST, Abdalla MM, Gürdal Z. Optimization of Variable-Stiffness Panels for Maximum Buckling Load Using Lamination Parameters. AIAA J 2010;48:134–43. https://doi.org/10.2514/1.42490.

[125] Ijsselmuiden ST, Abdalla MM, Gürdal Z. Thermomechanical design optimization of variable stiffness composite panels for buckling. J Therm Stress 2010;33:977–92. https://doi.org/10.1080/01495739.2010.510701.

[126] Khani A, Abdalla M, Gürdal Z. Maximum Buckling Load Design of General Cross-section Cylinders Using Lamination Parameters. 13th AIAA/ISSMO Multidiscip Anal Optim Conf 2010. https://doi.org/10.2514/6.2010-9182.

[127] Khani A, Abdalla MM, Gürdal Z. Circumferential stiffness tailoring of general cross section cylinders for maximum buckling load with strength constraints. Compos Struct 2012;94:2851–60. https://doi.org/10.1016/j.compstruct.2012.04.018.

[128] Khani A, Abdalla MM, Gürdal Z. Optimum tailoring of fibre-steered longitudinally stiffened cylinders. Compos Struct 2015;122:343–51. https://doi.org/10.1016/j.compstruct.2014.11.071.

[129] Dillinger JKS, Klimmek T, Abdalla MM, Gürdal Z. Stiffness Optimization of Composite Wings with Aeroelastic Constraints. J Aircr 2013;50:1159–68. https://doi.org/10.2514/1.C032084.

[130] Beckwith S. Designing with Composites: Suggested “Best Practices” Rules. SAMPE J 2009;45:16–7.

[131] Bailie JA, Ley RP, Pasricha A. A SUMMARY AND REVIEW OF COMPOSITE LAMINATE Design Guidelines. NASA Contract NAS1-19347 1997.

[132] IJsselmuiden S, Abdalla M, Pilaka V, Gürdal Z. Design of variable stiffness composite structures for advanced fibre placement technology. SAMPE Symp … 2010:14–6.

[133] Svanberg K. Methods Based on Conservative Convex Separable. Society 2002;12:555–73.

[134] Olhoff N. Multicriterion structural optimization via bound formulation and mathematical programming. Struct Optim 1989;1:11–7. https://doi.org/10.1007/BF01743805.

[135] Fleury C. CONLIN: An efficient dual optimizer based on convex approximation concepts. Struct Optim 1989;1:81–9. https://doi.org/10.1007/BF01637664.

[136] Abdalla MM, Kassapoglou C, Gürdal Z. Formulation of composite laminate robustness constraint in lamination parameters space. Collect Tech Pap -

AIAA/ASME/ASCE/AHS/ASC Struct Struct Dyn Mater Conf 2009:1–15. https://doi.org/10.2514/6.2009-2478.

[137] Peeters DMJ. Design Optimisation of Practical Variable Stiffness and Thickness Laminates. 2016.

[138] Campen J Van, Seresta O, Abdalla M, Gürdal Z. General blending definitions for stacking sequence design of composite laminate structure. 4th AIAA Multidiscip Des Optim Spec Conf 2008:7–10.

[139] Autio M. Determining the real lay-up of a laminate corresponding to optimal lamination parameters by genetic search. Struct Multidiscip Optim 2000;20:301–10. https://doi.org/10.1007/s001580050160.

[140] Gangadharan S, Nagendra S, Fiocca Y. Response surface based laminate stacking sequence optimization under stability constraints (AIAA). 38th Struct. Struct. Dyn. Mater. Conf., Reston, Virigina: American Institute of Aeronautics and Astronautics; 1997. https://doi.org/10.2514/6.1997-1236.

[141] Todoroki A, Haftka R. Lamination parameters for efficient genetic optimization of the stacking sequences of composite panels. 7th AIAA/USAF/NASA/ISSMO Symp. Multidiscip. Anal. Optim., Reston, Virigina: American Institute of Aeronautics and Astronautics; 1998. https://doi.org/10.2514/6.1998-4816.

[142] TERADA Y, TODOROKI A, SHIMAMURA Y. Stacking Sequence Optimizations Using Fractal Branch and Bound Method for Laminated Composites. JSME Int 2001;44.

[143] Todoroki A, Terada Y. Improved Fractal Branch and Bound Method for Stacking-Sequence Optimizations of Laminates. AIAA J 2004;42:141–8. https://doi.org/10.2514/1.9038.

[144] Todoroki A, Sekishiro M. New iteration fractal branch and bound method for stacking sequence optimizations of multiple laminates. Compos Struct 2007;81:419–26. https://doi.org/10.1016/j.compstruct.2006.09.001.

[145] Van Campen JMJF, Kassapoglou C, Gürdal Z. Generating realistic laminate fiber angle distributions for optimal variable stiffness laminates. Compos Part B Eng 2012;43:354–60. https://doi.org/10.1016/j.compositesb.2011.10.014.

[146] IJsselmuiden ST, Abdalla MM, Seresta O, Gürdal Z. Multi-step blended stacking sequence design of panel assemblies with buckling constraints. Compos Part B Eng 2009;40:329–36. https://doi.org/10.1016/j.compositesb.2008.12.002.

[147] Irisarri F-X, Abdalla MM, Gürdal Z. Improved Shepard's Method for the Optimization of Composite Structures. AIAA J 2011;49:2726–36. https://doi.org/10.2514/1.J051109.

[148] Peeters DMJ, Hesse SH, Abdalla MM. Multi-Objective and Multi-Constraint Optimisation of Variable Stiffness Composite Laminates. ECCM-16th Eur Conf Compos Mater 2014:22–6.

[149] Van Campen J, Kassapoglou C, Gürdal Z. Design of Fiber-steered Variable-stiffness Laminates Based on a Given Lamination Parameters Distribution. 52nd

AIAA/ASME/ASCE/AHS/ASC Struct Struct Dyn Mater Conf 2011:AIAA 2011-1894. https://doi.org/10.2514/6.2011-1894.

[150] Brooks TR, Martins JRRA. On manufacturing constraints for tow-steered composite design optimization. Compos Struct 2018;204:548–59. https://doi.org/10.1016/j.compstruct.2018.07.100.

[151] Albazzan MA, Harik R, Tatting BF, Gürdal Z, Blom-Schieber AW, Rassaian M, et al. Optimization of cylinders with holes under bending using nonconventional laminates. AIAA/ASCE/AHS/ASC Struct. Struct. Dyn. Mater. Conf. 2018, Reston, Virginia: American Institute of Aeronautics and Astronautics; 2018. https://doi.org/10.2514/6.2018-1377.

[152] Liu B, Haftka R. Composite wing structural design optimization with continuity constraints. 19th AIAA Appl. Aerodyn. Conf., Reston, Virigina: American Institute of Aeronautics and Astronautics; 2001. https://doi.org/10.2514/6.2001-1205.

[153] Soremekun G, Gürdal Z, Kassapoglou C, Toni D. Stacking sequence blending of multiple composite laminates using genetic algorithms. Compos Struct 2002;56:53–62. https://doi.org/10.1016/S0263-8223(01)00185-4.

[154] Adams DB, Watson LT, G??rdal Z, Anderson-Cook CM. Genetic algorithm optimization and blending of composite laminates by locally reducing laminate thickness. Adv Eng Softw 2004;35:35–43. https://doi.org/10.1016/j.advengsoft.2003.09.001.

[155] Seresta O, Zafer G. A Genetic Algorithm Based Blending Scheme for Design of Multiple Composite Laminates 2009:2699.

[156] Irisarri FX, Lasseigne A, Leroy FH, Le Riche R. Optimal design of laminated composite structures with ply drops using stacking sequence tables. Compos Struct 2014;107:559–69. https://doi.org/10.1016/j.compstruct.2013.08.030.

[157] Meddaikar YM, Irisarri FX, Abdalla MM. Laminate optimization of blended composite structures using a modified Shepard's method and stacking sequence tables. Struct Multidiscip Optim 2017;55:535–46. https://doi.org/10.1007/s00158-016-1508-0.

[158] Peeters DMJ, Peeters DMJ. Optimizing the ply dropping order in variable stiffness , variable thickness laminates using stacking sequence tables. ECCM17 n.d.:26–30.

[159] Blom AW, Abdalla MM, Gürdal Z. Optimization of course locations in fiber-placed panels for general fiber angle distributions. Compos Sci Technol 2010;70:564–70. https://doi.org/10.1016/j.compscitech.2009.12.003.

[160] Lozano GG, Tiwari A, Turner C. A design algorithm to model fibre paths for manufacturing of structurally optimised composite laminates. Compos Struct 2018;204:882–95. https://doi.org/10.1016/j.compstruct.2018.07.088.

[161] Blom AW, Lopes CS, Kromwijk PJ, Gürdal Z, Camanho PP. A Theoretical Model to Study the Influence of Tow-drop Areas on the Stiffness and Strength of Variable-stiffness Laminates. J Compos Mater 2009;43:403–25. https://doi.org/10.1177/0021998308097675.

[162] Blom-Schieber A, Kang LS, Vandenbrande JH. Fiber Placement Optimization for Steered-Fiber Plies. US10169492B2, 2019.

[163] Piegl L, Tiller W. The NURBS book. vol. 35. Springer Berlin Heidelberg; 1997. https://doi.org/10.5860/choice.35-0952.

[164] Hughes TJR, Cottrell JA, Bazilevs Y. Isogeometric analysis: CAD, finite elements, NURBS, exact geometry and mesh refinement. Comput Methods Appl Mech Eng 2005;194:4135–95. https://doi.org/10.1016/j.cma.2004.10.008.

[165] Fleury C, Schmit LA. Dual Methods and Approximation Concepts in Structural Synthesis. 1980.

[166] Seyranian AP, Lund E, Olhoff N. Multiple eigenvalues in structural optimization problems. Struct Optim 1994;8:207–27. https://doi.org/10.1007/BF01742705.

[167] Lambe A, Martins J. Extensions to the design structure matrix for the description of multidisciplinary design, analysis, and optimization processes. Struct Multidiscip Optim 2012;46:273–84. https://doi.org/10.1007/s00158-012-0763-y.

[168] Foadi J. Gradient , Divergence and Curl in Curvilinear Coordinates. 2011.

[169] Blom A. W. Structural performance of fiber-placed, variable-stiffness composite conical and cylindrical shells. 2010.

[170] Ahn CW. Advances in Evolutionary Algorithms: Theory, Design and Practice. 2006. https://doi.org/10.1007/3-540-31759-7.

[171] Tatting BF, Gürdal Z. Automated Finite Element Analysis of Elastically-Tailored Plates. Nasa/Cr-2003-212679 2003.

[172] Van Campen JMJF. Optimum lay-up design of variable stiffness composite structures. 2011.

[173] Tatting BF. Analysis and Design of Variable Stiffness Composite Cylinders. Virginia Polythecnic Institute and State University, 1998.

[174] Sun M, Hyer MW. Use of material tailoring to improve buckling capacity of elliptical composite cylinders. AIAA J 2008;46:770–82. https://doi.org/10.2514/1.32495.

[175] Paschero M, Hyer MW. Improvement of Axial Load Capacity of Elliptical Cylindrical Shells. AIAA J 2009;47:142–56. https://doi.org/10.2514/1.37012.

[176] Celebi M, Gürdal Z, Tatting B, Blom-Schieber A, Rassaian M, Wanthal SP. Effects of Size and Location of a Circular Cutout on Buckling and Failure of a Cylindrical Shell in Bending. 58th AIAA/ASCE/AHS/ASC Struct Struct Dyn Mater Conf 2017:1–18. https://doi.org/10.2514/6.2017-0433.

[177] Schultz MR, Nemeth MP. Buckling imperfection sensitivity of axially compressed orthotropic cylinders. Collect Tech Pap - AIAA/ASME/ASCE/AHS/ASC Struct Struct Dyn Mater Conf 2010. https://doi.org/10.2514/6.2010-2531.

[178] Ifayefunmi O, Błachut J. Imperfection Sensitivity: A Review of Buckling Behavior of Cones, Cylinders, and Domes. J Press Vessel Technol Trans ASME 2018;140. https://doi.org/10.1115/1.4039695.

[179] Fajuyitan OK, Sadowski AJ. Imperfection sensitivity in cylindrical shells under uniform bending. Adv Struct Eng 2018;21:2433–53. https://doi.org/10.1177/1369433218804928.

[180] Starnes JH. The Effect of a Circular Hole on the Buckling of Cylindrical Shells - CaltechTHESIS. 1970.

[181] Peeters DMJ, Lozano GG, Abdalla MM. Effect of steering limit constraints on the performance of variable stiffness laminates. Comput Struct 2018;196:94–111. https://doi.org/10.1016/j.compstruc.2017.11.002.

[182] Wehbe R, Tatting B, Gürdal Z, Harik R. Fiber Tow Deformations During Layup of Steered Paths Using Automated Fiber Placement Process. SAMPE 2019 Conf. Proceeding, 2019. https://doi.org/10.33599/nasampe/s.19.1591.

[183] Wehbe RY, Harik R, Gürdal Z. In-plane tow deformations due to steering in automated fiber placement. AIAA Scitech 2019 Forum, American Institute of Aeronautics and Astronautics; 2019. https://doi.org/10.2514/6.2019-1271.

[184] Harik R, Saidy C, Williams SJ, Gürdal Z, Grimsley B. Automated fiber placement defect identity cards: cause, anticipation, existence, significance, and progression. SAMPE Conf. Proc., 2018.

[185] Wehbe R. TOW-PATH CHARACTERIZATION FOR AUTOMATED FIBER PLACEMENT. University of South Carolina, 2020.

[186] iCPS-INGERSOLL COMPOSITE PROGRAMMING SYSTEM THE INTEGRATED SUITE FOR COMPOSITE MANUFACTURING. n.d.

[187] Lopes CS. Damage and Failure of Non-Conventional Composite Laminates. 2009.